

Germar Rudolf

Periodic Nodal Surfaces

and their

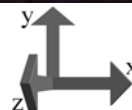
Application in Structural Chemistry

Thesis submitted
in order to obtain the
Degree of Doctor of Exact Sciences
Department of Natural Sciences
Faculty of Chemistry
Stuttgart University
Stuttgart
1993
and after threats
again withdrawn in 1996

© The main part of this thesis has been prepared with means of the Max Planck Institute for Solid State Research, Stuttgart, Germany, and with a scholarship by the Max Planck Society, Munich, Germany. It is published on the condition that anyone who consults it is understood to recognize that the copyright rests with its author and the Max Planck Society and that no quotation from the thesis and no information derived from it which is exceeding fair use may be published without prior written consent of the author and the Max Planck Society.



The periodic nodal surface $PP - JP_4$ ("amphora")
 $^{215}\langle(110);(111)^{\pi/4}\rangle$; x,y,z from $-1/2$ to $1/2$, see pp. 62f.



Contents

	Page
Preface.....	5
1. Introduction.....	9
1.1. Historical Overview.....	9
1.2. Task.....	11
2. Summary and Critique of Previous Approaches.....	13
2.1. Periodic Minimal Surfaces, PMS.....	13
2.2. Periodic Equi- and Zero-Potential Surfaces, PEPS/P0PS.....	16
2.3. Periodic Nodal Surfaces, PNS.....	17
3. Systematic Generation of Periodic Nodal Surfaces, PNS.....	25
3.1. Introductory Remarks.....	25
3.2. Characteristic Structure Factors $S(hkl)$ of the Cubic Space Groups.....	25
3.2.1. Symmetry Patterns.....	25
3.2.2. Tables for $S(hkl)$ of Cubic Space Groups.....	31
3.2.3. Application of the Tables.....	38
3.3. Periodic Nodal Surfaces PNS with Cubic Symmetry.....	40
3.3.1. Calculations.....	40
3.3.2. Nomenclature.....	41
3.3.3. Tables.....	42
3.3.4. Illustrations.....	56
3.4. Characteristic Structure Factors $S(hkl)$ of Hexagonal and Trigonal Space Groups.....	68
3.4.1. Symmetry Patterns.....	68
3.4.2. Tables for $S(hkl)$ of Hexagonal and Trigonal Space Groups.....	69
3.5. Periodic Nodal Surfaces PNS with hexagonal and trigonal Symmetry.....	76
4. Mathematical Analysis of PNS and their Generating Functions.....	79
4.1. Degree of Freedom of the Generating Function.....	79
4.2. Extrema and Line Segment Graphs of Generating Functions.....	79
4.3. Surface Area and Volume Distribution of Nodal Surfaces.....	82
4.4. Symmetry of PNS.....	87
4.4.1. Nodal Surfaces with Black-White Symmetry.....	87
4.4.2. ‘Mirror Surfaces’ and ‘Double Surfaces’.....	88
4.4.3. Nodal Surfaces with Reduced Symmetry.....	89
4.5. Topology of PNS.....	92
4.5.1. Introductory Remarks.....	92
4.5.2. Genera of Nodal Surfaces.....	94
4.5.3. Topology as a Function of Cell Metrics.....	97
5. Hyperbolic, Graphite-Like Carbon Networks.....	101
5.1. On the Theory of Three-Dimensional Networks.....	101
5.1.1. The Curvature of $(n,3)$ Networks.....	101
5.1.2. On the Topology of $(n,3)$ Networks.....	102

5.1.3. On the Symmetry of Hyperbolic Networks.....	107
5.2. Construction of Hyperbolic ($n,3$) Carbon Networks.....	108
5.2.1. Simulation Using Analog Computers	108
5.2.2. Feasibility as Chemical Structure.....	115
6. Organization of Chemical Structures by PNS	117
6.1. Introductory Remarks.....	117
6.2. Elements	118
6.2.1. Diamond	118
6.2.2. α -Manganese.....	119
6.3. Compounds.....	119
6.3.1. Compounds of the Cr_3Si type.....	119
6.3.2. Barium Cuprate, BaCuO_2	121
6.3.3. $\text{Bi}_{22}\text{Sr}_{36}\text{Al}_{48}\text{O}_{141}$	122
6.3.4. Molybdate-Phosphates	123
6.3.5. Lithium Nitrido-Silicate, Li_2SiN_2	124
6.3.6. $\text{Na}_2\text{Ca}_3\text{Al}_2\text{F}_{14}$	126
6.3.7. $\text{Ta}_6\text{Cl}_{15}$	126
6.3.8. Zeolites	127
6.3.8.1. Zeolites of the Sodalite Type	144
6.3.8.2. Paulingite	145
6.3.8.3. Melanophlogite	145
6.3.8.4. Faujasite and Dodecasile-3C	146
6.3.8.5. Analcime and Garnet	147
6.3.9. Hyperbolic Surface Area Demand of Several Zeolites	148
6.4. Summarizing Overview.....	150
7. Potential Areas of Application of the PNS Method.....	153
7.1. Bonding Theory of the Solid State.....	153
7.2. Phase Transitions.....	153
7.3. Physics of Interfaces.....	154
7.4. Description of Non-Crystalline Systems.....	154
7.5. Electron Localization Function ELF	156
8. Summary	157
9. Acknowledgements	159
10. Annex	161
10.1. References	161
10.2. List of Abbreviations and Symbols.....	174
10.3. List of Illustrations and Charts	175
10.4. List of Tables.....	176

Preface

When I was offered to write a PhD thesis at the prestigious Max Planck Institute for Solid State Research in Stuttgart, Germany, in the summer of 1990, it goes without saying that I was thrilled at the prospect and happily agreed, although the topic I was to work on seemed rather exotic and incomprehensible to me at first. Most readers of my thesis will probably agree. But as a student I merely considered this to be a matter of ignorance on my part. To come to understand what I hadn't understood so far was just one more challenge to tackle on my way to a promising academic career.

When I started to work on the topic presented in this thesis, I found myself in the middle of some nasty exchanges between my late supervisor Prof. Hans Georg von Schnering and my predecessor, who had worked on a similar topic until a few months before I showed up. I never quite understood the reason for their vitriolic yelling contests, but the effect of it was that my predecessor was absolutely disinclined to help me getting started, and my supervisor, as the acting director of an entire research institute, was always too busy to give me an introduction. As exotic as the topic was, there was no literature to fall back on, nor was there really anybody else in the world having any knowledge about the issue, save a professor in Zurich and another one somewhere in Sweden, although they both had other priorities than to cater to my needs.

While I was struggling along to get a mental grip on things, my supervisor repeatedly burst into my little room asking me to try certain variations of structure factors in order to create a space divider with a certain symmetry. Sometimes he failed, but sometimes he had success with this approach. Being a systematic person who loves to approach issues logically, I was very much dismayed by this haphazard approach to creating what my supervisor perceived as being something very fundamental and important. So after several months of being completely out at sea with no help from anyone, I set out to find a pattern behind what my supervisor was doing. I wanted to find the laws that govern the creation of certain symmetries by certain structure factors.

I was $\frac{3}{4}$ done with this work when, in the spring of 1991, my supervisor once more suddenly burst into my room one afternoon, this time venting with excitement about his idea that it should be possible to approach in a systematic way the relationships between structure factors and the symmetry they can generate. I listened to him patiently, and

when he was done I mentioned that I had already been working on this for several weeks and that I am almost done with this, showing him the results which I had put in tabular form. At the sight of my results his jaw merely dropped. “Very good” was all he said, and he went back into his office.

Ever since that day, my supervisor has held me in relatively high esteem – until the day when he started reading the first draft of my thesis in early 1993. The first, yet minor reason was the preface with which I had garnished my thesis. In it I deliberated about the dichotomies pervading our world, starting with those close to the topic dealt with in the present thesis. Via crystalline versus amorphous, order versus chaos, and energy versus entropy, I arrive at life versus death, where life – driven by energy – is the power that makes all things different, whereas death – driven by entropy – is the power that makes all things equal, although neither can exist (or makes sense) without the other. I then extended these thoughts to our social world, applying the same pattern: the ideology of egalitarianism is the ideology of death, whereas identity movements are the ideologies of life, which led to an excursion into what is “left” and “right,” politically speaking. This thought finally led me to a brief discussion of how societal taboos prevent social scientists from exploring these complementary opposites in depth while giving both sides their due.

My supervisor ordered me to remove this preface without substitution. Well, I did.

This was not the worst part of my first draft in my supervisor’s eyes, though, for I had dared to express my doubt that the entire topic I had been working on over the past two years was worth the time I had spent on it. And I still maintain that employing mathematical laws of group theory – or simply put: of symmetry – on simple sine and cosine functions could not possibly result in more than mathematical functions with a certain symmetry. My supervisor’s high-flying expectations have always been that these beautiful space dividers might unlock a treasure trove of information about links between chemical or physical features of solid structures on the one hand and their symmetry on the other. Nothing of that sort has ever panned out, nor was it likely to. After all, just putting a few sine and cosine functions together to produce some pretty, curved planes is hardly an approach to explain the properties of solid compounds. If you put only symmetry into it, you can get only symmetry out of it. Where symmetry laws force solids into a certain shape, their physical and chemical properties are certainly affected by this. But that is as far as it goes.

Other than that, the space dividers presented in this thesis are very convenient di-

dactic tools enabling us to recognize or understand better the often extremely complex and frequently non-Gaussian, “warped” organization of crystalline structures. They also doubtlessly have an esthetical value, if that is of any importance to a scientist.

It goes without saying that my supervisor, who had invested so much of his time, his resources and his hopes into his pet topic, didn’t like my iconoclastic statements at all. “You still haven’t understood a thing,” he yelled at me. He ordered me to excise them as well and to replace them with his view of the topic.

I didn’t quite follow his order, but tried to find a compromise by putting my statements into the form of questions left unanswered and by adding his views to the roster. This my supervisor let pass.

I also managed to get a few “ugly” examples into my thesis which clearly show the limitations of the concept developed in this thesis: sine and cosine functions do not always neatly follow nature’s patterns. As a matter of fact, the principle followed during my research was: find something that looks nice and use it. That which doesn’t look too good we ignore and discard. Well, I tried to steer a little against that prevailing current of the selective use of evidence and put in some examples of what can hardly pass as useful for anything: convoluted space dividers good for nothing.

Where does that leave us?

In his work *The Logic of Scientific Discovery*, Karl R. Popper described the various anti-scientific methods to immunize one’s theory against critique.¹ One of them is the arbitrary selection or elimination of data to make one’s theory look good. That was the tendency of the work leading up to my thesis, and I didn’t like it at all. I could not discuss this with my authoritarian supervisor. Hence my colleagues at the institute served as partners to discuss the ethical implications of doing research on a topic which put me on an unwanted career track or maybe even into a dead end of my career, which wasted taxpayer money, and which forced me to bend my scientific principles.

How many more students have found and are finding themselves in a similar position as I found myself in back then? What has science come to when evidence counts less than the “authority” of a recognized “expert”?

A few years later I discovered that I am not at all alone with this view. Dr. Halton Arp, professor of astrophysics at the Max Planck Institute for Astrophysics near Munich, has summarized the tragedy that is brewing today in science generally as follows:²

¹ Hutchinson & Co., London 1968, pp. 82-97.

² Halton Arp, “What has Science Come to?,” *Journal of Scientific Exploration*, 14(3) (2000), pp. 447-454.

“The most harmful aspect of what science has become is the deliberate attempt to hide evidence that contradicts the current paradigm. [...] In a quite human fashion, however, they [the peers] act in an exactly opposite manner – judging that ‘if an observation disagrees with what we know to be correct, then it must be wrong.’ The tradition of ‘peer review’ of articles published in professional journals has degenerated into almost total censorship.”

Later in my life I have encountered many other scientists who have found themselves in a similar position. A friend of mine, for instance, has been trying to finish his PhD thesis on a topic of the social sciences for twenty years. He has always been put under pressure to come to certain conclusions by his supervisors, although those conclusions were not supported by the evidence. He has changed topics and supervisors numerous times in search of an opportunity to write what he thinks the evidence forces him to. Another acquaintance of mine has written a habilitation thesis in Germany which no professor is willing to accept, because the results are running contrary to the *zeitgeist*. And so the story goes on.

My disappointment was not limited to my own thesis and its supervisor. It went beyond that. Having worked within a Max Planck Institute for three years made me also realize that this institution had become ossified to such a degree that many, if not most scientists there behaved more like public employees than like pioneers at the adventurous frontier of human discovery.

In view of all this it may no longer be such a great surprise that I risked my fledgling academic career at this renowned German research institution with research work I was simultaneously pursuing in private. I will not elaborate on this research here, because it is a different matter entirely. The interested reader can find out about it by searching the internet. Suffice it to say that the topic of my private research was and is very controversial and that therefore the pressure exerted by the public at large to come to foregone conclusions is nowhere as huge as it is there. But the beauty of this independent research was that nobody could order me how to do my research and to which conclusions I should come. After all, I wasn’t doing it to “earn” a degree or any other distinction, or to further my career or social status. Hence there was no supervisor, employer or academic board I had to answer to. I just wanted to satisfy my curiosity and get it right. And that’s ultimately what science should be about. Wrong or right, I was a free man.

And I am again.

Germar Rudolf, Red Lion, Pennsylvania, June 25, 2014

1. Introduction

1.1. Historical Overview

It is not known how long mankind has been pondering about the phenomenon of surface tension and thus the formation of minimal surfaces. During the 19th century mathematicians like Schwarz, Neovius, and Bonnet first focused intensively on periodic minimal surfaces (PMS), which are minimal surfaces defined by a given frame which can be perpetuated periodically while maintaining their steady curvature (Plateau's problem).^[1-3] The mathematical formalism for their parameterization has been deduced by Weierstrass, who already recognized that analytical expressions can be given only for certain minimal surfaces.^[4] In the early 20th century even Hilbert condoned the use of soap bubble experiments in order to investigate minimal surfaces, just as the famous architectural constructions by Frei Otto of the 1960s have been "calculated" with such experiments.

Interest in the topic increased again in the 1960s, most notably advanced by investigations by Schoen, who characterized 17 new PMS in a study prepared for NASA.^[5]

Nissen as well as Donnay and Dawson showed in 1969 that the macroscopic shapes of calcite skeletons of various echinodermata (sea urchin, sea cucumber, starfish etc.) have a strong resemblance with the shape of space-dividing periodic minimal surfaces.^[6,7] This observation raised the question which biochemical parameters result in the minimization of the contact surface between inorganic skeleton material and organic tissue.

In chemistry the application of space dividers in the shape of curved surfaces occurred for the first time in 1976, when Scriven^[8] suggested using a continuous, isotropical distribution of two phases, separated by a minimal surface, in order to describe cubic phases of liquid crystals in the lipid-water system. Previous attempts at explaining those phases as cubic packings of spheres or rods had failed, as this could not explain the high diffusion coefficients of the lipid molecules within these liquid crystals.^[9-13] For his approach Scriven resorted to the – at that time roughly a century old – works by Neovius and Schwarz as well as the more recent work by Schoen. Briefly before that, Kléman had predicted the formation of minimal surfaces during the phase transition from smectic to nematic phases of liquid crystals for energetic reasons.^[14] In the ensuing discus-

sion, Scriven's thesis prevailed that a cubic two-phase system exists whose interface can be described as a minimal surface.^[15-23] Even polymer chemists, whose mixed phases have properties similar to those of emulsions, turned to minimal surfaces in their search for suitable theories explaining their cubic phases.^[24-28]

The application of the concept of periodic space dividers to crystalline structures in general was initiated by Andersson on the basis of the works by Schoen, Schwarz, Neovius, and Bonnet. Contributions by Andersson in 1983 and by Andersson, Hyde, and v. Schnering in 1984^[29,30] demonstrated the organization of complex inorganic structures by space-dividing periodic minimal surfaces. That same year v. Schnering and Nesper, while discussing the relevance of PMS for the polar structures of salts, arrived at a fundamentally different approach for space dividers: periodic zero(0)-potential surfaces (POPS).^[31-35] It turned out swiftly that:

1. POPS and the periodic equi-potential surfaces (PEPS) parallel to them can be obtained much easier than PMS using the Ewald method^[36] generally used to calculate lattice potentials. (The required computer program MADKUG had been available since 1962.)
2. POPS are very similar to known PMS, and we know today that and why the deviations are minimal.^[37,38]
3. For considerations of pure symmetry, POPS can be found whose analogous PMS are yet unknown. (For instance the S^* and the Q^* surfaces, see later.)
4. Space dividers and their labyrinths have direct and tight relations to crystallographic point configurations. They can be organized following group-subgroup relations. Their number must be constraint.
5. Unequivocal relations exist to certain physical properties.
6. POPS can be transformed continuously, which opens new insights into phase transitions.

In subsequent years, this POPS approach has been studied thoroughly with regard to a variety of aspects by Oehme in his dissertation.^[39]

After a study by Hyde on general connections between PMS and crystalline matter^[40] as well as several topical observations,^[41-44] research interest increasingly focused on the theory of minimal surfaces. Fischer and Koch elucidated group-theoretical aspects of minimal surfaces,^[45-48] whereas especially Hyde, Andersson, and Lidin performed profound research on mathematical topics such as topology, graph theory, and differential geometry.^[49-55]

In 1987 v. Schnering and Nesper tried the second method of calculating zero-potential surfaces^[56] based on Bertaut's approach of calculating lattice energies or rather lattice potentials.^[57] The crucial difference between Bertaut's and Ewald's approach is that Bertaut assigns different factors to his summands from reciprocal and real space. The structure part itself can be described with only a few Fourier coefficients from reciprocal space. In 1988 Mackay discovered this formalism as well,^[58] although by using topological analogies between PMS and POPS on one hand and certain Fermi surfaces and their mathematical descriptions on the other hand.^[59] Oehme applied this approach successfully in his thesis as well.

In 1990 v. Schnering and Nesper discovered the fundamental importance of periodic nodal surfaces (PNS) as general structure invariants. They succeeded to formally reduce the Fourier series used to calculate the PNS to merely geometric structure factors S_{hkl} and symmetry-inducing phases α_{hkl} .^[60-62]

As will have to be shown, the PNS permit, due to their purely mathematical, group-theoretical nature, a fundamental description of the organization of crystalline as well as quasi-crystalline matter.

An overview of the research dedicated to the topic of minimal surfaces, space dividers, and geometric descriptions of interfaces is offered by the anthology of contributions to the International Workshop on Geometry and Interfaces, which took place in the summer of 1990.^[63]³

1.2. Task

In his PhD thesis Hyde investigated the relationship between minimal surfaces and the organization of crystalline matter. A large part of his work was dedicated to mathematical analyses of minimal surfaces.^[40] By so doing, he mainly focused on topological issues as well as on connections between geometric transformations of minimal surfaces and phases transitions in solid state chemistry. Oehme's dissertation centers around zero-potential surfaces and their use in structural chemistry.^[32,39] Oehme also explored how second order phase transitions can be modeled with dynamically modulated potential surfaces. As mentioned earlier, Oehme also made first steps into the generation and

³ For a comprehensive summary about minimal surfaces in physics, chemistry, and biology including research results mainly up to 1992/1993 see: S. Hyde, S. Andersson, K. Larsson, Z. Blum, T. Landh, S. Lidin, B.W. Ninham, *The Language of Shape*, Elsevier, Amsterdam 1997.

application of periodic nodal surfaces.

The task of this present work will be to investigate as thorough as possible the concept of periodic nodal surfaces and their usefulness for the analysis of the structure and organization of crystalline compounds. An introduction into the three concepts – minimal, zero-potential, and nodal surfaces – with main focus on nodal surfaces is meant to permit a comparison. In the third chapter I will develop the general formalism of *characteristic structure factors*, with whose help PNS of any desired symmetry can be generated. Furthermore all nodal surfaces generated so far will be introduced and characterized. During the fourth chapter these nodal surfaces plus their generating functions will be subjected to a mathematical analysis. The subsequent chapter deals with hypothetical hyperbolic networks of graphite-like carbon, whose topology and symmetry have a remarkable similarity with the space dividers discussed in this thesis. The sixth chapter will investigate how one can gain new insights into the organization of crystalline matter – both elements and compounds – by applying appropriate space dividers as previously developed.

The thesis ends with a brief chapter on possible other areas of application of nodal surfaces, which have partly been investigated already with the other, older methods.

2. Summary and Critique of Previous Approaches

2.1. Periodic Minimal Surfaces, PMS

Mathematicians have always had a predilection for harmonic geometric objects, to which minimal surfaces no doubt belong. The first documented studies by Schwarz and Neovius^[1,2] were considerably expanded a century later by Schoen.^[5] Karcher^[64] and Nitsche^[65-69] focused on thorough mathematical treatises of minimal surfaces. Besides the dissertations by Hyde^[40] and Oehme,^[39] mainly the papers by Fischer, Hyde, and Lidin et al. give an excellent overview about the history of research on minimal surfaces and about the properties of three-dimensional periodic minimal surfaces, which are of interest in this context.^[45,48,49,53-55] Only the most important characteristics of minimal surfaces will be discussed here, based on the papers quoted above.

Minimal surfaces are surfaces which assume such a shape within a given frame (boundary condition) that their surface area is minimal. Even after the introduction of powerful digital computers it is still considered normal to resort to natural materials for the discovery and investigation of minimal surfaces: a soap bubble within a given frame. We know since Gauß's research^[70] that the curvature of a soap bubble is proportional to its surface tension. As long as the gas pressure on both sides of the surface is equal, the *average curvature* H at any point of the soap bubble's surface needs to disappear so that this point is free of any force with regard to the gas phase, which is a prerequisite for the soap surface being stable. (Regarding analogous equilibrium conditions of lipid-water mixtures see the work by Marmus.^[20]) This is true both for surfaces free of any curvature as well as for curved surfaces, for which the integral over all curvatures at any point as a function of the direction α , k_α , – mathematically the second derivative of the function describing the soap surface – has to be zero:

$$H = \frac{1}{n} \int_{\alpha=0}^{\pi} k_\alpha d\alpha = 0 \quad (1)$$

Hence, minimal surfaces are characterized by the fact that they have either no curvature at all or that they have curvatures of identical absolute values but inverse sign in different directions. Gauss furthermore showed that one can find at any point of a minimal surface two directional vectors orthogonal to each other which have a maximum

absolute value of curvature k_i . For these *main curvatures* k_1 and k_2 the following holds:^[71]

$$k_1 = -k_2 \quad (2)$$

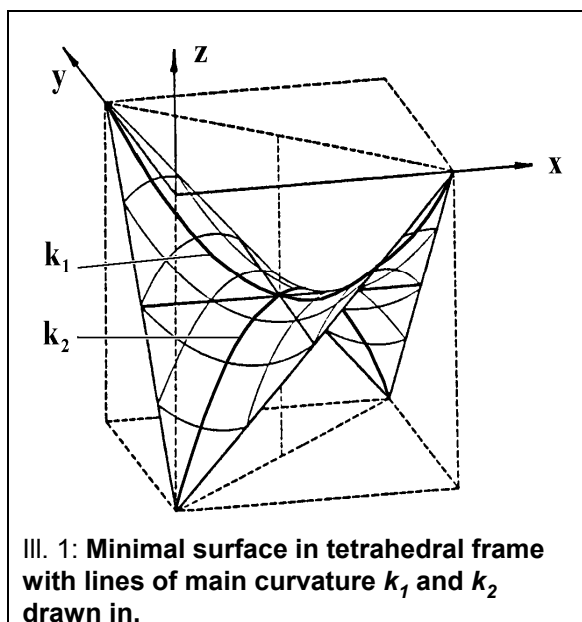
Thus the mean curvature can be defined as:

$$H = \frac{k_1 + k_2}{2} = 0 \quad (3)$$

The product of both main curvatures k_1 and k_2 is called *Gaussian curvature* G . In the case of minimal surfaces with the condition given in eq. (2) we receive:

$$G = k_1 \cdot k_2 \leq 0 \quad (4)$$

From this it follows that minimal surfaces consist exclusively of inflection points ($k_\alpha=0$) as well as of saddle or hyperbolic points ($H=0$, $k_\alpha \neq 0$). In contrast to surfaces with $G > 0$, which assume spherical or elliptical shapes, surfaces with negative Gaussian curvature are called hyperbolic. Ill. 1 (p. 14) shows a minimal surface, generated by using the frame of the four edges of a tetrahedron, with the lines of main curvature drawn in bold. This surface section itself is not yet



a translationally periodic minimal surface (PMS). Rather, such a surface has to be constructed by applying appropriate symmetry operations of the according space group,^[67] in which case the resulting minimal surface has to be continuously differentiable at the lines of connection of the surface sections. This two-dimensional surface section therefore corresponds to the zero-dimensional point configurations in crystallography.

With the availability of powerful computers minimization problems became easier to solve, such as minimal surfaces or the proverbial example of the traveling salesman who wants to visit a variety of places while reducing to a minimum the total mileage he has to travel. The calculation of minimum surfaces requires the numerical solution of elliptical integrals which defy analytical solutions. These integrals project the mathemati-

cal information from a plane of complex numbers into real space.^[38,54,66,72,73] The effort needed to calculate a minimal surface with known boundary conditions is extreme. In practice, this approach is used only to seek non-periodic minimal surfaces.^[74] It is therefore understandable why up to the end of the 20th century new minimal surfaces were still being discovered with the aid of the construction and novel assembly of surface sections by means of soap bubbles.^[47] Lidin^[55] as well as Fischer and Koch^[75] have investigated the symmetry restrictions of the boundary conditions (the defining framework of the soap bubble), which are given by the properties of minimal surfaces. By so doing, Fischer and Koch have determined how many different types of boundary conditions can exist for the generation of surface sections and which properties they must have.

Apart from their difficult accessibility as well as their restricted variability due to symmetry requirements, there is also a physical reason which has prevented the concept of minimal surfaces to be more widely accepted in crystallography. The physical reason for the relevance of minimal surfaces in special areas of biology,^[6,7,76-78] in the field of lipid crystals and lipid-water mixtures,^[8,15-23,63,79-84] is identical to that in the case of soap bubbles: dynamic systems try to minimize the interaction between two phases. But since the structure-determining interactions in static crystals are much more complicated, no obvious physical link exists here between minimal surface and structure. There have nevertheless been isolated attempts at regarding crystals as cases of minimized surface energies, although in this case no real geometric surfaces are meant but rather interfaces of different areas of interaction.^[85] The problem of this approach is that the limits of such areas of interaction are difficult to define and hardly determinable, quite in contrast to phase interfaces. It is therefore not surprising that more than 80% of all the contributions to the 1990 International Workshop on Geometry and Interfaces focused on the application of minimal surfaces on lipid crystalline phases and lipid-water mixtures.^[63]

In 1988 Andersson et. al. gave an overview of the results gained until then regarding the application of minimal surfaces in chemistry and its neighboring disciplines.^[86]⁴

⁴ It should be noted in passing that minimal surfaces are also being applied in relativistic physics for the description of the space-time-continuum.^[88,89]

2.2. Periodic Equi- and Zero-Potential Surfaces, PEPS/POPS

In the early 1960s v. Schnering developed a computer program capable of determining lattice potential values of crystals.^[89] This program can find possible locations in a crystal with ideal potential values for adding further atoms. It also allows the determination of the most likely theoretical position of protons in crystalline hydroxo compounds, often in close agreement with experimental results, since protons are expected to be located at the most negative potential on a sphere around their according oxygen atoms.^[90]

Instead of calculating lattice potentials only of a predefined location, as in the works mentioned above, Nesper and v. Schnering expanded this approach in the early 1980s to encompass the entire unit cell of a crystal, which for this purpose is divided into a fine grid work. This grid work is searched for certain potential values, which can then be connected to form potential surfaces.^[31-35] As a result, zero-potential surfaces are being generated, which can be flat (intersecting planes) or curved (spherical or hyperbolic). The same holds for surfaces of certain non-zero potential values, so-called equi-potential surfaces. It turned out that many zero-potential surfaces of certain periodic charge distributions have great similarity to known minimal surfaces. The zero-potential surfaces, however, have the advantage that they can be generated mathematically far easier than minimal surfaces and that, in addition to this, they are basically infinitely variable, depending on the choice of charge distribution. At the beginning of research on zero-potential surfaces in crystal chemistry, the Ewald method was used, which calculates potentials numerically and iteratively. For his PhD thesis Oehme already used Fourier series, which will be further discussed in the next chapter due to their importance for periodic nodal surfaces.^[39]

Except for v. Schnering and his co-workers^[31-39] it was basically only Hyde^[40] who – albeit rather superficially – focused on potential surfaces in structural chemistry. Even when dealing with ion conductors, for which a physical link between potential surfaces and conduction mechanism can hardly be overlooked, minimal surfaces of a similar geometry have been used.^[41,91] The reason for this may be that new concepts usually have difficulties to get recognized, especially when competing against already established methods. The advantage of potential surfaces over minimal surfaces (mathematical accessibility, unrestricted variability) are contrasted by the fact that the concept of electrostatic potentials is bound to a specific physical phenomenon, which seems to impede

more far-reaching interpretations and hence applications in crystal chemistry. v. Schnering and Nesper have pointed out that the charge configurations used to generate the potential surfaces are required merely in order to produce the desired symmetry, topology, and geometry. The resulting space-dividing periodic potential surfaces are subsequently investigated regarding their general usefulness to organize crystalline compounds independent of possible properties of the original generating charge configuration.^[35] This does, however, not remove the de facto link of the potential surface to its electrostatic origin. Even the sheer multitude of possible potential surfaces can be more of a bane than a boon, as the number of surfaces leads to new confusion instead of elucidating relationships in the organization of crystalline structure. A final obstacle for the application of zero-potential surfaces is certainly their clumsy nomenclature.^[32,35] Even though a proper nomenclature is necessary for an unequivocal characterization, it complicates the communication between scientists, quite in contrast to the convenient “trivial names” of most minimal surfaces.⁵

2.3. Periodic Nodal Surfaces, PNS

The second method for the calculation of potential surfaces as found by v. Schnering and Nesper^[56] is based on Bertaut’s theory of lattice energies and electrostatic lattice potentials, respectively.^[57] According to Bertaut, the lattice energy of a crystal can be calculated in a somewhat simplified form as follows: (cp. ^[61]):

$$U = \frac{1}{2V} \sum_h \frac{F_h^2 \Phi_h^2}{h^2} - \frac{3}{5} \cdot \frac{1}{R} \sum_i q_i^2 \quad (5)$$

with U = lattice energy
 V = cell volume
 F = geometric structure factors
 h = reciprocal lattice vectors
 Φ = Fourier transform of the charge distribution
 R = ion distance
 q_i = charge of ion i

⁵ The minimal surfaces named by Schoen^[5] obtained their names mostly from abbreviations of polyhedra which are similar to surface sections of the minimal surfaces. Since this nomenclature is neither strictly analytical nor has it been applied in a strict sense – frequently quite imaginative names or those pointing at their discoverers are being used – this expression may be permitted.

Table 1: Relation between Melting Enthalpy ΔH_M and Evaporation Enthalpy ΔH_E of some Elements and Compounds				
Element	Evaporation Enthalpy ΔH_E [kJ/mol]	Melting Enthalpy ΔH_M [kJ/mol]	$\frac{\Delta H_E}{\Delta H_M}$	Ref.
Aluminium	284.0	11.0	26.0	[92]
Argon	6.5	1.2	5.4	[92]
Bromium	30.0	12.5	2.4	[93]
Caesium	66.0	2.1	31.0	[94]
Cerium	422.0	8.9	47.0	[95]
Hydrogen	0.9	0.1	7.5	[92]
Iron	354.0	16.0	22.0	[92]
Lithium	134.0	3.0	45.0	[94]
Lutetium	427.0	19.0	22.0	[95]
Mercury	58.0	2.0	29.0	[92]
Phosphorus	12.4	2.5	5.0	[93]
Platinum	510.0	22.0	23.0	[92]
Scandium	376.0	16.0	24.0	[95]
Silver	254.0	12.0	21.0	[92]
Sulfur	90.0	1.7	53.0	[93]
Thulium	233.0	18.0	13.0	[95]
Tungsten	799.0	35.0	23.0	[93]
Ytterbium	153.0	9.0	17.0	[95]
Compound	Evaporation Enthalpy ΔH_E [kJ/mol]	Melting Enthalpy ΔH_M [kJ/mol]	$\frac{\Delta H_E}{\Delta H_M}$	Ref.
AgCl	199.0	12.7	15.7	[92]
AlBr ₃	23.0	11.3	2.0	[92]
As ₂ O ₃	30.8	49.8	0.6	[93]
BaCl ₂	210.0	22.5	9.3	[92]
C ₂ H ₅ OH	38.7	5.0	7.7	[92]
C ₆ H ₆	31.0	9.9	3.1	[92]
COS	18.5	4.7	3.9	[93]
CrO ₂ Cl ₂	35.1	41.5	0.9	[93]
FeCl ₃	25.2	43.1	0.6	[93]
H ₂ O	40.7	6.0	6.8	[92]
IrF ₆	7.4	8.4	0.9	[93]
NaCl	170.0	28.8	5.9	[92]
NaOH	144.0	6.4	22.5	[93]
NH ₃	23.4	5.7	4.1	[92]
P ₄ O ₁₀	86.5	71.5	1.2	[93]
PbO	213.0	11.7	18.2	[93]
SiH ₄	12.1	0.7	18.0	[93]
SO ₃	42.0	2.0	21.0	[93]
WOCl ₄	68.0	5.9	11.5	[93]

The equivalent equation for the lattice potential $P(r)$ is:

$$P(r) = \frac{1}{\pi V} \sum_h F_h \frac{|\Phi_h|^2}{|h|^2} e^{-2\pi i h r} - \frac{q}{\pi} \int \frac{\Phi_h^2}{h^2} dh \quad (6)$$

Both eq. (5) and (6) consist of two terms. The right-hand term contains the background charge, characterized by a spherical charge q with a radius R without any further information about structure of this environment. This is an arrangement as it can be found in liquids, if integrated over time. This right-hand term of the energy eq. (5) therefore gives that part of the lattice energy which is released during condensation of the respective matter from the gaseous to the liquid phase.

The left-hand term in turn introduces a correction from the amorphous (\approx liquid) to the crystalline state by adding the energy gained due to the periodic organization of the matter in a crystal. This organization is described in eq. (5) by means of a Fourier series, whose coefficients obey the group theoretical selection and permutation laws of the respective crystal symmetry.

In Table 1 (p. 18) the melting and evaporation enthalpies of several representative elements and compounds are listed. It follows from these data that, particularly in case of elements, evaporation enthalpies are regularly many times larger than melting enthalpies, in case of metals usually by more than the factor 20. Even for chemical compounds there is a predominance of those whose evaporation enthalpy is markedly higher than the melting enthalpy, even though there are a number of exceptions for highly volatile compounds. The right-hand term of the above equations therefore usually contributes the largest share to the total lattice energy of a crystal. The left-hand term, describing the transition from the amorphous to the crystalline state, frequently adds only a relatively minor correction to the total energy. The same is true for both terms of the potential eq. (6).

Crystal structures are periodic arrangements of objects in three-dimensional space. Trigonometric functions are therefore predestined to describe such objects, as they can be approximated to any periodically arranged object – in the following $f(r)$ – by a series:^[96]

$$f(r) = \sum_{h=-\infty}^{\infty} a_h \cos(2\pi h r) + b_h \sin(2\pi h r) \quad \text{with } h \in \mathbb{N}. \quad (7)$$

The constants a_h and b_h are hereafter replaced by the function $f(h)$. If transiting to infinitesimal steps with rational values of h and converting to the complex plane, eq. (7)

yields the Fourier transformation equation, which can be used to describe any object, even those not translationally periodic:

$$f(r) = \int_{h=-\infty}^{\infty} f(h) \cos(2\pi hr) dh \quad -i f(r) = \int_{h=-\infty}^{\infty} f(h) \sin(2\pi hr) dh \quad (8)$$

respectively:

$$f(r) = \int_{h=-\infty}^{\infty} f(h) e^{-2\pi i(hr)} dh. \quad (9)$$

This fundamental equation as well as its inverted equation (inverse Fourier transformation equation) for the characterization of individual structure factors $f(h)$:

$$f(r) = \int_r f(r) e^{2\pi i(hr)} dr \quad (10)$$

are the mathematical basis for the analysis of crystal structures, in which case, due to the translational periodicity, the structure factors h assume discrete, integer values, as a consequence of which simple sums instead of integrals can be used. The equation for the calculation of the electron density ρ in a crystal, which is responsible for the diffraction of x-rays, is therefore.^[97]

$$\rho(x,y,z) = \frac{1}{V} \sum_{h=-\infty}^{\infty} \sum_{k=-\infty}^{\infty} \sum_{l=-\infty}^{\infty} F(hkl) e^{-2\pi i(hx + ky + lz)}. \quad (11)$$

with $\rho(x,y,z)$ = electron density
 x,y,z = fractions of real cell axes
 V = volume of the unit cell
 h,k,l = multiples of reciprocal cell axes
 $F(hkl)$ = structure factors

Since crystals are periodic, the real space parameters in this equation are given in fractions of the cell axes (x,y,z) , and the reciprocal space parameters as multiples of the reciprocal axes (h,k,l) . Complete information about the distribution of the electron density in space is obtained only if the cell metrics are known. The structure factor $F(hkl)$ contains not only information about the symmetry of the crystal but also about the dependence of x-ray diffraction as a function of the angle of incidence (e.g. scatter length of atoms, experimental geometry, etc., compare^[98]).

Friedel's law enforces real electron densities with the following relation between $F(hkl)$ and $F(\bar{h}\bar{k}\bar{l})$:

$$F(hkl) = A' + iB'; \quad F(\bar{h}\bar{k}\bar{l}) = A' - iB'; \quad |F(hkl)|^2 = A'^2 + B'^2. \quad (12)$$

Thus results:

$$A' = |F(hkl)| \cos \alpha(hkl); \quad B' = |F(hkl)| \sin \alpha(hkl); \quad \text{with } \alpha(hkl) = \arctan\left(\frac{B'}{A'}\right). \quad (13)$$

Hence, eq. (11) turns into:

$$\rho(x,y,z) = \frac{1}{V} \sum_{h=-\infty}^{\infty} \sum_{k=-\infty}^{\infty} \sum_{l=-\infty}^{\infty} |F(hkl)| \cos(2\pi(hx + ky + lz) - \alpha(hkl)) \quad (14)$$

Because the integral over trigonometric functions covering one phase (2π) is always zero, the summands with at least one reciprocal coefficient unequal to zero describe merely the distribution of the function value $\rho(x,y,z)$ around the integral mean value of zero. A central role is therefore assigned to the summand whose coefficients are all zero, which is the one projected onto the origin of the reciprocal lattice. This summand yields a value proportional to the respective structure factor $F(000)$ at all locations x,y,z of the function, since $\cos \alpha(hkl)$ is constant. The trigonometric functions therefore describe, within a periodic unit, the distribution of a value defined by the origin's summand. Bertaut^[57] used similar mathematical series to describe lattice potentials of crystals whose value, integrated over the entire unit cell, has to be zero due to the condition of electro-neutrality ($F(000)=0$).

For the relationships of phases and signs of the structure factors of the Friedel reflexes the following holds:

$$\alpha(hkl) = -\alpha(\bar{h}\bar{k}\bar{l}); \quad F(hkl) = -F(\bar{h}\bar{k}\bar{l}). \quad (15)$$

Since furthermore the following is true:

$$\cos(2\pi(\bar{h}x + \bar{k}y + \bar{l}z) + \alpha(hkl)) = -\cos(2\pi(hx + ky + lz) - \alpha(hkl)) \quad (16)$$

this leads to the fact that in case of the Friedel reflexes sign changes of h,k,l and α on one hand and of $F(hkl)$ on the other hand cancel each other out. As a result, it is necessary to sum up only four of the eight octants of reciprocal space. If summing up only those space octants with $l \geq 0$, eq. (14) turns into:

$$\rho(x,y,z) = \frac{2}{V} \sum_{h=-\infty}^{\infty} \sum_{k=-\infty}^{\infty} \sum_{l=0}^{\infty} |F(hkl)| \cos(2\pi(hx + ky + lz) - \alpha(hkl)) \quad (17)$$

If replacing the charge distribution by a dimensionless δ -function, one receives a purely geometric, dimensionless structure factor $S(hkl)$ instead of the structure factor

$F(hkl)$ with the dimension of the elementary charge e^- . As a consequence one receives a function $f(x,y,z)$ with no link to any physical phenomenon:

$$f(x,y,z) = \sum_{h,k,l} |S(hkl)| \cos(2\pi(hx + ky + lz) - \alpha(hkl)) \quad (18)$$

$f(x,y,z)$ = function value

$S(hkl)$ = geometric structure factor

Nesper, Oehme, and v. Schnering^[39,56] used eq. (18) initially to approximate zero-potential surfaces of crystalline structure with a series quickly converging to its final value. In 1990 v. Schnering and Nesper realized that this approach merely contained the distribution of function values (δ -functions) following group-theoretical symmetry laws without any link to physical phenomena.^[60,61]

Like in the case of zero-potential surfaces, where $\rho(x,y,z)$ of eq. (17) is set to zero, the calculation of periodic nodal surfaces equally sets $f(x,y,z) = 0$ in eq. (18). The reasons for this are:

1. In case of a physical context, the Fourier sums ascertain a symmetrical distribution of the respective physical quantity. At those locations where the Fourier sums are zero and hence do not contribute to the symmetric distribution, they obviously are as structurally invariant as possible. At their zero locations, these functions are without any influence on and without any relation to physical phenomena.
2. The integrals over trigonometric functions of an entire phase (2π) are always zero. Purely mathematically viewed, the zero value surfaces of trigonometric functions in three-dimensional space are characterized by the fact that to the 'left' as well as to the 'right' of these surfaces the same total function value density can be found. Zero value surfaces are therefore surfaces of particularly high symmetry.

The independence from any physical inheritance doubtlessly has the advantage that results obtained with this approach are universally applicable within the framework of the laws of group theory. On the other hand, the question naturally arises whether this general mathematical, group-theoretical approach is at all useful for the interpretation of any physical phenomenon beyond pure symmetry considerations. It will be one of the tasks of this work to evaluate this.

In contrast to the methods introduced in the previous chapters, this approach has furthermore the advantage that the mathematical generation of nodal surfaces is extremely simple,⁶ even if resorting in most cases to numerical-iterative approximations, and their

⁶ S. Hyde et al. (see footnote 3 on p. 7, Hyde's p. 260), A.L. Mackay ("Periodic Minimal Surfaces from finite element methods", *Chem. Phys. Lett.* **221** (1994), pp. 317-321), as well as J. Klinowski, A. L.

variability is constrained only by the laws of group theory with the option to effortlessly generate any desired symmetry. More about this will be said in the next chapter.

When comparing the three methods discussed here, PMS – POPS – PNS, the question arises if and to which degree the results, i.e. the respective surfaces, are either completely different in nature, similar, or even identical. First of all it should not be expected that the results of different mathematical procedures yield identical results. Barnes, Hyde, and Ninham^[37] have shown for Schwarz's P-surface and their analogous surfaces obtained with the other methods that the results of all three methods can be astonishingly similar, yet are never identical. Within the framework of investigations for this work, control calculations yielded that the position of zero values resulting from the potential surface method are not identical to those resulting from the nodal surface method.

Particularly interesting is the comparison of the potential method with the nodal method. Whereas the generation of the zero-potential surface P* using Ewald's method requires several hundred to thousand summands in order to achieve a result with an error margin of $10^{-6}\%$, already the very first term of the nodal surface approach yields a result which deviates only 5% from the end result. This indicates that the very first terms of the sum always contribute the vast majority to the lattice potential, whereas all later terms contribute only minor corrections. This shows that the calculation of physical phenomena similar to lattice potentials yields a result very close to the final value already after the first summand.

Fogden has furthermore shown that the Fourier series of our PNS are identical to the first terms of the mathematical series of the exact Weierstrass integrals used to calculate minimal surfaces and that they are larger than all following terms by a factor of 50.^[38] As a result, deviations between PNS and their PMS counterparts are minor.

Mackay, and H. Terrones ("Curved surfaces in chemical structures", *Phil. Trans. R. Soc. Lond. A*, **354** (1996), pp. 1975-1987, here pp. 1979f.) consider PNS primarily as mathematical shortcuts to the calculation of surfaces closely resembling minimal surfaces.

3. Systematic Generation of Periodic Nodal Surfaces, PNS

3.1. Introductory Remarks

In order to find periodic nodal surfaces, early attempts have tried to recreate surfaces already discovered with the POPS approach (see chapter 2.2.).^[39,56] For this, structure factor calculations have been performed using charge distributions as given by the potential method. The resulting structure factors closest to the origin of reciprocal space and with the highest values have been chosen and used to calculate nodal surfaces.

The same approach was initially used for this work in order to get clues as to which structure factors are relevant. The main goal, however, has been to no longer generate periodic nodal surfaces by means of empirical searches following the guidance of the potential method, but rather to determine how the variety of possible structure factors for a certain given symmetry is governed by the laws of group symmetry.

The relationship between symmetry in real space on the one hand and the values and phases α in reciprocal space on the other hand are sufficiently documented and listed.^[99] However, this information does not fully meet the requirements of the PNS method. In order to receive periodic nodal surfaces of a certain symmetry, first all those $S(hkl)$ have to be excluded which are forbidden in general or with a certain phase. The application of $S(hkl)$ which in general or with a certain α belong to a supergroup of the respective targeted space group, generate a PNS with a different, higher symmetry than the one aimed at. Such $S(hkl)$, although permitted, are therefore not *characteristic*. A systematic approach to the generation of PNS therefore required the solution of the problem of *characteristic structure factors*.

3.2. Characteristic Structure Factors $S(hkl)$ of the Cubic Space Groups

3.2.1. Symmetry Patterns

In all five cubic crystal classes $m\bar{3}m - O_h$, $\bar{4}3m - T_d$, $432 - O$, $m\bar{3} - T_h$ and $23 - T$ the indices hkl of the structure factors are cyclicly permutable with constant $|S(hkl)|$ and $\alpha(hkl)$. In case of a sign change of the indices, changes of $\alpha(hkl)$ occur with unchanged

$|S(hkl)|$, which are characteristic for the respective symmetry. Acyclic permutations are permitted only for space groups with diagonal mirror planes ($|S(hkl)| = |S(khl)|$). In case of inversion centres, α is always a multiple of π ($\alpha = m\pi$) for centric setups of the inversion centre, or $\alpha = m\pi \pm \pi/2$ and $\alpha = m\pi \pm \pi/4$ for shifted origins. The crystal classes can be divided accordingly into four groups:

1. Such with inversion centre $\bar{1}$ and mirror or glide mirror planes $m, c, n \parallel \{110\}$; this is restricted to crystal class $m\bar{3}m$ with $\alpha = m\pi$ (or for shifted origins $\alpha = m\pi \pm \pi/2$ and $\alpha = m\pi \pm \pi/4$, respectively) and $|S(hkl)| = |S(khl)|$.
2. Mirror or glide mirror planes $m, c, n \parallel \{110\}$; crystal classes $\bar{4}3m$ and 432 with freely variable $\alpha(hkl) = \pm \alpha(khl)$ with $|S(hkl)| = |S(khl)|$.
3. Inversion center $\bar{1}$; crystal class $m\bar{3}$ with $\alpha = m\pi$ (or for shifted origin $\alpha = m\pi \pm \pi/2$ or $\alpha = m\pi \pm \pi/4$, respectively) and $|S(hkl)| \neq |S(khl)|$.
4. Crystal class 23 with freely variable $\alpha(hkl) \neq \alpha(khl)$ and $|S(hkl)| \neq |S(khl)|$.

An $S(hkl)$ generating a Fourier series of a certain symmetry is a *characteristic structure factor* for this symmetry: this $S(hkl)$ possesses as its *eigen symmetry* the symmetry of this space group.

An $S(hkl)$ permitted for a certain symmetry of a space group but not generating that particular symmetry itself within a Fourier series is called a *non-characteristic structure factor*. This $S(hkl)$ has as its eigen symmetry the symmetry of a supergroup of this space group.

This nomenclature is equivalent to the *characteristic* and *non-characteristic point configurations* as introduced by Wondratschek^[100] and as comprehensively deduced by Engel et al.^[101]

Even the combination of two *non-characteristic* structure factors $S(hkl)$ can, under certain circumstances, yield the desired symmetry. The reason for this is that frequently a *non-characteristic* $S(hkl)$ lacks only one feature to be *characteristic*. This missing feature can be added with a second $S(hkl)$, which in turn may lack other features required to produce the aimed-at symmetry.

Among $S(hkl)$ with missing features are those with a different Bravais lattice type (face- or body-centered). Although these structure factors otherwise have all the features necessary to produce a Fourier sum of the aimed-at symmetry, they are not characteristic. Such $S(hkl)$ are called *partly characteristic*. If adding to such a *partly characteristic* $S(hkl)$ an arbitrary, permitted structure factor which corrects the Bravais lattice type, the correct symmetry is obtained. The exclusive use of structure factors of the

types *ggg* and *uug* (*g*=gerade/even; *u*=ungerade/odd), for instance, basically leads to a body-centered cubic symmetry. The use of such structure factors for the generation of a primitive cubic symmetry therefore requires the additional use of an $S(hkl)$ of the type *ugg* or *uuu* (in case of *ugg*; *ggg+uuu* would result in a face-centered symmetry).

There is a variety of possibilities to obtain the proper symmetry by combining *non-characteristic* $S(hkl)$. This has so far not yet been thoroughly investigated, so only two examples may suffice here:

1. *Characteristic structure factors* of the crystal classes 23 and $m\bar{3}$ not only have to be formally cyclicly permutable. In addition to this, the acyclicly permuted $S(hkl)$ have to differ, which is impossible for the types *h00*, *hh0*, *hhl* and *hhh*. Hence, if taking such an $S(hkl)$, this missing feature can be added by a second *non-characteristic* of the type *hk0* or *hkl*.
2. An $S(hkl)$ which would be characteristic for a certain space group with regard to its permutations may have the same phases as those of a supergroup, which renders it *non-characteristic*. But if adding to this a second $S(hkl)$ of an arbitrary yet permitted type whose phases differ from that of the supergroup, one obtains the correct symmetry. To this case belong those examples in which acentric space groups with certain phases α yield centric supergroups with a shifted origin.

The deduction of the so-called *characteristic structure factors* can cause considerable difficulties. This will be elucidated with one example for each of the above listed cases.

1. In order to generate functions with a symmetry for which $S(hkl) \neq S(khl)$ (crystal classes $m\bar{3}$ and 23) – be that due to $\alpha(hkl) \neq \alpha(khl)$ or due to $|S(hkl)| \neq |S(khl)|$ – it is obligatory that $|h| \neq |k| \neq |l| \neq |h|$. Hence, the symmetry of these space groups without diagonal mirror operations is only obtainable with structure factors of the types $S(hk0)$ or $S(hkl)$, but not with the types *hhl* or *hhh*. Special cases exist if the aimed at space group has no supergroup whose symmetry would for instance be generated by $S(hhl)$. Hence, in $Pa\bar{3}$ (No. 205) *cP*-typical structure factors of the type $S(hhl)$ are characteristic because no translationally equivalent supergroup exists (see p. 39).
2. For the *cF* space group $F\bar{4}3m$ (No. 216) only the structure factors of the type *ggg* and *uuu* are permitted. In addition it holds: $|S(hkl)| = |S(khl)|$. The phase is unrestrained. The following results for the *hkl* permutations:

$$\alpha(hkl) = \alpha(klh) = \alpha(lhk) = -\alpha(\bar{h}\bar{k}\bar{l}) = -\alpha(\bar{h}kl) = \alpha(h\bar{k}\bar{l}) = \alpha(hk\bar{l}) = \alpha(khl)$$

Each structure factor $S(ggg)$ generates cI symmetry. Each one of them is a multiple of a type uug (cI -typical), ugg (cP -typical) or uuu (cF -typical). The type $S(ggg)$ within $F\bar{4}3m$ generates the symmetry $I\bar{4}3m$ (No. 217), as long as the structure factor is typical for this space group, which is to say: if $h, k, l \neq 0$. Otherwise the resulting symmetry is $Im\bar{3}m$ due to the \bar{I} symmetry.

Since $I\bar{4}3m$ and $F\bar{4}3m$ have the same α permutations, an $F\bar{4}3m$ symmetry can be enforced by adding any $S(uuu)$ not forbidden in $F\bar{4}3m$ to an $S(ggg)$ characteristic for $I\bar{4}3m$. Hence, these $S(ggg)$ are *partly characteristic structure* factors in $F\bar{4}3m$.

If choosing $\alpha(uuu) = m\pi$, the centric supergroup $Fm\bar{3}m$ is generated. This is generally true if $h \vee k \vee l = 0$.

Further complications arise due to such phases $\alpha \neq m\pi$ which can be attributed to centro-symmetric space groups with a shifted origin. This is true not only for the space groups $Pn\bar{3}$, $Fd\bar{3}$, $Pn\bar{3}m$, $Fd\bar{3}m$, and $Fd\bar{3}c$, for which the *International Tables* list characteristics for shifted origins, but actually for all centric space groups.

The shifts $\Delta\alpha$ which are relevant in this context are restricted to a few cases resulting from certain shifts of the origin along $[111]$, which are:

$$\Delta\alpha = m \cdot \pi/4, \text{ that is } |\sin\Delta\alpha| = |\cos\Delta\alpha| \text{ or } \sin\Delta\alpha = 0 \text{ or } \cos\Delta\alpha = 0. \quad (19)$$

These $\Delta\alpha$ are equivalent to permutations of multiples of $\pi/4$. In real space this equals shifts of $\frac{n}{8}$ along $[111]$. All other cases need not be discussed.

The phase α' of a setup shifted by $\frac{1}{n} \frac{1}{n} \frac{1}{n}$ is:

$$\alpha'_{hkl} = \alpha_{hkl} + \frac{2\pi}{n} \cdot \sum_i h_i \quad (20)$$

In case of $F\bar{4}3m$ one obtains, for instance, with $\alpha = -\pi/4$ the symmetry of $Fd\bar{3}m$ in acentric setup (origin in $\bar{4}3m$; shifted by $\frac{1}{8} \frac{1}{8} \frac{1}{8}$ against $\bar{3}m$); with $\alpha = \pi/2$, however, one obtains the symmetry of $Fm\bar{3}m$ in acentric setup (origin in $\bar{4}3m$; shifted by $\frac{1}{4} \frac{1}{4} \frac{1}{4}$ against $m\bar{3}m$), which is not listed in the *International Tables*, since it is not a standard setup.

The *intrinsic centro-symmetry* generated by $\alpha = -\pi/4$ or $\alpha = \pi/2$ can be destroyed by adding a structure factor whose permutation laws are different than those of the supergroup with the shifted origin. If, for instance, adding $S(200)$ to $S(111)$ with $\alpha = -\pi/4$, this will force a $F\bar{4}3m$ symmetry onto the function, since $S(200)$ must have a phase $\alpha = m\pi$ in $F\bar{4}3m$ (see PNS F^* (D), Table 8), whereas in $Fd\bar{3}m$ in an acentric setup it must have $\alpha = \pm\pi/2$. It would be different with $S(400)$, because for this type of factor even in $Fd\bar{3}m$

Table 2: α Permutations in $Im\bar{3}m$ with and without Phase Shift $\Delta\alpha = -\pi/4$					
$\Sigma h_i \neq 4n$; $h,k = 4n \neq l$	Centric α	Acentric α'	$\Sigma h_i = 4n$; $h,k = 4n + 2 \neq l$	centric α	acentric α'
$hkl (842)$	$m\pi$	$m\pi + \pi/2$	$hkl (642)$	$m\pi$	$m\pi + \pi$
$\bar{h}kl (\bar{8}42)$	$m\pi$	$m\pi + \pi/2$	$\bar{h}kl (\bar{6}42)$	$m\pi$	$m\pi$
$h\bar{k}l (8\bar{4}2)$	$m\pi$	$m\pi + \pi/2$	$h\bar{k}l (6\bar{4}2)$	$m\pi$	$m\pi + \pi$
$hk\bar{l} (84\bar{2})$	$m\pi$	$m\pi - \pi/2$	$hk\bar{l} (64\bar{2})$	$m\pi$	$m\pi$
$\Sigma h_i \neq 4n$; $h,k,l \neq 4n$	Centric α	Acentric $\alpha' (\triangleq I\bar{4}3m)$	same for $h,k,l = 4n$ (e.g. (12 84))		
$hkl (10\ 62)$	$m\pi$	$m\pi - \pi/2$			
$\bar{h}kl (\bar{1}0\ 62)$	$m\pi$	$m\pi + \pi/2$			
$h\bar{k}l (10\ \bar{6}2)$	$m\pi$	$m\pi + \pi/2$			
$hk\bar{l} (10\ 6\bar{2})$	$m\pi$	$m\pi + \pi/2$			

Table 3: α Permutations in $Fd\bar{3}m$; Acentric: $\Delta\alpha = -\pi/4$					
$\Sigma h_i \neq 4n$; $h,k = 4n \neq l$	centric α	acentric α' ($\triangleq I\bar{4}3m$)	$\Sigma h_i = 4n$; $h,k = 4n + 2 \neq l$	centric α	acentric α' ($\triangleq Im\bar{3}m$)
$hkl (842)$	$m\pi$	$m\pi + \pi/2$	$hkl (642)$	$m\pi + \pi$	$m\pi$
$\bar{h}kl (\bar{8}42)$	$m\pi + \pi$	$m\pi - \pi/2$	$\bar{h}kl (\bar{6}42)$	$m\pi$	$m\pi$
$h\bar{k}l (8\bar{4}2)$	$m\pi + \pi$	$m\pi - \pi/2$	$h\bar{k}l (6\bar{4}2)$	$m\pi + \pi$	$m\pi$
$hk\bar{l} (84\bar{2})$	$m\pi$	$m\pi - \pi/2$	$hk\bar{l} (64\bar{2})$	$m\pi$	$m\pi$
$\Sigma h_i \neq 4n$; $h,k,l \neq 4n$	centric α	acentric $\alpha' (\triangleq Im\bar{3}m)$	same for $h,k,l = 4n$ (e.g. (12 84))		
$hkl (10\ 62)$	$m\pi$	$m\pi - \pi/2$			
$\bar{h}kl (\bar{1}0\ 62)$	$m\pi$	$m\pi + \pi/2$			
$h\bar{k}l (10\ \bar{6}2)$	$m\pi$	$m\pi + \pi/2$			
$hk\bar{l} (10\ 6\bar{2})$	$m\pi$	$m\pi + \pi/2$			

of an acentric setup a phase $\alpha=m\pi$ is prescribed.

In order to generate an $F\bar{4}3m$ symmetry with just one structure factor, a factor type $S(uuu)$ with $\alpha \neq m\pi/4$ needs to be used. If using $S(uuu)$ with $\alpha = \pm \pi/2$ or $\alpha = m\pi \pm \pi/4$, then an additional appropriate structure factor is needed to suppress the intrinsic centro-symmetry.

When using a factor type $S(ggg)$ with $\alpha \neq \pm \pi/2$, then one has to add an $S(uuu)$ of any phase α ($\alpha=m\pi+\pi/4$ does not lead to a shift of origin for centro-symmetric cI space groups).

When using a factor type $S(ggg)$ with $\alpha = \pm \pi/2$, then several special cases must be considered, which apply accordingly to the space group $I\bar{4}3m$:

- If $h + k + l = 4n$ ($\Sigma h_i = 4n$), then the function has $I\bar{4}3m$ symmetry under any circumstance, since $\alpha=m\pi$ for all shifted or unshifted setups of the supergroup $Im\bar{3}m$ (Table 2).
- If $\Sigma h_i \neq 4n$ and also $h,k,l = 4n + 2$, then the resulting function is centro-symmetric ($Im\bar{3}m$; $[111]$ shift with $\alpha=m\pi+\pi/4$; not listed in the Int. Tables; see Table 2).

- If $\Sigma h_i \neq 4n$ and $h, k = 4n \neq l$, then centro-symmetry is obtained, although in the *cF* space group $Fd\bar{3}m$ in acentric setup, since a shift $\Delta\alpha$ in $Im\bar{3}m$ never leads to the required phase permutations (see $S(842)$, Tables 2 and 3).

The permutations of hkl and $\alpha(hkl)$ for the space group $Fd\bar{3}m$ as given by the *International Tables*^[99] are listed in Table 3 for the structure factors $S(842)$, $S(642)$ and $S(10\bar{6}2)$. If $\Sigma h_i = 4n$ or $h, k, l \neq 4n$, then the phase permutations of $S(ggg)$ of $Fd\bar{3}m$ can be achieved within $Im\bar{3}m$ by means of an appropriate origin shift $\Delta\alpha$, but not in case of $h, k = 4n \neq l$. The phase permutations of the latter factor type in acentric setup of $Fd\bar{3}m$ are identical to those in $I\bar{4}3m$ with $\alpha = m\pi \pm \pi/4$. In $Im\bar{3}m$ this factor type has different permutations of $\alpha \neq m\pi$ than $Fd\bar{3}m$ (and $I\bar{4}3m$) and in centric setup it has always $\alpha = m\pi$, in contrast to $Fd\bar{3}m$ (and $I\bar{4}3m$).

Since the phase permutation laws in case of sign changes of h, k, l for the structure factor type $S(ggg)$ are identical for both the space group $Ia\bar{3}d$ and $Im\bar{3}m$, there does not exist a centric *cI* space group with the Patterson symmetry $m\bar{3}m$ which has $Fd\bar{3}m$ -like permutation laws for an $S(ggg)$ with $h, k = 4n \neq l$. There is, however, a *cP* space group with identical permutation laws. If reducing the indices of $S(ggg)$ with $h, k = 4n \neq l$ by a factor of two, one obtains the structure factor type ugg of the supergroup of $Fd\bar{3}m$, namely $Pn\bar{3}m$.

Hence, second order structure factors $S(2u, 2g, 2g)$ of $Pn\bar{3}m$ are not *cI*- but rather *cF*-typical.

Apart from an analogous case in space group $Fd\bar{3}$, this is the only case where a factor type $S(ggg)$ is characteristic for a *cF* symmetry, which has not yet been reported as far as we know.

Hence, if using a factor of the type $S(ggg)$ with a phase $\alpha = \pm\pi/2$ in $F\bar{4}3m$, then this factor is only *partly characteristic* provided that $\Sigma h_i = 4n$, because only $S(ggg)$ of this type are *characteristic* for $I\bar{4}3m$. But just like in the case of $S(uuu)$, the symmetry of the respective shifted setup of the centro-symmetric supergroup can be cancelled by adding another structure factor.

Table 4: Permutations of $S(531)$ in $F\bar{4}3m$							
Permutation	α	Permutation	α	Permutation	α	Permutation	α
hkl (531)	$\pi/2$	$h\bar{k}l$ ($5\bar{3}1$)	$-\pi/2$	khl (351)	$\pi/2$	$k\bar{h}l$ ($3\bar{5}1$)	$-\pi/2$
lhk (153)	$\pi/2$	$l\bar{h}k$ ($1\bar{5}3$)	$-\pi/2$	lkh (135)	$\pi/2$	$l\bar{k}h$ ($1\bar{3}5$)	$-\pi/2$
klh (315)	$\pi/2$	$k\bar{l}h$ ($3\bar{1}5$)	$-\pi/2$	$h\bar{l}k$ (315)	$\pi/2$	$h\bar{l}k$ (513)	$-\pi/2$
$\bar{h}kl$ ($\bar{5}31$)	$-\pi/2$	$h\bar{k}\bar{l}$ ($53\bar{1}$)	$-\pi/2$	$\bar{k}hl$ ($\bar{3}51$)	$-\pi/2$	$k\bar{h}\bar{l}$ ($35\bar{1}$)	$-\pi/2$
$\bar{l}hk$ ($\bar{1}53$)	$-\pi/2$	$\bar{l}\bar{h}k$ ($\bar{1}\bar{5}3$)	$-\pi/2$	$\bar{l}kh$ ($\bar{1}35$)	$-\pi/2$	$\bar{l}\bar{k}h$ ($\bar{1}\bar{3}5$)	$-\pi/2$
$k\bar{l}h$ ($31\bar{5}$)	$-\pi/2$	$k\bar{l}\bar{h}$ ($3\bar{1}\bar{5}$)	$-\pi/2$	$h\bar{l}\bar{k}$ ($51\bar{3}$)	$-\pi/2$	$h\bar{l}k$ ($5\bar{1}3$)	$-\pi/2$

The required permutations of the general structure factor $S(531)$ with $\alpha = \pi/2$ are listed in Table 4. This is the first cubic structure factor (i.e., closest to the origin) which can be *characteristic* for all cF space groups.

3.2.2. Tables for $S(hkl)$ of Cubic Space Groups

The **characteristic structure factors** $S(hkl)$ of the cubic space groups are listed in Tables 5.1., 5.2. and 5.3. To each structure factor type hkl the required phase $\alpha(hkl)$ is assigned, where the symbol α denotes a freely variable phase. Although *partly characteristic* $S(hkl)$ are characteristic only for a different space group, they still follow identical permutation laws (different Bravais type). They are marked by the space group number of the characteristic space group of the correct Bravais type with an index to the phase: $\alpha_{\langle \dots \rangle}$.

If the supergroup is set up acentrically, then the phase shift $\Delta\alpha$ is a multiple n of $\pi/4$. If multiplying $n \cdot \pi/4$ with Σh_i of each hkl permutation, one obtains for it the shift $\Delta\alpha_{hkl} = n \cdot \pi/4 \cdot \Sigma h_i$ of the supergroup given in the index (see eq. (20), p. 28). This is given in the tables as $\alpha_{\langle \dots \rangle} n\Sigma$.

If $S(hkl)$ is neither prohibited nor characteristic, the space group characteristic for this $S(hkl)$ is given: $\langle \dots \rangle$. Prohibited $S(hkl)$ are given as $|S| = 0$. If the factor type is algebraically impossible, \notin is given. The type $hh0$, for instance, can be of the pattern uug only if $2h = 4n + 2$.

Following the columns with structure factor types typical for the Bravais type dealt with in each table are columns giving the characteristic space group (supergroup) when using $\alpha = m\pi$; $\alpha = m\pi \pm \pi/2$; and $\alpha = m\pi \pm \pi/4$ (the latter only for cF space groups). However, this is only relevant for the space groups without inversion center (crystal classes $\bar{4}3m$, 432, and 23). In each case the respective shifts for $\Delta\alpha$ are given.

Note: When adding an additional structure factor not possessing the characteristics of

this supergroup, its symmetry is cancelled out (see earlier)!

The lowest rows finally contain the $S(hkl)$ closest to the origin of reciprocal space for each factor type.

For this work the *characteristic structure factors* have been deduced from the literature.^[99] This method is rather error prone. It should be possible to calculate the *characteristic* $S(hkl)$ following group theoretical laws analogous to the method used by Engel.^[102] For this, his concept needs to be adapted to the laws of reciprocal space. Bienenstock and Ewald showed already in 1962 that the analytical deduction of reciprocal symmetry groups with their symmetry elements is possible.^[103] By so doing, they determined that all symmetry elements in reciprocal space have to run through the origin. In order to take into account the phase α , complex symmetry operations have to be used in reciprocal space. So far and to our knowledge, the laws governing reciprocal symmetry operations have not yet been analyzed for all space groups.^[104] Only after those have been established will it be possible to systematically and analytically determine the characteristic structure factors following Engel's approach.

Characteristic Structure Factors $S(hkl)$ Table 5.1.: cI Space Groups

It holds: $|S(hkl)| = |S(h\bar{k}l)| = |S(hk\bar{l})| = |S(h\bar{k}\bar{l})| = |S(khl)| = |S(kh\bar{l})|$; $|S(hkl)| = |S(h\bar{k}l)|$; $\alpha(hkl) = |S(hkl)|$; $\alpha(hkl) -$ relations in *Intern. Tables*, Vol. I (1976) 367-525.
 For each structure factor type the characteristic phase $\alpha(hkl)$ is given [α stands for $0 \leq \alpha(hkl) \leq 2\pi$]. If $\alpha(hkl)$ generates a different symmetry (non-characteristic $S(hkl)$), then the respective space group is given in $\langle \dots \rangle$. In case of a deviation from the standard setup, the phase shift $\Delta\alpha$ is given as a multiple n of $\pi/4$: $\langle \dots \rangle n \Sigma$, with $\Sigma = \Sigma h_i$. $S(ggg)$ merely generate multiple translations with the symmetry of the respective $S(g_2 g_2 g_2)$. Algebraically impossible structure factor types are marked with \emptyset .

Cristal class	Space Group		$ S(hkl) $ $\alpha(hkl)$	Σh_i	$h00$	$hh0$		$hk0$		hhl / hhh		hkl		$\alpha = m\pi$		$\alpha = \pm \pi/2$		Σh_i
						uug	ggg	uug	ggg	uug	ggg	uug	ggg	uug	ggg	uug	ggg	
$\bar{m}3m$ O_h	$Ia\bar{3}d$ $Im\bar{3}m$	230	$ S(hkl) = S(khl) $ $\alpha(hkl) = m\pi$	4n	$\langle 229 \rangle$	\emptyset	$\langle 229 \rangle$	$ S = 0$	$\langle 229 \rangle$	$m\pi$	$\langle 229 \rangle$	$m\pi$	$\langle 229 \rangle$	$\langle 230 \rangle$	$\langle 229 \rangle$	—	—	4n
		229		4n+2	$\langle 229 \rangle$	$ S = 0$	\emptyset	$ S = 0$	$m\pi$	$m\pi$	$ S = 0$	$\langle 229 \rangle$	$m\pi$	$\langle 230 \rangle$	$\langle 230 \rangle$	—	—	4n+2
$\bar{4}3m$ T_d	$\bar{I}43d$ $\bar{I}43m$	220		4n	$\langle 229 \rangle$	\emptyset	$\langle 229 \rangle$	$m\pi + \pi/2$	$\langle 229 \rangle$	$m\pi$	$\langle 217 \rangle$	α	$\langle 217 \rangle$	$\langle 230 \rangle$	$\langle 229 \rangle$	—	—	4n
		217	$ S(hkl) = S(khl) $ $0 \leq \alpha(hkl) \leq 2\pi$	4n+2	$ S = 0$	$ S = 0$	\emptyset	$m\pi + \pi/2$	$\langle 230 \rangle$	$ S = 0$	$\langle 217 \rangle$	α	α	$\langle 230 \rangle$	$\langle 230 \rangle$	—	—	4n+2
432 O	$I4_132$ $I432$	214		2n	$\langle 229 \rangle$	$\langle 229 \rangle$	$\langle 229 \rangle$	$\langle 229 \rangle$	$\langle 229 \rangle$	α	α	α	$\langle 229 \rangle$	$\langle 229 \rangle$	4n : $\langle 217 \rangle$ $h,k \neq 4n : \langle 229 \rangle \pm \Sigma$ $h,k = 4n \neq l : \langle 227 \rangle \pm \Sigma$	—	—	2n
		211	$ S(hkl) = S(khl) $ $0 \leq \alpha(hkl) \leq 2\pi$	4n	$\langle 229 \rangle$	\emptyset	$\langle 229 \rangle$	$m\pi + \pi/2$	$\langle 229 \rangle$	$m\pi + \pi/2$	$\langle 230 \rangle$	$\langle 229 \rangle$	α	$\langle 211 \rangle$	$\langle 230 \rangle$	—	—	4n
$\bar{m}3$ T_h	$Ia\bar{3}$ $Im\bar{3}$	206	$ S(hkl) \neq S(khl) $ $\alpha(hkl) = m\pi$	4n	$\langle 229 \rangle$	\emptyset	$\langle 229 \rangle$	$ S = 0$	$\langle 204 \rangle$	$\langle 230 \rangle$	$\langle 229 \rangle$	$m\pi$	$\langle 204 \rangle$	$\langle 206 \rangle$	$\langle 229 \rangle$	—	—	4n
		204		4n+2	$\langle 229 \rangle$	$ S = 0$	\emptyset	$ S = 0$	$\langle 204 \rangle$	$m\pi$	$\langle 229 \rangle$	$m\pi$	$\langle 204 \rangle$	$\langle 206 \rangle$	$\langle 206 \rangle$	—	—	4n+2
23 T	$I2_13$ $I23$	199		2n	$\langle 229 \rangle$	$\langle 214 \rangle$	$\langle 229 \rangle$	$m\pi$	$m\pi + \pi/2$	$\langle 204 \rangle$	$\langle 217 \rangle$	α	$\langle 197 \rangle$	$\langle 204 \rangle$	$\langle 206 \rangle$	—	—	2n
		197	$ S(hkl) \neq S(khl) $ $0 \leq \alpha(hkl) \leq 2\pi$	2n	$\langle 229 \rangle$	$\langle 229 \rangle$	$\langle 229 \rangle$	$\langle 204 \rangle$	$\langle 204 \rangle$	$\langle 204 \rangle$	$\langle 217 \rangle$	α	α	$\langle 204 \rangle$	$\langle 204 \rangle$	4n : $\langle 217 \rangle$ $h,k \neq 4n : \langle 204 \rangle \pm \Sigma$ $h,k = 4n \neq l : \langle 203 \rangle \pm \Sigma$	—	—
Closest to the origin $S(hkl)$ ($\Sigma h_i^2 = \min.$)				4n	400	\emptyset	220	310	620	112/ \emptyset	422/444	314	642					
				4n+2	200	110	\emptyset	510	420	114/ \emptyset	622/222	312	842					

Characteristic Structure Factors $S(hkl)$

Table 5.2.: cF Space Groups													
It holds: $ S(hkl) = S(hkh) = S(khl) : S(hkl) = S(h\bar{k}l) = S(hk\bar{l}) $; $\alpha(hkl)$ -relations in <i>Intern. Tables</i> , Vol. I (1976) 367-525.													
For each structure factor type the characteristic phase $\alpha(hkl)$ is given [α stands for $0 \leq \alpha(hkl) \leq 2\pi$]. If $\alpha(hkl)$ generates a different symmetry (non-characteristic $S(hkl)$), then the respective spacegroup is given in (...). For partly characteristic factors $S(ggg)$ with a corresponding cI space group, its number is given in an index to α . In case of a deviation from the standard setup, the phase shift $\Delta\alpha$ is given as a multiple n of $\pi/4$: $\langle \dots \rangle n \Sigma$, with $\Sigma = \Sigma h_i$. Algebraically impossible structure factor types are marked with \emptyset . For $Fd\bar{3}m$, $Fd\bar{3}c$ and $Fd\bar{3}$ the centro-symmetric setup is used (choice 2).													
Cristal Class	Space Group	$ S(hkl) $	Structure Factor Types uuu					Structure Factor Types ggg, cI Type					Σh_i
			hkl	$\alpha = m\pi$	$\alpha = \pm \pi/2$	$\alpha = m\pi \pm \pi/4$	$h00$	$hh0$	$hk0$	hhh / hhl	hkl		
$m\bar{3}m$ O_h	$Fd\bar{3}c$	228	\emptyset	\emptyset	\emptyset	\emptyset	$\langle 229 \rangle$	$\langle 227 \rangle$	$\langle 227 \rangle$	$\langle 227 \rangle$	$\langle 227 \rangle$	$4n$	
			$ S = 0$	$m\pi$	\emptyset	\emptyset	$ S = 0$	$ S = 0$	$ S = 0$	$ S = 0$	$\langle 227 \rangle$	$\neq 4n$	
	$Fd\bar{3}m$	227	$ S(hkl) = S(khl) $ $\alpha(hkl) = m\pi$	\emptyset	\emptyset	\emptyset	$\langle 229 \rangle$	$h, k = 4n: \langle 229 \rangle$ $h, k \neq 4n: m\pi_{(229)} \bar{\Sigma}$	$h, k, l = 4n: \langle 229 \rangle$ $h, k \neq 4n = l: m\pi_{(229)} \bar{\Sigma}$	$\langle 229 \rangle$	$4n$		
			$m\pi$	$m\pi$	\emptyset	$ S = 0$	$ S = 0$	$ S = 0$	$h, k, l \neq 4n: \langle 229 \rangle$ $h, k = 4n \neq l: m\pi$	$\langle 229 \rangle$	$\neq 4n$		
			$ S = 0$	$m\pi$	\emptyset	$ S = 0$	$\langle 229 \rangle$	$\langle 229 \rangle$	$\langle 229 \rangle$	$\langle 229 \rangle$	n		
$\bar{4}3m$ T_d	$Fm\bar{3}c$	226	$m\pi$	\emptyset	\emptyset	\emptyset	$m\pi_{(229)}$	$m\pi_{(229)}$	$m\pi_{(229)}$	$m\pi_{(229)}$	n		
	$Fm\bar{3}m$	225	$ S = 0$	α	$\langle 226 \rangle \pm 2\Sigma$	$\langle 228 \rangle \pm 3 \Sigma$	$\langle 229 \rangle$	$\langle 229 \rangle$	$\langle 217 \rangle$	$\langle 217 \rangle$	n		
432 O	$F\bar{4}3c$	219	$ S(hkl) = S(khl) $	α	$\langle 226 \rangle \pm 2\Sigma$	$\langle 228 \rangle \pm 3 \Sigma$	$\langle 229 \rangle$	$\langle 229 \rangle$	$\langle 217 \rangle$	$\langle 217 \rangle$	n		
	$F\bar{4}3m$	216	$0 \leq \alpha(hkl) \leq 2\pi$	α	$\langle 225 \rangle \pm 2\Sigma$	$\langle 227 \rangle \pm \Sigma$	$\langle 229 \rangle$	$\langle 229 \rangle$	$\alpha_{(217)}$	$\alpha_{(217)}$	n		
	$F4_132$	210	$ S(hkl) = S(khl) $ $0 \leq \alpha(hkl) \leq 2\pi$	α	$\langle 226 \rangle$	$\langle 210 \rangle$	$\langle 214 \rangle$	$\langle 214 \rangle$	$\langle 214 \rangle$	$4n: \langle 211 \rangle$ $4n+2: \alpha_{(214)}$	n		
$m\bar{3}$ T_h	$F432$	209	$ S(hkl) \neq S(khl) $ $0 \leq \alpha(hkl) \leq 2\pi$	α	$\langle 226 \rangle \pm 2\Sigma$	\emptyset	$\langle 229 \rangle$	$\langle 229 \rangle$	$\langle 229 \rangle$	$\alpha_{(211)}$	n		
	$Fd\bar{3}$	203	$ S(hkl) \neq S(khl) $ $\alpha(hkl) = m\pi$	\emptyset	\emptyset	\emptyset	$\langle 229 \rangle$	$\langle 227 \rangle$	$h, k = 4n: \langle 204 \rangle$ $h, k \neq 4n: m\pi_{(204)} \bar{\Sigma}$	$h, k, l = 4n: \langle 204 \rangle$ $h, k \neq 4n = l: m\pi_{(204)} \bar{\Sigma}$	$4n$		
	$Fm\bar{3}$	202	$ S(hkl) \neq S(khl) $ $\alpha(hkl) = m\pi$	$m\pi$	\emptyset	\emptyset	$ S = 0$	$ S = 0$	$\langle 227 \rangle$	$h, k, l \neq 4n: \langle 204 \rangle$ $h, k = 4n \neq l: m\pi$	$\neq 4n$		
23 T	$F\bar{m}\bar{3}$	202	$ S(hkl) \neq S(khl) $ $0 \leq \alpha(hkl) \leq 2\pi$	$m\pi$	\emptyset	\emptyset	$\langle 203 \rangle \pm \Sigma$	$\langle 229 \rangle$	$m\pi_{(204)}$	$m\pi_{(204)}$	n		
	$F23$	196	$ S(hkl) \neq S(khl) $ $0 \leq \alpha(hkl) \leq 2\pi$	α	$\langle 202 \rangle \pm 2\Sigma$	\emptyset	\emptyset	$\langle 229 \rangle$	$\langle 202 \rangle$	$\langle 217 \rangle$	n		
		Closest to the origin $S(hkl)$ ($\Sigma h_i^2 = \min.$)	\emptyset	\emptyset								$4n$	
			113	531								$4n+1$	
			\emptyset	\emptyset								$4n+2$	
			111	731								$4n+3$	
													$4n+3$

Characteristic Structure Factors $S(hkl)$ Table 5.3.: cP Space Groups

It holds: $|S(hkl)| = |S(h\bar{k}l)| = |S(khl)| : |S(hkl)| = |S(h\bar{k}l)| = |S(hkl)|$; $\alpha(hkl)$ relations in Intern. Tables, Vol. I (1976) 367-525. For each structure factor type the characteristic phase $\alpha(hkl)$ is given [α stands for $0 \leq \alpha(hkl) \leq 2\pi$]. If $\alpha(hkl)$ generates a different symmetry (non-characteristic $S(hkl)$), then the respective spacegroup is given in (...). The partly characteristic $S(ggg)$ as well as $S(uug)$ and $S(uuu)$, respectively, belong to the corresponding cI and cF groups, respectively, whose numbers are given in an index to α . $S(hkl)$ of cI and cF factor types not listed behave as those in the corresponding cI and cF space groups of the general structure factor type hkl (Tab. 5.1. and 5.2.). In case of a deviation from the standard setup, the phase shift $\Delta\alpha$ is given as a multiple n of $\pi/4$; (...) n Σ , with $\Sigma = \Sigma h_i$. For $Pn\bar{3}m$, $Pn\bar{3}n$ and $Pn\bar{3}$ the centro-symmetric setup is used (choice 2).

Crystal class	Space Group		$ S(hkl) $ $\alpha(hkl)$	$\Sigma h_i = 2n+1, cP$ typical $S(ugg)$								cF type	$\Sigma h_i = 2n, cI$ type	
	Symbol	No.		$h00$ ugg	$hk0$ ugg	hhl ggu	hkl ugg	$\alpha = m\pi$ ugg	$\alpha = \pm \pi/2$ ugg	hkl uuu	uug		hkl ggg	
$\bar{m}\bar{3}m$	$Pn\bar{3}m$	224	$ S(hkl) = S(khl) $ $\alpha(hkl) = m\pi$	$ S = 0$	$ S = 0$	$m\pi$	$m\pi$	$\langle 224 \rangle$	—	$\langle 225 \rangle$	$m\pi_{(229)}$	$\langle 229 \rangle$		
	$Pm\bar{3}n$	223		$ S = 0$	$m\pi$	$ S = 0$	$m\pi$	$\langle 223 \rangle$	—	$m\pi_{(226)}$	$\langle 229 \rangle$	$\langle 229 \rangle$		
	$Pn\bar{3}n$	222		$ S = 0$	$ S = 0$	$ S = 0$	$m\pi$	$\langle 222 \rangle$	—	$\langle 226 \rangle$	$\langle 224 \rangle$	$\langle 229 \rangle$		
O_h	$Pm\bar{3}m$	221	$ S(hkl) = S(khl) $ $0 \leq \alpha(hkl) \leq 2\pi$	$m\pi$	$m\pi$	$m\pi$	$m\pi$	$\langle 221 \rangle$	—	$m\pi_{(225)}$	$m\pi_{(229)}$	$m\pi_{(229)}$		
	$P4_3n$	218		$ S = 0$	$\langle 223 \rangle$	$ S = 0$	α	$\langle 223 \rangle$	$\langle 222 \rangle \pm 2\Sigma$	$\alpha_{(219)}$	$\langle 217 \rangle$	$\langle 217 \rangle$		
	$P4_3m$	215		$\langle 221 \rangle$	$\langle 221 \rangle$	α	α	$\langle 221 \rangle$	$\langle 224 \rangle \pm 2\Sigma$	$\alpha_{(216)}$	$\alpha_{(217)}$	$\alpha_{(217)}$		
432	$P4_32$	213	$ S(hkl) = S(khl) $ $0 \leq \alpha(hkl) \leq 2\pi$	$ S = 0$	uug: $m\pi + \pi/2$ gug: $m\pi$	α	α	$\langle 213 \rangle$ $hhl: \langle 205 \rangle$	$\langle 213 \rangle$	$\alpha_{(210)}$	$\alpha_{(214)}$	$\alpha_{(214)}$		
	$P4_32$	212		as 213								as 213	as 213	
	$P4_32$	208		$ S = 0$		$\langle 215 \rangle$	α	$\langle 223 \rangle$	$\langle 224 \rangle \pm 2\Sigma$	$\langle 209 \rangle$	$\langle 211 \rangle$	$\langle 211 \rangle$		
$\bar{m}\bar{3}$	$P4_32$	207	$ S(hkl) \neq S(khl) $ $\alpha(hkl) = m\pi$	$\langle 221 \rangle$	$\langle 223 \rangle$	$\langle 215 \rangle$	α	$\langle 223 \rangle$	$\langle 222 \rangle \pm 2\Sigma$	$\alpha_{(209)}$	$\alpha_{(211)}$	$\alpha_{(211)}$		
	$Pa\bar{3}$	205		$ S = 0$	$m\pi$	$m\pi$	$m\pi$	$\langle 205 \rangle$	—	$\langle 202 \rangle$	$m\pi_{(206)}$	$\langle 204 \rangle$		
	$Pn\bar{3}$	201		$ S = 0$	$ S = 0$	$\langle 224 \rangle$	$m\pi$	$\langle 201 \rangle$	—	$\langle 202 \rangle$	$m\pi_{(204)}$	$\langle 204 \rangle$		
T_h	$Pm\bar{3}$	200	$ S(hkl) \neq S(khl) $ $0 \leq \alpha(hkl) \leq 2\pi$	$\langle 221 \rangle$	$m\pi$	$\langle 221 \rangle$	$m\pi$	$\langle 200 \rangle$	—	$m\pi_{(202)}$	$m\pi_{(204)}$	$m\pi_{(204)}$		
	$P2_13$	198		$ S = 0$	$\langle 205 \rangle$	$\langle 213 \rangle$	α	$\langle 205 \rangle$	$\langle 198 \rangle$	$\langle 196 \rangle$	$\alpha_{(199)}$	$\langle 197 \rangle$		
	$P23$	195		$\langle 221 \rangle$	$\langle 200 \rangle$	$\langle 215 \rangle$	α	$\langle 200 \rangle$	$\langle 201 \rangle \pm 2\Sigma$	$\alpha_{(196)}$	$\alpha_{(197)}$	$\alpha_{(197)}$		
Closest to the origin: $S(hkl)$ ($\Sigma h_i^2 = \min.$)			100	120	221	142	Tab. 5.2.						Tab. 5.1.	

Table 6.1.: Characteristic Structure Factors $S(hkl)$ of the cI Space Groups

characteristic : ● ; non-characteristic: ▽ ; extinguished: empty box.																														
SG (No.)	hkl	110	200	211	220	310	222	321	400	330	411	420	332	422	431	510	521	440	433	530	442	600	532	611	620	541	622	631	444	543
Ia3d (230)		▽	●	●	▽	▽	▽	●	▽	▽		●	●	▽	●		●	▽	▽		▽	▽	●	●	▽	●	▽	●	▽	●
Im3m (229)	●	●	●	●	●	●	●	●	●	●	●	●	●	●	●	●	●	●	●	●	●	●	●	●	●	●	●	●	●	●
I43d (220)			●	▽	▽	●		●	▽			▽	●	▽	●	●		▽		●			●	▽	●			▽	●	
I43m (217)	▽	▽	●	●	▽	▽	●	●	▽	▽	●	▽	●	●	●	▽	●	▽	▽	▽	●	▽	●	●	▽	●	●	▽	●	●
I4132 (214)	●		▽	▽	▽	●	▽	●	▽	●	●	▽	▽	▽	●	▽	●	▽	▽	●	▽			▽	▽	▽	▽	▽	▽	●
I432 (211)	▽	▽	▽	▽	▽	▽	▽	▽	▽	▽	▽	▽	▽	▽	●	▽	●	▽	▽	▽	▽	▽	●	▽	▽	▽	▽	▽	▽	●
Ia3 (206)		▽	▽	▽	▽		▽	●	▽		●	▽	▽	▽	●		●	▽	●		▽	▽	●	▽	▽	▽	▽	▽	▽	●
Im3 (204)	▽	▽	▽	▽	▽	●	▽	●	▽	▽	▽	●	▽	▽	●	●	●	▽	▽	●	▽	▽	●	▽	●	▽	▽	▽	▽	●
I213 (199)	▽	▽	▽	▽	▽	●	▽	●	▽	▽	▽	▽	▽	▽	●	●	●	▽	▽	●	▽	▽	●	▽	▽	▽	▽	▽	▽	●
I23 (197)	▽	▽	▽	▽	▽	▽	▽	●	▽	▽	▽	▽	▽	▽	●	▽	●	▽	▽	▽	▽	▽	●	▽	▽	▽	▽	▽	▽	●

Table 6.2.: Characteristic Structure Factors $S(hkl)$ of the cF Space Groups

characteristic : ● ; partly characteristic (different Bravais type: ○ ; non-characteristic: ▽ ; extinguished: empty box.																															
SG (No.)	hkl	111	200	220	311	222	400	331	420	422	333	511	440	531	442	600	620	533	622	444	551	711	640	642	553	731	800	733	644	820	
Fd3c (228)				▽		▽	▽			▽			▽	●	▽		▽		▽	▽				▽		●	▽			▽	
Fd3m (227)	●		○		●	▽	▽	●		○	●	●	▽	●	●		○		●	▽	●	●		○	●	●	▽	●		○	
Fm3c (226)			▽	▽		▽	▽		▽	▽			▽	●	▽	▽	▽		▽	▽			▽	▽		●	▽		▽	▽	
Fm3m (225)	●		○	○	●	○	○	●	○	○	●		○	●	○	○	○	○	○	○	●	●	○	○	●	○	○	●	○	○	
F43c (219)			▽	▽		▽	▽		▽	▽			▽	▽	▽	▽	▽		▽	▽			▽	▽		●	▽		▽	▽	
F43m (216)	●		▽	▽	●	○	▽	●	▽	○	●	●	▽	▽	○	▽	▽	●	○	○	●	●	▽	○	●	▽	●	○	○	▽	
F432 (210)	▽		▽	▽	▽	▽	▽	▽	▽	▽	▽	▽	▽	●	▽		▽	▽	▽	▽	▽	▽	▽	▽	▽	●	▽	▽	▽	▽	
F432 (209)	▽		▽	▽	▽	▽	▽	▽	▽	▽	▽	▽	▽	●	▽	▽	▽	▽	▽	▽	▽	▽	▽	▽	▽	●	▽	▽	▽	▽	
Fd3 (203)	▽			▽	▽	▽	▽	▽		▽	▽	▽	▽	●	▽		○	▽	▽	▽	▽	▽		○	▽	●	▽	▽	▽	▽	
Fm3 (202)	▽	▽	▽	▽	▽	▽	▽	▽	○	▽	▽	▽	▽	●	▽	▽	▽	▽	▽	▽	▽	▽	○	○	▽	●	▽	▽	▽	○	
F2 (196)	▽	▽	▽	▽	▽	▽	▽	▽	▽	▽	▽	▽	▽	●	▽	▽	▽	▽	▽	▽	▽	▽	▽	▽	▽	●	▽	▽	▽	▽	

Table 6.3.: Characteristic Structure Factors $S(hkl)$ of the cP Space Groups																																
characteristic : \bullet ; partly characteristic (different Bravais type: \circ ; non-characteristic: ∇ ; extinguished: empty box.																																
SG (No.)	hkl	100	110	111	200	210	211	220	221	300	310	311	222	320	321	400	322	410	330	411	331	420	421	332	422	430	500	431	510	333		
$Pn\bar{3}m$ (224)		\circ	∇	∇	∇	\circ	∇	∇	\bullet		\circ	∇	∇		\circ	∇	\bullet		\circ	∇	∇	\bullet	\circ	∇	∇		\circ	\circ	∇			
$Pm\bar{3}n$ (223)		∇		∇	∇	\bullet	∇	∇			∇		∇	\bullet	∇	∇		\bullet	∇			\bullet	∇	∇	\bullet		∇	∇	∇			
$Pn\bar{3}n$ (222)		∇	∇	∇	∇		∇	∇			∇	∇	∇		∇	∇			∇	∇	∇	\bullet	∇	∇			∇	∇	∇			
$Pm\bar{3}m$ (221)	\bullet	\circ	\circ	\circ	\circ	\bullet	\circ	\circ	\bullet	\bullet	\circ	\circ	\circ	\bullet	\circ	\circ	\bullet	\bullet	\circ	\circ	\circ	\bullet	\circ	\circ	\bullet	\bullet	\circ	\circ	\circ			
$P43n$ (218)		∇		∇	∇	∇	∇	∇			∇		∇	∇	∇	∇		∇	∇			\bullet	∇	∇	∇		∇	∇	∇			
$P43m$ (215)	∇	∇	\circ	∇	∇	∇	\circ	∇	\bullet	∇	∇	\circ	\circ	∇	\circ	∇	\bullet	∇	∇	\circ	∇	\bullet	\circ	\circ	∇	∇	\circ	∇	\circ			
$P4_32$ (213)		\circ	∇			\bullet	∇	∇	\bullet		\circ	∇	∇	\bullet	\circ	∇	\bullet	\bullet	\circ	\circ	∇	\bullet	∇	∇	\bullet		\circ	\circ	∇			
$P4_32$ (212)	\circ	∇		∇		\bullet	∇	∇	\bullet	\bullet	\circ	∇	∇	\bullet	\circ	∇	\bullet	\bullet	\circ	\circ	∇	\bullet	∇	∇	\bullet		\circ	\circ	∇			
$P4_32$ (208)		∇	∇	∇	∇	∇	∇	∇	∇		∇	∇	∇	∇	∇	∇	∇	∇	∇	∇	∇	\bullet	∇	∇	∇		∇	∇	∇			
$P432$ (207)	∇	∇	∇	∇	∇	∇	∇	∇	∇	∇	∇	∇	∇	∇	\circ	∇	∇	∇	∇	∇	∇	\bullet	∇	∇	∇	∇	\circ	∇	∇			
$Pa\bar{3}$ (205)			∇	∇	∇	\bullet	∇	∇	\bullet	\bullet		∇	∇	\bullet	\circ	∇	\bullet	\bullet		\circ	∇	\bullet	∇	∇	\bullet		\circ		∇			
$Pn\bar{3}$ (201)			∇	∇	∇		∇	∇	∇		\circ	∇	∇		\circ	∇	∇		∇	∇	∇	\bullet	∇	∇			\circ	∇	∇			
$Pm\bar{3}$ (200)	∇	∇	∇	∇	∇	\bullet	∇	∇	∇	∇	\circ	∇	∇	\bullet	\circ	∇	∇	\bullet	∇	∇	∇	\bullet	∇	∇	∇	∇	\circ	\circ	∇			
$P2_13$ (198)		∇	∇	∇	∇	∇	∇	∇	∇		\circ	∇	∇	∇	\circ	∇	∇	∇	∇	∇	∇	\bullet	∇	∇			\circ	\circ	∇			
$P23$ (195)	∇	∇	∇	∇	∇	∇	∇	∇	∇	∇	∇	∇	∇	∇	\circ	∇	∇	∇	∇	∇	∇	\bullet	∇	∇	∇	∇	\circ	\circ	∇			

3.2.3. Application of the Tables

From Tables 5.1. to 5.3. it can be gleaned which structure factors $S(hkl)$ are required for the generation of a Fourier sum of a desired symmetry and which ones are permitted without generating the desired symmetry. Apart from the prohibited and hence excluded $S(hkl)$, the (*partly*) *characteristic* $S(hkl)$ are of central importance. In principle, this rendering of the symmetry laws corresponds to what is intrinsically included in the International Tables.^[99]

Tables 6.1. to 6.3. (pp. 36f.) give the 29 $S(hkl)$ closest to the origin of reciprocal space for all three cubic Bravais types and all cubic space groups. Together with the non-prohibited, not characteristic $S(hkl)$, this sets the frame within which Fourier series with the desired symmetry of the cubic space groups can be generated. For several space groups with far-reaching restrictions, only a few $S(hkl)$ close to the origin exist with which the targeted symmetry can be generated. Particularly cF as well as in general space groups with a low symmetry are affected by this. The number of characteristic structure factors close to the origin is approximately correlated to the number of point configurations characteristic for this space group. Thus the space group $Pn\bar{3}n$ (No. 222), for instance, has only one specific point configuration: position 48i.^[101,105] In addition, the high multiplicity of 48 requires high indices of the descriptive Fourier coefficients. Table 6.3. (p. 37) therefore yields as the first characteristic structure factor for this space group one with relatively high indices $S(421)$.

The application of the tables will be demonstrated in the following:

Wanted are the conditions to generate a Fourier series $f(r)$ with the symmetry $P4_132$ (No. 213). Since $P4_132$ belongs to the cP space groups and to crystal class $432 - O$, we refer to Table 5.3. Since structure factors with $\Sigma h_i = 2n$ automatically lead to a cI space group, this is given as an index to $\alpha(\alpha_{214}; I4_132)$. If adding a structure factor with $\Sigma h_i = 2n + 1$ to the Fourier series, this immediately leads to the desired symmetry $P4_132$. – with one exception: combinations of $S(ggg)$ and $S(uuu)$ lead to $F4_132$.

If choosing *non-characteristic* $S(hkl)$, such simple corrections do not suffice. For example, if picking a structure factor type $\Sigma h_i = 2n$ within $P\bar{4}3n$ (No. 218), this leads to $I\bar{4}3m$ (No. 217), whose permutation laws are *non-characteristic* for $P\bar{4}3n$. In this case one has to add at least one *partly characteristic structure factor* with $\Sigma h_i = 2n + 1$. For a cI -typical $S(uug)$ this would for instance have to be an $S(uuu)$, which is *characteristic*

for $F\bar{4}3c$ (No. 219).

For $P4_132$ only the factor types $S(hkl)$ and $S(hhl)$ in general as well as $S(hk0)$ of the pattern ugg and with a fixed α ($\alpha = m\pi \pm \pi/2$ for ugg ; $\alpha = m\pi$ for gug) are *characteristic* without restrictions. Since no centric space group of the same permutation laws exists due to the unique permutations of the phase of $S(hkl)$ with $h \neq k \neq l$, $S(hkl)$ remains a *characteristic structure factor* even if $\alpha = m\pi$. Only if $h=k$ ($S(hhl)$), then $\alpha=m\pi$ leads to $Pa\bar{3}$ (No. 205). The two space groups $P4_132$ and $P4_332$ are an exception because only in these space groups does $\alpha=m\pi$ not necessarily lead to an inversion center. This peculiarity results from the screw axes 4_1 and 4_3 , respectively, which are typical exclusively for those two enantiomorphic space groups.

The space groups $Pa\bar{3}$ (No. 205) and $Ia\bar{3}$ (No. 206) are similar exceptions, as they lack mirror operations $\parallel \{110\}$: $|S(hkl)| \neq |S(khl)|$. Yet despite the fact that structure factors of the types $S(hhl)$, $S(hh0)$, and $S(hhh)$ can be acyclicly permuted only formally, they nevertheless do **not** ($Pa\bar{3}$) or only in **special** cases ($Ia\bar{3}$) lead to different space groups. This stands in contrast to the space groups in the crystal classes $m\bar{3} - T_h$ and $23 - T$, where those factor types do not produce symmetries of these classes. In $Pa\bar{3}$ this exception is caused by the glide mirror plane, which exists only in this cP space group. In $Ia\bar{3}$ this special case is restricted to factors of the type $S(hhl)$ with $\Sigma h_i = 4n + 2$, which are missing in the supergroup $Ia\bar{3}d$ due to the d glide mirror plane.

As mentioned above, acentric space groups have permitted structure factors with $\alpha=m\pi$. Their centro-symmetry can be cancelled with any $S(hkl)$ with a free α . Hence the combination of the *non-characteristic* cP structure factor of the type $hk0$ in $P\bar{4}3n$, for example, together with any *non-characteristic* cI structure factor with freely variable α yields the proper symmetry, since the latter cancels the centro-symmetry. The same is true for $S(hkl)$ of this type in $P432$, $P2_13$, and $P23$ in combination with any *non-characteristic* cP - $S(hkl)$ of the type hhl . Analogously, one can generate the symmetry of $I23$ (No. 197) by combining an $S(hkl)$ of the type $hk0$ with an $S(hkl)$ of the type hhl or hhh .

Another variation exists, for instance, in $I4_132$ (No. 214) for the *non-characteristic* $S(hk0)$ of the pattern ggg with $\Sigma h_i = 4n + 2$ or for $S(hhl)$ of the pattern uug with $\Sigma h_i = 4n$ and with $\alpha = m\pi$. These two types are *characteristic* for the centro-symmetric supergroup $Ia\bar{3}d$ (No. 230). One obtains the symmetry $I4_132$ only if adding an $S(hkl)$ with freely variable α differing from $I\bar{4}3d$ (No. 220). This is successful even when choosing certain *non-characteristic* factor types with free α ($hhh = ggg$ with

$\Sigma h_i = 4n + 2$ and $hkl = ggg$ with $\Sigma h_i = 4n$).

As mentioned earlier, the fact that a *non-characteristic structure factor* is merely formally acyclicly permutable can be corrected with a second factor. For instance, the symmetry $I2_13$ (No. 199) can be generated with the *non-characteristic* $S(hhl)$ or $S(hh0)$

of the pattern uug with $\Sigma h_i = 4n + 2$ (*characteristic* for $I4_132$) by adding an equally *non-characteristic* factor $S(hk0)$ or $S(hkl)$ of the pattern ggg . The first two structure factors have freely variable phases of the correct permutations (recognizable by way of the supergroup $I4_132$), but the indices can be permuted only formally in an acyclic way. This is corrected by the latter two centro-symmetric factor types obeying different permutation laws

Table 7: **Some Combinations of two $S(hkl)$ Close to the Origin of the Space Group $I\bar{4}3d$**

$I\bar{4}3d$	●211	●310	●321	$\nabla 220$	$\nabla 400$
●211	α	α	α	α	α
●310	α	α	α	α	α
●321	α	α	α	α	α
$\nabla 220$	α	α	α	$\langle 229 \rangle$	$\langle 229 \rangle$
$\nabla 400$	α	α	α	$\langle 229 \rangle$	$\langle 229 \rangle$

3.3. Periodic Nodal Surfaces PNS with Cubic Symmetry

3.3.1. Calculations

The data contained in Tables 6.1. to 6.3. permit the direct generation of all Fourier series based only on one *characteristic* $S(hkl)$. Together with the *non-characteristic* $S(hkl)$ from Tables 5.1. to 5.3. we compiled tables in order to determine all possible combinations of two structure factors – both characteristic and non-characteristic $S(hkl)$. Table 7 gives an example of such a table for the space group $I\bar{4}3d$, where characteristic $S(hkl)$ are marked with a ● and non-characteristic factors with ∇ . In this case the combination of two non-characteristic factors never yields the desired symmetry but rather the space group $Im\bar{3}m$ (No. 229). In addition to this, the phase α can be varied for those factors with freely variable α (acentric space groups, whereas it has to be $\alpha = m\pi$ for the centro-symmetric space groups (crystal classes $m\bar{3}m - O_h$ and 432 – O). In case of acentric space groups we limited α to values of $n\cdot\pi/4$. Due to the multitude of possible combinations, only those combinations were tried where nodal surfaces had not yet been discovered or where additional alternatives were desired or expected.

For the computational generation, depiction, and analysis of the periodic nodal surfaces and their generating functions we used various FORTRAN77 programs running on a SUN GX4000 workstation, some of which had already been used for previous

work and which have been expanded, rewritten, and complemented with newly programmed subroutines.^[106] The programs for the calculation of the nodal surfaces themselves are based on earlier works by v. Schnering.^[89,90]

3.3.2. Nomenclature

The nomenclature used for zero-potential surfaces originating from the potential method^[39] has also been used, with a few minor changes, for naming PNS. For this, the point configurations (*PC*) are given where the formal charges have been placed which generate the zero-potential surface. If, for instance, the special position 4e (*PC* F) in $Fm\bar{3}m$ (No. 225) has been occupied with the formal charge of $q=+3$ and the special position 4b with $q=-1$ as well as position 8e equally with $q=-1$ (*PC* $\frac{1}{2}\frac{1}{2}\frac{1}{2}$ F and $\frac{1}{4}\frac{1}{4}\frac{1}{4}$ P₂), then the thusly generated zero-potential surface has been called F – FP₂. The hyphen separates the point configurations of opposite charges. If the point configurations of opposite charges are commutative, the generated surface will be of the *cI* type. In such cases only one of the identical sets of *PC*s is given, marked with a star. If a point configuration occurs more than once, this is denoted by an exponent. Hence, the name of the POPS contains a large part of the information necessary to generate them. The use of the names derived from POPS for morphologically similar PNS, as introduced by Oehme, comes to an impasse where novel surfaces are generated which have no connection to any hitherto known POPS. However, if considering that the positions of the formal charges of the potential methods are at once extreme values of the potential, this concept can be transferred to extrema. But since most of the functions used here can be depicted merely implicitly, i.e., they are inaccessible to algebraic analysis, their extrema can be determined only numerically—iteratively. The extreme values of PNS determined this way exhibit several peculiarities, which will be investigated separately in chapter 4.2. To give just one example: some of the extrema are not certain point configurations but rather line segment configurations,^[62] meaning that the extrema have constant values along a defined line. The number of configurations of extrema can furthermore be so numerous that this kind of “extrema nomenclature” becomes unwieldy. Finally, this *PC* nomenclature can lead to identical names for surfaces with different symmetries. This fact has already been observed for POPS (see PNS (PJ)* from space groups No. 221 or No. 215, Ill. 4.a and 5.b, pp. 60 and 62). A rigorous nomenclature of the PNS

following this *PC* method has led to a change in names (see Table 8) as compared to those used in various publications,^[60-62] since in the latter cases the names had simply been transferred from POPS with a strong morphological resemblance. In most cases, however, PNS have a different distribution of extrema than analogous POPS.

The inadequacies of the “extrema nomenclature” as well as its missing relation to the generation of periodic nodal surfaces gave rise to the development of a separate nomenclature for PNS containing as much information as necessary to generate the surface thusly named. A complete set of information requires the generating space group, the *hkl* used, the phases α , and, in case multiple factors are used, the relative contribution of each factor. The structure factor indices $(hkl)_i$, surrounded by parentheses, obtain a phase α_i as an exponent, in case it deviates from 0. The amount of the factor $|S_i|$ is set as an index in case it deviates from 1. The *hkl* are set apart from one another with a semi-colon or comma, and the whole lot is surrounded by angle brackets, which have as a pre-exponent the number of the generating space group *gSG*. If the eigen symmetry of the generated surface differs from the symmetry of the generating function, then the number of this space group *eSG* appears as a post-exponent at the end of the name:⁷

$${}^{gSG}\langle (hkl)_{i|S_i|}^{\alpha_i} (hkl)_{j|S_j|}^{\alpha_j}, \dots \rangle^{eSG} \quad (21)$$

By giving the generating space group, the permutation laws of the structure factors are defined as well as for the respective phases α . Hence the function is defined unequivocally. Since these names contain only numbers, this “generator nomenclature” is not easy to use in day-to-day conversation. We therefore continued the nomenclature of the old methods (extrema nomenclature derived from POPS and “trivial names” from minimal surfaces) in the following tables and in the text in order to facilitate references to these other methods. The new nomenclature is used in the subsequent text and for illustrations so that the generating functions are immediately recognizable.⁸

3.3.3. Tables

Table 8 gives the main characteristics of several PNS generated during the studies leading to the present work. Column 1 contains the systematic name of the PNS follow-

⁷ Although developed in 1992 during research for the present work, later publications used a slightly modified nomenclature for PNS, with the position of phase and factor value swapped, see e.g.: A. Zürn, PhD Thesis, University of Stuttgart, 1998, p. 28.

⁸ See footnote 5 on p. 17.

ing the extrema nomenclature (see above). Columns 2 to 4 contain in this order the hkl , the relative structure factor values $|S|$, and their phases α of the generating Fourier series. Column 4 contains the space group of the generating Fourier series, column 5 the implicit trigonometric function of the PNS (deducted with the help of ^[99]). Column 6 contains the space group of the generated PNS, which in case of black-white symmetry (identical partial spaces) is a supergroup of the generating space group. Column 7 contains the extrema of the generating Fourier series with function values and point configurations equivalent to the extrema, which defines the name of the PNS according to the “extrema nomenclature”. The subsequent chapter contains illustrations for each of these nodal surfaces.

Table 8.: Data of some 3D Periodic Nodal Surfaces ($|S|$ = structure factor amplitude, α = phase angle, PC = point configuration)

name	hkl	$ S $	α	generating space group	$f(X, Y, Z) = 0$ with $X=2\pi \cdot x$, $Y=2\pi \cdot y$, $Z=2\pi \cdot z$	eigen symmetry of surface	extrema of $f(x, y, z)$ Wyckoff positions and values	PC
$I_2 - Y^{**}V^*$	211 220	1 1	0 0	$Ia\bar{3}d$	$-2 \cdot [\sin 2X \cdot \cos Y \cdot \sin Z + \sin X \cdot \sin 2Y \cdot \cos Z + \cos X \cdot \sin Y \cdot \sin 2Z]$ $+ \cos 2X \cdot \cos 2Y + \cos 2Y \cdot \cos 2Z + \cos 2X \cdot \cos 2Z = 0$	$Ia\bar{3}d$	16a: +6 16b: -6 24c: -6	I_2 Y^{**} V^*
$Y^{**} - S^*$	211 220	1 1	0 π	$Ia\bar{3}d$	$+2 \cdot [\sin 2X \cdot \cos Y \cdot \sin Z + \sin X \cdot \sin 2Y \cdot \cos Z + \cos X \cdot \sin Y \cdot \sin 2Z]$ $+ \cos 2X \cdot \cos 2Y + \cos 2Y \cdot \cos 2Z + \cos 2X \cdot \cos 2Z = 0$	$Ia\bar{3}d$	32e: +6; $x = 0$ to 1 24d: -6	Y^{**} S^*
$I_{xxx} - J^*$	110 200	1 1	0 π	$Im\bar{3}m$	$2 \cdot [\cos X \cdot \cos Y + \cos Y \cdot \cos Z + \cos X \cdot \cos Z]$ $- [\cos 2X + \cos 2Y + \cos 2Z] = 0$	$Im\bar{3}m$	16f: +3; $x = 0$ to 1 6b: -5	I_{xxx} J^*
$IJ^* - P_2$	110 200	1 1	0 0	$Im\bar{3}m$	$2 \cdot [\cos X \cdot \cos Y + \cos Y \cdot \cos Z + \cos X \cdot \cos Z]$ $+ \cos 2X + \cos 2Y + \cos 2Z = 0$	$Im\bar{3}m$	2a: +9 6b: +1 8c: -3	I J^* P_2
$IW^* - I_z$	211	1	0	$Im\bar{3}m$	$\cos 2X \cdot \cos Y \cdot \cos Z + \cos X \cdot \cos 2Y \cdot \cos Z + \cos X \cdot \cos Y \cdot \cos 2Z = 0$	$Im\bar{3}m$	2a: 12 12d: 4 12e: -6	I W^* I_z
F_{xx}^*	531	1	0	$Fd\bar{3}c$	$\cos(5X + 3Y) \cdot \cos Z + \sin(5X - 3Y) \cdot \sin Z + \cos(X - 5Y) \cdot \cos 3Z - \sin(X + 5Y) \cdot \sin 3Z$ $+ \cos(3X + Y) \cdot \cos 5Z - \sin(3X - Y) \cdot \sin 5Z$ $- [\cos(3X + 5Y) \cdot \cos Z - \sin(3X - 5Y) \cdot \sin Z + \cos(X + 3Y) \cdot \cos 5Z + \sin(X - 3Y) \cdot \sin 5Z +$ $\cos(5X - Y) \cdot \cos 3Z - \sin(5X + Y) \cdot \sin 3Z] = 0$	$Pn\bar{3}m$	96g: ± 10.4 ; $x^+ = \frac{1}{2} - x^- = \frac{1}{6}$	F_{xx}
D^*	111	1	0	$Fd\bar{3}m$	$\cos(X - Y) \cdot \cos Z + \sin(X + Y) \cdot \sin Z = 0$	$Pn\bar{3}m$	8a/b: $\pm 2\sqrt{2}$	D
$(DT)^*$	311	1	0	$Fd\bar{3}m$	$\cos(3X + Y) \cdot \cos Z - \sin(3X - Y) \cdot \sin Z + \cos(X + 3Y) \cdot \cos Z$ $+ \sin(X - 3Y) \cdot \sin Z + \cos(X - Y) \cdot \cos 3Z - \sin(X + Y) \cdot \sin 3Z = 0$	$Pn\bar{3}m$	8b/a: ± 8.48 16c/d: ± 6	D T
$D - DT$	111 220	$\frac{5}{2}$ 1	0 π	$Fd\bar{3}m$	$\frac{5}{2} \cdot \cos(X - Y) \cdot \cos Z + \sin(X + Y) \cdot \sin Z$ $+ \cos(2X - 2Y) + \cos 2Y \cdot \cos 2Z + \sin 2Y \cdot \sin 2Z$ $+ \cos 2X \cdot \cos 2Z + \sin 2X \cdot \sin 2Z = 0$	$Fd\bar{3}m$	8a: 13.1 8b: -1.1 16c: -5; $x = \frac{1}{8}$	D D T
$(DTD_{xxx}D_{xxx})^*$	111 331	1 1	0 0	$Fd\bar{3}m$	$- [\cos(X - Y) \cdot \cos Z + \sin(X + Y) \cdot \sin Z]$ $+ \cos(3X - 3Y) \cdot \cos Z - \sin(3X + 3Y) \cdot \sin Z$ $+ \cos(X + 3Y) \cdot \cos 3Z - \sin(X - 3Y) \cdot \sin 3Z$ $+ \cos(3X + Y) \cdot \cos 3Z + \sin(3X - Y) \cdot \sin 3Z = 0$	$Pn\bar{3}m$	8a/b: ± 5.66 16c/d: ± 4 32c: ± 5.74 ; $x^+ = \frac{1}{2} + x^- = .71$ 96g: ± 5.71 ; $x^+ = .09$ $y^+ = \frac{1}{2} + y^- = .782$	D T D_{xxx} D_{xxx}

Table 8.: continued

name	hkl	$ S $	α	generating space group	$f(X,Y,Z) = 0$ with $X=2\pi \cdot x$, $Y=2\pi \cdot y$, $Z=2\pi \cdot z$	eigen symmetry of surface	extrema of $f(x,y,z)$ Wyckoff positions and values	PC
(DTD _{zxx})*	111 331	1 1	π 0	Fd $\bar{3}m$	$\cos(X - Y) \cdot \cos Z + \sin(X + Y) \cdot \sin Z$ + $\cos(3X - 3Y) \cdot \cos Z - \sin(3X + 3Y) \cdot \sin Z$ + $\cos(X + 3Y) \cdot \cos 3Z - \sin(X - 3Y) \cdot \sin 3Z$ + $\cos(3X + Y) \cdot \cos 3Z + \sin(3X - Y) \cdot \sin 3Z = 0$	Pn $\bar{3}m$	8a/b: ± 11.31 16c/d: ± 8 96g: ± 3.25 ; $x^{\pm} = .082$ $y^+ = \frac{1}{2} + y^- = .797$	D T D _{zxx}
P _{zxx} *	531	1	0	Fm $\bar{3}c$	$\cos 5X \cdot \cos 3Y \cdot \cos Z + \cos X \cdot \cos 5Y \cdot \cos 3Z + \cos 3X \cdot \cos Y \cdot \cos 5X$ - $[\cos 3X \cdot \cos 5Y \cdot \cos Z + \cos X \cdot \cos 3Y \cdot \cos 5Z + \cos 5X \cdot \cos Y \cdot \cos 3X] = 0$	Pm $\bar{3}m$	96i: ± 11.9 ; $y^+ = -y^- = .102$ $z^+ = \frac{1}{2} + z^- = .686$	P _{zxx}
F*	111	1	0	Fm $\bar{3}m$	$\cos X \cdot \cos Y \cdot \cos Z = 0$	Im $\bar{3}m$	4a/b: ± 4	F
FF _{zx} - FP ₂	111 220	2 1	0 π	Fm $\bar{3}m$	$4 \cdot [\cos X \cdot \cos Y \cdot \cos Z]$ - $[\cos 2X \cdot \cos 2Y + \cos 2Y \cdot \cos 2Z + \cos 2X \cdot \cos 2Z] = 0$	Fm $\bar{3}m$	4a: +2 96j: +4; diff. x/y 4b: -14 8c: -6	F F _{zx} F P ₂
F - I	110 111	1 1	0 0	Pn $\bar{3}m$	$\cos X \cdot \cos Y + \cos Y \cdot \cos Z + \cos X \cdot \cos Z$ + $2 \cdot \sin X \cdot \sin Y \cdot \sin Z = 0$	Pn $\bar{3}m$	2a: +6 4c: -4	F I
IF _{xx} - I _{xxx} W*	111 211	1 1	0 0	Pn $\bar{3}m$	$\cos X \cdot \cos Y \cdot \cos Z$ - $[\cos 2X \cdot \sin Y \cdot \sin Z + \sin X \cdot \cos 2Y \cdot \sin Z + \sin X \cdot \sin Y \cdot \cos 2Z] = 0$	Pn $\bar{3}m$	2a: 12 24i: 4; y = 0 - 1 8e: -4.4; x = .44 12f: -6	I F _{xx} I _{xxx} W*
J*I _{zxx} - II _{xxx} W*	111 321	1 1	0 0	Pn $\bar{3}m$	$\cos X \cdot \cos Y \cdot \cos Z$ + $\sin 3X \cdot \cos 2Y \cdot \sin Z + \sin X \cdot \sin 3Y \cdot \cos 2Z + \cos 2X \cdot \sin Y \cdot \sin 3Z$ - $[\cos 2X \cdot \sin 3Y \cdot \sin Z + \sin X \cdot \cos 2Y \cdot \sin 3Z + \sin 3X \cdot \sin Y \cdot \cos 2Z] = 0$	Pn $\bar{3}m$	6d: 8 12g: 10.5; x = .044 24k: 7.8; x = .059; y = .859 2a: -24 8e: -9.28; x = .431 8e: -3.51; x = .077 12f: -8	J* I _z I _{zxx} I I _{xxx} I _{xxx} W*

Table 8.: continued

name	hkl	$ S $	α	generating space group	$f(X, Y, Z) = 0$ with $X=2\pi \cdot x$, $Y=2\pi \cdot y$, $Z=2\pi \cdot z$	eigen symmetry of surface	extrema of $f(x, y, z)$ Wyckoff positions and values	PC
W^*	210	1	0	$Pm\bar{3}n$	$\cos 2X \cdot \cos Y + \cos 2Y \cdot \cos Z + \cos X \cdot \cos 2Z$ $- [\cos X \cdot \cos 2Y + \cos Y \cdot \cos 2Z + \cos 2X \cdot \cos Z] = 0$	$Im\bar{3}m$	6d/c: ± 8	W
$P_2 - IW_z$	110 200 210	2 4 1	0 0 π	$Pm\bar{3}n$	$-2 \cdot [\cos X \cdot \cos Y + \cos Y \cdot \cos Z + \cos X \cdot \cos Z]$ $- 2 \cdot [\cos 2X + \cos 2Y + \cos 2Z]$ $+ \cos 2X \cdot \cos Y + \cos 2Y \cdot \cos Z + \cos X \cdot \cos 2Z$ $- [\cos X \cdot \cos 2Y + \cos Y \cdot \cos 2Z + \cos 2X \cdot \cos Z] = 0$	$Pm\bar{3}n$	8e: +12 2a: -24 12g: -8; $x = 0$ to 1	P_2 I W_z
$IW - I_z W_z$	210 211	1 1	0 0	$Pm\bar{3}n$	$\cos 2X \cdot \cos Y + \cos 2Y \cdot \cos Z + \cos X \cdot \cos 2Z$ $- [\cos X \cdot \cos 2Y + \cos Y \cdot \cos 2Z + \cos 2X \cdot \cos Z]$ $+ 2 \cdot [\cos 2X \cdot \cos Y \cdot \cos Z + \cos X \cdot \cos 2Y \cdot \cos Z + \cos Y \cdot \cos 2X \cdot \cos Z] = 0$	$Pm\bar{3}n$	2a: 12 6d: 12 12f: -6; $x = \frac{2}{3}$ 12g: -4; $x = .225$	I W I_z W_z
$IWI_{zx} - J^*P_2$	210 211 220	1 2 4	0 0 $0/\pi$	$Pm\bar{3}n$	$\cos 2X \cdot \cos Y + \cos 2Y \cdot \cos Z + \cos X \cdot \cos 2Z$ $- [\cos X \cdot \cos 2Y + \cos Y \cdot \cos 2Z + \cos 2X \cdot \cos Z]$ $+ 4 \cdot [\cos 2X \cdot \cos Y \cdot \cos Z + \cos X \cdot \cos 2Y \cdot \cos Z + \cos Y \cdot \cos X \cdot \cos 2Z]$ $- 4 \cdot [\cos 2X \cdot \cos 2Y + \cos 2Y \cdot \cos 2Z + \cos 2X \cdot \cos 2Z] = 0$	$Pm\bar{3}n$	2a: ± 0 6d: 24 24k: 4.13; $y = .887$; $z = .84$ 6b: -32 8e: -24	I W I_{zx} J^* P_2
I^*_{xyz}	421	1	0	$Pn\bar{3}n$	$\sin 4X \cdot \sin 2Y \cdot \cos Z + \cos X \cdot \sin 4Y \cdot \sin 2Z + \sin 2X \cdot \cos Y \cdot \sin 4Z$ $- [\sin 2X \cdot \sin 4Y \cdot \cos Z + \sin X \cdot \sin 2Y \cdot \sin 4Z + \sin 4X \cdot \cos Y \cdot \sin 2Z] = 0$	$Im\bar{3}m$	48i: ± 11.25 ; $x^+ = \frac{1}{2} + x^- = .080$ $y^+ = -y^- = .938$ $z^+ = -z^- = .672$	I_{xyz}

Table 8.: continued

name	hkl	$ S $	α	generating space group	$f(X, Y, Z) = 0$ with $X=2\pi \cdot x, Y=2\pi \cdot y, Z=2\pi \cdot z$	eigen symmetry of surface	extrema of $f(x, y, z)$ Wyckoff positions and values	PC
$P_2 I_{xyz} - I J^* I_{xyz}$	200 421	4 1	0 0	$Pn\bar{3}n$	$\cos 2X + \cos 2Y + \cos 2Z$ $- [\sin 4X \cdot \sin 2Y \cdot \cos Z + \cos X \cdot \sin 4Y \cdot \sin 2Z + \sin 2X \cdot \cos Y \cdot \sin 4Z]$ $+ \sin 2X \cdot \sin 4Y \cdot \cos Z + \sin X \cdot \sin 2Y \cdot \sin 4Z + \sin 4X \cdot \cos Y \cdot \sin 2Z = 0$	$Pn\bar{3}n$	8c: 12 48i: 14.9; $x = .051$; $y = .152$; $z = .561$ 2a: -12 6b: -12 48i: -9.8; $x = .084$ $y = .186$; $z = .88$	P_2 I_{xyz} I J* I_{xyz}
P*	100	1	0	$Pm\bar{3}m$	$\cos X + \cos Y + \cos Z = 0$	$Im\bar{3}m$	1a/b: ± 3	P
(PJ)*	100 111	1 1	0 0	$Pm\bar{3}m$	$\cos X + \cos Y + \cos Z + 4 \cdot \cos X \cdot \cos Y \cdot \cos Z = 0$	$Im\bar{3}m$	1a/b: ± 7 3c/d: ± 3	P J
$PPJ - J_x$	110 111 220	4 2 1	0 0 0	$Pm\bar{3}m$	$4 \cdot [\cos X \cdot \cos Y + \cos Y \cdot \cos Z + \cos X \cdot \cos Z]$ $+ 4 \cdot \cos X \cdot \cos Y \cdot \cos Z$ $+ \cos 2X \cdot \cos 2Y + \cos 2Y \cdot \cos 2Z + \cos 2X \cdot \cos 2Z = 0$	$Pm\bar{3}m$	1a: +76 1b: +44 3c: +12 12h: -24	P P J J _x
$PPJP_{xxx} - J$	110 111 210	$\sqrt{2}$ 1 1	0 0 π	$Pm\bar{3}m$	$\sqrt{2} \cdot [\cos X \cdot \cos Y + \cos Y \cdot \cos Z + \cos X \cdot \cos Z]$ $+ 2 \cdot [\cos X \cdot \cos Y \cdot \cos Z]$ $- [\cos 2X \cdot \cos Y + \cos 2Y \cdot \cos Z + \cos X \cdot \cos 2Z]$ $+ \cos X \cdot \cos 2Y + \cos Y \cdot \cos 2Z + \cos 2X \cdot \cos Z = 0$	$Pm\bar{3}m$	1a: +0.4 1b: +6.4 3c: +5.2 8c: +5.9; $x = .146$ 3d: -10.8	P P J P_{xxx} J
S*	211	1	$\frac{\pi}{2}$	$I\bar{4}3d$	$\cos 2X \cdot \sin Y \cdot \cos Z + \cos X \cdot \cos 2Y \cdot \sin Z + \sin X \cdot \cos Y \cdot \cos 2Z = 0$	$I\bar{4}3d$	12a/b: ± 5.675	S
$I_2 Y^{**} - SS_z$	220 310	2 1	0 $\frac{\pi}{2}$	$I\bar{4}3d$	$2 \cdot [\cos 2X \cdot \cos 2Y + \cos 2Y \cdot \cos 2Z + \cos 2X \cdot \cos 2Z]$ $+ \sin 3X \cdot \cos Y + \sin 3Y \cdot \cos Z + \cos X \cdot \sin 3Z$ $+ \sin X \cdot \cos 3Y + \sin Y \cdot \cos 3Z + \cos 3X \cdot \sin Z = 0$	$I\bar{4}3d$	16c: 14.5; $x = .031$ 12b: -9.66 24d: -5.54; $x = .19$	$I_2 Y^{**}$ S S_z
$(SI_2 Y^{**})^*$	310	1	$\frac{\pi}{2}$	$I\bar{4}3d$	$\sin 3X \cdot \cos Y + \sin 3Y \cdot \cos Z + \cos X \cdot \sin 3Z$ $+ \sin X \cdot \cos 3Y + \sin Y \cdot \cos 3Z + \cos 3X \cdot \sin Z = 0$	$I\bar{4}3d$	12a/b: ± 5.66 16c: ± 6 ; $x^+ = -x^- = \frac{1}{16}$	S $I_2 Y^{**}$

Table 8.: continued

name	hkl	$ S $	α	generating space group	$f(X, Y, Z) = 0$ with $X=2\pi \cdot x$, $Y=2\pi \cdot y$, $Z=2\pi \cdot z$	eigen symmetry of surface	extrema of $f(x, y, z)$ Wyckoff positions and values	PC
$(W_{xyz}^2)^*$	421	1	$\frac{\pi}{4}$	$\bar{P}43n$	$\cos 4X \cdot \cos 2Y \cdot \cos Z + \cos X \cdot \cos 4Y \cdot \cos 2Z + \cos 2X \cdot \cos Y \cdot \cos 4Z$ – $[\sin 4X \cdot \sin 2Y \cdot \sin Z + \sin X \cdot \sin 4Y \cdot \sin 2Z + \sin 2X \cdot \sin Y \cdot \sin 4Z]$ – $[\cos 2X \cdot \cos 4Y \cdot \cos Z + \cos X \cdot \cos 2Y \cdot \cos 4Z + \cos 4X \cdot \cos Y \cdot \cos 2Z]$ + $\sin 2X \cdot \sin 4Y \cdot \sin Z + \sin X \cdot \sin 2Y \cdot \sin 4Z + \sin 4X \cdot \sin Y \cdot \sin 2Z = 0$	$\bar{I}43m$	6d/c: ± 11.3 24i: ± 8.78 ; $x^+ = y^- = .05$ $y^+ = x^- = .27$ $z^+ = z^- = .84$ 24i: ± 10.25 ; $x^+ = y^- = .08$ $y^+ = x^- = .19$ $z^+ = z^- = .35$	W I_{xyz} I_{xyz}
$II_{xxx} W^* - I_{xxx}$	211	1	$-\frac{\pi}{4}$	$\bar{I}43m$	$\cos 2X \cdot \cos Y \cdot \cos Z + \cos X \cdot \cos 2Y \cdot \cos Z + \cos X \cdot \cos Y \cdot \cos 2Z$ – $[\sin 2X \cdot \sin Y \cdot \sin Z + \sin X \cdot \sin 2Y \cdot \sin Z + \sin X \cdot \sin Y \cdot \sin 2Z] = 0$	$\bar{I}43m$	2a: $+8.5$ 8c: $+4.45$; $x = \frac{1}{6}$ 12d: $+2\sqrt{2}$ 8c: -6.57 ; $x = \frac{5}{6}$	I I_{xxx} W^* I_{xxx}
$IJ^* I_{xxx} - I_{xxx} W^*$	220 211	1 1	0 $-\frac{\pi}{2}$	$\bar{I}43m$	$\cos 2X \cdot \cos 2Y + \cos 2Y \cdot \cos 2Z + \cos 2X \cdot \cos 2Z$ – $2 \cdot [\cos 2X \cdot \cos Y \cdot \cos Z + \cos X \cdot \cos 2Y \cdot \cos Z + \cos X \cdot \cos Y \cdot \cos 2Z]$ – $[\sin 2X \cdot \sin Y \cdot \sin Z + \sin X \cdot \sin 2Y \cdot \sin Z + \sin X \cdot \sin Y \cdot \sin 2Z] = 0$	$\bar{I}43m$	2a: 6 6b: 6 8c: 10.3; $x = .196$ 8c: -6.9 ; $x = .352$ 12d: -2	I J^* I_{xxx} I_{xxx} W^*
$F^* (D)$	111 200	$\sqrt{2}$ 1	$\frac{\pi}{4}$ 0	$F\bar{4}3m$	$4 \cdot [\cos X \cdot \cos Y \cdot \cos Z - \sin X \cdot \sin Y \cdot \sin Z]$ + $\cos 2X + \cos 2Y + \cos 2Z = 0$	$F\bar{d}3m$	4a/b: ± 6.96	F ; in $227: D$
$(PP_{xxx})^*$	100 111	1 1	0 $-\frac{\pi}{2}$	$\bar{P}43m$	$\cos X + \cos Y + \cos Z$ – $4 \cdot [\sin X \cdot \sin Y \cdot \sin Z] = 0$	$\bar{I}43m$	1a/b: ± 3 4c: ± 4.38 ; $x^+ = x^- + \frac{1}{2} = .21$	P P_{xxx}
$(PJ)^*$	100 111	$\sqrt{2}$ 1	0 $\frac{\pi}{4}$	$\bar{P}43m$	$\cos X + \cos Y + \cos Z + \cos X \cdot \cos Y \cdot \cos Z$ – $\sin X \cdot \sin Y \cdot \sin Z = 0$	$\bar{I}43m$	1a/b: ± 7.06 3c/d: ± 1.42	P J
$PP - JP_4$	110 111	1 1	0 $\frac{\pi}{4}$	$\bar{P}43m$	$\cos X \cdot \cos Y + \cos Y \cdot \cos Z + \cos X \cdot \cos Z$ + $\sqrt{2} \cdot [\cos X \cdot \cos Y \cdot \cos Z - \sin X \cdot \sin Y \cdot \sin Z] = 0$	$\bar{P}43m$	1a: $+8.83$ 1b: $+3.17$ 3d: -4.82 4c: $-2\sqrt{2}$	P P J P_4

Table 8.: continued

name	hkl	$ S $	α	generating space group	$f(X, Y, Z) = 0$ with $X=2\pi \cdot x, Y=2\pi \cdot y, Z=2\pi \cdot z$	eigen symmetry of surface	extrema of $f(x, y, z)$ Wyckoff positions and values	PC
$(PJP_{xxx}^2 P_z P_{zxx})^*$	221	1	$\frac{\pi}{4}$	$P\bar{4}3m$	$\cos 2X \cdot \cos 2Y \cdot \cos Z + \cos X \cdot \cos 2Y \cdot \cos 2Z + \cos 2X \cdot \cos Y \cdot \cos 2Z$ $- [\sin 2X \cdot \sin 2Y \cdot \sin Z + \sin X \cdot \sin 2Y \cdot \sin 2Z + \sin 2X \cdot \sin Y \cdot \sin 2Z] = 0$	$I\bar{4}3m$	1a/b: ± 8.5 3c/d: $\pm 2\sqrt{2}$ 4e: ± 6.71 ; $x^+ = \frac{1}{2} + x^- = .845$ 4e: ± 6.18 ; $x^+ = \frac{1}{2} + x^- = .635$ 6g/f: ± 5.83 ; $x^+ = \frac{1}{2} + x^- = .230$ 12i: ± 4.6 ; $x^+ = \frac{1}{2} + x^- = .301$ $y^+ = \frac{1}{2} + y^- = .072$	P J P_{xxx} P_{xxx} P_z P_{zxx}
Y^{**}	110	1	$\frac{\pi}{2}$	$I4_132$	$\sin X \cdot \cos Y + \sin Y \cdot \cos Z + \cos X \cdot \sin Z = 0$	$I\bar{4}3d$	8a/b: ± 3	Y^*
$(YY_{xx})^*$	110 310	3 2	$\frac{\pi}{2}$ $\frac{\pi}{2}$	$I4_132$	$3 \cdot [\sin X \cdot \cos X + \sin Y \cdot \cos Z + \cos X \cdot \sin Z]$ $+ 2 \cdot [\sin 3X \cdot \cos Y + \cos X \cdot \sin 3Z + \sin 3Y \cdot \cos Z]$ $- \sin X \cdot \cos 3Y - \cos 3X \cdot \sin Z - \sin Y \cdot \cos 3Z = 0$	$I\bar{4}3d$	8a/b: ± 10.5 24g/h: ± 4.2 ; $x^+ = \frac{1}{2} + x^- = .181$	Y^* Y_{xx}^*
$(Y_{xxx} Y_{xyz})^*$	221	1	$\frac{\pi}{2}$	$P4_332$	$\sin 2X \cdot \cos 2Y \cdot \cos Z + \cos X \cdot \cos 2Y \cdot \cos 2Z + \cos 2X \cdot \cos Y \cdot \sin 2Z = 0$	$I4_132$	8c: ± 5.57 $x^+ = \frac{1}{2} + x^- = .059$ 24e: ± 5.03 ; $x^+ = \frac{1}{2} + x^- = .013$ $y^+ = \frac{1}{2} + y^- = .402$ $z^+ = \frac{1}{2} + z^- = .808$	Y_{xxx} Y_{xyz}
Y^*	111 210	1 $\sqrt{2}$	$\frac{\pi}{4}$ π	$P4_332$	$[\cos X \cdot \cos Y \cdot \cos Z + \sin X \cdot \sin Y \cdot \sin Z]$ $+ \sin 2Y \cdot \sin Y + \sin 2Y \cdot \sin Z + \sin X \cdot \sin 2Z$ $+ \cos X \cdot \sin 2Y + \cos Y \cdot \sin 2Z + \sin 2X \cdot \cos Z = 0$	$I4_132$	4a/b: ± 9.9	^+Y
$(YY_{xxx} Y_{xx})^*$	111 210	1 $\sqrt{2}$	$\frac{\pi}{4}$ 0	$P4_332$	$- [\cos X \cdot \cos Y \cdot \cos Z + \sin X \cdot \sin Y \cdot \sin Z]$ $+ \sin 2Y \cdot \sin Y + \sin 2Y \cdot \sin Z + \sin X \cdot \sin 2Z$ $+ \cos X \cdot \sin 2Y + \cos Y \cdot \sin 2Z + \sin 2X \cdot \cos Z = 0$	$I4_132$	4a/b: $\pm 5\sqrt{2}$ 8c: ± 3.93 ; $x^+ = \frac{1}{2} + x^- = .452$ 12d: $\pm 3\sqrt{2}$; $y^+ = -y^- = \frac{3}{8}$	^+Y Y_{xxx} Y_{xx}

Table 8.: continued

name	hkl	$ S $	α	generating space group	$f(X, Y, Z) = 0$ with $X=2\pi \cdot x$, $Y=2\pi \cdot y$, $Z=2\pi \cdot z$	eigen symmetry of surface	extrema of $f(x, y, z)$ Wyckoff positions and values	PC
P_{xxx}^*	200 321 231	2 1 1	0 π π	$la\bar{3}$	$\cos 2X + \cos 2Y + \cos 2Z$ $+ 2 \cdot [\sin 3X \cdot \sin 2Y \cdot \cos Z + \cos X \cdot \sin 3Y \cdot \sin 2Z + \sin 2X \cdot \cos Y \cdot \sin 3Z]$ $+ 2 \cdot [\sin 2X \cdot \cos 3Y \cdot \sin Z + \sin X \cdot \sin 2Y \cdot \cos 3Z + \cos 3X \cdot \sin Y \cdot \sin 2Z] = 0$	$la\bar{3}d$	16c: ± 12.91 ; $x^+ = \frac{1}{4}$; $x^- = .069$	P_{xxx}
$P_2 P_{2xxx} - P_{2xyz}$	220 321 231	2 1 1	0 π π	$la\bar{3}$	$\cos 2X \cdot \cos 2Y + \cos 2Y \cdot \cos 2Z + \cos 2X \cdot \cos 2Z$ $+ \sin 3X \cdot \sin 2Y \cdot \cos Z + \cos X \cdot \sin 3Y \cdot \sin 2Z + \sin 2X \cdot \cos Y \cdot \sin 3Z$ $+ \sin 2X \cdot \sin 3Y \cdot \cos Z + \cos X \cdot \sin 2Y \cdot \sin 3Z + \sin 3X \cdot \cos Y \cdot \sin 2Z = 0$	$la\bar{3}$	8b: +12 16c: +14.6; $x = .055$ 48e: -7.8; $x = .038$ $y = .125$; $z = .306$	P_2 P_{2xxx} P_{2xyz}
F_{xxx}^*	210	1	0	$Pa\bar{3}$	$\sin 2X \cdot \sin Y + \sin 2Y \cdot \sin Z + \sin X \cdot \sin 2Z = 0$	$la\bar{3}$	8c: ± 4.62 ; $x^+ = \frac{1}{2}$; $x^- = .152$	F_{xxx}
F_{xxx}^*	111 210	1 1	0 π	$Pa\bar{3}$	$2 \cdot [\cos X \cdot \cos Y \cdot \cos Z]$ $+ \sin 2X \cdot \sin Y + \sin 2Y \cdot \sin Z + \sin X \cdot \sin 2Z = 0$	$la\bar{3}$	8c: ± 5.66 ; $x^+ = \frac{1}{2}$; $x^- = \frac{1}{8}$	F_{xxx}
$(FF_{xxx})^*$	111 210	1 1	0 0	$Pa\bar{3}$	$-2 \cdot [\cos X \cdot \cos Y \cdot \cos Z]$ $+ \sin 2X \cdot \sin Y + \sin 2Y \cdot \sin Z + \sin X \cdot \sin 2Z = 0$	$la\bar{3}$	4a/b: ± 4 8c: ± 4 ; $x^+ = \frac{1}{2}$; $x^- = \frac{1}{6}$	F F_{xxx}
$F_{xyz} - F_{xxx}^2$	111 211	1 1	0 0	$Pa\bar{3}$	$\cos X \cdot \cos Y \cdot \cos Z$ $- [\sin 2X \cdot \cos Y \cdot \sin Z + \sin X \cdot \sin 2Y \cdot \cos Z + \cos X \cdot \sin Y \cdot \sin 2Z] = 0$	$Pa\bar{3}$	24d: +5; $x = 0$; $y = .141$; $z = .895$ 8c: -7.62; $x = .391$ 8c: -4.76; $x = .138$	F_{xyz} F_{xxx} F_{xxx}
$FF_{xxx} - FF_{xxx}$	111 210 220	2 1 1	0 π π	$Pa\bar{3}$	$4 \cdot [\cos X \cdot \cos Y \cdot \cos Z]$ $+ \sin 2X \cdot \sin Y + \sin 2Y \cdot \sin Z + \sin X \cdot \sin 2Z$ $- [\cos 2X \cdot \cos 2Y + \cos 2Y \cdot \cos 2Z + \cos 2X \cdot \cos 2Z] = 0$	$Pa\bar{3}$	4b: 14 8c: 7.54; $x = .294$ 4a: -2 8c: -7.22; $x = .114$	F F_{xxx} F F_{xxx}
$(F_{xxx} F_{xyz})^*$	221	1	0	$Pa\bar{3}$	$\cos 2X \cdot \sin 2Y \cdot \sin Z + \sin X \cdot \cos 2Y \cdot \sin 2Z + \sin 2X \cdot \sin Y \cdot \cos 2Z = 0$	$la\bar{3}$	8c: ± 5.57 ; $x^+ = \frac{1}{2}$; $x^- = .191$ 24d: ± 5.03 ; $x^+ = \frac{1}{2}$; $x^- = .058$ $y^+ = \frac{1}{2}$; $y^- = .152$ $z^+ = \frac{1}{2}$; $z^- = .737$	F_{xxx} F_{xyz}

Table 8.: continued

name	hkl	$ S $	α	generating space group	$f(X, Y, Z) = 0$ with $X=2\pi \cdot x, Y=2\pi \cdot y, Z=2\pi \cdot z$	eigen symmetry of surface	extrema of $f(x, y, z)$ Wyckoff positions and values	PC
$FF_{xxx} - F_{xyz}$	111 210 220	2 1 1	0 0 0	$\overline{Pa3}$	$4 \cdot [\cos X \cdot \cos Y \cdot \cos Z]$ $- [\sin 2X \cdot \sin Y + \sin 2Y \cdot \sin Z + \sin X \cdot \sin 2Z]$ $+ \cos 2X \cdot \cos 2Y + \cos 2Y \cdot \cos 2Z + \cos 2X \cdot \cos 2Z = 0$	$\overline{Pa3}$	4a: +14 8c: 7.3; $x = .284$ 24d: -5.66; $x = .022$ $y = .116; z = .336$	F F_{xxx} F_{xyz}
I_{zx}^*	310 130	1 1	0 π	$\overline{Im3}$	$\cos 3X \cdot \cos Y + \cos 3Y \cdot \cos Z + \cos X \cdot \cos 3Z$ $- [\cos X \cdot \cos 3Y + \cos Y \cdot \cos 3Z + \cos 3X \cdot \cos Z] = 0$	$\overline{Im3m}$	24g: ± 6.58 ; $x^+ = y^- = .162$ $y^+ = x^- = .391$	I_{zx}
$(J_X^* I_{zx})^*$	321 231	1 1	0 π	$\overline{Im3}$	$\cos 3X \cdot \cos 2Y \cdot \cos Z + \cos X \cdot \cos 3Y \cdot \cos 2Z + \cos 2X \cdot \cos Y \cdot \cos 3Z$ $- [\cos 2X \cdot \cos 3Y \cdot \cos Z + \cos X \cdot \cos 2Y \cdot \cos 3Z + \cos 3X \cdot \cos Y \cdot \cos 2Z] = 0$	$\overline{Im3m}$	12e: ± 12.3 ; $x^+ = \frac{1}{2} + x^- = .85$ 24g: ± 7.55 ; $y^+ = z^- = .176$ $z^+ = y^- = .297$	J_X^* I_{zx}
$J^* I_{xxx} I_{zx} - IP_2 I_z$	310 222	1 1	0 π	$\overline{Im3}$	$\cos 3X \cdot \cos Y + \cos 3Y \cdot \cos Z + \cos X \cdot \cos 3Z$ $- 2 \cdot [\cos 2X \cdot \cos 2Y \cdot \cos 2Z] = 0$	$\overline{Im3}$	6b: 6 16f: 3.33; $x = .142$ 24g: 49; $x = .745; y = .792$ 2a: -2 8c: -4 12d: -6.42; $x = .28$	J^* I_{xxx} I_{zx} I P_2 I_z
$IJ_X^* I_{xxx} - I_z$	211 321	1 1	0 $0/\pi$	$\overline{Im3}$	$\cos 2X \cdot \cos Y \cdot \cos Z + \cos X \cdot \cos 2Y \cdot \cos Z + \cos X \cdot \cos Y \cdot \cos 2Z$ $+ \cos 3X \cdot \cos 2Y \cdot \cos Z + \cos X \cdot \cos 3Y \cdot \cos 2Z + \cos 2X \cdot \cos Y \cdot \cos 3Z = 0$	$\overline{Im3}$	2a: 24 12e: 11.0; $x = .196$ 16f: 1.78; $x = .183$ 12d: -8; $x = \frac{1}{4}$	I J_X^* I_{xxx} I_z
$IJ_X^* I_{xxx} I_{zx} - J^* J_X^* I_{zx}$	222 321	1 1	0 π	$\overline{Im3}$	$\cos 2X \cdot \cos 2Y \cdot \cos 2Z$ $- [\cos 3X \cdot \cos 2Y \cdot \cos Z + \cos X \cdot \cos 3Y \cdot \cos 2Z + \cos 2X \cdot \cos Y \cdot \cos 3Z] = 0$	$\overline{Im3}$	2a: 8 12e: 11.0; $x = .304$ 16f: 4.55; $x = .2$ 24g: 4.63; $x = .13; y = .31$ 6b: -8 12e: -8; $x = .004$ 24g: -6.58; $x = .31; y = .74$	I J_X^* I_{xxx} I_{zx} J^* J_X^* I_{zx}

Table 8.: continued

name	<i>hkl</i>	$ S $	α	generating space group	$f(X, Y, Z) = 0$ with $X=2\pi \cdot x, Y=2\pi \cdot y, Z=2\pi \cdot z$	eigen symmetry of surface	extrema of $f(x, y, z)$ Wyckoff positions and values	<i>PC</i>
$I_{I_{zx}} - J^* I_{xxx}$	$\begin{matrix} 200 \\ 211 \\ 310 \end{matrix}$	$\begin{matrix} 1 \\ 1 \\ 1 \end{matrix}$	$\begin{matrix} 0 \\ \pi \\ \pi \end{matrix}$	$Im\bar{3}$	$- [\cos 2X + \cos 2Y + \cos 2Z]$ $+ 4 \cdot [\cos 2X \cdot \cos Y \cdot \cos Z + \cos X \cdot \cos 2Y \cdot \cos Z + \cos X \cdot \cos Y \cdot \cos 2Z]$ $2 \cdot [\cos 3X \cdot \cos Y + \cos 3Y \cdot \cos Z + \cos X \cdot \cos 3Z] = 0$	$Im\bar{3}$	2a: 15 24g: 4.7; $x = .2275$ $y = .645$ 6b: -9 16f: -3.75; $x = .145$	I $I_{I_{zx}}$ J^* I_{xxx}
$J^* I_{I_{zx}} - IP_2 I_{I_{zx}}$	$\begin{matrix} 220 \\ 310 \end{matrix}$	$\begin{matrix} 1 \\ 1 \end{matrix}$	$\begin{matrix} 0 \\ 0 \end{matrix}$	$Im\bar{3}$	$\cos 2X \cdot \cos 2Y + \cos 2Y \cdot \cos 2Z + \cos 2X \cdot \cos 2Z$ $+ \cos 3X \cdot \cos Y + \cos 3Y \cdot \cos Z + \cos X \cdot \cos 3Z = 0$	$Im\bar{3}$	12e: 5.48; $x = .304$ 24g: 4.1; $x = .222$ $y = .161$ 2a: -12 8c: -6 24g: -4.3; $x = .059$ $y = .407$	J^*_x $I_{I_{zx}}$
$IP^* I_{I_{xxx}} I_{I_{zx}} - I_{I_{I_{zx}}}$	$\begin{matrix} 220 \\ 321 \end{matrix}$	$\begin{matrix} 1 \\ 1 \end{matrix}$	$\begin{matrix} 0 \\ 0 \end{matrix}$	$Im\bar{3}$	$\cos 2X \cdot \cos 2Y + \cos 2Y \cdot \cos 2Z + \cos 2X \cdot \cos 2Z$ $+ 2 \cdot [\cos 3X \cdot \cos 2Y \cdot \cos Z + \cos X \cdot \cos 3Y \cdot \cos 2Z + \cos 2X \cdot \cos Y \cdot \cos 3Z] = 0$	$Im\bar{3}$	2a: 18 12e: 8.16; $x = .348$ 16f: 6.4; $x = .207$ 24g: 3.78; $x = .158; y = .313$ 12d: -6.83; $x = .22$ 24g: -6.48; $x = .35; y = .285$	I J^*_x I_{xxx} $I_{I_{zx}}$
$(DTD^2_{xxx} D_{xyz})^*$	531	1	0	$Fd\bar{3}$	$\cos(5X + 3Y) \cdot \cos Z + \sin(5X - 3Y) \cdot \sin Z$ $+ \cos(X - 5Y) \cdot \sin 3Z - \sin(X + 5Y) \cdot \sin Z$ $+ \cos(3X + Y) \cdot \cos 5Z - \sin(3X - Y) \cdot \sin 5Z = 0$	$Pn\bar{3}$	8a/b: ± 8.48 16c/d: ± 6 32e: ± 4.04 ; $x^+ = \frac{1}{2} + x^- = .56$ 32e: ± 4.04 ; $x^+ = \frac{1}{2} + x^- = .56$ 96g: ± 6.3 $x^\pm = .03; y^\pm = .33$ $z^+ = \frac{1}{2} + z^- = .085$	D T D_{xxx} D_{xxx} D_{xyz}
$(PJ_x)^*$	$\begin{matrix} 110 \\ 210 \end{matrix}$	$\begin{matrix} 1 \\ 1 \end{matrix}$	$\begin{matrix} 0 \\ 0 \end{matrix}$	$Pm\bar{3}$	$2 \cdot [\cos 2X \cdot \cos Y + \cos 2Y \cdot \cos Z + \cos X \cdot \cos 2Z]$ $+ \cos X + \cos Y + \cos Z = 0$	$Im\bar{3}$	1a/b: ± 9 6g/f: ± 4.56 $x^+ = \frac{1}{2} + x^- = .189$	P J_x

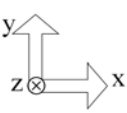
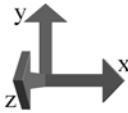
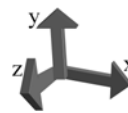
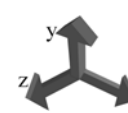
Table 8.: continued

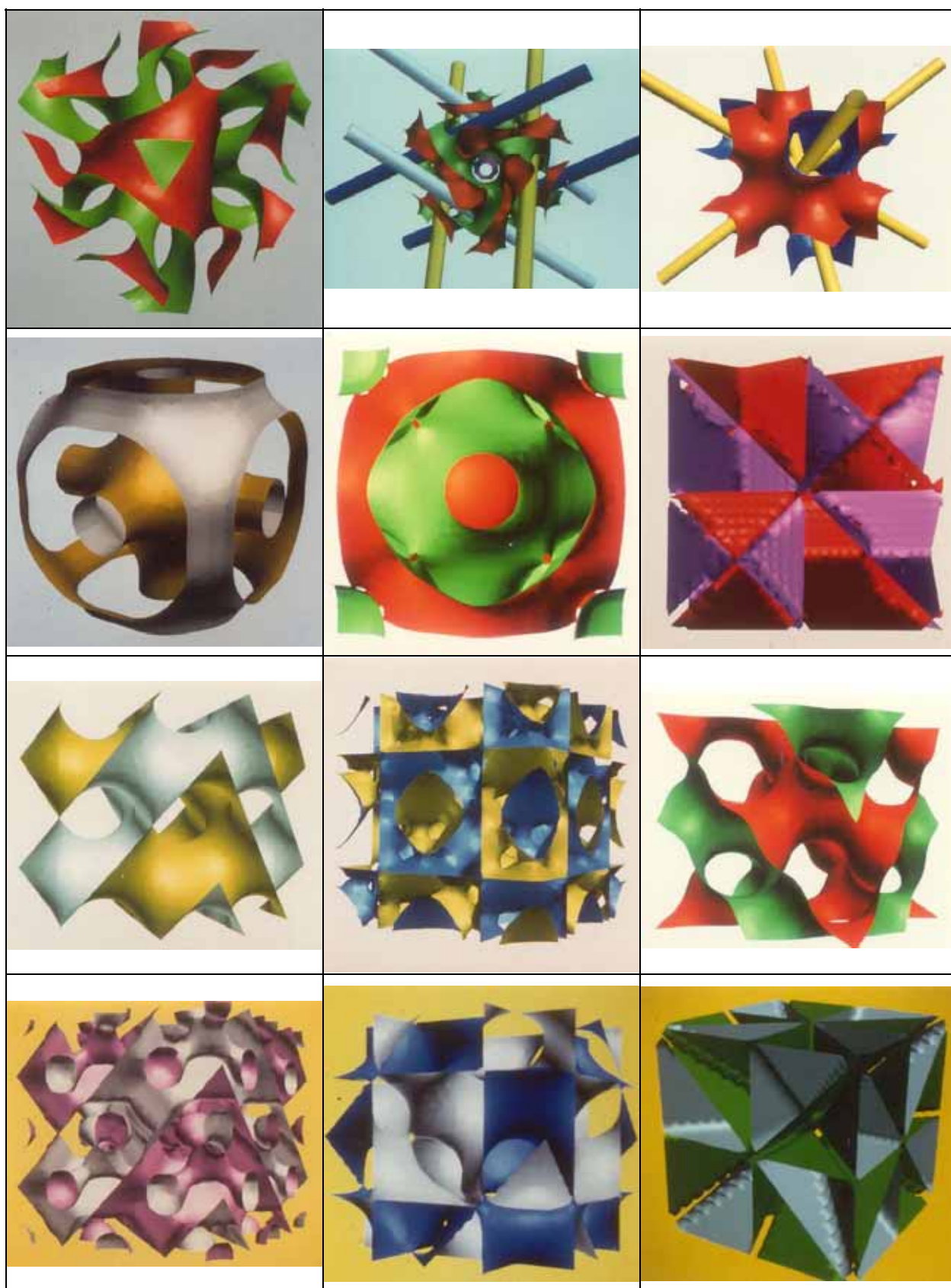
name	hkl	$ S $	α	generating space group	$f(X, Y, Z) = 0$ with $X=2\pi \cdot x$, $Y=2\pi \cdot y$, $Z=2\pi \cdot z$	eigen symmetry of surface	extrema of $f(x, y, z)$ Wyckoff positions and values	PC
$(PJ_X)^*$	210	1	0	$Pm\bar{3}$	$\cos 2X \cdot \cos Y + \cos 2Y \cdot \cos Z \cdot \cos X \cdot \cos 2Z = 0$	$Im\bar{3}$	1a/b: ± 6 6g/f: ± 4.25 ; $x^+ = \frac{1}{2} + x^- = .210$	P J_x
$(PJ_X P_{Zx})^*$	100 210	2 1	0 π	$Pm\bar{3}$	$\cos X + \cos Y + \cos Z$ $- [\cos 2X \cdot \cos Y + \cos 2Y \cdot \cos Z + \cos X \cdot \cos 2Z] = 0$	$Im\bar{3}$	1a/b: ± 0 6g/f: ± 4 ; $x^+ = \frac{1}{2} + x^- = \frac{1}{4}$ 12k/j: ± 5 ; $y^+ = \frac{1}{2} + y^- = \frac{1}{4}$ $z^+ = \frac{1}{2} + z^- = \frac{1}{3}$	P J_x P_{Zx}
$(P_2Y^*SV P_2Y_{yz}^*)^*$	222 321	1 1	$\frac{\pi}{2}$ $\frac{\pi}{2}$	$I2_13$	$\sin 2X \cdot \sin 2Y \cdot \sin 2Z$ $+ \cos 3X \cdot \cos 2Y \cdot \sin Z + \sin X \cdot \cos 3Y \cdot \cos 2Z + \cos 2X \cdot \sin Y \cdot \cos 3Z = 0$	$Ia\bar{3}$	8a: ± 8.657 ; $x^+ = -x^- = .188$ 12b: ± 7.52 ; $x^+ = \frac{1}{2} - x^- = .675$ 24c: ± 4.55 ; $x^+ = -x^- = .029$ $y^+ = -y^- = .442$ $z^+ = -z^- = .325$	P_2Y^* SV $P_2Y_{yz}^*$
$(P_2Y^*SV^2P_2Y_{yz}^*)^*$	222 321	2 1	$\frac{\pi}{2}$ $\frac{\pi}{2}$	$I2_13$	$-2 \cdot [\sin 2X \cdot \sin 2Y \cdot \sin 2Z]$ $+ \cos 3X \cdot \cos 2Y \cdot \sin Z + \sin X \cdot \cos 3Y \cdot \cos 2Z + \cos 2X \cdot \sin Y \cdot \cos 3Z = 0$	$Ia\bar{3}$	8a: ± 8.37 ; $x^+ = -x^- = .385$ 12b: ± 7.52 ; $x^+ = -x^- = .675$ 12b: ± 4.223 ; $x^+ = -x^- = .982$ 24c: ± 8.93 ; $x^+ = -x^- = .11$ $y^+ = -y^- = .15$ $z^+ = -z^- = .346$	P_2Y^* SV SV $P_2Y_{yz}^*$
$(P_2Y_{xxx} P_2Y_{xyz})^*$	310	1	$\frac{\pi}{2}$	$I2_13$	$\sin 3X \cdot \cos Y + \sin 3Y \cdot \cos Z + \cos X \cdot \sin 3Z = 0$	$Ia\bar{3}$	8a: ± 5.28 ; $x^+ = -x^- = .075$ 24c: ± 3.78 ; $x^+ = -x^- = .023$ $y^+ = -y^- = .759$ $z^+ = -z^- = .075$	P_2Y_{xxx} P_2Y_{xyz}




Table 8.: continued

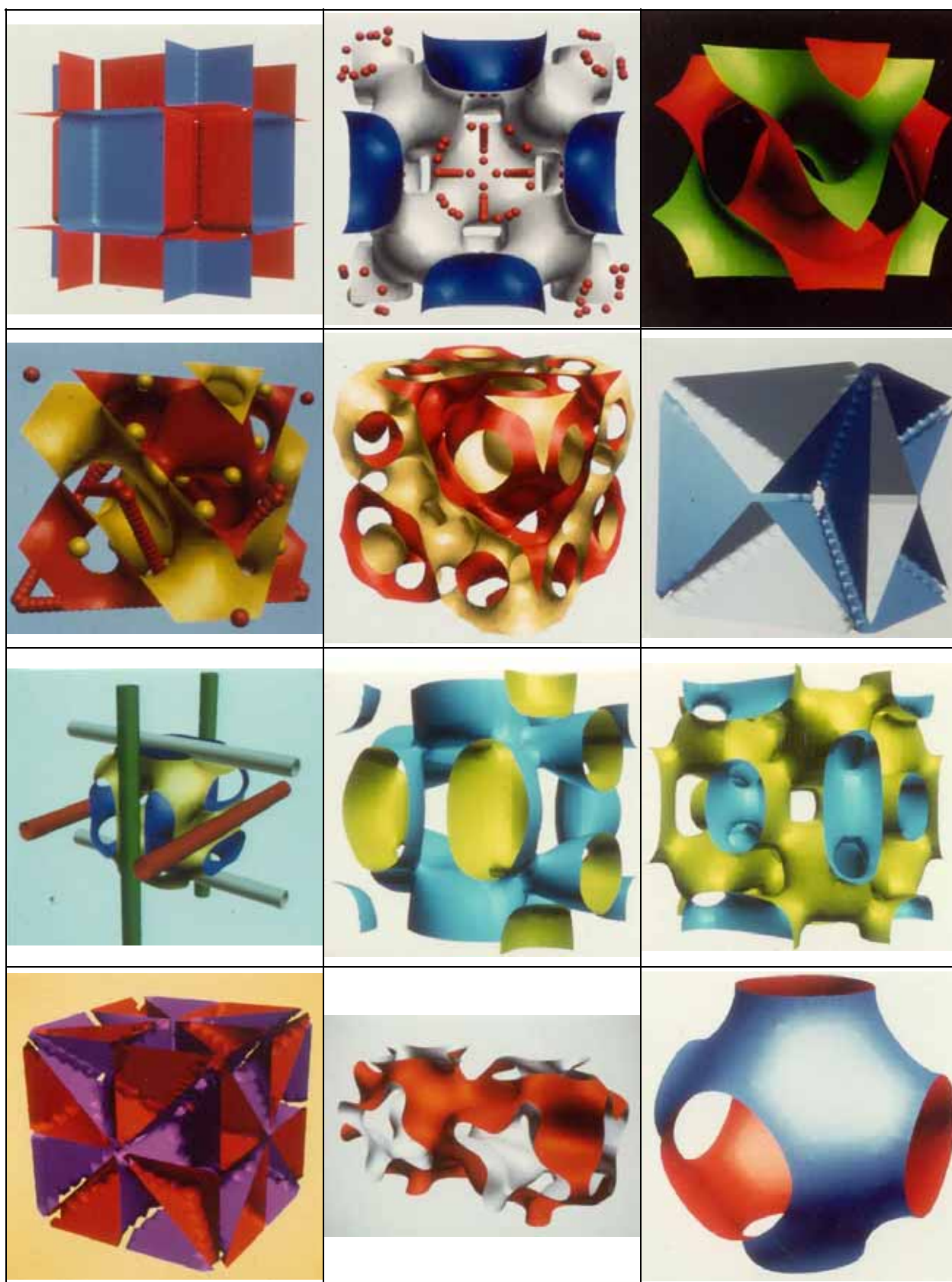
name	hkl	$ S $	α	generating space group	$f(X,Y,Z) = 0$ with $X=2\pi \cdot x, Y=2\pi \cdot y, Z=2\pi \cdot z$	eigen symmetry of surface	extrema of $f(x,y,z)$ Wyckoff positions and values	PC
$(I_{xxx}^2 I_{xyz})^*$	321	1	$\frac{\pi}{2}$	I23	$\sin 3X \cdot \sin 2Y \cdot \sin Z + \sin X \cdot \sin 3Y \cdot \sin 2Z + \sin 2X \cdot \sin Y \cdot \sin 3Z = 0$	$\text{Im}\bar{3}$	8c: ± 6.6 ; $x^+ = -x^- = .39$ 8c: ± 4.1 ; $x^+ = -x^- = .207$ 24f: ± 6.78 ; $x^+ = -x^- = .095$ $y^+ = -y^- = .36$ $z^+ = -z^- = .26$	I_{xxx} I_{xxx} I_{xyz}
$IJ^* I_{xxx} I_{xyz} - I_{xxx}^2 I_{xyz}$	222 321	1 1	0 $\frac{\pi}{2}$	I23	$\cos 2X \cdot \cos 2Y \cdot \cos 2Z$ $- [\sin 3X \cdot \sin 2Y \cdot \sin Z + \sin X \cdot \sin 3Y \cdot \sin 2Z + \sin 2X \cdot \sin Y \cdot \sin 3Z] = 0$	I23	2a: 4 6b: 4 8c: 6.6; $x = .392$ 24f: 7.5; $x = .081$ $y = .321$; $z = .246$ 8c: -6.56; $x = .111$ 8c: -6.91; $x = .283$ 12d: -4; $x = \frac{1}{4}$ 24f: -6.8; $x = .09$ $y = .391$; $z = .727$	I J* I_{xxx} I_{xyz} I_{xxx} I_{xxx} I_z I_{xyz}
$(PJ_x^2 P_{xyz})^*$	100 231 321	4 1 1	0 $\frac{3\pi}{4}$ $\frac{\pi}{4}$	P23	$\sqrt{2} \cdot \cos X + \cos Y + \cos Z$ $+ \cos 2X \cdot \cos 3Y \cdot \cos Z - \sin 2X \cdot \sin 3Y \cdot \sin Z$ $+ \cos X \cdot \cos 2Y \cdot \cos 3Z - \sin X \cdot \sin 2Y \cdot \sin 3Z$ $+ \cos 3X \cdot \cos Y \cdot \cos 2Z - \sin 3X \cdot \sin Y \cdot \sin 2Z$ $- [\cos 3X \cdot \cos 2Y \cdot \cos Z - \sin 3X \cdot \sin 2Y \cdot \sin Z$ $+ \cos X \cdot \cos 3Y \cdot \cos 2Z - \sin X \cdot \sin 3Y \cdot \sin 2Z$ $+ \cos 2X \cdot \cos Y \cdot \cos 3Z - \sin 2X \cdot \sin Y \cdot \sin 3Z] = 0$	P23	1a/b: ± 12 6h: ± 11.12 ; $x = \frac{1}{2} - x^- = .142$ 6h: ± 6.50 ; $x = \frac{1}{2} - x^- = .338$ 12j: ± 11.72 ; $x = \frac{1}{2} + x^- = .056$ $y^+ = .31$; $y^- = .315$ $z^+ = .81$; $z^- = .815$	P J_x J_x P_{xyz}

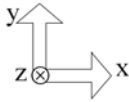
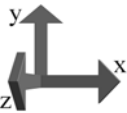
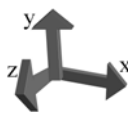
3.3.4. Illustrations

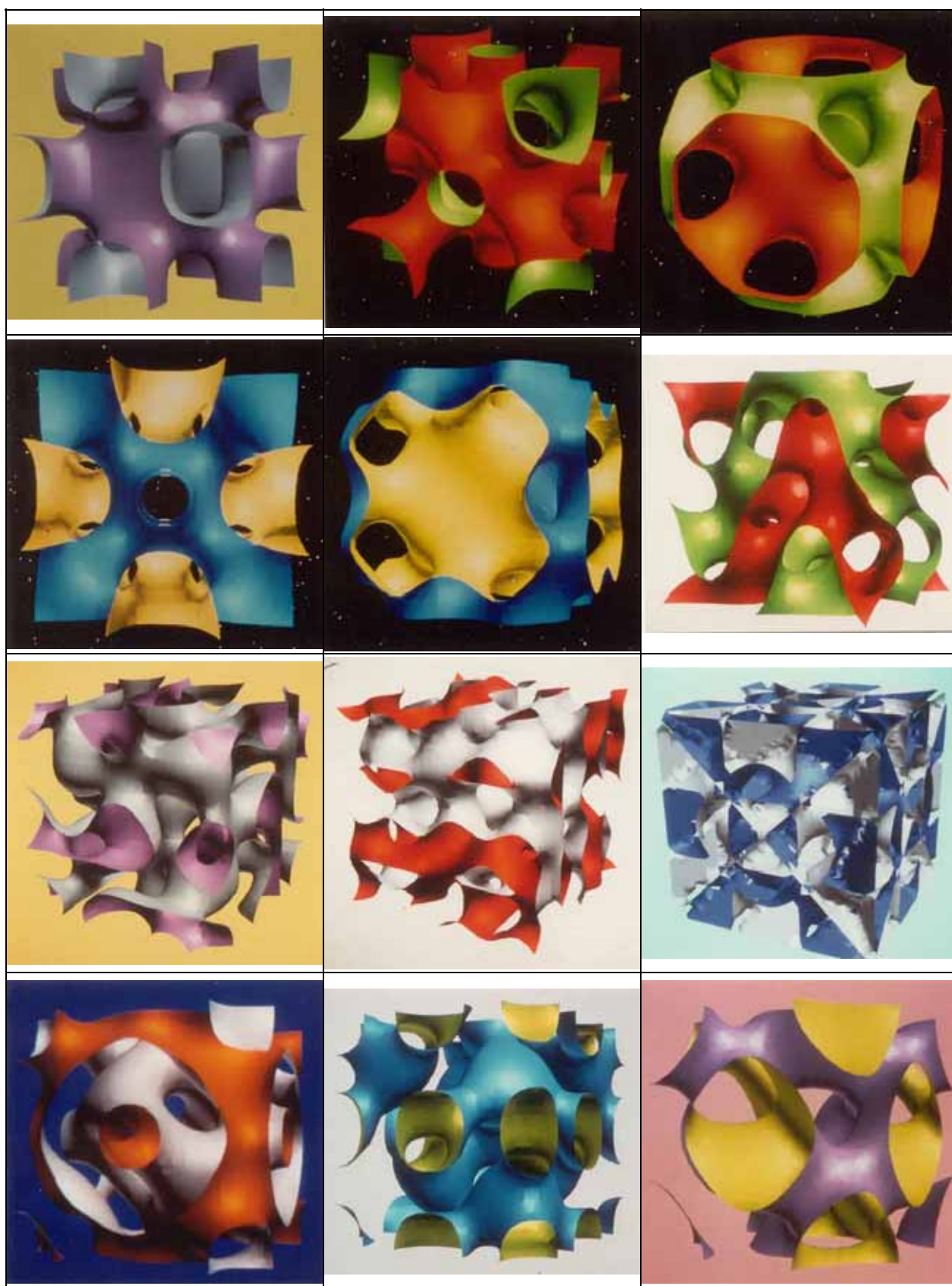
<p>Ill. 2.a</p> $I_2 - Y^{**}V^*$ $^{230}\langle(211);(220)\rangle$ <p>Setup 4 acc. to Oehme^[39]</p>	<p>Ill. 2.b</p> $Y_{xxx}^{**} - S^*$ $^{230}\langle(211);(220)^\pi\rangle$ <p>with Y_{xxx}^{**} graph Setup 4</p>	<p>Ill. 2.c</p> $I_{xxx} - J^*$ $^{229}\langle(110);(200)^\pi\rangle$ <p>with I_{xxx} graph Setup 3</p>
<p>Ill. 2.d</p> $IJ^* - P_2$ $^{229}\langle(110);(200)\rangle$ <p>Setup 3</p>	<p>Ill. 2.e</p> $IW^* - I_z$ $^{229}\langle 211 \rangle$ <p>Setup 1</p>	<p>Ill. 2.f</p> F_{xx}^* $^{228}\langle 531 \rangle^{224}$ <p>x,y,z from 0 to $\frac{1}{2}$ (1st octand of the unit cell) 000 at 43m Setup 1</p>
<p>Ill. 2.g</p> D^* $^{227}\langle 111 \rangle^{224}$ <p>000 at $\bar{3}m$ Setup 2</p>	<p>Ill. 2.h</p> $(DT)^*$ $^{227}\langle 311 \rangle^{224}$ <p>000 at $\bar{3}m$ Setup 2</p>	<p>Ill. 2.i</p> $D - DT$ $^{227}\langle(111)_{5/2};(220)^\pi\rangle$ <p>000 at $\bar{3}m$ Setup 2</p>
<p>Ill. 2.j</p> $(DTD_{xxx}D_{zzx})^*$ $^{227}\langle(111);(331)\rangle^{224}$ <p>000 at $\bar{3}m$ topological: D* & F – I Setup 2</p>	<p>Ill. 2.k</p> $(DTD_{zzx})^*$ $^{227}\langle(111)^\pi;(331)\rangle^{224}$ <p>x,y,z from 0 to $\frac{1}{2}$ (1st octand of the unit cell) 000 at $\bar{3}m$ Setup 2</p>	<p>Ill. 2.l</p> $(P_{2zx})^*$ $^{226}\langle 531 \rangle^{211}$ <p>x,y,z from 0 to $\frac{1}{2}$ (1st octand of the unit cell) Setup 3</p>
<p>Setup 1: </p> <p>Setup 2: </p> <p>Setup 3: </p> <p>Setup 4: </p>		

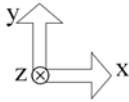
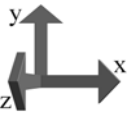
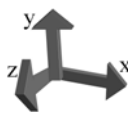


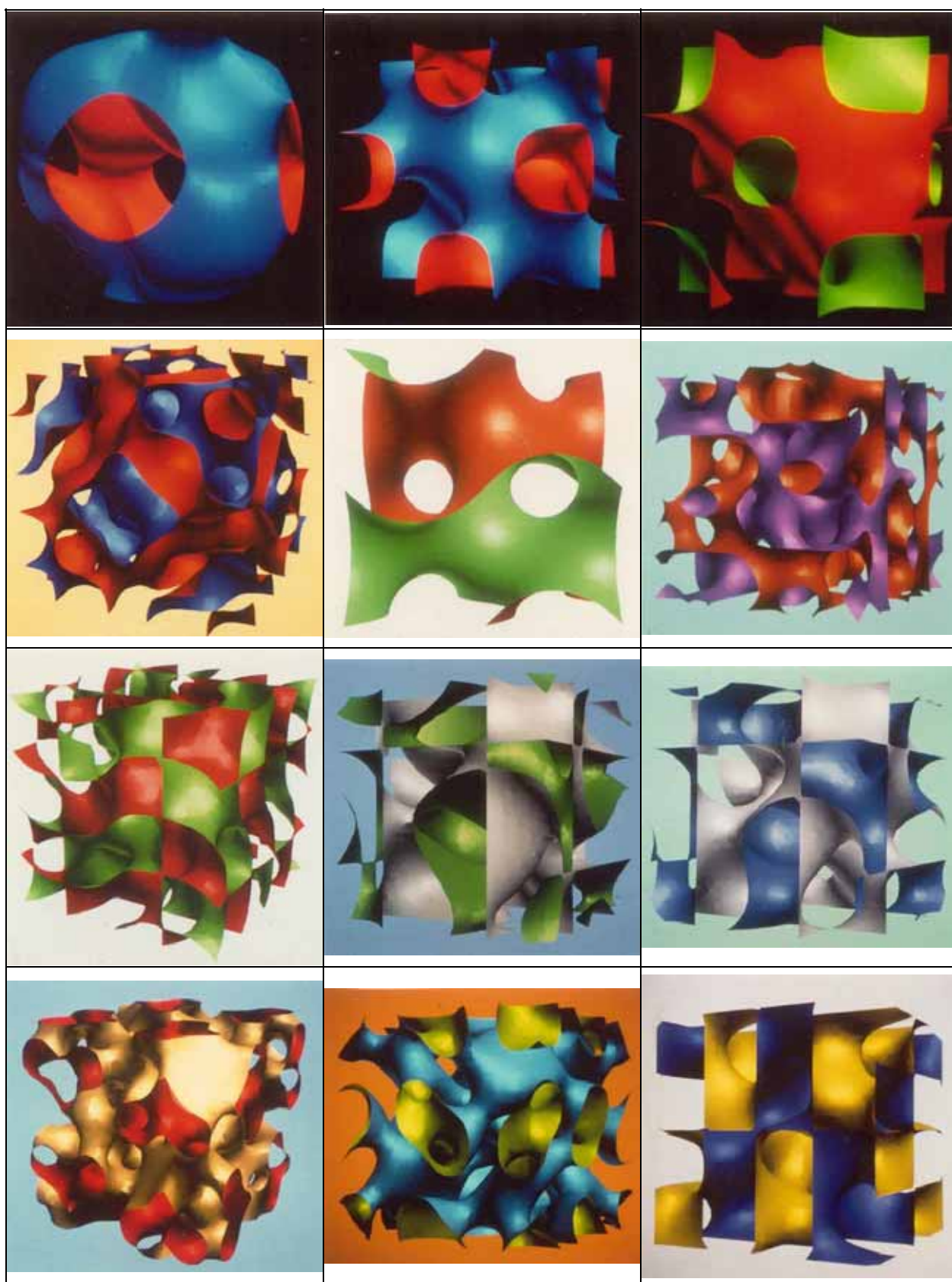
<p>Ill. 3.a</p> F^* $^{225}\langle 111 \rangle^{229}$ <p>Setup 2</p>	<p>Ill. 3.b</p> $FF_{zx} - FP_2$ $^{225}\langle (111)_2; (220)^\pi \rangle$ <p>With some extrema of the point configuration F_{zx} as balls, forming the main circles of a deformed sphere</p> <p>Setup 1</p>	<p>Ill. 3.c</p> $F - I$ $^{224}\langle (110); (111) \rangle$ <p>000 at $\bar{3}m$</p> <p>Setup 2</p>
<p>Ill. 3.d</p> $IF_{xx} - I_{xxx}W^*$ $^{224}\langle (111); (211) \rangle$ <p>Extrema as balls, with F_{xx} graph</p> <p>000 at $\bar{3}m$</p> <p>Setup 2</p>	<p>Ill. 3.e</p> $J^*I_zI_{zxx} - II_{xxx}W^*$ $^{224}\langle (111), (321) \rangle$ <p>000 at $\bar{3}m$</p> <p>Setup 3</p>	<p>Ill. 3.f</p> W^* $^{223}\langle 210 \rangle^{229}$ <p>Setup 2</p>
<p>Ill. 3.g</p> $P_2 - IW_z$ $^{223}\langle (110)_2; (200)_4; (210)^\pi \rangle$ <p>With W_z graph (three-rod packing)</p> <p>Setup 3</p>	<p>Ill. 3.h</p> $IW - I_zW_z$ $^{223}\langle (210); (211) \rangle$ <p>Setup 2</p>	<p>Ill. 3.i</p> $IWI_{zx} - J^*P_2$ $^{223}\langle (210); (211)_2; (220)_4 \rangle$ <p>Setup 2</p>
<p>Ill. 3.j</p> I_{xyz}^* $^{222}\langle 421 \rangle^{229}$ <p>x,y,z from 0 to $\frac{1}{2}$</p> <p>(1st octant of the unit cell)</p> <p>Setup 3</p>	<p>Ill. 3.k</p> $P_2I_{xyz} - IJ^*I_{xyz}$ $^{222}\langle (220)_4; (421) \rangle$ <p>x,y,z from 0 to $\frac{1}{2}$</p> <p>(1st octant of the unit cell)</p> <p>Setup 3</p>	<p>Ill. 3.l</p> P^* $^{221}\langle 100 \rangle^{229}$ <p>Setup 3</p>
<p>Setup 1: </p> <p>Setup 2: </p> <p>Setup 3: </p>		

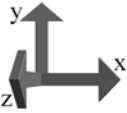
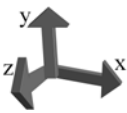


<p>III. 4.a</p> <p>(PJ)*</p> $^{221}\langle (100);(111)\rangle^{229}$ <p>Setup 2</p>	<p>III. 4.b</p> <p>PPJ – J_x</p> $^{221}\langle (110)_4;(111)_2;(220)\rangle$ <p>Setup 3</p>	<p>III. 4.c</p> <p>PPJ – J_x</p> $^{221}\langle (110)_4;(111)_2;(220)\rangle$ <p>x,y,z from $-\frac{1}{2}$ to $\frac{1}{2}$</p> <p>Setup 3</p>
<p>III. 4.d</p> <p>PPJP_{xxx} – J</p> $^{221}\langle (110)_{\sqrt{2}};(111);(210)^{\pi}\rangle$ <p>Setup 1</p>	<p>III. 4.e</p> <p>PPJP_{xxx} – J</p> $^{221}\langle (110)_{\sqrt{2}};(111);(210)^{\pi}\rangle$ <p>x,y,z from $-\frac{1}{2}$ to $\frac{1}{2}$</p> <p>Setup 2</p>	<p>III. 4.f</p> <p>S*</p> $^{220}\langle (211)^{\pi/2}\rangle^{230}$ <p>Setup 2</p>
<p>III. 4.g</p> <p>I₂Y** – SS_z</p> $^{220}\langle (220)_2;(310)^{\pi/2}\rangle$ <p>Setup 3</p>	<p>III. 4.h</p> <p>(SI₂Y**)*</p> $^{220}\langle (310)^{\pi/2}\rangle^{230}$ <p>Setup 3</p>	<p>III. 4.i</p> <p>(WI_{xyz}²)*</p> $^{218}\langle (421)^{\pi/4}\rangle^{217}$ <p>Setup 3</p>
<p>III. 4.j</p> <p>II_{xxx}W* – I_{xxx}</p> $^{217}\langle (211)^{-\pi/4}\rangle$ <p>Setup 2</p>	<p>III. 4.k</p> <p>IJ*I_{xxx} – I_{xxx}W*</p> $^{217}\langle (220);(211)^{-\pi/2}\rangle$ <p>Setup 2</p>	<p>III. 4.l</p> <p>F* (D)</p> $^{216}\langle (111)_{\sqrt{2}}^{-\pi/4};(200)\rangle^{227}$ <p>Setup 2</p>
<p>Setup 1: </p> <p>Setup 2: </p> <p>Setup 3: </p>		

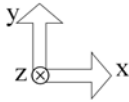
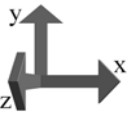
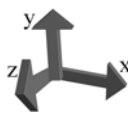


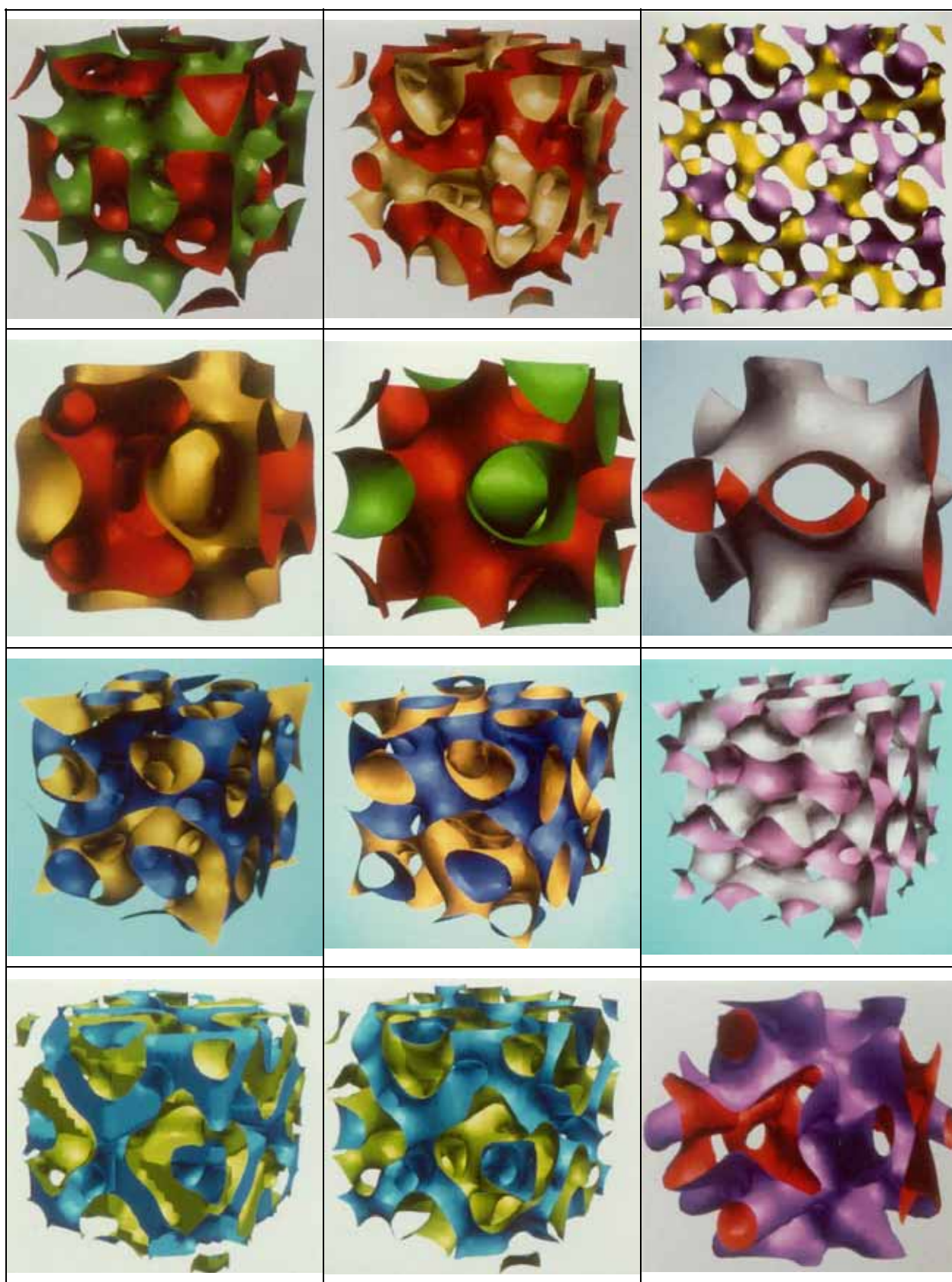
<p>Ill. 5.a</p> $(PP_{xxx})^*$ $^{215}\langle(100);(111)^{-\pi/2}\rangle^{217}$ <p>Setup 2</p>	<p>Ill. 5.b</p> $(PJ)^*$ $^{215}\langle(100)\sqrt{2};(111)^{\pi/4}\rangle^{217}$ <p>Setup 2</p>	<p>Ill. 5.c</p> $PP - JP_4$ $^{215}\langle(110);(111)^{\pi/4}\rangle$ <p>Setup 2</p>
<p>Ill. 5.d</p> $(PJP_{xxx}^2 P_z P_{zzx})^*$ $^{215}\langle(221)^{\pi/4}\rangle^{217}$ <p>Setup 3</p>	<p>Ill. 5.e</p> Y^{**} $^{214}\langle(110)^{\pi/2}\rangle^{230}$ <p>Setup 1</p>	<p>Ill. 5.f</p> $(YY_{xx})^*$ $^{214}\langle(110)_3^{\pi/2};(310)_2^{\pi/2}\rangle^{230}$ <p>Setup 2</p>
<p>Ill. 5.g</p> $(Y_{xxx} Y_{xyz})^*$ $^{212}\langle(221)^{\pi/2}\rangle^{214}$ <p>Setup 3</p>	<p>Ill. 5.h</p> Y^* $^{212}\langle(111)^{-\pi/4};(210)^{\pi/\sqrt{2}}\rangle^{214}$ <p>Setup 2</p>	<p>Ill. 5.i</p> $(YY_{xxx} Y_{xx})^*$ $^{212}\langle(111)^{-\pi/4};(210)\sqrt{2}\rangle^{214}$ <p>Setup 2</p>
<p>Ill. 5.j</p> P_{xxx}^* $^{206}\langle(200)_2;(321)^\pi;(231)^\pi\rangle^{230}$ <p>Setup 3</p>	<p>Ill. 5.k</p> $P_2 P_{2xxx} - P_{2xyz}$ $^{206}\langle(220)_2;(321)^\pi;(231)^\pi\rangle$ <p>Setup 2</p>	<p>Ill. 5.l</p> F_{xxx}^* $^{205}\langle 210 \rangle^{206}$ <p>Setup 2</p>
<p>Setup 1: </p> <p>Setup 2: </p> <p>Setup 3: </p>		



<p>Ill. 6.a</p> $^{205}\langle (111);(210)^\pi \rangle^{206}$ <p>Setup 2</p>	<p>Ill. 6.b</p> $^{205}\langle (111);(210) \rangle^{206}$ <p>Setup 2</p>	<p>Ill. 6.c</p> $^{205}\langle (111);(211) \rangle$ <p>Setup 2</p>
<p>Ill. 6.d</p> $^{205}\langle (111)_2;(210)^\pi;(220)^\pi \rangle$ <p>Setup 2</p>	<p>Ill. 6.e</p> $^{205}\langle (221) \rangle^{206}$ <p>Setup 2</p>	<p>Ill. 6.f</p> $^{205}\langle (111)_2;(210);(220) \rangle$ <p>Setup 2</p>
<p>Ill. 6.g</p> $^{204}\langle (310);(130)^\pi \rangle^{229}$ <p>Setup 3</p>	<p>Ill. 6.h</p> $^{204}\langle (321);(231)^\pi \rangle^{229}$ <p>Setup 3</p>	<p>Ill. 6.i</p> $^{204}\langle (310);(222)^\pi \rangle$ <p>Setup 3</p>
<p>Ill. 6.j</p> $^{204}\langle (211);(321) \rangle$ <p>Setup 3</p>	<p>Ill. 6.k</p> $^{204}\langle (222);(321)^\pi \rangle$ <p>Setup 3</p>	<p>Ill. 6.l</p> $^{204}\langle (200);(211)^\pi;(310)^\pi \rangle$ <p>Setup 2</p>
<p>Setup 2:  Setup 3: </p>		



<p>III. 7.a</p> $\frac{J_x^* I_{zx} - I P_2 I_{zx}}{204} \langle (220); (310) \rangle$ <p>Setup 3</p>	<p>III. 7.b</p> $\frac{I J_x^* I_{xxx} I_{zx} - I_z I_{zx}}{204} \langle (220); (321) \rangle$ <p>Setup 3</p>	<p>III. 7.c</p> $\frac{(D T D_{xxx}^2 D_{xyz})^*}{203} \langle 531 \rangle^{201}$ <p>x,y from 0 to 1 z from $\frac{7}{8}$ to 1</p> <p>Setup 1</p>
<p>III. 7.d</p> $\frac{(P J_x)^*}{200} \langle (110); (210) \rangle^{204}$ <p>Setup 2</p>	<p>III. 7.e</p> $\frac{(P J_x)^*}{200} \langle 210 \rangle^{204}$ <p>Setup 2</p>	<p>III. 7.f</p> $\frac{(P J_x P_{zx})^*}{200} \langle (100)_2; (210)^\pi \rangle^{204}$ <p>Setup 2</p>
<p>III. 7.g</p> $\frac{(P_2 Y^* S V P_2 Y_{yz}^*)^*}{199} \langle (222)^{\pi/2}; (321)^{\pi/2} \rangle^{206}$ <p>Setup 3</p>	<p>III. 7.h</p> $\frac{(P_2 Y^* S V P_2 Y_{yz}^*)^*}{199} \langle (222)_2^{-\pi/2}; (321)^{\pi/2} \rangle^{206}$ <p>Setup 3</p>	<p>III. 7.i</p> $\frac{(P_2 Y_{xxx} P_2 Y_{xyz})^*}{199} \langle (310)^{\pi/2} \rangle^{206}$ <p>Setup 3</p>
<p>III. 7.j</p> $\frac{(I_{xxx}^2 I_{xyz})^*}{197} \langle (321)^{\pi/2} \rangle^{204}$ <p>Setup 3</p>	<p>III. 7.k</p> $\frac{I J^* I_{xxx} I_{xyz} - I_{xxx}^2 I_z I_{xyz}}{197} \langle (222); (321)^{\pi/2} \rangle$ <p>Setup 3</p>	<p>III. 7.l</p> $\frac{(P J_x^2 P_{xyz})^*}{195} \langle (100)_4; (231)^{-3\pi/4}; (321)^{\pi/4} \rangle$ <p>Setup 2</p>
<p>Setup 1: </p> <p>Setup 2: </p> <p>Setup 3: </p>		



3.4. Characteristic Structure Factors $S(hkl)$ of Hexagonal and Trigonal Space Groups

3.4.1. Symmetry Patterns

Due to their non-orthogonal axes in the x-y-plane, hexagonal and trigonal space groups have a fourth, calculated index $i = -(h+k)$. While keeping the value of the structure factor constant, only the three indices h , k , and i can be permuted cyclicly: $|S(hkl)| = |S(ihk)| \neq |S(lhi)|$. Since the vectors \bar{h} , \bar{k} , \bar{i} are not orthogonal to one another, $|S(hkl)| \neq |S(\bar{h}\bar{k}\bar{l})|$. Due to their reduced symmetry from sixfold to threefold rotations, in trigonal crystal classes we have $|S(hk.l)| \neq |S(hk.\bar{l})|$. The rhombohedral space groups are a special case within the trigonal crystal class, because if setup rhombohedrally we have $a_r = b_r = c_r$, resulting in: $|S(hkl)| = |S(lhk)|$ but unlike cubic symmetries, due to $\alpha_r = \beta_r = \gamma_r \neq 90$ we have: $|S(hkl)| \neq |S(\bar{h}\bar{k}\bar{l})|$. These rhombohedral space groups can be setup trigonally when tripling the cell volume. They then obey the laws of the respective trigonal space groups. If symmetry operations $\parallel \{11.0\}$ exist, the respective hexagonal and trigonal space groups permit acyclic permutations of hki : $|S(hk.l)| = |S(kh.l)|$. Hence the hexagonal and trigonal crystal classes can be divided into four groups:

1. Inversion centre $\bar{1}$ and symmetry elements m , c and $2 \parallel \{11.0\}$, crystal classes $6/mmm$ and $\bar{3}m1$ or $\bar{3}1m$, respectively, with $\alpha = m\pi$ and $|S(hk.l)| = |S(kh.l)|$.
2. Symmetry elements m , c and $2 \parallel \{11.0\}$: crystal classes $62m$ (or $6m2$), $6mm$, 622 , $3m1$ (or $31m$) and 321 (or 312) with freely variable α and $|S(hk.l)| = |S(kh.l)|$.
3. Inversion center $\bar{1}$: crystal classes $\bar{3}$ and $6/m$ with $\alpha = m\pi$ and $|S(hk.l)| \neq |S(kh.l)|$.
4. Crystal classes $\bar{6}$, 6 and 3 with freely variable $\alpha(hk.l) \neq \alpha(kh.l)$ and $|S(hk.l)| \neq |S(kh.l)|$.

As no centering of the unit cell exists as such for hexagonal and trigonal space groups, most complications known from the cubic space groups are absent here. During the preparation of this work the question has not been investigated whether or not there are any cases where certain phase permutations of acentric space groups are equivalent to those of acentrically setup centric space groups.

3.4.2. Tables for $S(hkil)$ of Hexagonal and Trigonal Space Groups

In analogy to the tables for the cubic space groups (pp. 33ff.), Tables 9.1.1., 9.1.2., 9.2., 9.3.1., and 9.3.2. contain information about whether or not a certain structure factor is *characteristic* or even prohibited for the respective hexagonal, trigonal, and rhombohedral space group. The column to the right of the general conditions of the structure factor S and phase α for the respective crystal class gives the modulus j , which has to be entered into the equation in the head row of the subsequent columns with which the type of index l is determined. In absence of a screw axes with a value higher than 2 the permutation laws distinguish only between $l = 2n$ and $l = 2n + 1$. In case of screw axes $6_2/6_4$, $3_1/3_2$ and $6_1/6_5$, the laws are organized according to the multiplicity of the respective axis.

Characteristic Structure Factors $S(hkil)$

Table 9.1.2.: <i>hP</i> Space Groups with Patterson Symmetry 6/ <i>m</i>																
It holds: $ S(hkil) = S(ihkl) = S(kihl) $; $ S(hkil) = S(h\bar{k}il) $; $ S(hkil) = S(h\bar{k}\bar{l}) $; $ S(hkil) = S(h\bar{k}l) $; $ S(hkil) = S(h\bar{k}\bar{l}) $ r relations in Intern. Tables, Vol. I (1976) 367-525.																
For each structurr factor typ <i>hkil</i> the characteristic phase $\alpha(hkil)$ is given [α stands for $0 \leq \alpha(hkil) \leq 2\pi$]. If $\alpha(hkil)$ generates a differentsymmetry (non-characteristic structure factor), then the respective space group is given in (...).																
Crystal Class	Space Group		$ S(hkil) $ $\alpha(hkil)$	j	<i>l</i> = in						<i>l</i> = in ± 1					
	Symbol	No.			00. <i>l</i>	hh.0	h0.0	hk.0	hh. <i>l</i>	h0. <i>l</i>	hk. <i>l</i>	$\alpha = m\pi$	00. <i>l</i>	hh. <i>l</i>	h0. <i>l</i>	hk. <i>l</i>
6/ <i>m</i>	P ₆₃ / <i>m</i>	176	$ S(hkil) \neq S(khil) $	2	$\langle 191 \rangle$	$\langle 191 \rangle$	$\langle 191 \rangle$	$\langle 175 \rangle$	$\langle 191 \rangle$	$\langle 175 \rangle$	$\langle 175 \rangle$	$\langle 193 \rangle$	$m\pi$	$m\pi$	$m\pi$	$\langle 176 \rangle$
	P ₆ / <i>m</i>	175	$\alpha(hkil) = m\pi$		$\langle 191 \rangle$	$\langle 191 \rangle$	$\langle 191 \rangle$	$m\pi$	$\langle 191 \rangle$	$m\pi$	$\langle 175 \rangle$	$\langle 191 \rangle$	$m\pi$	$m\pi$	$m\pi$	$\langle 175 \rangle$
$\bar{6}$, C _{3h}	P $\bar{6}$	174	$ S(hkil) \neq S(khil) $ $0 \geq \alpha(hkil) \leq m\pi$	2	$\langle 191 \rangle$	$\langle 189 \rangle$	α	α	$\langle 189 \rangle$	α	$\langle 175 \rangle$	$\langle 189 \rangle$	α	α	α	$\langle 175 \rangle$
	P ₆₃	173		2	$\langle 183 \rangle$	$\langle 191 \rangle$	$\langle 191 \rangle$	$\langle 175 \rangle$	$\langle 183 \rangle$	$\langle 168 \rangle$	$\langle 168 \rangle$	$\alpha/m\pi + \pi/2$; $\langle 182 \rangle$	α	α	α	$\langle 175 \rangle$
C ₆	P ₆₄	172		3	$\langle 183 \rangle$	$\langle 191 \rangle$	$\langle 191 \rangle$	$\langle 175 \rangle$	$\langle 183 \rangle$	$\langle 168 \rangle$	$\langle 168 \rangle$	$\langle 176 \rangle$	$\langle 181 \rangle$	α	α	$\langle 172 \rangle$
	P ₆₂	171	$ S(hkil) \neq S(khil) $		$\langle 183 \rangle$	$\langle 191 \rangle$	$\langle 191 \rangle$	$\langle 175 \rangle$	$\langle 183 \rangle$	$\langle 168 \rangle$	$\langle 168 \rangle$	$\langle 176 \rangle$	$\langle 180 \rangle$	α	α	$\langle 171 \rangle$
	P ₆₅	170	$0 \geq \alpha(hkil) \leq m\pi$	6	$\langle 183 \rangle$	$\langle 191 \rangle$	$\langle 191 \rangle$	$\langle 175 \rangle$	$\langle 183 \rangle$	$\langle 168 \rangle$	$\langle 168 \rangle$	$\langle 176 \rangle$	$\langle 179 \rangle$	$6n \pm 1$: α	$6n \pm 2$: $\langle 171/2 \rangle$	$\langle 170 \rangle$
	P ₆₁	169	$\langle 183 \rangle$		$\langle 191 \rangle$	$\langle 191 \rangle$	$\langle 175 \rangle$	$\langle 183 \rangle$	$\langle 168 \rangle$	$\langle 168 \rangle$	$\langle 176 \rangle$	$\langle 178 \rangle$	$6n \pm 3$: $\langle 173 \rangle$			
	P ₆	168		2	$\langle 183 \rangle$	$\langle 191 \rangle$	$\langle 191 \rangle$	$\langle 175 \rangle$	$\langle 183 \rangle$	α	α	$\langle 183 \rangle$	α	α	α	$\langle 175 \rangle$
Closest to the origin <i>S(hkil)</i> ($\sum f_j = \min.$)				00. ℓ	11.0	10.0	12.0	11. ℓ	10. ℓ	12. ℓ		00. ℓ	11. ℓ	10. ℓ	12. ℓ	
				00. ℓ	22.0	20.0	13.0	22. ℓ	20. ℓ	13. ℓ		00. ℓ	22. ℓ	20. ℓ	13. ℓ	

Characteristic Structure Factors $S(hkil)$ Table 9.2.: trP Space Groups with Patterson Symmetry 6/m

It holds: $ S(hkil) = S(ihkl) = S(kihl) $; $ S(hkil) \neq S(hkl) $; $ S(hkil) \neq S(hkl) $; $ S(hkil) \neq S(hkl) $ relations in Intern. Tables, Vol. I (1976) 367-525. For each structurr factor $hkil$ the characteristic phase $\alpha(hkil)$ is given [α stands for $0 \leq \alpha(hkil) \leq 2\pi$]. If $\alpha(hkil)$ generates a differentsymmetry (non-characteristic structure factor), then the respective space group is given in (...).																																	
Crystal Class	Space Group Symbol	Space Group No.	$ S(hkil) $ $\alpha(hkil)$	j	$l = jn$												$l = jn \pm 1$																
					00.l	hh.0	h0.0	hk.0	hh.l	h0.l	hk.l	$\alpha = m\pi$	00.l	hh.l	h0.l	hk.l	$\alpha = m\pi$	00.l	hh.l	h0.l	hk.l	$\alpha = m\pi$											
$\bar{3}m1$ v.v. D_{3d}	$P\bar{3}c1$	165	$ S(hkil) = S(khil) $ $\alpha(hkil) = m\pi$	2	$\langle 162 \rangle$	$\langle 191 \rangle$	$\langle 191 \rangle$	$\langle 191 \rangle$	$\langle 162 \rangle$	$\langle 164 \rangle$	$\langle 164 \rangle$	$\langle 164 \rangle$	$ S = 0$	$\langle 162 \rangle$	$\langle 162 \rangle$	$ S = 0$	$\langle 164 \rangle$	$ S = 0$	$\langle 162 \rangle$	$\langle 162 \rangle$	$ S = 0$	$\langle 165 \rangle$	$ S = 0$	$\langle 162 \rangle$	$\langle 162 \rangle$	$ S = 0$	$\langle 165 \rangle$	$ S = 0$	$\langle 162 \rangle$	$\langle 162 \rangle$	$ S = 0$	$\langle 165 \rangle$	
	$P\bar{3}m1$	164			$\langle 162 \rangle$	$\langle 191 \rangle$	$\langle 191 \rangle$	$\langle 191 \rangle$	$\langle 162 \rangle$	$\langle 164 \rangle$	$\langle 164 \rangle$	$\langle 164 \rangle$	$ S = 0$	$\langle 162 \rangle$	$\langle 162 \rangle$	$ S = 0$	$\langle 164 \rangle$	$ S = 0$	$\langle 162 \rangle$	$\langle 162 \rangle$	$ S = 0$	$\langle 165 \rangle$	$ S = 0$	$\langle 162 \rangle$	$\langle 162 \rangle$	$ S = 0$	$\langle 165 \rangle$	$ S = 0$	$\langle 162 \rangle$	$\langle 162 \rangle$	$ S = 0$	$\langle 165 \rangle$	
	$P\bar{3}1c$	163			$\langle 162 \rangle$	$\langle 191 \rangle$	$\langle 191 \rangle$	$\langle 191 \rangle$	$\langle 162 \rangle$	$\langle 164 \rangle$	$\langle 164 \rangle$	$\langle 164 \rangle$	$ S = 0$	$\langle 162 \rangle$	$\langle 162 \rangle$	$ S = 0$	$\langle 164 \rangle$	$ S = 0$	$\langle 162 \rangle$	$\langle 162 \rangle$	$ S = 0$	$\langle 165 \rangle$	$ S = 0$	$\langle 162 \rangle$	$\langle 162 \rangle$	$ S = 0$	$\langle 165 \rangle$	$ S = 0$	$\langle 162 \rangle$	$\langle 162 \rangle$	$ S = 0$	$\langle 165 \rangle$	
	$P\bar{3}1m$	162			$m\pi$	$\langle 191 \rangle$	$\langle 191 \rangle$	$\langle 191 \rangle$	$m\pi$	$m\pi$	$m\pi$	$m\pi$	$m\pi$	$m\pi$	$m\pi$	$m\pi$	$m\pi$	$m\pi$	$m\pi$	$m\pi$	$m\pi$	$m\pi$	$m\pi$	$m\pi$	$m\pi$	$m\pi$	$m\pi$	$m\pi$	$m\pi$	$m\pi$	$m\pi$	$m\pi$	$m\pi$
$3m1$ v.v. C_{3v}	$P31c$	159	$ S(hkil) = S(khil) $ $0 \geq \alpha(hkil) \leq m\pi$	2	$\langle 157 \rangle$	$\langle 189 \rangle$	$\langle 191 \rangle$	$\langle 189 \rangle$	$\langle 157 \rangle$	$\langle 157 \rangle$	$\langle 156 \rangle$	$\langle 164 \rangle$	$ S = 0$	$\langle 157 \rangle$	$\langle 157 \rangle$	$ S = 0$	$\langle 164 \rangle$	$ S = 0$	$\langle 157 \rangle$	$\langle 157 \rangle$	$ S = 0$	$\langle 165 \rangle$	$ S = 0$	$\langle 157 \rangle$	$\langle 157 \rangle$	$ S = 0$	$\langle 165 \rangle$	$ S = 0$	$\langle 157 \rangle$	$\langle 157 \rangle$	$ S = 0$	$\langle 165 \rangle$	
	$P3c1$	158			$\langle 157 \rangle$	$\langle 191 \rangle$	$\langle 187 \rangle$	$\langle 187 \rangle$	$\langle 157 \rangle$	$\langle 157 \rangle$	$\langle 156 \rangle$	$\langle 164 \rangle$	$ S = 0$	$\langle 157 \rangle$	$\langle 157 \rangle$	$ S = 0$	$\langle 164 \rangle$	$ S = 0$	$\langle 157 \rangle$	$\langle 157 \rangle$	$ S = 0$	$\langle 165 \rangle$	$ S = 0$	$\langle 157 \rangle$	$\langle 157 \rangle$	$ S = 0$	$\langle 165 \rangle$	$ S = 0$	$\langle 157 \rangle$	$\langle 157 \rangle$	$ S = 0$	$\langle 165 \rangle$	
	$P31m$	157			α	$\langle 189 \rangle$	$\langle 191 \rangle$	$\langle 189 \rangle$	α	α	α	α	α	α	α	α	α	α	α	α	α	α	α	α	α	α	α	α	α	α	α	α	
	$P3m1$	156			$\langle 157 \rangle$	$\langle 191 \rangle$	$\langle 187 \rangle$	$\langle 187 \rangle$	$\langle 157 \rangle$	$\langle 157 \rangle$	$\langle 150 \rangle$	$\langle 164 \rangle$	$ S = 0$	$\langle 157 \rangle$	$\langle 157 \rangle$	$ S = 0$	$\langle 164 \rangle$	$ S = 0$	$\langle 157 \rangle$	$\langle 157 \rangle$	$ S = 0$	$\langle 165 \rangle$	$ S = 0$	$\langle 157 \rangle$	$\langle 157 \rangle$	$ S = 0$	$\langle 165 \rangle$	$ S = 0$	$\langle 157 \rangle$	$\langle 157 \rangle$	$ S = 0$	$\langle 165 \rangle$	
321 v.v. D_3	$P3_21$	154	$ S(hkil) = S(khil) $ $0 \geq \alpha(hkil) \leq m\pi$	3	$\langle 162 \rangle$	$\langle 189 \rangle$	$\langle 191 \rangle$	$\langle 189 \rangle$	$\langle 157 \rangle$	$\langle 157 \rangle$	$\langle 164 \rangle$	$\langle 150 \rangle$	$ S = 0$	$\langle 162 \rangle$	$\langle 162 \rangle$	$ S = 0$	$\langle 164 \rangle$	$ S = 0$	$\langle 162 \rangle$	$\langle 162 \rangle$	$ S = 0$	$\langle 165 \rangle$	$ S = 0$	$\langle 162 \rangle$	$\langle 162 \rangle$	$ S = 0$	$\langle 165 \rangle$	$ S = 0$	$\langle 162 \rangle$	$\langle 162 \rangle$	$ S = 0$	$\langle 165 \rangle$	
	$P3_212$	153			$\langle 162 \rangle$	$\langle 191 \rangle$	$\langle 187 \rangle$	$\langle 187 \rangle$	$\langle 162 \rangle$	$\langle 149 \rangle$	$\langle 149 \rangle$	$\langle 162 \rangle$	$ S = 0$	$\langle 162 \rangle$	$\langle 162 \rangle$	$ S = 0$	$\langle 164 \rangle$	$ S = 0$	$\langle 162 \rangle$	$\langle 162 \rangle$	$ S = 0$	$\langle 165 \rangle$	$ S = 0$	$\langle 162 \rangle$	$\langle 162 \rangle$	$ S = 0$	$\langle 165 \rangle$	$ S = 0$	$\langle 162 \rangle$	$\langle 162 \rangle$	$ S = 0$	$\langle 165 \rangle$	
	$P3_21$	152			$\langle 162 \rangle$	$\langle 189 \rangle$	$\langle 191 \rangle$	$\langle 189 \rangle$	$\langle 157 \rangle$	$\langle 164 \rangle$	$\langle 150 \rangle$	$\langle 164 \rangle$	$ S = 0$	$\langle 162 \rangle$	$\langle 162 \rangle$	$ S = 0$	$\langle 164 \rangle$	$ S = 0$	$\langle 162 \rangle$	$\langle 162 \rangle$	$ S = 0$	$\langle 165 \rangle$	$ S = 0$	$\langle 162 \rangle$	$\langle 162 \rangle$	$ S = 0$	$\langle 165 \rangle$	$ S = 0$	$\langle 162 \rangle$	$\langle 162 \rangle$	$ S = 0$	$\langle 165 \rangle$	
	$P3_112$	151			$\langle 162 \rangle$	$\langle 191 \rangle$	$\langle 187 \rangle$	$\langle 187 \rangle$	$\langle 162 \rangle$	$\langle 149 \rangle$	$\langle 149 \rangle$	$\langle 162 \rangle$	$ S = 0$	$\langle 162 \rangle$	$\langle 162 \rangle$	$ S = 0$	$\langle 164 \rangle$	$ S = 0$	$\langle 162 \rangle$	$\langle 162 \rangle$	$ S = 0$	$\langle 165 \rangle$	$ S = 0$	$\langle 162 \rangle$	$\langle 162 \rangle$	$ S = 0$	$\langle 165 \rangle$	$ S = 0$	$\langle 162 \rangle$	$\langle 162 \rangle$	$ S = 0$	$\langle 165 \rangle$	
	$P321$	150			$\langle 162 \rangle$	$\langle 189 \rangle$	$\langle 191 \rangle$	$\langle 189 \rangle$	$\langle 157 \rangle$	$\langle 164 \rangle$	α	$\langle 164 \rangle$	$ S = 0$	$\langle 162 \rangle$	$\langle 162 \rangle$	$ S = 0$	$\langle 164 \rangle$	$ S = 0$	$\langle 162 \rangle$	$\langle 162 \rangle$	$ S = 0$	$\langle 165 \rangle$	$ S = 0$	$\langle 162 \rangle$	$\langle 162 \rangle$	$ S = 0$	$\langle 165 \rangle$	$ S = 0$	$\langle 162 \rangle$	$\langle 162 \rangle$	$ S = 0$	$\langle 165 \rangle$	
	$P312$	149			$\langle 162 \rangle$	$\langle 191 \rangle$	$\langle 187 \rangle$	$\langle 187 \rangle$	$\langle 162 \rangle$	α	α	α	α	α	α	α	α	α	α	α	α	α	α	α	α	α	α	α	α	α	α	α	α
$\bar{3}, C_{3i}$	$P\bar{3}$	147	$ S(hkil) \neq S(khil) $ $\alpha(hkil) = m\pi$	2	$\langle 162 \rangle$	$\langle 191 \rangle$	$\langle 175 \rangle$	$\langle 175 \rangle$	$\langle 162 \rangle$	$m\pi$	$m\pi$	$m\pi$	$\langle 147 \rangle$	$\langle 162 \rangle$	$\langle 162 \rangle$	$\langle 147 \rangle$	$\langle 147 \rangle$	$\langle 162 \rangle$	$\langle 162 \rangle$	$\langle 147 \rangle$	$\langle 147 \rangle$	$\langle 147 \rangle$	$\langle 147 \rangle$	$\langle 162 \rangle$	$\langle 162 \rangle$	$\langle 147 \rangle$	$\langle 147 \rangle$	$\langle 162 \rangle$	$\langle 162 \rangle$	$\langle 147 \rangle$	$\langle 147 \rangle$	$\langle 147 \rangle$	$\langle 147 \rangle$
	$P3_2$	145			$\langle 157 \rangle$	$\langle 189 \rangle$	$\langle 174 \rangle$	$\langle 174 \rangle$	$\langle 157 \rangle$	$\langle 143 \rangle$	$\langle 143 \rangle$	$\langle 147 \rangle$	$\langle 157 \rangle$	$\langle 157 \rangle$	$\langle 154 \rangle$	$\langle 147 \rangle$	$\langle 157 \rangle$	$\langle 157 \rangle$	$\langle 154 \rangle$	$\langle 147 \rangle$	$\langle 147 \rangle$	$\langle 147 \rangle$	$\langle 157 \rangle$	$\langle 157 \rangle$	$\langle 154 \rangle$	$\langle 147 \rangle$	$\langle 157 \rangle$	$\langle 157 \rangle$	$\langle 154 \rangle$	$\langle 147 \rangle$	$\langle 147 \rangle$	$\langle 147 \rangle$	
	$P3_1$	144			$\langle 157 \rangle$	$\langle 189 \rangle$	$\langle 174 \rangle$	$\langle 174 \rangle$	$\langle 157 \rangle$	$\langle 143 \rangle$	$\langle 143 \rangle$	$\langle 147 \rangle$	$\langle 157 \rangle$	$\langle 157 \rangle$	$\langle 154 \rangle$	$\langle 147 \rangle$	$\langle 157 \rangle$	$\langle 157 \rangle$	$\langle 154 \rangle$	$\langle 147 \rangle$	$\langle 147 \rangle$	$\langle 147 \rangle$	$\langle 157 \rangle$	$\langle 157 \rangle$	$\langle 154 \rangle$	$\langle 147 \rangle$	$\langle 157 \rangle$	$\langle 157 \rangle$	$\langle 154 \rangle$	$\langle 147 \rangle$	$\langle 147 \rangle$	$\langle 147 \rangle$	
	$P3$	143			$\langle 157 \rangle$	$\langle 189 \rangle$	$\langle 174 \rangle$	$\langle 174 \rangle$	$\langle 157 \rangle$	α	α	α	$\langle 147 \rangle$	$\langle 157 \rangle$	$\langle 157 \rangle$	α	$\langle 147 \rangle$	$\langle 157 \rangle$	$\langle 157 \rangle$	α	α	α	$\langle 147 \rangle$	$\langle 157 \rangle$	$\langle 157 \rangle$	α	α	α	α	α	α	α	α
Closest to the origin $S(hkil) (\sum l^2 = \min.)$					00. ℓ	11.0	10.0	12.0	11. ℓ	10. ℓ	12. ℓ		00. ℓ	11. ℓ	10. ℓ	12. ℓ		00. ℓ	11. ℓ	10. ℓ	12. ℓ		00. ℓ	11. ℓ	10. ℓ	12. ℓ		00. ℓ	11. ℓ	10. ℓ	12. ℓ		
					00. ℓ	22.0	20.0	13.0	22. ℓ	20. ℓ	13. ℓ		00. ℓ	22. ℓ	20. ℓ	13. ℓ		00. ℓ	22. ℓ	20. ℓ	13. ℓ		00. ℓ	22. ℓ	20. ℓ	13. ℓ		00. ℓ	22. ℓ	20. ℓ	13. ℓ		

Characteristic Structure Factors $S(hkl)$

Table 9.3.1.: trR Space Groups, Rhombohedral Setup									
It holds: $ S(hkl) = S(lhk) = S(klh) $; $ S(hkl) \neq S(hkl) $; $\alpha(hkl)$ relations in Intern. Tables, Vol. I (1976) 367-525. For each structure factor type hkl the characteristic phase $\alpha(hkl)$ is given [α stands for $0 \leq \alpha(hkl) \leq 2\pi$]. If $\alpha(hkl)$ generates a difference symmetry (non-characteristic structure factor), then the respective space group is given in (...). In case of appropriate cell metrics, structure factor types $h00$ have cubic symmetry; the respective space group e is given as an index to the phases: $\alpha_{(\dots)}$.									
Crystal Class	Space Group	$ S(hkl) $	$\Sigma h_i = 2n$						$\Sigma h_i = 2n + 1$
Symbol	No.	$\alpha(hkl)$	$h00$	$hh0$	$hk0$	hhh	hhl	hkl	$\alpha = m\pi$
$\bar{3}m$	R3c	167	$\langle 166 \rangle$	$\langle 166 \rangle$	$\langle 166 \rangle$	$\langle 166 \rangle$	$\langle 166 \rangle$	$\langle 166 \rangle$	$\alpha = m\pi$
D_{3d}	$R\bar{3}m$	166	$m\pi_{(221)}$	$m\pi$	$m\pi$	$m\pi$	$m\pi$	$m\pi$	$\langle 166 \rangle$
$3m$	R3c	161	$\langle 160 \rangle$	$\langle 160 \rangle$	$\langle 160 \rangle$	$\langle 160 \rangle$	$\langle 160 \rangle$	$\langle 160 \rangle$	α
C_{3v}	R3m	160	$\alpha'_{(215)}$	α	α	α	α	α	$\langle 166 \rangle$
32	R32	155	$\langle 166 \rangle$	$\langle 166 \rangle$	α	$\langle 166 \rangle$	$\langle 166 \rangle$	α	$\langle 166 \rangle$
D_3	$\bar{3}$	148	$\langle 166 \rangle$	$\langle 166 \rangle$	$m\pi$	$\langle 166 \rangle$	$\langle 166 \rangle$	$m\pi$	$\langle 148 \rangle$
C_{3i}	R3	146	$\langle 160 \rangle$	$\langle 160 \rangle$	α	$\langle 160 \rangle$	$\langle 160 \rangle$	α	$\langle 148 \rangle$
Closest to the origin $S(hkl)$ ($\Sigma h_i = \min.$)									
			200	110	310	222	112	321	100
			400	220	420	444	114	421	300
									210
									320
									111
									221
									421
									423

Characteristic Structure Factors $S(hkil)$

Table 9.3.2.: trR Space Groups, trP Setup									
The same laws apply as in Table 9.2. The characteristic structure factors of rhombohedral symmetry in trigonal setup behave as the space groups of trigonal symmetry given underneath. In addition to this the following holds for an obverse setup: $-h + k + l = 3n$.									
trP Space Group	R3c, 167	$R\bar{3}m$, 166	R3c, 161	R3m, 160	R32, 155	$R\bar{3}$, 148	R3, 146		
trR Space Group	$P\bar{3}c1$, 165	$P\bar{3}m1$, 164	$P3c1$, 158	$P3m1$, 156	$P321$, 150	$P\bar{3}$, 147	$P3$, 143		

Tab. 10.1.: <i>hP</i> Space Groups, Characteristic $S(hk.l)$				
Crystal Class	Space group	j	Structure Factor Types	
			$\ell = jn$	$\ell = jn \pm 1$
6/mmm D _{6h}	194, P _{6₃} /mmc	2	–	h0. ℓ , hk. ℓ
	193, P _{6₃} /mcm		–	hh. ℓ , hk. ℓ
	192, P _{6₃} /mcc		–	hk. ℓ
	191, P _{6₃} /mmm		general	general
62m	190, P $\bar{6}2c$	2	–	hk. ℓ
6m2	189, P $\bar{6}2m$		hh.0, hk.0, hh. ℓ , hk. ℓ	hh. ℓ , hk. ℓ
D _{3h}	188, P $\bar{6}c2$		–	hk. ℓ
	187, P $\bar{6}m2$		h0.0, hk.0, h0. ℓ , hk. ℓ	h0. ℓ , hk. ℓ
6mm C _{6v}	186, P _{6₃} mc	2	–	h0. ℓ , hk. ℓ
	185, P _{6₃} cm		–	hh. ℓ , hk. ℓ
	184, P $\bar{6}cc$		–	hk. ℓ
	183, P $\bar{6}mm$		00. ℓ , hh. ℓ , h0. ℓ , hk. ℓ	general
622 D ₆	182, P _{6₃} 22	2	–	hh. ℓ , hk. ℓ
	181, P _{6₄} 22	3	–	hh. ℓ , h0. ℓ , hk. ℓ
	180, P _{6₂} 22		–	hk. ℓ , hh. ℓ , h0. ℓ
	179, P _{6₅} 22	6	–	6n \pm 1: hh. ℓ , h0. ℓ , hk. ℓ
	178, P _{6₁} 22		–	6n \pm 1: hh. ℓ , h0. ℓ , hk. ℓ
	177, P $\bar{6}22$	2	hk. ℓ	hk. ℓ
6/m C _{6h}	176, P _{6₃} /m	2	–	h0. ℓ , hk. ℓ
	175, P $\bar{6}$ /m		hk.0, h0. ℓ , hk. ℓ	h0. ℓ , hk. ℓ
$\bar{6}$ / C _{3h}	174, P $\bar{6}$		h0.0, hk.0, h0. ℓ , hk. ℓ	h0. ℓ , hk. ℓ
6 C ₆	173, P _{6₃}	2	–	hh. ℓ , h0. ℓ , hk. ℓ
	172, P _{6₄}	3	–	h0. ℓ , hk. ℓ
	171, P _{6₂}		–	h0. ℓ , hk. ℓ
	170, P _{6₅}	6	–	6n \pm 1: h0. ℓ , hk. ℓ
	169, P _{6₁}		–	6n \pm 1: h0. ℓ , hk. ℓ
	168, P $\bar{6}$	2	h0. ℓ , hk. ℓ	h0. ℓ , hk. ℓ

Tab. 10.2.: <i>trP</i> Space Groups, Characteristic $S(hk.l)$				
Crystal Class	Space Group	j	Structure Factor Types	
			$\ell = jn$	$\ell = jn \pm 1$
$\bar{3}m1$ v.v. D_{3d}	165, $P\bar{3}c1$	2	–	$hk.l$
	164, $P\bar{3}m1$		$h0.l, hk.l$	$h0.l, hk.l$
	163, $P\bar{3}1c$		–	$hk.l$
	162, $P\bar{3}1m$		$00.l, hh.l, h0.l, hk.l$	$00.l, hh.l, h0.l, hk.l$
$3m1$ v.v. C_{3v}	159, $P31c$	2	–	$h0.l, hk.l$
	158, $P3c1$		–	$hk.l$
	157, $P31m$		$00.l, hh.l, h0.l, hk.l$	$00.l, hh.l, h0.l, hk.l$
	156, $P3m1$		$h0.l, hk.l$	$h0.l, hk.l$
321 v.v. D_3	154, $P3_221$	3	–	$hh.l, h0.l, hk.l$
	153, $P3_212$		–	$hh.l, h0.l, hk.l$
	152, $P3_121$		–	$hh.l, h0.l, hk.l$
	151, $P3_112$		–	$hh.l, h0.l, hk.l$
	150, $P321$	2	$hk.l$	$hk.l$
	149, $P312$		$h0.l, hk.l$	$h0.l, hk.l$
$\bar{3} / C_{3i}$	147, $P\bar{3}$	2	$h0.l, hk.l$	$h0.l, hk.l$
3 C_3	145, $P3_2$	3	–	$h0.l, hk.l$
	144, $P3_1$		–	$h0.l, hk.l$
	143, $P3$	2	$h0.l, hk.l$	$h0.l, hk.l$

Tab. 10.3.1.: <i>trR</i> Space Groups, <i>R</i> Setup, Characteristic $S(hkl)$				10.3.2.: <i>trR</i> Space Groups, <i>trP</i> Setup, Characteristic $S(hk.l)$; General Condition: $-h+k+l=3n$ (obverse)		
Crystal Class	Space Group	Structure Factor Types		Crystal Class	Space Group	cp. <i>trP</i> SG No. (Tab. 10.2)
		$\Sigma h_j = 2n$	$\Sigma h_j = 2n+1$			
$\bar{3}m$	167, $R\bar{3}c$	–	$hk0, hk\ell$	$\bar{3}m$	167, $R\bar{3}c$	165
D_{3d}	166, $R\bar{3}m$	General	general	D_{3d}	166, $R\bar{3}m$	164
$3m$	161, $R3c$	–	$hk0, hk\ell$	$3m$	161, $R3c$	158
C_{3v}	160, $R3m$	General	general	C_{3v}	160, $R3m$	156
$32 / D_3$	155, $R32$	$hk0, hk\ell$	$hk0, hk\ell$	$32 / D_3$	155, $R32$	150
$\bar{3} / C_{3i}$	148, $R\bar{3}$	$hk0, hk\ell$	$hk0, hk\ell$	$\bar{3} / C_{3i}$	148, $R\bar{3}$	147
$3 / C_3$	146, $R3$	$hk0, hk\ell$	$hk0, hk\ell$	$3 / C_3$	146, $R3$	143

3.5. Periodic Nodal Surfaces PNS with hexagonal and trigonal Symmetry

As for the PNS with cubic symmetry (Tables 6.1.to 6.3., pp. 36f.), one can glean from the Tables 10.1. to 10.3.2. the characteristic structure factors for all space groups of the hexagonal (hP), trigonal (trP), and the rhombohedral (trR) symmetry classes. Since these classes have different laws regarding the index l , no explicit $S(hkil)$ and $S(hkl)$, respectively, are given. Together with the non-characteristic $S(hk(i)l)$, this again sets the frame within which Fourier series with the desired symmetries of the respective hexagonal and trigonal space groups can be generated. Here as well space groups with low symmetry – and especially in absence of screw axes of higher order – have severe restrictions regarding the number of $S(hk(i)l)$ close to the reciprocal origin allowing the generation of a function with the aimed-at symmetry.

The computational generation and naming of the PNS follows the rules as developed for the cubic nodal surfaces.

The subsequent Table 11 (p. 77) lists the main characteristics of periodic nodal surfaces generated prior to and during the preparation of the current work, in analogy to the pattern described for the cubic surfaces (Table 8, p. 44ff.).

Name	hkl	$ S $	α	Generating Space Group	Eigen Symmetry	Extrema	Point Configuration
P – G	00.1 10.0	1 1	0 0	P6/mmm	P6/mmm	1a: 4 2d: -2.5	P G
P _c – E ²	10.0 00.2	1 1	0 0	P6/mmm	P6/mmm	2a: 4 2c/d: -2.5	P _c E
(PGP _x P _{xx̄})*	20.1 21.1	1 1	0 0	P6/mmm	P6/mmm	1a/b: ± 18 ; 2d/c: ± 9 6k/j: ± 8.83 ; x = 0.22 6l/m: ± 4.66 ; x = 0.218	P; G P _{6x} P _{6xx̄}
(PGNP _{6xx̄})*	11.1 20.1	1 1	0 0	P6/mmm	P6/mmm	1a/b: ± 12 ; 2c/d: ± 3 ; 3f/g: ± 4 6m/l: ± 5 ; x = $\frac{1}{6}$	P; G; N P _{6xx̄}
PG – P _x	00.1 11.0 10.1	2 1 1	0 0 π	P6/mmm	P6/mmm	1a: 5 2c: 5 6k: -2.5 ; x = $\frac{1}{3}$	P G P _{2x}
PN ² – G _z P _{xx̄z}	00.2 20.0 10.1	1 1 1	0 0 0	P6/mmm	P6/mmm	1a: 10; 3f: 2; 3g: 6 4h: -3.63 ; z = 0.12 12o: -3.05 ; x = 0.11, y = 0.43	P; N; N G _z P _{xx̄z}
E*	10.1	1	0	P6 ₃ /mmc	P6/mmm	2c/d: ± 5.20	E
(Pc _{3x})*	11.1	1	0	P6 ₃ /mcm	P6/mmm	6g: ± 5.20 ; x ⁺ = $-x^-$ = $\frac{1}{3}$; y [±] = 0	Pc _{3x}
P* (E in ^[39])	00.1 10.0	1 1	0 $-\frac{\pi}{2}$	P6m2	P6 ₃ /mmc	1c/e: ± 3.60	P
(P _{2z})*	10.0	1	$-\frac{\pi}{2}$	P6m2	P6/mmm	2h/i: ± 2.60 ; z = 0 – 1	P _{2z}
Q*	10.1	1	0	P6 ₂ 22	P6 ₄ 22	3c/d: ± 4	⁺ Q
P ² P ² _{6xx̄} P _{6xz} – P _{6xz}	00.2 11.1	1 1	0 π	P31m	P31m	1a/b: 1 6i/j: 1; x = 0.34 6k: 4.20; x = $\frac{1}{3}$; y = $\frac{1}{4}$ 6k: -6.20 ; x = $\frac{1}{3}$; y = $\frac{3}{4}$	P P _{6xx̄} P _{6xz} P _{6xz}
P _{2z} G _{2z} P _{6xz2y} – PG _{2z} P _{6xz}	11.1 11.2	1 1	0 0	P31m	P31m	2e: 6; z = $\frac{1}{2}$; 4h: 6; z = $\frac{1}{4}$ 12l: $4\frac{1}{8}$; x = 0; y = $\frac{1}{3}$; z = 0.07 1a: -6 ; 4h: -6 ; z = 0 6k: -8.20 ; x = $\frac{2}{3}$; y = $\frac{1}{4}$	P _{2z} ; G _{2z} P _{6xz2y} P; G _{2z} P _{6xz}
(P _{6xz})*	11.1	1	0	P31m	P6/mmm	6k: ± 5.20 ; x ⁺ = $-x^-$ = $\frac{1}{3}$; z [±] = $\frac{1}{4}$	P _{6xz}

4. Mathematical Analysis of PNS and their Generating Functions

4.1. Degree of Freedom of the Generating Function

Some of the periodic nodal surfaces introduced here require for their generation merely one structure factor $S(hkl)$, others need two or even three. In general each characteristic structure factor generates a periodic nodal surface without any need for additional structure factors. In many cases, however, the use of only one $S(hkl)$ generates nodal surfaces with point-like intersections (singularities, see Ill. 2.e), with spherical surfaces or with at times very narrow tunnels of high curvature (see Ill. 7.i). In order to generate surfaces without intersections and with a more evenly distributed curvature, it is necessary to sometimes use a second or even third structure factor (see Ill. 7.d, 7.e).

Intersections along a line are observed more frequently (Ill. 3.a, 3.f) and are also known from zero-potential surfaces.^[39]

If using several $S(hkl)$, the choice of the relative value of the structure factors $|S(hkl)|$ and their phases α is frequently restricted only by the requirement to avoid intersections and objects of positive Gaussians curvature (spheres). This determines the scope within which these parameters can be freely set and can also be adjusted to fit individual features of certain chemical structures.

One mathematical characteristic of PNS is therefore their degree of freedom DF , when calculating them. If using only one $S(hkl)$, then $DF=0$. Hence, the PNS generated with just one characteristic $S(hkl)$ depict fundamental symmetry properties. With growing numbers of $S(hkl)$ used for the generation, the degree of freedom rises accordingly with the combinatorial possibilities.

4.2. Extrema and Line Segment Graphs of Generating Functions

Since the generating Fourier series consist of trigonometric functions with coefficients hkl of a low order, their function values vary moderately within space. Extreme gradients cannot exist. The distribution of the function values obeys the symmetry laws of the respective generating space group. The same is true for special values of the function: zero values (nodes) and extrema. We will subsequently focus on extrema.

A special program has been used to determine the extrema of all PNS-generating

functions investigated during this work.^[106] The position of the extrema permits the determination of the symmetry of both the generating function as well as of the generated nodal surface (chapter 4.4.).

The point configuration correlating to these positions yield the names for these surfaces following the extrema nomenclature. The same program also allows determining which value the function has along certain line segments, spheres or isohypses.

The extrema of the generating functions of several nodal surfaces do not consist of certain (zero-dimensional) point-like positions but stretch out along lines throughout the entire unit cell. These are one-dimensional extrema lines which generate a *line graph* of constant function values throughout the labyrinth of the nodal surface. Following the term point configuration, these *line graphs* make up a specific *line configuration*.

There are furthermore cases where the function's values decrease only slightly between two point-like extrema. In such and similar cases one can construct a *graph* within the maze of the nodal surface which connects the extrema along such extreme value ridges. We call the connecting lines *line segments*. Orthogonal to these *line segments* the function's values decrease steadily. Hence, if analyzing a two-dimensional cross-section of the function's space orthogonal to the *line segment*, the point where it cuts through the *line segment* is always an extremum. The fragments of such *line segment graphs* correlating to point configurations we term accordingly: *line segment configurations*. In contrast to *line graphs* with constant maximum values running linearly through the entire unit cell, the connecting points of *line segments* within a *line segment graph* are also locations of change of direction of the graph as well as frequently also points of furcations.

Similar to equi-potential surfaces, the use of Fourier series also allows the use of function values $f(x,y,z) \neq 0$ to generate surfaces, although these are not nodal surfaces (\equiv zero-value surfaces). With increasing approximation of this value to the extrema of the generating functions, the thusly created surface spatially and morphologically increasingly resembles extrema graphs. In such cases the eigen symmetry of the surfaces is always identical to the generating symmetry. Hence, besides the zero values, the extrema are function values of particular interest. They serve:

- a) to analyze the symmetry (chapter 4.4., p. 87),
- b) to analyze the genus of the nodal surface (chapter 4.5., p. 92).

In Table 12 (p. 84) the *line graphs* and *line segment graphs* of several PNS are listed. Column 1 contains the name following the extrema nomenclature, columns 2 to 4 in this

order hkl , $|S|$, α . Column 5 gives the generating symmetry (in parentheses the eigen symmetry of the surface, if different), and column 6 the point configuration of the extrema (with function value in parentheses), which constitutes the point configuration (\Rightarrow italics) of the graph. The latter is generated by the given variation of the free parameter(s) of this point configuration (e.g. for $I_2 - Y^{**}V^*$: $y = 0 \rightarrow 1$ for $0 \leq y \leq 1$). If both partial spaces exhibit black-white symmetry (cp. chapter 4.4.1.) then the respective point configurations of the graphs are merged into a point configuration of the according supergroup (brace). Column 7 contains the name of the *line segment configuration*. The nomenclature of these *line segment configurations* closely follows the rules for the description of homogeneous networks as introduced by Hellner, Koch, and Reinhardt.^[107] It starts with the capital letters of the point configuration PC of the generating, partly special position (x,y,z) , followed by the parameters of the partly special position in parentheses and as its index i and exponent e the lower and upper limit of the variation of the free parameter(s) of this partly special position, respectively:

$$PC(x,y,z)_i^e \quad (22)$$

Since the labyrinths of many nodal surfaces are characterized by at times curved *line segments* generated by general positions, this method cannot be used to universally characterize PNS. But already the naming of linear *line segment graphs* can be cumbersome, as is demonstrated by the *line segment graph* $Y^{**}(x,y,z)_{x=3/8, y=0, z=1/4}^{x=5/16, y=1/16, z=3/8}$, which connects the point configuration S^* .

All graphs in the mazes of PNS mentioned in the present work have been known and described before.^[49,52,107,108] Some of them will nevertheless be discussed here before going into more details in connection with chemical structures (chapter 6., pp. 117ff.).

Four of the *line segment graphs* listed in Table 12 consist of *line graphs* of constant values in both partial spaces, where (one of) the free parameter(s) runs through the entire unit cell from 0 to 1. These are the PNS $Y_{xxx}^{**} - S^*$, $I_{xxx} - J^*$, $P_2 - IW_z$ and $IF_{xx} - I_{xxx}W^*$. Hence, in these cases we are dealing with *line configurations* instead of *line segment configurations*.

The constant *line graphs* of the PNS $P_2 - IW_z \triangleq {}^{223}\langle (110)_2^\pi; (200)_4^\pi; (210) \rangle$ and $Y_{xxx}^{**} - S^* \triangleq {}^{230}\langle (211)^\pi; (220) \rangle$ constitute the well-known three and four rod packings, respectively (Ill. 3.g and 2.b). The generating functions of these PNS generate in one of the partial spaces a constant distribution of extrema identical to these rod packings. The associated PNS wrap these rod packings.^[62] The graphs of the other partial spaces allow

conclusions about the topology of the respective surfaces (chapter 4.5., pp. 92f.).

The PNS $FF_{zx} - FP_2 \triangleq {}^{225}\langle(111)_2; (220)^\pi\rangle$ is an exception (Ill. 3.b). Except for small geometric deviations, this surface is almost identical to the minimal surface F-RD.^[5] To our illustration have been added the extrema of the generating function, rendered as spheres with a radius proportional to the value of the function. Due to the iterative detection of these extrema, there are gaps between the spheres in this illustration. In reality, the extrema of constant values form the main circles of a slightly deformed sphere around the position $\frac{1}{2}\frac{1}{2}0$. The sphere has a radius of $a/6$ along $[100]$ and $\sqrt{(a/8)^2 + (a/8)^2} = 0.1768 \times a$ along $[110]$, which is a deformation ratio of 1:1.061. The generating point configuration is F_{zx} with various values for x and y . The huge “hollow” space of this partial space of this PNS with 12 exits (the vertices of a cuboctahedron) is therefore not generated by just one extremum as in most other PNS but instead by a spherical arrangement of three extremum ellipses. The ratio of the radii of the PNS-equivalent of the P^* surface, by the way, have the reverse deformation value. The circular openings at the border of the unit cell has a ratio of radii $r[100]/r[110]$ of $a/4 : \sqrt{(a/6)^2 + (a/6)^2}$, which amounts to 1.061:1.

4.3. Surface Area and Volume Distribution of Nodal Surfaces

As has been described already by Schoen^[5] and has later also been used by Oehme,^[39] the dimensionless reduced surface area F_R^0 of a repetitive unit of a PMS or POPS can be used as a measure to gauge the surface requirement of a space divider. This quantity can be seen as a measure for the complicatedness or complexity of a space divider. The higher the surface need within a unit cell, the higher the average curvature of the respective space divider. For the reduced surface area F_R^0 the surface area F is set into relation to the volume V of the *primitive* unit cell:

$$F_R^0 = \frac{F/\mathfrak{z}}{(V/\mathfrak{z})^{2/3}} = \frac{F_R}{\mathfrak{z}^{1/3}} \quad (23)$$

$$\begin{aligned} \text{with } \mathfrak{z} &= 1 \text{ for } P\text{-types} \\ \mathfrak{z} &= 2 \text{ for } I\text{-, } A\text{-, } B\text{- and } C\text{-types} \\ \mathfrak{z} &= 3 \text{ for trigonally set-up } trR\text{-types} \\ \mathfrak{z} &= 4 \text{ for } F\text{-types} \\ F_R &= F/V^{2/3} \end{aligned}$$

The centricity index \mathfrak{z} corrects the value for non-primitive unit cells. The value of F_R^0 for several nodal surfaces is given in the last column of Table 13. The column before

this gives the reduced surface area F_R of the entire unit cell. This is listed because only rarely are centered structures given in their primitive setup in the literature. The unreduced surface area F has been calculated by the PNS-generating computer program.^[106] Due to restricted computer memory no higher accuracies of this value could be calculated.

Column 6 of Table 13 gives the ratios of the volumes of each partial space (+R and -R) for the PNS listed, calculated by determining iteratively the ratio of the number of positive and negative function values in the unit cell. Although the integral of the function values will always yield identical values for both partial space, the volumina themselves can be different as long as the surface does not have black-white symmetry (chapter 4.4.1.). In cases of asymmetric volumina, the partial space with smaller volume has accordingly higher function values and higher gradients.

Table 12: Some Graph-Generating 3D Nodal Surfaces ($|S|$ = Struktur Faktor Value, α = Phase)

Name	hkl	$ S $	α	Symmetry (Eigen)	Graph-Generating Point Configurations (Function Value $f(x,y,z)$) \Rightarrow Point Configurations of the Graph, Parameter Variation	Line Segment Configuration
$I_2 - Y^{**}V^*$	211 220	1 1	0 0	$Ia\bar{3}d$	$16b(-6) + 24c(-6) \Rightarrow 48g, y = 0 \rightarrow \frac{1}{8}$	$Y^{**}(\frac{1}{2}, y, \bar{y} + \frac{1}{4})_{y=0}^{y=1/8}$
$Y_{xxx}^{**} - S^*$	211 220	1 1	0 π	$Ia\bar{3}d$	$32e(+6), x = 0 \rightarrow 1$ $24d(-6) \Rightarrow 96h, x = \frac{3}{8} \rightarrow \frac{5}{8}; y = 0 \rightarrow \frac{1}{16}, z = \frac{1}{4} \rightarrow \frac{3}{8}$	$Y^{**}(x, x, x)_{x=1}^{x=1}$ $Y^{**}(x, y, z)_{x=5/16, y=1/16, z=3/8}^{x=1/16, y=1/16, z=1/4}$
$I_{xxx} - J^*$	110 200	1 1	0 π	$Im\bar{3}m$	$16f(+3), x = 0 \rightarrow 1$ $6b(-5) \Rightarrow 24g, x = 0 \rightarrow \frac{1}{2}$	$I(x, x, x)_{x=1}^{x=1}$ $J^*(x, 0, \frac{1}{2})_{x=0}^{x=1/2}$
$IJ^* - P_2$	110 200	1 1	0 0	$Im\bar{3}m$	$2a(+9) + 6b(+1) \Rightarrow 12e, z = 0 \rightarrow \frac{1}{2}$	$I(x, 0, 0)_{z=0}^{z=1/2}$
D^*	111	1	0	$Fd\bar{3}m$ ($Pn\bar{3}m$)	$8a(+2.83) \Rightarrow 32e, x = 0 \rightarrow \frac{3}{8}$ $8b(-2.83) \Rightarrow 32e, x = \frac{1}{2} \rightarrow \frac{5}{8}$ $\left. \vphantom{\begin{matrix} 8a \\ 8b \end{matrix}} \right\} 8e, x = 0 \rightarrow \frac{1}{4} \text{ in } Pn\bar{3}m$	$I(x, x, x)_{x=0}^{x=1/4}$
(DT)*	311	1	0	$Fd\bar{3}m$ ($Pn\bar{3}m$)	$8b(+8.5) + 16c(6) \Rightarrow 32e, x = 0 \rightarrow \frac{1}{8}$ $8a(-8.5) + 16d(-6) \Rightarrow 32e, x = \frac{1}{4} \rightarrow \frac{3}{8}$ $\left. \vphantom{\begin{matrix} 8b \\ 8a \end{matrix}} \right\} 8e, x = 0 \rightarrow \frac{1}{4} \text{ in } Pn\bar{3}m$	$I(x, x, x)_{x=0}^{x=1/4}$
$D - DT$	111 220	$\frac{5}{2}$ 1	$-\frac{\pi}{4}$ 0	$Fd\bar{3}m$	$8a(+13) \Rightarrow 32e, x = 0 \rightarrow \frac{1}{8}$ $8a(-1) + 16c(-5) \Rightarrow 32e, x = \frac{1}{2} \rightarrow \frac{5}{8}$	$D(x, x, x)_{x=1/8}^{x=1/8}$ $D(x, x, x)_{x=5/8}^{x=1/2}$
$FF_{zx} - FP_2$	111 220	2 1	0 π	$Fm\bar{3}m$	$96j(+4), (\frac{1}{2} + x, \frac{1}{2} + y, 0) \text{ with } \sqrt{x^2 + y^2} \approx \frac{1}{6}$ $4b(-14) + 8c(-6) \Rightarrow 32f, x = \frac{1}{4} \rightarrow \frac{1}{2}$	$F(\frac{1}{2} + x, \frac{1}{2} + y, 0)_{x=1/2}^{x=1/2}$ $F(x, x, x)_{x=1/4}^{x=1/4}$

Table 12: continued

Name	hkl	$ S $	α	Symmetry (Eigen)	Graph-Generating Point Configurations \Rightarrow Point Configurations of the Graph, Parameter Variation	Line Segment Configuration
$IF_{xx} - I_{xxx} W^*$	111 211	1 1	0 0	$Pn\bar{3}m$	$24i (+4); y = 0 \rightarrow 1$	$F(\frac{1}{2}, y, \bar{y})_{y=0}^{y=1}$
$F - I$	110 111	1 1	0 π_2	$Pn\bar{3}m$	$2a (+6) \Rightarrow 8e, x = \frac{1}{4} \rightarrow \frac{1}{2}$	$I(x, x, x)_{x=1/4}^{x=1/2}$
$P_2 - IW_z$	110 200 210	2 4 1	π π 0	$Pm\bar{3}n$	$8e (+12) + 6d (+8) \Rightarrow 24j, y = \frac{1}{2} \rightarrow \frac{1}{2}$ $12g (-8) x = 0 \rightarrow 1$	$W_{xx}(\frac{1}{4}, y, y + \frac{1}{2})_{x=1/4}^{y=1/2}$ $W(x, 0, \frac{1}{2})_{x=0}$
P^*	100	1	0	$Pm\bar{3}m$ ($Im\bar{3}m$)	$1a (+3) + 3d (+1) \Rightarrow 6e, x = 0 \rightarrow \frac{1}{2}$ $1b (-3) + 3c (-1) \Rightarrow 6f, x = 0 \rightarrow \frac{1}{2}$ $12e, x = 0 \rightarrow \frac{1}{2}$ in $Im\bar{3}m$	$I(x, 0, 0)_{x=0}^{x=1/2}$
$(PJ)^*$	100 111	1 1	0 0	$Pm\bar{3}m$ ($Im\bar{3}m$)	$1a (+7) + 3c (+3) \Rightarrow 12i, y = 0 \rightarrow \frac{1}{2}$ $1b (-7) + 3d (-3) \Rightarrow 12j, y = 0 \rightarrow \frac{1}{2}$ $24h, y = 0 \rightarrow \frac{1}{2}$ in $Im\bar{3}m$	$I(0, y, y)_{y=0}^{y=1/2}$
$PPJ - J_x$	110 111 220	4 2 1	0 0 0	$Pm\bar{3}m$	$1a (+76) + 1b (+44) \Rightarrow 8g, x = 0 \rightarrow \frac{1}{2}$ $1b (+44) + 3c (+12) \Rightarrow 6f, x = 0 \rightarrow \frac{1}{2}$	$P(x, x, x)_{x=0}^{x=1/2}$ $P(x, \frac{1}{2}, \frac{1}{2})_{x=0}$
Y^{**}	110	1	π_2	$I4_132$ ($Ia\bar{3}d$)	$8a (+3) \Rightarrow 24h, y = 0 \rightarrow \frac{1}{8}$ $8b: (-3) \Rightarrow 24g, y = \frac{3}{8} \rightarrow \frac{1}{2}$ $48g, y = 0 \rightarrow \frac{1}{8}$ in $Ia\bar{3}d$	$Y^{**}(\frac{1}{8}, y, \bar{y} + \frac{1}{4})_{y=0}^{y=1/8}$
$(FF_{xxx})^*$	111 210	1 1	π π	$Pa\bar{3}$ ($Ia\bar{3}$)	$4a (+4) + 8c (+4) \Rightarrow 8c, x = 0 \rightarrow \frac{1}{6}$ $4b: (-4) + 8c (-4) \Rightarrow 8c, y = \frac{1}{3} \rightarrow \frac{1}{2}$ $16c, x = 0 \rightarrow \frac{1}{6}$ in $Ia\bar{3}$	$P_2(x, x, x)_{y=0}^{y=1/6}$

Table 13: Volume Ratios and Surface Areas of some PNS ($ S $ = strukture factor value, α = phase, a = cell axis, for β see eq. (23))							
Name	hkl	$ S $	α	Generating Space Group	$\frac{\text{volume}^+R}{\text{volume}^-R}$	$\frac{F_R}{(a^2 \cdot V^{-2/3})}$	$\frac{F_R^0}{(a^2 \cdot V^{-2/3} \cdot \beta^{1/3})}$
$I_2 - Y^{**}V^*$	$\begin{smallmatrix} 211 \\ 220 \end{smallmatrix}$	$\begin{smallmatrix} 1 \\ 1 \end{smallmatrix}$	$\begin{smallmatrix} 0 \\ 0 \end{smallmatrix}$	$Ia\bar{3}d$	1.25	5.4	4.3
$Y_{xxx}^{**} - S^*$	$\begin{smallmatrix} 211 \\ 220 \end{smallmatrix}$	$\begin{smallmatrix} 1 \\ 1 \end{smallmatrix}$	$\begin{smallmatrix} 0 \\ \pi \end{smallmatrix}$	$Ia\bar{3}d$	0.98	5.8	4.6
$I_{xxx} - J^*$	$\begin{smallmatrix} 110 \\ 200 \end{smallmatrix}$	$\begin{smallmatrix} 1 \\ 1 \end{smallmatrix}$	$\begin{smallmatrix} 0 \\ \pi \end{smallmatrix}$	$Im\bar{3}m$	1.13	3.6	2.9
$IJ^* - P_2$	$\begin{smallmatrix} 110 \\ 200 \end{smallmatrix}$	$\begin{smallmatrix} 1 \\ 1 \end{smallmatrix}$	$\begin{smallmatrix} 0 \\ 0 \end{smallmatrix}$	$Im\bar{3}m$	0.59	3.7	2.9
$IW^* - I_z$	$\begin{smallmatrix} 211 \\ 211 \end{smallmatrix}$	$\begin{smallmatrix} 1 \\ 1 \end{smallmatrix}$	$\begin{smallmatrix} 0 \\ 0 \end{smallmatrix}$	$Im\bar{3}m$	0.97	5.4	4.3
D^*	111	1	0	$Fd\bar{3}m$	1	3.8	2.4
$(DT)^*$	311	1	0	$Fd\bar{3}m$	1	9.3	5.9
$D - DT$	$\begin{smallmatrix} 111 \\ 220 \end{smallmatrix}$	$\begin{smallmatrix} 5/2 \\ 1 \end{smallmatrix}$	$\begin{smallmatrix} -\pi/4 \\ 0 \end{smallmatrix}$	$Fd\bar{3}m$	0.65	3.8	2.4
F^*	111	1	0	$Fm\bar{3}m$	1	5.8	3.7
$FF_{zx} - FP_2$	$\begin{smallmatrix} 111 \\ 220 \end{smallmatrix}$	$\begin{smallmatrix} 2 \\ 1 \end{smallmatrix}$	$\begin{smallmatrix} 0 \\ \pi \end{smallmatrix}$	$Fm\bar{3}m$	1.31	4.9	3.1
$F - I$	$\begin{smallmatrix} 110 \\ 111 \end{smallmatrix}$	$\begin{smallmatrix} 1 \\ 1 \end{smallmatrix}$	$\begin{smallmatrix} 0 \\ -\pi/2 \end{smallmatrix}$	$Pn\bar{3}m$	0.76	3.3	3.3
$IF_{xx} - I_{xxx}W^*$	$\begin{smallmatrix} 111 \\ 211 \end{smallmatrix}$	$\begin{smallmatrix} 1 \\ 1 \end{smallmatrix}$	$\begin{smallmatrix} 0 \\ 0 \end{smallmatrix}$	$Pn\bar{3}m$	0.99	5	5
W^*	210	1	0	$Pm\bar{3}n$	1	8.2	8.2
$P_2 - IW_z$	$\begin{smallmatrix} 110 \\ 200 \\ 210 \end{smallmatrix}$	$\begin{smallmatrix} 2 \\ 4 \\ 1 \end{smallmatrix}$	$\begin{smallmatrix} \pi \\ \pi \\ 0 \end{smallmatrix}$	$Pm\bar{3}n$	1.11	4.4	4.4
$IWI_{zx} - J^*P_2$	$\begin{smallmatrix} 210 \\ 211 \\ 220 \end{smallmatrix}$	$\begin{smallmatrix} 1 \\ 2 \\ 4 \end{smallmatrix}$	$\begin{smallmatrix} 0 \\ 0 \\ m\pi \end{smallmatrix}$	$Pm\bar{3}n$	1.31	6.3	6.3
P^*	100	1	0	$Pm\bar{3}m$	1	2.4	2.4
$(PJ)^*$	$\begin{smallmatrix} 100 \\ 111 \end{smallmatrix}$	$\begin{smallmatrix} 1 \\ 1 \end{smallmatrix}$	$\begin{smallmatrix} 0 \\ 0 \end{smallmatrix}$	$Pm\bar{3}m$	1	3.9	3.9
$PPJ - J_x$	$\begin{smallmatrix} 110 \\ 111 \\ 220 \end{smallmatrix}$	$\begin{smallmatrix} 4 \\ 2 \\ 1 \end{smallmatrix}$	$\begin{smallmatrix} 0 \\ 0 \\ 0 \end{smallmatrix}$	$Pm\bar{3}m$	0.87	3.8	3.8

Table 13: continued							
Name	hkl	$ S $	α	Generating Space Group	$\frac{\text{volume}^+R}{\text{volume}^-R}$	F_R ($a^2 \cdot V^{-2/3}$)	F_R^0 ($a^2 \cdot V^{-2/3} \cdot \tilde{g}^{-1/3}$)
PPJP _{xxx} – J	110	$\sqrt{2}$	0	Pm $\bar{3}$ m	1.0	4.5	4.5
	111	1	0				
	210	1	π				
S*	211	1	$\pi/2$	I $\bar{4}$ 3d	1	5.5	4.4
I ₂ Y** – SS _z	220	2	0	I $\bar{4}$ 3d	0.76	6.7	5.3
	310	1	$\pi/2$				
II _{xxx} W* – I _{xxx}	211	1	$\pi/4$	I $\bar{4}$ 3m	1.25	5.2	4.1
F* (D)	111	$\sqrt{2}$	$-\pi/4$	F $\bar{4}$ 3m	1	4.1	2.6
	200	1	0				
(PP _{xxx})*	100	1	0	P $\bar{4}$ 3m	1	3.2	3.2
	111	1	$\pi/2$				
(PJ)*	100	$\sqrt{2}$	0	P $\bar{4}$ 3m	1	3.7	3.7
	111	1	$\pi/4$				
PP – JP ₄	110	1	0	P $\bar{4}$ 3m	0.94	3.5	3.5
	111	1	$\pi/4$				
Y**	110	1	$\pi/2$	I4 ₁ 32	1	3.1	2.5

4.4. Symmetry of PNS

4.4.1. Nodal Surfaces with Black-White Symmetry

Fischer and Koch have published several papers on the symmetry of minimal surfaces.^[45–47,109] In the center of attention have been the symmetry elements of minimal surfaces and their position on or relative to the surface. The issue of black-white symmetry has also been touched upon.

The symmetry restrictions of minimal surfaces regarding their shape (only inflection and hyperbolic points) and their realizability for certain space groups, as mentioned in chapter 2.1., do not exist for nodal surfaces. The affiliation of a generated nodal surface to a certain symmetry is usually determined by the choice of characteristic $S(hkl)$.

Due to the mathematical symmetry of the nodal surfaces (integral over the function of both partial spaces, separated by the surface, is identical within an entire unit cell, see chapter 2.3.) black-white symmetry can be observed both for PMS and for PNS, in which case the surface itself has the symmetry of a supergroup of the generating space group. In such a case both partial spaces can be transposed into each other with either a twofold rotation, if twofold rotational axes are located on the surface, with a mirror op-

eration along the surface itself, or with a point mirror operation using an inversion center located on the surface. In the latter two cases, and if no twofold rotational axes are located on the surface, the nodal surface is a so-called non-Euclidian mirror,^[35] which transposes a left-handed into a right-handed partial space and vice versa (chapter 4.4.2.).

The black-white symmetry of a nodal surface can be determined by way of their extrema (chapter 4.2.). In case of black-white symmetry the function's extrema form commutative point configurations with identical values but opposite signs as well as different parameters. They are merged into one point configuration of a *cI* supergroup (Table 12, p. 84). In Table 8. (pp. 44ff) one can recognize the black-white symmetry of a surface by the fact that its eigen symmetry is a supergroup of the generating function's space group.

4.4.2. 'Mirror Surfaces' and 'Double Surfaces'

If a surface separates two partial spaces which are geometrically identical in every regard except perhaps their chirality ('*mirror surfaces*'), and if the mirror-symmetrical double labyrinth system thusly created does not possess constrictions which are too narrow, then a nodal surface can be found which consists of *two* identical (partial) surfaces, although they are generated only by *one* function. Both parts of this '*double surface*' are mirror-symmetrically arranged to the '*mirror surface*' in its double labyrinth and they divide the space into three partial spaces. Of these three partial spaces, two are mirror-symmetrical to each other whereas the third partial space separates the other two and evenly envelops the '*mirror surface*'. The generating space group of this '*double surface*' is at once the eigen symmetry of its '*mirror surface*', just as the graph describing the two mirror symmetrical labyrinths of the '*double surface*' is identical to the graphs describing the '*mirror surface*'.

If twofold rotational axes lie on the '*mirror surface*', which can transpose both half spaces into each other in addition to a mirror operation on the surface itself, then this surface is not a '*mirror surface*' in the more strict sense that the two partial spaces are not chiral to each other. If such rotational axes are missing, though, and if both partial spaces can be transposed into each other only by way of an inversion centre located on the surface or by a mirror operation on that surface itself, then this surface is a true

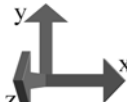

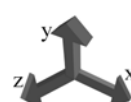
‘*mirror surface*’, forming a non-Euclidian mirror which transposes two chiral half spaces into each other, which in turn are described by helical graphs.

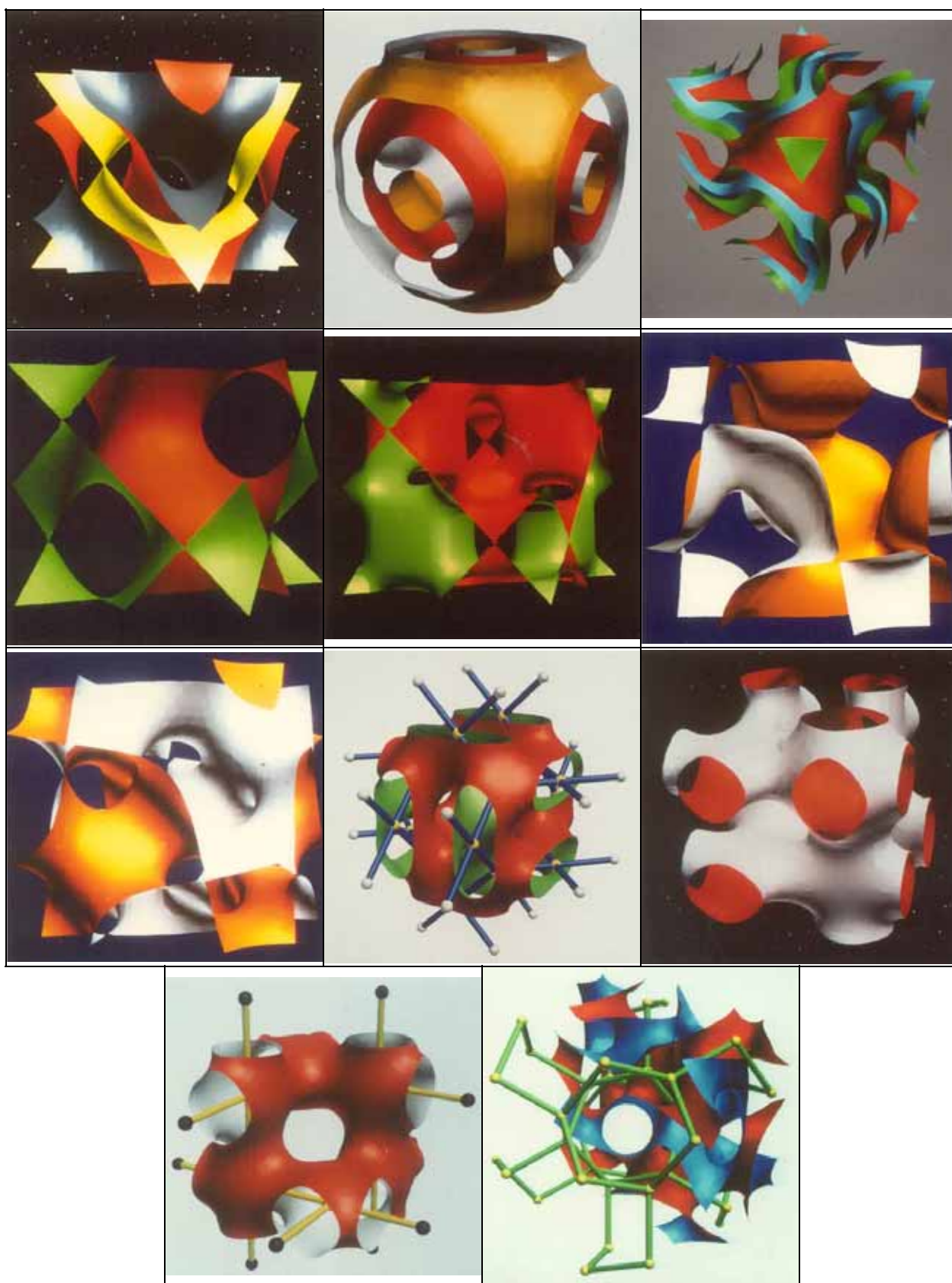
As abstract as this may sound in theory, it can indeed be observed for PNS. Ill. 8.a to 8.c (p. 90) each show a parallel ‘*double surface*’ combined with its respective ‘*mirror surface*’. The term ‘parallel’, however, is not meant strictly mathematically. Since the generating functions usually can be rendered only intrinsically, a geometrical analysis cannot be performed. When using the term ‘parallel’ it merely refers to the fact that the surfaces keep an almost constant distance from one another, allowing for some minor deviations (e.g. P^* relative to $IJ^* - P_2$, Ill. 8.b). Among the three examples illustrated here the third deserves special attention (Ill. 8.c). This is so far the only known case of a true ‘*mirror surface*’ combined with the respective ‘*double surface*’ consisting of two chiral half surfaces.

The combined volume of the two mirror-symmetrical partial spaces of these ‘*double surfaces*’ is smaller, sometimes even considerably so, than the volume of the space which separates the surfaces and which contains function values of the opposite sign (Table 13, p. 86).

4.4.3. Nodal Surfaces with Reduced Symmetry

Some nodal surfaces have morphologically and topologically similar surfaces in subgroups. This relation can be recognized in some cases already due to the similarity of the structure factors used. Some nodal surfaces of the crystal class $m\bar{3}m$, for instance, can be rendered within the crystal class $\bar{4}3m$ by foisting a tetrahedral symmetry onto them, cf. the group – subgroup pairs $P^* \wedge (PP_{xxx})^* ({}^{221}\langle 100 \rangle^{229} \wedge {}^{215}\langle (100);(111)^{\pi/2} \rangle^{217}$, Ill. 3.1 and 5.a) and $PPJ - J_x \wedge PP - JP_4 ({}^{221}\langle (110)_4;(111)_2;(220) \rangle \wedge {}^{215}\langle (110);(111)^{\pi/4} \rangle$, Ill. 4.b and 5.c). Although the pair $IJ^* - P_2 \wedge II_{xxx}W^* - I_{xxx} ({}^{229}\langle (110);(200) \rangle \wedge {}^{217}\langle (211)^{\pi/4} \rangle$, Ill. 2.d and 4.j) has different structure factors, there exists the PNS $IW^* - I_z ({}^{229}\langle 211 \rangle$, Ill. 2.e), containing intersections which strongly resembles the PNS $IJ^* - P_2$. The names derived from the extrema nomenclature for the group – subgroup pair ${}^{221}\langle (100);(111) \rangle^{229}$ and ${}^{215}\langle (100)_{1,4};(111)^{\pi/4} \rangle^{217}$ (Ill. 4.a and 5.b), both made up of the point configurations $(PJ)^*$, clearly show the limit of this naming method, since no information is included denoting the generating space group.

<p>Ill. 8.a</p> <p>Double Surface $F - I \triangleq {}^{224}\langle(110);(111)\rangle$ and 1st octant of the non-chiral ‘mirror surface’ $D^* \triangleq {}^{227}\langle 111 \rangle^{224}$ (golden); Setup 2</p>	<p>Ill. 8.b</p> <p>Double Surface $IJ^* - P_2 \triangleq {}^{229}\langle(110);(200)\rangle$ and non-chiral ‘mirror surface’ $P^* \triangleq {}^{221}\langle 100 \rangle^{229}$ (red); Setup 3</p>	<p>Ill. 8.c</p> <p>Chiral Double Surface $I_2 - Y^{**}V^* \triangleq {}^{230}\langle(211);(220)\rangle$ (‘Christmas Star’^[39]) and true ‘mirror surface’ $Y^{**} \triangleq {}^{214}\langle(110)^{\pi/2}\rangle^{230}$ (blue); Setup 4</p>	
<p>Ill. 8.d</p> <p>$P^* \triangleq {}^{221}\langle 100 \rangle^{229}$ Origin at $\frac{1}{4} \frac{1}{4} \frac{1}{4}$ from $m\bar{3}m$ straight lines at cell borders correspond to C_2-Axes, ‘frame’ of minimal surfaces, complementary to $(PJ)^*$ from SG No. 221; Setup 2</p>	<p>Ill. 8.e</p> <p>$(PJ)^* \triangleq {}^{221}\langle(100);(111)\rangle^{229}$ Origin at $\frac{1}{4} \frac{1}{4} \frac{1}{4}$ from $m\bar{3}m$ straight lines at cell borders correspond to C_2-Axes, ‘frame’ of minimal surfaces, complementary to P^* from SG No. 221; Setup 2</p>	<p>Ill. 8.f</p> <p>$(PP_{xxx})^* \triangleq {}^{215}\langle(100);(111)^{\pi/2}\rangle^{217}$ Origin at $\frac{1}{4} \frac{1}{4} \frac{1}{4}$ from $m\bar{3}m$ bent ‘frame’ of minimal surfaces, complementary to $(PJ)^*$ from SG No. 215; Setup 2</p>	
<p>Ill. 8.g</p> <p>$(PJ)^* \triangleq {}^{215}\langle(100)_{1,4};(111)^{\pi/4}\rangle^{217}$ Origin at $\frac{1}{4} \frac{1}{4} \frac{1}{4}$ from $m\bar{3}m$ bent ‘frame’ of minimal surfaces, complementary to $(PP_{xxx})^*$ from SG No. 215; Setup 2</p>	<p>Ill. 8.h</p> <p>$P_2 - I W_z \triangleq {}^{223}\langle(110)_2^{\pi};(200)_4^{\pi};(210)\rangle$ Including graph $W_{xx}(\frac{1}{4},y,y + \frac{1}{2})_{y=1/4}^{y=1/2}$ in one partial space; Setup 3</p>	<p>Ill. 8.i</p> <p>$P_2 - I W_z \triangleq {}^{223}\langle(110)_2^{\pi};(200)_4^{\pi};(210)\rangle$ Origin at $\frac{1}{4} \frac{1}{4} \frac{1}{4}$ from $m\bar{3}$; Setup 3</p>	
	<p>Ill. 8.j</p> <p>PNS $I_{xxx} - J^* \triangleq {}^{229}\langle(110);(200)^{\pi}\rangle$ Origin at $\frac{1}{4} \frac{1}{4} \frac{1}{4}$ from $m\bar{3}m$, with graph $J^*(x,0,\frac{1}{2})_{x=0}^{x=1/2}$ of the other partial space; Setup 3</p>	<p>Ill. 8.k</p> <p>PNS $Y_{xxx}^{**} - S^* \triangleq {}^{230}\langle(211);(220)^{\pi}\rangle$ from $z = 0$ to $\frac{1}{2}$, with S^*-Graph $Y^{**}(x,y,z)_{x=3/8, y=0, z=1/4}^{x=5/16, y=1/16, z=3/8}$; Setup 4</p>	
<p>Setup 2:</p> 	<p>Setup 3:</p> 	<p>Setup 4:</p> 	

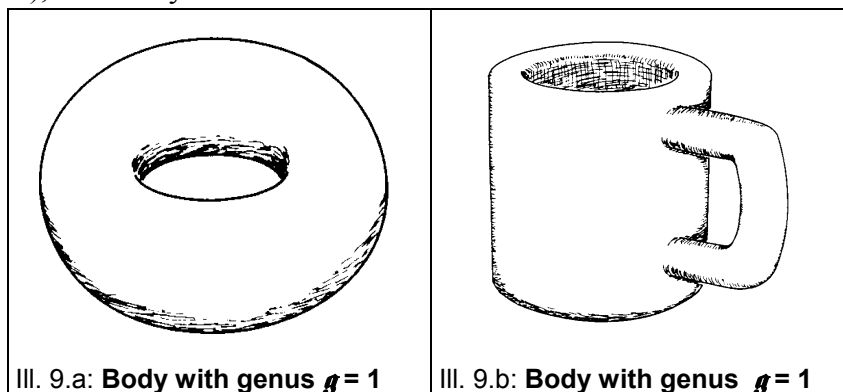


Schoen developed the concept of complementary minimal surfaces.^[5] Two minimal surfaces are complementary, if they are defined by the same boundary conditions – in case of soap bubbles this would mean identical frameworks – but are geometrically different. The nodal surfaces depicted in Ill. 3.1 and 4.a correspond to the minimal surfaces P and c(P) (Neovius Surface), respectively. They are complementary to each other, since they are suspended along the same ‘frame’, which, analytically speaking, means that they have the same set of twofold rotational axes. When calculating the corresponding PNS starting at $\frac{1}{4}\frac{1}{4}\frac{1}{4}$ from $m\bar{3}m$, they look as depicted in Ill. 8.d and 8.e. Both nodal surfaces therefore have the same straight zero-value lines which are called “frame” in the case of minimal surfaces and which in both cases are twofold rotational axes. In case of the two PNS with reduced symmetry from the subgroup $P\bar{4}3m$ both surfaces do have the same ‘frame’ as well, although in this case this frame is curved (Ill. 8.f, 8.g).

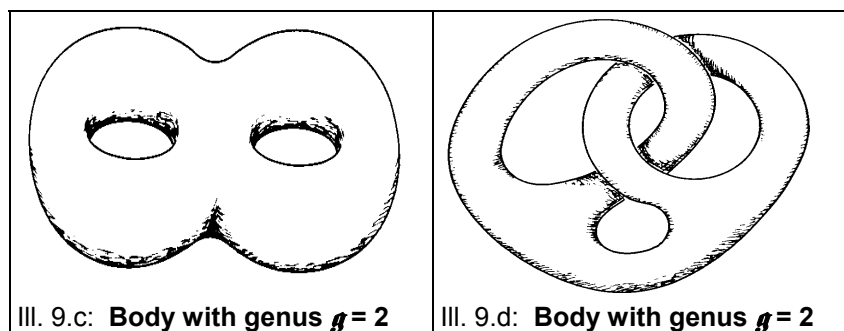
4.5. Topology of PNS

4.5.1. Introductory Remarks

The periodic nodal surfaces will be analyzed in the following using graph theory, which is a part of topology. Graphs are systems where various elements are connected to one another in a defined way, building a network. This can be applied to PNS if the spaces separated by (a) surface(s) consist of tunnel-like systems which can be described with graphs (networks). The topology of graphs analyzes the kind of connections between its elements without paying attention to geometric features like length, angle, and curvature of connecting lines.^[110] Two graphs or networks are topologically identical (isomorphic⁹), if the way their elements are connected to one another is identical.^[111]



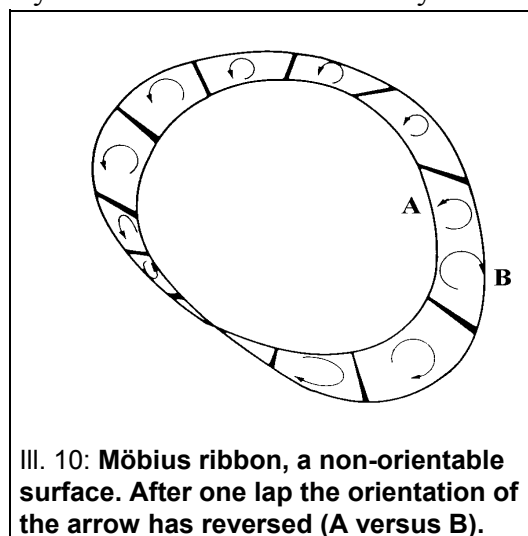
⁹ Not to be confused with crystallographic isomorphism, which refers to identical symmetry (space group), while ignoring chirality.



The surfaces themselves can be analyzed topologically as well. Two objects formed by finite or infinite surfaces are topologically identical (homeomorphic) if they can be transformed into each other without breaching the surface in the process. Of the four objects shown in Ill. III. 9.a-d only those in the upper row can be thusly transformed, whereas all other transformations are possible only if breaching the surface.

The nomenclature of topologically different graphs is difficult due to the enormous variability^[107,108,112-114] and has not been standardized to this day.¹⁰ As mentioned earlier (p. 81), this present work will closely follow the rules established by Hellner, Koch, and Reinhardt^[107] for naming graphs as they frequently occur in solid state chemistry.

In contrast to this, the nomenclature of objects defined by steady surfaces has been clearly standardized for quite a while. It is organized around the concepts of orientability and genus g .^[110,111,115] A surface is orientable if it has a right-hand and a left-hand side, which is not the case for the famous Moebius ribbon in Ill. 10. The genus of an object indicates how often it has to be cut open so that it can be deformed to form a sphere. The ob-



Ill. 10: Möbius ribbon, a non-orientable surface. After one lap the orientation of the arrow has reversed (A versus B).

jects in the upper row of Ill. 9, for instance, have the genus $g = 1$, whereas those in the lower row have $g = 2$. A sphere has $g = 0$ according to this nomenclature.

The nodal surfaces investigated in this work as well as minimal surfaces and zero-potential surfaces are all orientable. It is mathematically possible, however, to transform minimal surfaces from orientable to non-orientable surfaces without changing their genus.^[53,116]

¹⁰ Which is not to say that a standardization is not being attempted; see e.g., O. Delgado-Friedrichs, A.W.M. Dress, D.H. Huson, J. Klinowski, A.L. Mackay, "Systematic enumeration of crystalline networks", *Nature* **400** (12.8.1999) pp. 644-647; O. Delgado-Friedrichs, M. O'Keefe, O.M. Yaghi, "Taxonomy of periodic nets and the design of materials," *Phys. Chem. Chem. Phys.* **9** (2007) pp. 1035-1043, with further references.

4.5.2. Genera of Nodal Surfaces

The same methods to determine the genus of minimal surfaces as they have been developed by Schoen,^[5] Hyde^[40,49,53] and Fischer & Koch^[48] can be used for nodal surfaces with separated, periodic tunnel systems. The two most commonly used methods are:

1. The *labyrinth-graph method*: The tunnel system of a periodic surface is described by a graph. The genus of the surface is a function of the number of furcation points and connecting lines of the graph.
2. The Euler method: The target surface is generated by way of tessellation using different polygons. The kind and number of polygons used directly yields the genus of the surface via the Euler-Schläfli equation.

While the second method will be discussed in detail in chapter 5. (pp. 101ff.), I will focus on the first method in the following.

The labyrinth-graph method: Each finite and infinite surface divides space in two parts. The genus has to be determined only for one of these parts, as the other part must have an identical genus. A graph is constructed throughout the surface's maze in such a way that each furcation of the surface's tunnel system has an equivalent furcation of the graph. The genus of this graph is equal to the number of cuts necessary to obtain a branched graph without closed loops (cycles). Hence, the number of cycles to be opened is equal to the genus of the surface.

The reasoning for the determination of the number of cycles within a unit cell goes as follows: A graph without cycles always has one (end)point \mathcal{E} more than lines \mathcal{K} connecting such points: $\mathcal{E}-1=\mathcal{K}$. (Prerequisite: each line ends with a point). In order to close a cycle, two points have to be connected with an additional line. Hence the number of cycles Z of a graph is:

$$Z = \mathcal{K} - \mathcal{E} + 1 \quad (24)$$

In order to take into consideration the periodicity of periodic nodal surfaces, the following holds:

1. Each line \mathcal{K} of a furcation point is connected with another furcation point and therefore counts only half.
2. Furcation points \mathcal{E} on a unit cell's faces count as half points, those on edges as quarter points, and those on corners as eighths points. The same is true for lines.

Since the number of cycles of a graph describing the tunnel system of a surface is

equivalent to the surface's genus g , we obtain:

$$g = \mathcal{K} - \mathcal{E} + 1 \quad (25)$$

Thus, it becomes evident that the genus of a body is identical with the cycle number of the graph describing it.

For demonstration purposes I will clarify this concept with a few examples using PNS described by their labyrinth graphs. Ill. 8.h (p. 90) shows the periodic nodal surface $P_2 - IW_Z \triangleq {}^{223}\langle(110)_2^\pi; (200)_4^\pi; (210)\rangle$ with its labyrinth graph, generated by the point configurations P_2 and W_{XX} . The graph contains 14 points and 24 line segments, for which eq (25) yields $g = 11$. The same PNS has been calculated starting at $\frac{1}{4}\frac{1}{4}\frac{1}{4}$ from $m\bar{3}$, Ill. 8.i. Since the other partial space contains the three rod packing which does not describe this tunnel system, no graph has been included in this illustration. It is easily recognizable, though, that with $\mathcal{K} = 18$ and $\mathcal{E} = 8$ this partial space has the same genus $g = 11$.

Ill. 2.c (p. 56) shows the PNS $I_{xxx} - J^* \triangleq {}^{229}\langle(110); (200)^\pi\rangle$ with the graph generated by the point configuration I_{xxx} in one of the partial spaces. With 8 line segments and only 2 furcation points we obtain: $g = 7$. Ill. 8.j shows the same surface calculated starting at $\frac{1}{4}\frac{1}{4}\frac{1}{4}$ from $m\bar{3}m$ and augmented with the graph describing the other partial space. 12 line segments and 6 furcation points once more yield $g = 7$.

The PNS $Y_{xxx}^{**} - S^* \triangleq {}^{230}\langle(211)^\pi; (220)\rangle$ has a labyrinth graph in one of its partial spaces generated by the point configuration S^* (graph name: $Y^{**}(x,y,z)_{x=5/16, y=1/16, z=3/8, x=3/8, y=0, z=1/4}$, p. 84; Ill. 8.k). From each of its 24 furcation points of the position 24d four lines branch off. This effectively yields 48 line segments, resulting in a genus $g = 25$.

The determination of the genus of a minimal surface, for which a fitting graph cannot always be found as easily as for most PNS (cf. chapter 4.2., p. 79), is therefore error prone.^[117] Hyde,^[83] for instance, gives a genus of $g = 3$ for the minimal surface Y (an analogous surface to the PNS $Y^{**} \triangleq {}^{214}\langle(110)^{\pi/2}\rangle^{230}$) instead of the correct genus $g = 5$, and a genus $g = 6$ (instead of 21) for the surface F-RD (analogous to PNS $FF_{zx} - FP_2 \triangleq {}^{225}\langle(111)_2; (220)^\pi\rangle$). Hyde's genera are correct only if they refer to the respective *primitive* unit cell. But since he gives, in the same table, the correct value for the body-centered setup of the surface I-WP (analogous to PNS $I_{xxx} - J^* \triangleq {}^{229}\langle(110); (200)^\pi\rangle$) with $g = 7$ (cP: $g = 4$), he must have made a mistake in either case.

The genus of a periodic object is indeed commonly referring to its primitive unit cell.^[48] If transiting from a primitive to a body-centered rendering, one formally connects two primitive topological units with each other. Hence one obtains one cycle more

than the sum of the cycles of the two isolated primitive cells. The transition from primitive to face-centered comes with three such additional connections, hence three more cycles than the sum of four isolated primitive units. The genus g_{ni} of n topological, repetitive units i connected to one another is therefore linked to the genus g_i of the topological unit i as follows:

$$g_{ni} = n \cdot g_i - (n-1) \quad (26)$$

The genus of several PNS in primitive as well as centered setups is listed in Table 14. The ‘mirror surfaces’ $F - I$, $IJ^* - P_2$, $I_2 - Y^{**}V^*$ and $II_{xxx}W^* - I_{xxx}$ are characterized by the fact that their two mirror-symmetrical partial spaces have identical genera differing from that of the third partial space separating the two. It has not been investigated whether or not there is a relationship between the genera of these different partial spaces, because in lack of a tunnel character the third, separating partial space cannot be described with the graph method. Table 14 therefore only lists the genus of the two mirror-symmetrical partial spaces.

Minimal surfaces can be divided into subunits which, when applying appropriate symmetry operations, can yield the complete surface, as mentioned above (chapter 2.1.).^[47,67,109] PNS offer a similar possibility. In addition, the PNS can be considered to consist of topological subunits, in which case every furcation point of its labyrinth system is at once the centre of such a subunit. The PNS $FF_{zx} - FP_2 \triangleq {}^{225}\langle(III);(220)^\pi\rangle$ (Ill. 3.b, p. 58) for example, can be considered to be an assembly of tetrahedral and octahedral subunits, if viewed from one partial space, or of cuboctahedral subunits, if viewed from the other. Topologically identical subunits can in turn be used to construct other PNS. In connection with the construction of hyperbolic networks (chapter 5., p. 101) this topic will be investigated in more detail.

The method used here cannot successfully be applied to all PNS. Surfaces with intersection lines, for instance, do not divide space into labyrinth systems but rather into closed polyhedra. See for example the nodal surfaces $F^* \triangleq {}^{225}\langle III \rangle^{229}$ and $W^* \triangleq {}^{223}\langle 210 \rangle^{229}$ (Ill. 3.a, 3.f, p. 58) generated with only one $S(hkl)$, as well as the PNS $I_{zx}^* \triangleq {}^{204}\langle(130);(310)^\pi\rangle^{229}$ and $(J_x^*I_{zx})^* \triangleq {}^{204}\langle(321);(231)^\pi\rangle^{229}$ generated using two $S(hkl)$ (Ill. 6.g, 6.h).

It is possible in general to deduce information about the integral curvature of a surface from its genus. According to Carmo^[118] the integral over the value of the curvature $|k|$ of a periodic unit A of a surface is proportional to the genus g of the surface:

Table 14: Genus g of some Nodal Surfaces				
Nodal Surface, PNS		g Partial Space Bravais	g Partial Space Primitiv	F_R^0 (Half Surface)
$I_2 - Y^{**}V^*$	$^{230}\langle(211);(220)\rangle$	$2 \cdot 5 (cI)$	$2 \cdot 3$	4.3 (2.1)
$Y_{xxx}^{**} - S^*$	$^{230}\langle(211);(220)^\pi\rangle$	$25 (cI)$	13	4.6
$I_{xxx} - J^*$	$^{229}\langle(110);(200)^\pi\rangle$	$7 (cI)$	4	2.9
$IJ^* - P_2$	$^{229}\langle(110);(200)\rangle$	$2 \cdot 3 (cI)$	3	3.7 (1.9)
D^*	$^{227}\langle 111 \rangle^{224}$	$9 (cF)$	3	2.4
$D - DT$	$^{227}\langle(111)_{5/2};(220)^\pi\rangle$	$9 (cF)$	3	2.4
$FF_{zx} - FP_2$	$^{225}\langle(111)_2;(220)^\pi\rangle$	$21 (cF)$	6	3.1
$F - I$	$^{224}\langle(110);(111)\rangle$	3	3	3.3 (1.7)
$P_2 - IW_z$	$^{223}\langle(110)_2;(200)_4;(210)^\pi\rangle$	11	11	4.4
$IWI_{zx} - J^*P_2$	$^{223}\langle(210);(211)_2;(220)_4\rangle$	35	35	6.3
P^*	$^{221}\langle 100 \rangle^{229}$	3	3	2.4
$(PJ)^*$	$^{221}\langle(100);(111)\rangle^{229}$	9	9	3.9
$PPJ - J_x$	$^{221}\langle(110)_4;(111)_2;(220)\rangle$	10	10	3.8
$PPJP_{xxx} - J$	$^{221}\langle(110)_{1.4};(111);(210)^\pi\rangle$	14	14	4.5
S^*	$^{220}\langle(211)^{\pi/2}\rangle^{230}$	$13 (cI)$	7	4.4
$\Pi_{xxx}W^* - I_{xxx}$	$^{217}\langle(211)^{\pi/4}\rangle$	$2 \cdot 6 (cI)$	6	4.1
$F^*(D)$	$^{216}\langle(111)^{-\pi/4}_{1.4};(200)\rangle^{227}$	$17 (cF)$	5	2.6
$(PJ)^*$	$^{215}\langle(100)_{1.4};(111)^{\pi/4}\rangle^{217}$	9	9	3.7
$PP - JP_4$	$^{215}\langle(110);(111)^{\pi/4}\rangle$	6	6	3.5
Y^{**}	$^{214}\langle(110)^{\pi/2}\rangle^{230}$	$5 (cI)$	3	2.5

$$\int_A |k| dA = 4\pi (I - g) \quad (27)$$

Hence the genus is a measure for the complicatedness of the division of space caused by the surface. A comparison of the values of the reduced surface area F_R^0 (last column in Table 13) with the genus of the primitive unit cell accordingly reveals a correlation, as both quantities are a measure of curvature (cf. chapter 4.3.). This correlation between genus and curvature, however, is the only analytical connection between topology and geometry. Topology does not contain any other information about symmetrical or local geometric properties of an object.

4.5.3. Topology as a Function of Cell Metrics

In his dissertation Oehme has described a sizeable number of variations of POPS as a function of changing cell metrics.^[39] When changing the relative position of the formal charges to one another, the potential values between them inexorably change. This ine-

luctably changes the shape of the potential surface. This will not only change the geometrical features of the respective surface, but under certain circumstances also its topology.

In contrast to this, a change of cell metrics will not affect the topology of nodal surfaces, if eq. (18) (p. 22) is used for their generation, as it contains no term influenced by the cell's metric:

$$f(x,y,z) \neq f(\vec{r}) \quad (28)$$

with x,y,z = fraction of cell axes
 \vec{r} = coordinates in real space

However, if using the following equation,^[61]

$$f(r) = \frac{1}{\pi V} \sum_h S_h \frac{|\Phi_h|^2}{|h|^2} e^{-2\pi i \vec{h} \vec{r}} \quad (29)$$

which is used to calculate POPS and which has been derived directly from eq. (6) (p. 19), then the term $\frac{|\Phi_h|^2}{|h|^2}$ is a function of the cell's metrics.

This means that PNS generated within the cubic crystal system following eq. (18) can be transformed to lower crystal classes by way of appropriate hkl transformations without losing the PNS's topological features. Although a certain change in symmetry formally leads to a separation of some structure factors into independent $S(hkl)$, these formally split $S(hkl)$ are actually still degenerated, because the *value* of the structure factor $|S(hkl)|$ in eq. (18) is not influenced by such a transformation. Only if $|S(hkl)|$ is changed as a function of the changing reciprocal lattice plane distance $d^*(hkl)$ following the principles of eq. (29) will a split in independent structure factors occur.

There are a few cases, however, where *not even* an hkl transformation leads to a split of the structure factors into separate, formally independent $S(hkl)$. In such cases the topology of the nodal surface as well as the POPS calculated following eq. (29) is in any case independent of the cell metrics, hence cannot be changed.

Charts 1 and 2 (overleaf) show the correlations of the reciprocal lattice plane distance $d^*(hkl)$ as a function of the c/a axes ratio for trigonal and tetragonal body-centered cells, respectively. The reciprocal lattice plane distance has been normalized with respect to the cell volume V in order to make it independent of the metrics.

Chart 1 shows the volume-reduced reciprocal distances $d^*(hk.l) \cdot V^{1/3}$ of a trigonal unit cell as a function of the axes ratio c/a (abscissa). Focus lies on $hk.l$ complying with the rhombohedral condition ($-h + k + l = 3n$). At an axes ratio $c/a = \sqrt{3/2}$ the metrics is

cubic primitive (*cP*) with the transformation matrix *A* from trigonal to cubic cell axes, eq. (30) (analogous to the rhombohedral transformation). If doubling $c/a = \sqrt{6}$, then one obtains a face-centered cubic metrics (*cF*) with transformation matrix *C* starting from trigonal and *B* from cubic primitive (*cP*) metrics:

$$A \times B = C = \begin{pmatrix} 2/3 & 1/3 & 1/3 \\ -1/3 & 1/3 & 1/3 \\ -1/3 & -2/3 & 1/3 \end{pmatrix} \times \begin{pmatrix} 1 & 1 & -1 \\ -1 & 1 & 1 \\ 1 & -1 & 1 \end{pmatrix} = \begin{pmatrix} 2/3 & 4/3 & 1/3 \\ -4/3 & -2/3 & 1/3 \\ 2/3 & -2/3 & 1/3 \end{pmatrix} \quad (30)$$

At these special c/a ratios certain $d^*(hkl)$ are identical. They degenerate and form one cubic structure factor of the type *cP(hkl)* or *cF(hkl)* after the appropriate *hkl* transformations with either of the above matrices. Both for *cP* and *cF* transformations only the cubic structure factor types *h00* (trigonal the type *h0h*) do not split up.

Chart 2 contains the volume-reduced reciprocal lattice plane distances $d^*(hkl) \cdot V^{1/3}$ for the tetragonal body-centered lattice. Apart from the trivial case of $c/a = 1$, the transformation from the tetragonal to the face-centered cubic metrics is of interest in this context, where $c/a = \sqrt{2}$:

$$a(cF) = a(tl) + b(tl); \quad b(cF) = b(tl) - a(tl); \quad c(cF) = c(tl)$$

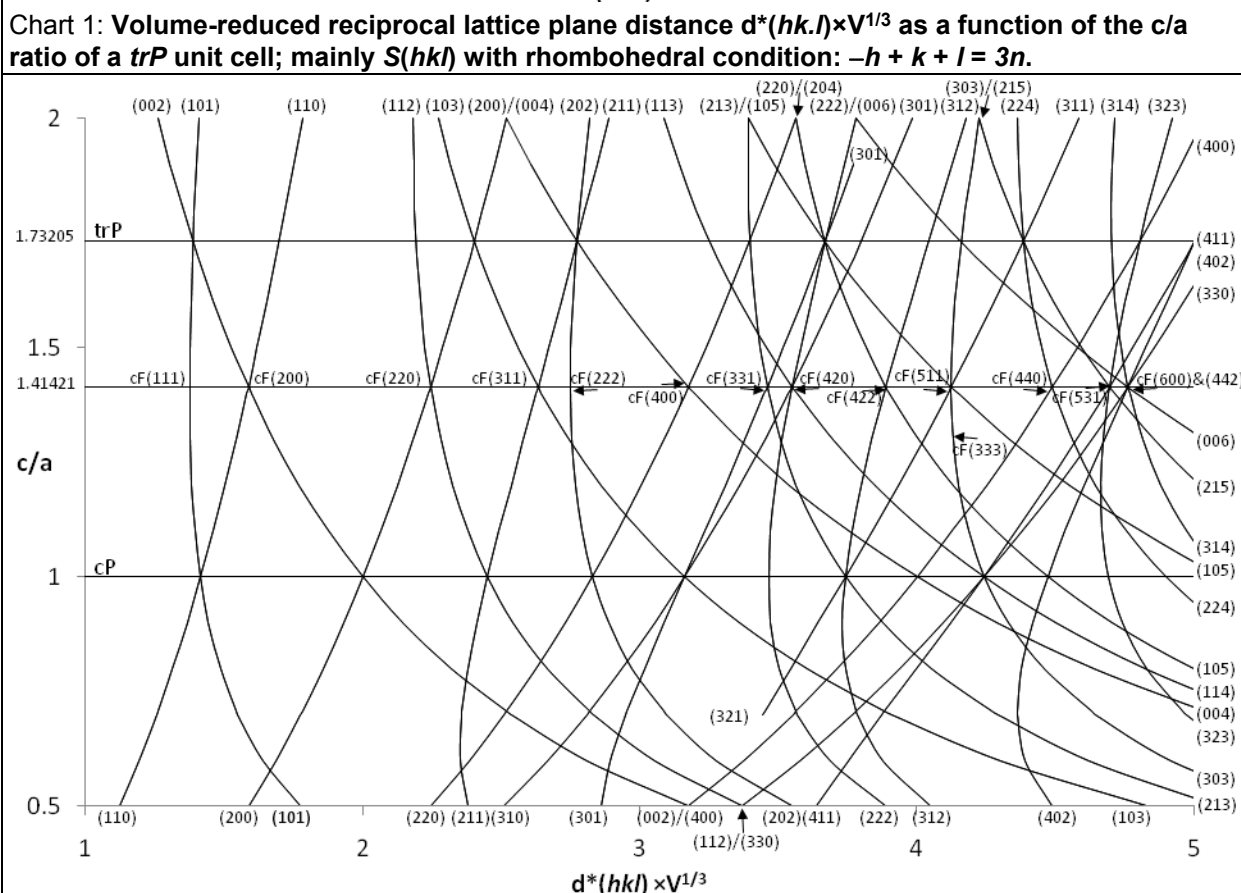
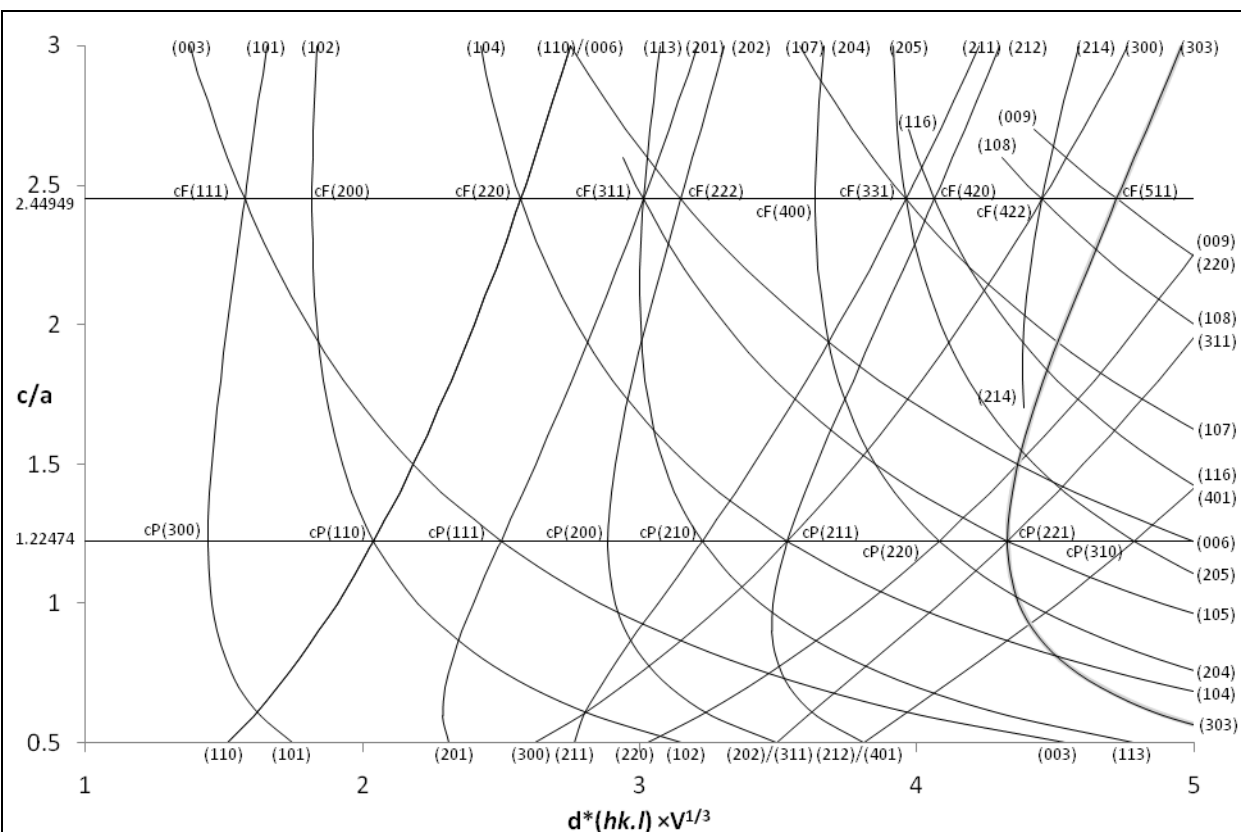
In this case cubic structure factors of the type *hhh* (*h0h* in the tetragonal metrics) are not split up, meaning that *cF* nodal surfaces generated with such structure factors cannot be varied when transformed into the tetragonal. Since such factor types don't split up when transformed into the orthorhombic crystal system either, thusly generated nodal surfaces can be transformed right down to the orthorhombic without affecting the topology.

This is true especially for the PNS $D^* \triangleq {}^{227}\langle III \rangle^{224}$ which can be transformed to the tetragonal (space group *I4₁/amd*, No. 141) and orthorhombic (space group *Fddd*, No. 70) crystal system without any possibility to change its function values and thus its topology (cf. chapter 6.3.5.).

It should be noted that a tetragonal cell can be set up trigonally in case of a c/a ratio of $\sqrt{3}$ (*trP*, see chart 2):

$$a(trP) = b(tl) - c(tl); \quad b(trP) = b(tl) + c(tl); \quad c(trP) = a(tl)$$

This is highlighted in chart 2 by the many $d^*(hkl)$ values crossing one another at $c/a = \sqrt{3}$.



5. Hyperbolic, Graphite-Like Carbon Networks

Already in 1966 did Jones predict the existence of Buckminster fullerenes.^[119] He suggested the name in honor of the famous U.S. architect Buckminster Fuller, who had used similar network patterns for the construction of vaulted ceilings. It should be noted, however, that such polygon patterns have been known and used since the Renaissance.^[120] Only some 20 years later did Kroto et al. manage to synthesize C_{60} , although without being able to isolate and characterize it fully.^[121] Shortly thereafter Krätschmer et al. succeeded in systematically synthesizing and characterizing C_{60} .^[122]

The broad variety of closed cages of trivalent carbon with 12 pentagons and an almost deliberate number of hexagons is astounding.^[123,124] But are other modifications of carbon possible beside the three known so far? Iijima pointed at carbon's potential to form needle- and tube-like objects.^[125] In 1991 Jones once more showed a new path by postulating the existence of foam-like carbon networks similar to those made of silicates, forming the basis for the chemistry of zeolites.^[126]

This chapter will investigate under which topological and geometrical conditions such networks could evolve.

5.1. On the Theory of Three-Dimensional Networks

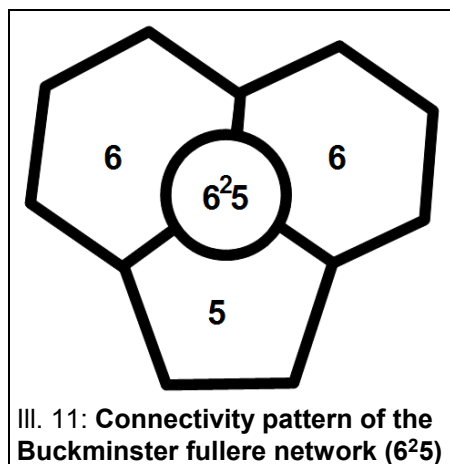
5.1.1. The Curvature of (n,3) Networks

Topologically seen, fullerenes are derivatives of the pentagon-dodecahedron, where three edges emanate from each vertex. This equates the s-bonds of sp^2 -hybridized carbon. The sum of all angles between the edges of a dodecahedron is 324° (thrice the angle between two adjacent edges of a pentagon). This is less than 360° , which is required for the tessellation of a Euclidian plane. Euclidian geometry pertains to straight lines, planes, and to space with orthogonal coordinates. Objects described with such coordinates are called parabolic. The sum of a triangle within a plane is 180° . For non-Euclidian geometry this sum is $\neq 180^\circ$. One distinguishes between hyperbolic and elliptic (Riemann) geometry, for which $\sum \alpha(\Delta) > 180^\circ$ and $\sum \alpha(\Delta) < 180^\circ$, respectively.^[127] The sum of all angles around the furcation points (henceforth \mathcal{E}) of a network of less than 360° closes this network to form a convex polyhedron. The continuous surface

Table 15: Curvature of Various Combinations of two m - and one n -Polygon, Connectivity per Connecting Point: $p = 3$ (Schläfli Symbol m^2n)					
Name	m	n	Sum of Angles	Gaussian curvature	Shape
Pentagon dodecahedron	5	5	324°	+	elliptic
Buckminster fullerene	6	5	348°	+	elliptic
Graphite	6	6	360°	0	parabolic
–	6	7	368.6°	–	hyperbolic
–	6	8	380°	–	hyperbolic
–	7	7	385.8°	–	hyperbolic
–	8	8	420°	–	hyperbolic

embedding these connecting points is *elliptic*, a rotational ellipsoid, in which case curvatures orthogonal to one another have the same sign. The Gaussian curvature is always positive (cf. chapter 2.1., p. 13).

The sum of angles in a plane around any connection point is 360° , hence the curvature of the embedding surface is zero. If the angle sum is $>360^\circ$, then curvatures of the embedding surface orthogonal to one another have opposite signs, the Gaussian curvature is negative, the surface embedding such a network is *hyperbolic*. The sum of angles of various, regular combinations of n -fold polygons therefore directly determines whether the object thusly formed is a closed, elliptic polyhedra or a hyperbolic, infinite network. We will subsequently investigate n -fold polygons with three connection lines at each corner ($n,3$ network). Table 15 lists the sum of angles and the sign of Gaussian curvature for some combinations of n -fold polygons exhibiting the tessellation pattern of fullerene, that is to say: which contain furcation points of the type (m^2n), where two m -fold polygons and one n -fold polygon meet at each furcation point (notation according to Schläfli, III. 11).

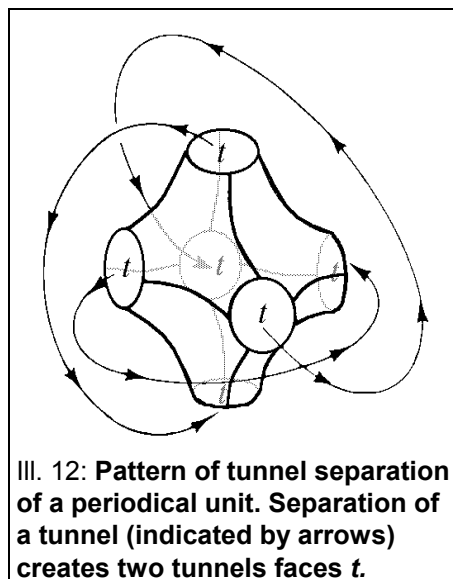


III. 11: Connectivity pattern of the Buckminster fullerene network (6^25)

5.1.2. On the Topology of ($n,3$) Networks

In this chapter we will explore networks viewed on one hand under aspects of group theory, which is a part of topology (see p. 92), and on the other hand under the aspects of the continuous surfaces formed by the network's furcation points. Each graph, there-

fore also each network, can be embedded into and therefore described by a continuous surface of an appropriate genus.^[128] Embedding means that each furcation point \mathcal{E} of the network lies on the surface and that all edges \mathcal{K} can be drawn onto the surface without crossing one another. A surface with the genus $g = 0$ is suitable only for spherical networks. It is expedient to use a surface of a minimal genus for such embeddings. The determination of the network's genus subsequently follows the Euler method as mentioned in chapter 4.5.2. (p. 94).



As already mentioned on p. 92, the nomenclature of graphs has not been unified to this day due to their huge variability. Since we will subsequently deal with rather complex networks, descriptions will be restricted to phenomenological observations which do not rely on existing, at times confusing and complicated rules.

When embedding infinite, hyperbolic networks into three-dimensional space, intersections of the curved network are readily possible. To avoid them, the networks have to be interconnected at these potential intersections. This changes the topology of the network. In this way a multitude of multi-furcated tunnel systems evolves. Such tunnel systems can be crystalline, quasi-crystalline, or amorphous. Crystalline networks can be systematized according to topological and symmetrical features. A.F. Wells has thoroughly described the topology of three-dimensional periodic networks.^[108] After a brief general introduction we will focus here on hyperbolic crystalline networks made up by hexagons and heptagons. According to the Euler-Schläfli equation the following relation holds for the number of i -dimensional elements N_i in a network:

$$\sum_{i=1}^j (-1)^i N_i = (-1)^j + 1 \quad (31)$$

For three-dimensional networks $j = 3$. We subsequently use the letter \mathcal{E} for the number of zero-dimensional elements N_0 (number of furcation points), \mathcal{K} for the number of one-dimensional elements (number of edges), and \mathcal{F} for the number of two-dimensional elements N_2 (number of polygons). If describing a network as a circumscription of a surface, this network divides space into two parts ($N_3 = 2$). We consequently obtain the already introduced Euler equation:

$$\mathcal{E} - \mathcal{K} + \mathcal{F} - 2 = 0 \quad (32)$$

A network is three-dimensionally periodic if it consists of an infinite amount of furcation points and edges and if it can be ‘cut’ at certain furcation points and edges in such a way that it splits up into an infinite number of identical partial networks. This does not necessarily have to be a translational partial network. Even the division into one or several topologically identical units which are non-translational, like a trigonal prism or a tetrahedron, can be regarded as a topological repetition. In such a case, however, the arrangement of several of such subunits has to lead to a translational unit.

These partial networks obtain additional furcation points, edges, and tunnel polygons (faces) t as a result of the cutting operation, which splits the tunnels of the infinite network. The additional furcation points and edges, however, void one another in the Euler equation due to their opposite sign (see Ill. 12).

Hence we obtain:

$$\mathcal{E} - \mathcal{K} + \mathcal{F} = 2 - t \quad (33)$$

The number of severed tunnels is equivalent to the genus g of this unit, in which case each severed tunnel leads to two tunnel polygons: $2t = g$.

The term $(2 - t)$ in eq. (33) is also referred to as the Euler-Poincaré characteristic of the described object.

Since the number of furcation points, edges, and polygons is directly linked to one another, above equation can be transformed. Because the number of furcation points \mathcal{E} is equal to the corners n of the respective polygon \mathcal{F}_n divided by the number p of polygons converging at this furcation point \mathcal{E} , the sum of all n -cornered polygons yields:

$$\mathcal{E} = \sum_{n=1}^m \frac{n}{p} \mathcal{F}_n \quad (34)$$

The number of edges \mathcal{K} is equal to half the number of edges n of the respective polygon \mathcal{F}_n , since each edge separates two polygons from another:

$$\mathcal{K} = \sum_{n=1}^m \frac{n}{2} \mathcal{F}_n \quad (35)$$

For the sum of all n -polygons we therefore obtain:

$$\mathcal{F} = \sum_{n=1}^m \mathcal{F}_n \quad (36)$$

Inserting these three equations into eq. (33), we obtain after transformation:

$$\sum_{n=1}^m \mathcal{F}_n \{4 - (n - 2)(p - 2)\} = 2p (2 - t) \quad (37)$$

with n = number of furcation points or edges per polygon, respectively, and p = number of edges per furcation point. Except for trivial cases (p or $n = 2$) and if using only one type of polygon, the factor in braces is zero if the resulting tessellation of space yields a plane: $p = 3 \rightarrow n = 6$ or vice versa, as well as $p = 4 \rightarrow n = 4$. Hence, if dealing with triple-connected networks ($p = 3$), the number of hexagons does not influence the value of this equation:

$$\sum_n \mathcal{F}_n \left(1 - \frac{n}{6}\right) = 2 - t \quad (38)$$

So if one wishes to obtain a closed, convex polyhedron with pentagons and hexagons, i.e. $t = 0$, then this requires 12 pentagons, independent of the number of hexagons. This result is, of course, widely known due to the fullerenes, whose broad variability with regard to the number of hexagons is restricted only downward due to the rising tension of the increasingly curved sphere. This is easily understandable, since within a triple-connected network hexagons can generate only a parabolic geometry, leaving the topology of the overall object untouched. The hexagon is therefore a neutral element for triple-connected networks, as the tetragon is neutral for quadruple-connected networks, and the triangle for the hexuple-(sixfold-)connected networks. If such neutral elements are included, the average number of corners per polygon of a certain object does therefore not permit any conclusion about the genus of this object. The average number of corners for various fullerenes for example, can vary between 5 at one extreme (dodecahedron) and 6 at the other extreme, which would be a hypothetical, infinitely large fullerene, i.e., an infinitely large graphene sheet with 12 pentagons. This has no influence on the genus of the respective object, as in all these cases $g = 0$.

One result of these considerations is that the genus of a triple-connected network increases only with the number of heptagons or larger polygons included. At the beginning of this chapter it has been shown that the sum of all angles between all edges emanating from one furcation point increases with increasing number of corners of the polygons converging at this furcation point. With an angle sum $>360^\circ$ the curvature at this location increases with increasing size of the polygons. The integral curvature of the entire object increases proportionally to this, if ignoring the topologically neutral hexagons. Both effects – increase of integral curvature *and* of the network's genus – are coupled via the size and number of non-neutral polygons. This complies with eq. (27) (p. 97), which determined an analytical connection between genus and integral curvature of an object.

Table 16: Number of n -Polygons \mathcal{F}_n in Topologically Repetitive Unit as a Function of Number of Tunnel Faces t with $p = 3$ (Schläfli Symbol n^3)								
n	t :	3	4	5	6	7	8	general
7		6	12	18	24	30	36	$6(t - 2)$
8		3	6	9	12	15	18	$3(t - 2)$
9		2	3	4	5	6	7	$t - 1$
10		—	3	—	6	—	9	$\frac{2}{3}(t - 2)$

Table 16 lists the number of required polygons with n corners ($n > 6$) for the generation of an integer number of tunnel faces t , and hence of a topological unit with a certain genus g for a triple-connected network in 3D space (Schläfli symbol n^3).

Topological units with an odd number of tunnel faces t , hence a fractional genus, can become translationally repetitive only if two of them are merged.

The same is true if using a mixture of different polygons with $n \neq 6$. The only prerequisite is that the number of resulting tunnel faces must be an integer, which in Table 16 in case of decagons is the case only for an even number of them. Table 17 gives as an example some possible combinations of triple-connected pentagons and octagons needed to obtain a 4-tunnel system ($g = 2$, $t = 4$, $p = 3$). The possibilities to link these polygons are galore; hence the Schläfli symbolism cannot be applied.

Table 17: Tessellation of Space with Pentagons and Octagons by Topological Units with $g = 2$ ($t = 4$, $p = 3$)				
\mathcal{F}_5 :	12	36	60	84
\mathcal{F}_8 :	12	24	36	48

The periodic minimal, zero-potential, and nodal surfaces belong to the objects whose topology can be characterized with such descriptions. The possibilities to tessellate space with certain topologically repetitive units of a particular number of tunnel faces and hence a certain genus g as given in Table 16 do not include sufficient information about the geometric and symmetric properties of these objects, whether or not, for instance, a particular combination is translationally periodic, i.e., crystalline, and which kinds of symmetry elements are contained in the unit cell. Schoen, for instance, gives five different options to form minimal surfaces of different geometry and symmetry with a translational, periodic unit of $g = 3$ (primitive unit cell).^[5] They differ with regard to their local curvatures. In a $(n,3)$ network with a given amount and arrangement of polygons with $n > 6$ this curvature is defined by the number and arrangement of hexagons, which are not included in the Euler equation, since it makes statements about topology only.

Chemically seen it is interesting to consider which of the options listed in Table 16 could be realized under which conditions. Since increased curvatures result in increased deviations from the ideal C–C bond angle of 120° in graphite, a reduction of the local negative Gaussian curvature by an increased number of hexagons seems necessary.

Since a high density of octagons (anti-aromatic) would destroy the continuous conjugation of the carbon network and because larger polygons would result in extreme changes of the C–C bonding angle, all subsequent considerations will be restricted to networks consisting of hexagons and heptagons.¹¹

5.1.3. On the Symmetry of Hyperbolic Networks

Considerations on symmetry allow to make decisive statements about the possible tessellations of a translationally periodic $(n,3)$ network made of hexagons and heptagons. It is for example impossible to have a fourfold axis run through hexagons or heptagons. Such axes have to run along tunnels and through tunnel openings (faces). In case of a cubic symmetry $3 \times m$ n -polygons have to be arranged symmetrically around threefold axes. Such an axis runs either through the center of a polygon with $3n$ corners or through the connection point of three equal polygons. $2 \times m$ n -polygons accordingly have to lie symmetrically around a twofold axis. Such an axis either runs through the center of a polygon with even corners or through the edge of two identical polygons.

Following the Euler equation, a network with three tunnel faces has to have 6 heptagons (the describing graph is trigonal planar; the graph's symmetry will be used henceforth to describe the networks investigated). One has to arrange three heptagons around a hexagon bearing the threefold axis on either side of the network in order to maintain the symmetry, and this does indeed generate such a network with $t = 3$, $\mathfrak{g} = 3/2$ (see III. 13-15).

The way of connecting polygons with an uneven number of corners to hexagons as well as the number of hexagons lying between them determines the curvature of the network and therefore the probability as a chemical structure. This pattern does also determine the existence of symmetry elements. If, for instance, mirror planes are to be re-

¹¹ Energy calculations suggest, though, that 8-membered rings need not reduce stability, probably since their distortion eliminates part of their anti-aromatic character and their larger flexibility in comparison to 7-rings permits a better relaxation of network tension. H. Terrones, A.L. Mackay, "Triply periodic minimal surfaces decorated with curved graphite", *Chem. Phys. Lett.* **207** (1993), pp. 45-50. Yet in order to reduce the problem considered here to a manageable size, a restriction to networks containing merely 7 and 6-rings may still be permitted.

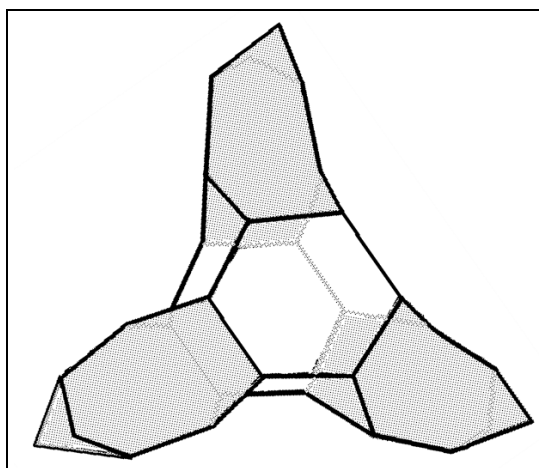
tained, polygons with an uneven number of corners parallel to the plane have to have a staggered arrangement, pointing at one another with either corners or edges. For some centric space groups the loss of mirror planes directly leads to the loss of the inversion center ($\bar{3} \rightarrow 3$). Further considerations about the symmetry of networks follow in the next chapter when dealing with specific examples.

5.2. Construction of Hyperbolic $(n,3)$ Carbon Networks

5.2.1. Simulation Using Analog Computers

The computational simulation of periodic networks with more than 100 furcation points and furcations quickly approaches the technical or reasonable temporal limits of modern computers, since the number of iterative calculation steps grows exponentially with the size of the network. Mathematicians call such problems which elude a deterministic polygonal solution np-complete. This means that so far no algorithm has been found to solve an np-complete problem with a number of calculation steps O which is a function of a constant exponent n of the number of operands x : $O \neq x^n$. In the most unfavorable of all cases the number of operands is actually the exponent so that the number of calculation steps necessary to solve the problem increases exponentially with the number of operands: $O = n^x$.^[129,130] Although Dress and Franz have shown that there is only a finite number of solutions for the tessellation of topologically defined objects obeying certain boundary conditions, their approach does not take into consideration the symmetry of the patterns used.^[131] We therefore resorted to the use of analog computers, that is to say: we built our models using molecule construction kits. These models may elucidate the acting patterning rules and symmetry laws of such networks.

The first most parsimonious possibility to realize a trigonal planar subunit for a network consisting of hexagons and heptagons ($g = 3/2$) is given by adjoining three heptagons directly to a central hexagon forming the threefold axis and by letting two edges of each heptagon coincide with identical



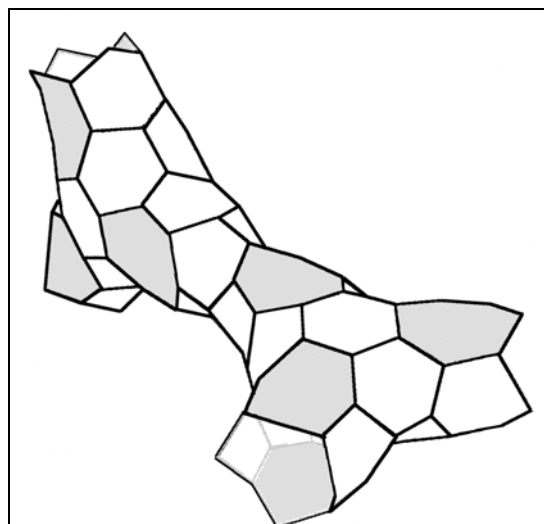
III. 13: First possibility to construct a network, consisting of hexagons and heptagons, with a unit of $g = 3/2$ (trigonal planar).

edges of the mirror-symmetrical heptagons on the other side of this subunit. The tunnel exits generated in such a way are formed by merely 4 corner points, which would be chemically rather unlikely due to the intense ring tension (Ill. 13, p. 108).

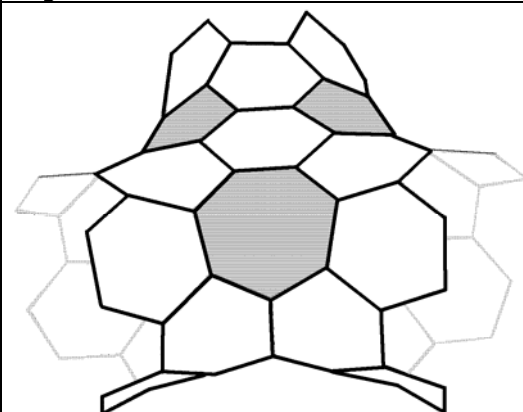
An expansion of this network unit can be achieved by either adding hexagons around the mirror plane perpendicular to the C_3 axis and/or by keeping a larger distance between the heptagons arranged around the central hexagon of the C_3 axis. Ill. 14 shows two subunits of the network in Ill. 13 with an additional row of hexagons added along the mirror plane perpendicular to the C_3 axis. Ill. 15 shows a network unit of the same genus but with the heptagons rotated by 60° .

The subunits with genus $3/2$ can become translational only if two of them are merged mirror-symmetrically, resulting in a network with $g = 2$ (Ill. 14). The minimum genus required for two dimensions is $g = 2$, for 3D

translationality $g = 3$. The number of possible ways to connect such subunits grows with the number of tunnel faces (=exits) and with the number of furcation points at these exits. While the subunit shown in Ill. 13 permits only planar, hexagonal networks to be formed (if preventing the direct connection of four heptagons at two merging tunnel faces), the unit in Ill. 14 permits the formation of a three-dimensional hexagonal network, as the topological units can be turned by 90° with each merging tunnel. The network depicted in Ill. 15 allows the formation of fourfold screw axes due to its eight possible furcation points at its tunnel exits. It would be desirable to connect this trigonal unit following the pattern of the periodic nodal surface $I_2 - Y^{**}V^*$ of the space group $Ia\bar{3}d$ (No. 230; Ill. 2.a, p. 56). The two nodal surfaces of this function divide space into three parts, two of which are chiral to each other, separated by the third. The generating function of this nodal surface has its extrema on the point configurations I_2 as well as Y^{**}



Ill. 14: Two linked subunits with an added row of hexagons, compared to Ill. 13, with two units of $g = 3/2$ (trigonal planar) $\rightarrow g = 4/2 = 2$.



Ill. 15: Unit made of hexagons and heptagons, $g = 3/2$. Position of heptagons rotated by 60° compared to Ill. 14.

Table 18: Symmetry of Topological Units of 3D Networks with $p = 3$, Arrangement of the Heptagons \mathcal{F}_7 around n -fold Axes C_n				
t	\mathcal{F}_7	Type of Polyhedron	Fulfillment of Euler equation	Point Group
3	6	trigonal planar	2·3 \mathcal{F}_7 around C_3 or 3·2 \mathcal{F}_7 around $C_2 = 6 \mathcal{F}_7$	$\bar{6}m2$
4	12	tetrahedral	2·4 \mathcal{F}_7 around $C_2 + 2·2 \mathcal{F}_7$ around C_2 or 6·2 \mathcal{F}_7 around $C_2 = 12 \mathcal{F}_7$	$\bar{4}3m$
		tetragonal planar	4·3 \mathcal{F}_7 around C_3 or 2·6 \mathcal{F}_7 around $C_2 = 12 \mathcal{F}_7$	mmm
5	18	trigonal bipyramidal	2·6 \mathcal{F}_7 around $C_3 + 3·2 \mathcal{F}_7$ around $C_2 = 18 \mathcal{F}_7$	$\bar{6}m2$
6	24	octahedral	8·3 \mathcal{F}_7 around $C_3 = 24 \mathcal{F}_7$	$m\bar{3}m$
7	30	pentagonal bipyramidal	5·6 \mathcal{F}_7 around C_2 or 2·5 \mathcal{F}_7 around $C_5 + 5 \cdot \left(2 + \frac{4}{2}\right) \mathcal{F}_7$ around $C_2 = 30 \mathcal{F}_7$	$\bar{10}m2$
8	36	cubic, non-translative	6·6 \mathcal{F}_7 around $C_2 = 36 \mathcal{F}_7$	$m\bar{3}$
		cubic	$8\frac{6}{2} \mathcal{F}_7$ around $C_3 + 6·2 \mathcal{F}_7$ around $C_2 = 36 \mathcal{F}_7$	$m\bar{3}$
12	60	cuboctahedral	8·6 \mathcal{F}_7 around $C_3 + 6·2 \mathcal{F}_7$ around C_2 or 8·3 \mathcal{F}_7 around $C_3 + 6·6 \mathcal{F}_7$ around $C_2 = 60 \mathcal{F}_7$	$m\bar{3}$
14	72	capped cubic	12·6 \mathcal{F}_7 around $C_2 = 72 \mathcal{F}_7$	$m\bar{3}m$

and V^* , respectively (see Table 11, p. 77). The point configurations Y^{**} and V^* generate within the chiral partial spaces equivalent chiral networks (graphs) consisting of trigonal subunits, namely the line segment graph $Y^{**}(\frac{1}{8}, Y, \bar{Y} + \frac{1}{4})_{Y=0}^{Y=1/8}$ as given in Table 12 (p. 84). The trigonal surface subunits surrounding this graph are the topological building units of the PNS $I_2-Y^{**}V^*$. The planes defined by these trigonal graph units run orthogonal to the space diagonal of the cubic unit cell. The torsion angle between two linearly connected trigonal graph units is therefore $70.52878\dots^\circ$ (exactly: $2 \times \arccos(\sqrt{2/3})$).

If connecting analogous tunnel networks with each other, then this happens by way of a natural number of furcation points n . Hence every possible connection torsion angle is a multiple of $360^\circ/n$. In order to achieve a torsion angle identical to that of the Y^{**} graph we must have:

$$m \cdot \frac{360}{n} = 2 \cdot \arccos(\sqrt{2/3}) \quad (39)$$

This is given only if $\arccos(\sqrt{2/3})$ can be rendered as a fraction of natural numbers (rational number). But since this is an irrational number, it follows that it is impossible to construct a translational periodic network analogous to the periodic nodal surface $I_2-Y^{**}V^*$. The same is true for the so-called Gyroid (minimal surface of the same space group) and the analogous PNS Y^{**} , both of which have partial spaces that are

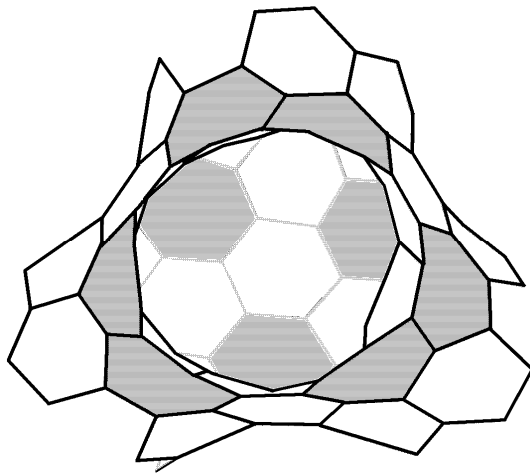
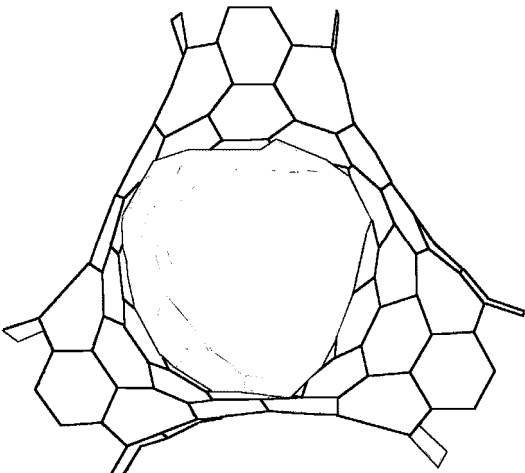
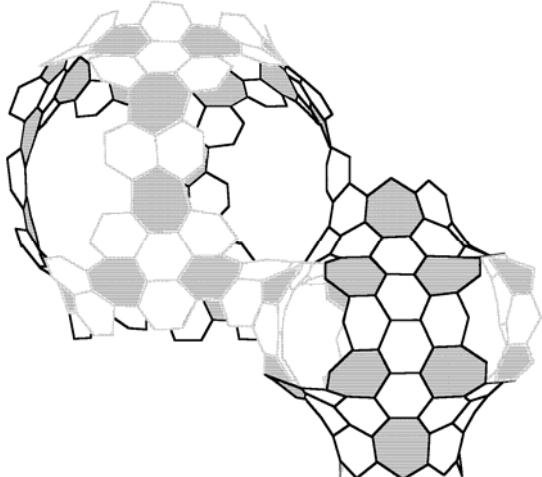
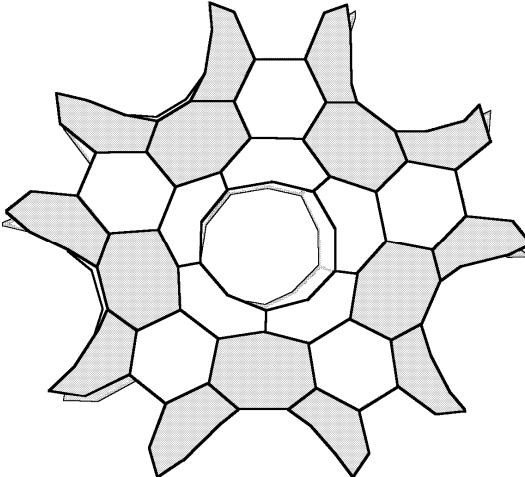
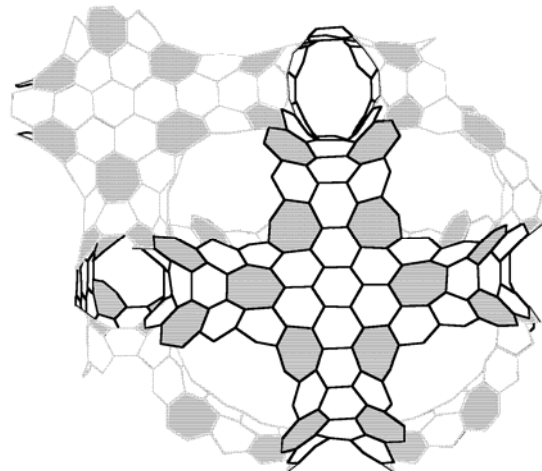
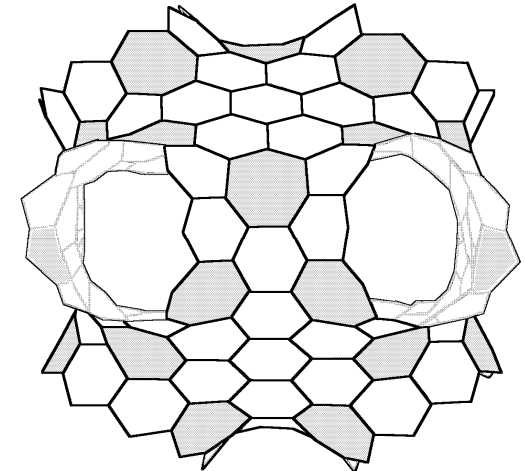
chiral to each other and are arranged around the network graph formed by the point configuration Y^{**} , although in this case without a third, separating partial space. (Ill. 5.e, p. 62)

Several solutions for networks of a higher genus are presented subsequently. Table 18 (p. 110) lists some topological construction units as a function of tunnel faces t . Column 2 contains the number of heptagons \mathcal{T}_7 prescribed by the Euler equation, column 3 the polyhedron of the respective genus ($g = t/2$), where the vertices of the polyhedra are equated to tunnel exits of the matching network unit. Column 4 lists several solutions to fulfill the required symmetry of each polyhedron with the needed number of heptagons according to Euler as well as their distribution around the respective symmetry elements. Column 5 contains the highest possible point group of this topological unit. Ill. 16-22 (pp. 112f.) show some of these construction units.

Ill. 18 depicts a network with $t = 6$ where both partial spaces have been tessellated to form an octahedron. It can easily be seen that both partial spaces are not identical. The reason for this is that the polygons surrounding the tunnel exits are linked via edges in one case but via corners in the other. The ratio of the distances of opposite edges and corners in a hexagon is irrational ($2:\sqrt{3}$).

It is therefore impossible to obtain equal curvatures and thus identical partial spaces, not even by connecting heptagons directly to one another, which would interrupt the continuous conjugation of the carbon network (see Ill. 16). This means that such carbon networks cannot generate hyperbolic surfaces equivalent to minimal surfaces with identical partial spaces such as Schwarz' P^* surface (an octahedral system with six tunnel faces per unit cell; Ill. 3.1, p. 58, shows the equivalent PNS) or the D^* surface (eigen symmetry $Pn\bar{3}m$, supergroup of $Fd\bar{3}m$, for its PNS equivalent see Ill. 2.g, p. 56).

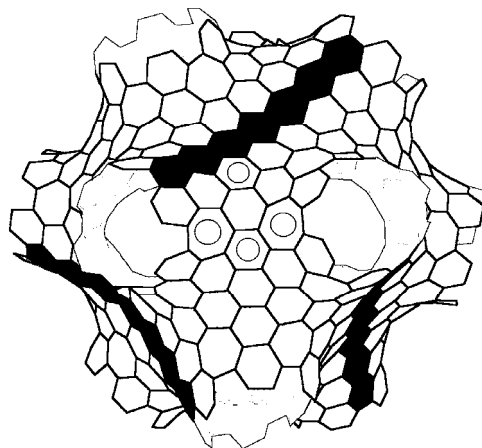
The topological unit with $g = 4$ ($t = 8$, Table 18) with cubic symmetry corresponds to the topological unit, i.e. the primitive unit cell of the well-known body-centered minimal surface I – WP as discovered by Schoen,^[5] which is very similar to the periodic nodal surface $I_{xxx} - J^*$ (Ill. 2.c, p. 56). Since the crystallographic unit cell consists of twice the content of a primitive cell (body-centered), the unit cell of the respective network requires 72 heptagons. The minimal surface I – WP has a genus of $g = 7$, which corresponds to 14 tunnel exits. This result is consistent with the value determined in chapter 4.5. (p. 92ff.) using the *labyrinth-graph method* with the relation between primitive and centric setups as given by eq. (26) (p. 96). The 14 tunnel exits of the PNS $I_{xxx} - J^*$, corresponding to the genus of 7 for the body-centered rendering, can be rec-

 <p>III. 16: Unit of a (6,7) network with $g = 2$ ($t = 4$) in tetrahedral arrangement.</p>	 <p>III. 17: Unit of a (6,7) network with $g = 5/2$ ($t = 5$) in trigonal-bipyramidal arrangement.</p>
 <p>III. 18: One unit each of the 'left' and 'right' partial space with $g = 3$ ($t = 6$) in octahedral arrangement.</p>	 <p>III. 19: Unit with $g = 7/2$ ($t = 7$) in pentagonal-bipyramidal arrangement of a quasi-crystalline (6,7) network.</p>
 <p>III. 20: Unit with $g = 4$ ($t = 8$) in cubic arrangement, including three units of the other partial space with $g = 2$ in tetragonal-planar arrangement.</p>	 <p>III. 21: Unit with $g = 4$ in cubic arrangement. Due to special choice of heptagon tessellation non-translative!</p>

ognized if calculating the surface acentrically (origin at $\frac{1}{4}\frac{1}{4}\frac{1}{4}$ from $\bar{3}m$, Ill. 8.j, p. 90): Two exits each are located at each of the six occupied corners of the cube plus two exits in the other partial space (the tunnel system itself, forming a ring in the body-centered unit cell of this rendering, has already $g = 1$, $t = 2$ even in the absence of any tunnel faces!). In this context one has to consider that exits located at edges and corners of the unit cell have different crystallographic values than those located at faces, since the first two cases always consist of furcation points of tunnels (in analogy to the *labyrinth-graph method*).

In order to determine the genus of a labyrinth structure following the *Euler method*, one first has to dismantle the maze into its constituent topological building units. By so doing each furcation point of tunnels is considered to be the center of a separate topological unit, which subsequently is connected to other units only via the face of a topological unit cell. This way the genus and the number of necessary n -polygons can be determined easily. The number of required n -polygons for the entire structure directly determines its genus via eq. (38) (p. 105). It is irrelevant which partial space – potentially made up of different building units – is assessed that way.

The topological base unit of the one partial space of the above-mentioned minimal surface I – WP, for instance, is a quadratic planar subunit, of which six are contained in a body-centered unit cell. 6×12 heptagons results in 72, just as 2×36 heptagons required for the two cubes of the other partial space. A network built by subunits similar to those mentioned above, requiring quadratic planar subunits, can be constructed only with tetragonal distortion when using hexagons and heptagons, since no fourfold axes can be realized with such polygons. Ill. 20 shows such a network, consisting of tetragonal planar units with four tunnel exits and 2×3 heptagons each in one partial space and made up of cubes in the other partial space (Table 18). The alternating arrangement of the six tetragonal subunits inexorably results in the fact that heptagons are lying on the border of the primitive unit cell, six each around each opening (C_3 ax-



Ill. 22: Unit with $g = 6$ in cuboctahedral arrangement. When removing the chains of black hexagons, one obtains an icosahedral arrangement of the tunnel faces. Another option is obtained when relocating the heptagons marked with circles onto the locations of the similarly marked hexagons.

Table 19: Comparison of PMS and PNS with Hypothetical Graphite Networks

PMS/PNS	SG Surface/ Partial Space	g of Partial Space (Primitive)	SG Network	Symmetry of Network Units
P/P*	$\text{Im}\bar{3}\text{m}/\text{Pm}\bar{3}\text{m}$	3	$\text{Pm}\bar{3}\text{m}$	octahedral
D/D*	$\text{Pn}\bar{3}\text{m}/\text{Fd}\bar{3}\text{m}$	3	$\text{Fd}\bar{3}\text{m}$	twice tetrahedral
G/Y**	$\text{Ia}\bar{3}\text{d}/\text{I4}_132$	3	—	—
$-\text{I}_2-\text{Y}^{**}\text{V}^*$	$\text{Ia}\bar{3}\text{d}$	twice 3	—	—
Neovius / (PJ)*	$\text{Pm}\bar{3}\text{m}$	9	$\text{Pm}\bar{3}$	cubeoctahedral + thrice tetragonal planar
I-WP/ I_{xxx} -J*	$\text{Im}\bar{3}\text{m}$	4	$\text{Im}\bar{3}$	twice cubic or sixfold tetragonal planar
F-RD / $\text{FF}_{\text{zx}}-\text{FP}_2$	$\text{Fm}\bar{3}\text{m}$	6	$\text{Fm}\bar{3}$	eightfold tetrahedral + fourfold cubic or fourfold cubeoctahedral
$\text{O}_2\text{C}-\text{TO} / \text{PPJ}-\text{J}_x$	$\text{Pm}\bar{3}\text{m}$	10	$\text{Pm}\bar{3}$	cubic + capped cubic

is), which therefore count only half for each unit. This tessellation pattern for a cubic unit is the second example listed in Table 18. In case of the first example all heptagons lie within the unit cell, which prevents the formation of planar subunits with four tunnel exits in the other partial space. If constructing cubic units one therefore has to keep in mind what subunits have to be generated in the other partial space. Hence, if the topological units of both partial spaces separated by the carbon network are different, the choice of polygon tessellation pattern following the Euler equation has to take into consideration all topological building units.

Further peculiarities arise for the distorted cubeoctahedral structure. The cubeoctahedron is related to the icosahedron. If reducing the network shown in Ill. 22 along the $\{100\}$ planes by the hexagon chains rendered black, then one obtains a structure with icosahedral symmetry. The topological unit shown in Ill. 22 can be connected in different ways. If connected to identical subunits via the tunnels, a network results with strong similarity to Schoen's minimal surface F – RD or the analogous PNS $\text{FF}_{\text{zx}} - \text{FP}_2$ (SG $\text{Fm}\bar{3}\text{m}$, 225, Ill. 3.b, p. 58). One partial space consists of four cubeoctahedrons, the other of a pattern well known from spinels: 13 tetrahedra linked via vertices plus four cubes, the dual polyhedron of the octahedron. This yields a genus $g = 21$ (240 heptagons) for this structure, or for the primitive cell: $g = 6$ (60 heptagons). Both cubeoctahedra listed in Table 18 are suited to build this structure, since in both cases appropriate tetrahedra can be generated. The second of the two structures shown in Table 18 can be generated from the first depicted in Ill. 22 by simply swapping the set of two heptagons marked with a circle with the equally marked hexagons.

Another structure accessible with cuboctahedra is Neovius' PMS or the equivalent PNS (PJ)* (Ill. 4.a, p. 60). In this case the cuboctahedra are connected via tetragonal planar subunits with four tunnels exits. In order to obtain these tetragonal planar subunits, only the first example of cuboctahedra listed in Table 18 is suitable, as here again 6 heptagons have to be located on the $\{100\}$ planes.

Table 19 (p. 114) lists several known minimal surfaces as well as PNS with their space groups SG and that of the partial space, if different (=generating symmetry). Column 3 contains the genus of the primitive unit cell. Column 4 lists the highest possible symmetry obtainable with corresponding carbon networks, if at all possible. The last column lists the topological units required for their construction, taken from Table 18.

5.2.2. Feasibility as Chemical Structure

Up to this date there does not seem to exist an analytical answer to the question whether or not a certain hyperbolic tessellation pattern leads to translational networks. The formation of structures in which two hexagons and one heptagon meet at each corner point (6^27 , pattern of fullerene C_{60}) will most certainly lead to amorphous networks, as the repetitive sevenfold site symmetry destroys all translational symmetry elements. When placing heptagons strategically, though, quite high symmetries can be obtained, although excluding C_4 axes perpendicular to the network. It should also be possible in certain cases to embed incommensurable networks in minimal or nodal surfaces of corresponding genus and geometry. This would correspond to minimal interfaces of lipid-water mixtures, which exhibit global symmetry while lacking local symmetry.^[15-28]

By subdividing the targeted structure into topological building units, it is facilitated to comprehend and thus construct them. This makes it easier to coordinate topological requirements as given by Euler's equation with symmetrical necessities of arranging heptagons around certain symmetry elements.

The geometry of hexagons prevents the formation of networks analogous to the minimal surfaces P and D, as the partial spaces separated by the network need to be identical (black-white symmetry).

With regard to a hypothetical synthesis of the networks described here it must be emphasized that the conditions for the formation of hyperbolic networks are profoundly different to those of elliptical structures like the fullerenes. While the use of 12 penta-

gons will always and ineluctably lead to a spherical structure no matter how many hexagons are involved, the formation of hyperbolic networks is completely undetermined. While building models, it seemed at times inevitable to us pentagons or even tetragons in order to reduce the tension which had built up by the heptagons within the sp^2 carbon network. The probability to obtain certain tessellation patterns of hexagons and heptagons as described here seems extremely unlikely. The formation of hyperbolic networks appears to be more likely if larger n -polygons are used, which, due to their internal flexibility, can alleviate the network tension. It goes without saying that sp^2 -hybridized carbon differs fundamentally from silicon, whose tetrahedral bonding angles are readily capable of forming hyperbolic networks. It therefore seems far more likely that hyperbolic topological units as described here, if at all obtainable, will be terminated by C_{30} hemispheres capping the tunnel exits, as this is, entropically seen, far more likely than the formation of infinite networks.

Lenosky et al., Adams et al., and Townsend et al. have performed calculations with hypothetical graphite networks similar to the P^* and D^* surfaces. According to this these structures lie energetically between C_{60} and diamond.^[132-134] O'Keefe, Adams, and Sanku have shown that hyperbolic carbon modifications consisting of hexagons and octagons should be very stable energetically.^[135] Such networks would resemble three-dimensional infinite [2.2.2] benzenophene-like scaffolds. Mackay and Terrones^[136] have given an overview of articles published about hyperbolic graphite structures.¹²

¹² For a more recent study covering not only "Schwarzites" (the name recently given to hypothetical hyperbolic sp^2 carbon networks) but also many other exotic carbon structures see: H. Terrones, M. Terrones, L. López-Urías, J.A. Rodríguez-Manzo, A.L. Mackay, "Shape and complexity at the atomic scale: the case of layered nanomaterials", *Phil. Trans. R. Soc. Lond. A* **363** (2004) pp. 2039-2063), with further references.

6. Organization of Chemical Structures by PNS

6.1. Introductory Remarks

This chapter will explore the structural organization of a range of exemplary element and compound structures by PNS. Since mainly PNS of the cubic crystal family have been investigated for this thesis, the focus will be on cubic structures in this chapter as well. In particular for complex structures the PNS approach will be tested regarding its ability to lucidly organize chemical structures and maybe even reveal new insights. This is especially true for non-Euclidian layer structures (cf. p. 101). When introducing minimal surfaces the terms of positive and negative Gaussian curvatures have been explained (pp. 13ff.). The chapter on hyperbolic graphite-like networks showed how networks with a positive Gaussian curvature form closed, elliptic objects whereas those with a negative Gaussian curvature form hyperbolic surfaces (pp. 101ff.).

It is common practice in solid state chemistry to regard chemical structures either as plane, Euclidian layers or as Euclidian packings of elliptic objects. By so doing only two of the three possible cases of Gaussian curvatures are used, namely those with $G = 0$, i.e. layered structures, and those with $G > 0$, i.e. packings of elliptic objects. Even assemblies of coordination polyhedra to larger clusters (scaling of substructures) or the arrangement of polyhedra to form layered packages all belong to structures with $G \geq 0$. In particular the common description of crystalline structures as Euclidian layers is a remarkable mathematical restriction, since the case of $G = 0$ is a special case with rather low probability, mathematically speaking. The subsequent subchapters will highlight examples of crystalline chemical networks which form non-Euclidian hyperbolically layered structures, smoothly arranged along hyperbolic surfaces. The concept of periodic nodal surfaces is predestined to serve as an instrument of discovery of such structural features, since the appropriate PNS intrinsically carry the crystal's symmetry and in most cases divide space with hyperbolic surfaces. The illustrations 23-30 referred to in the following subchapters are located on pp. 128-142.

6.2. Elements

6.2.1. Diamond

The PNS $D^* \triangleq {}^{227}\langle III \rangle^{224}$ (Ill. 2.g, p. 56) is frequently referred to as the ‘diamond surface’ in the literature. Since this surface has the eigen symmetry $Pn\bar{3}m$, this denomination is incorrect. The diamond network occupies only one of the two identical tunnel systems of the D^* surface, hence has $Fd\bar{3}m$ symmetry. Ill. 23.a shows a PNS with an eigen symmetry of $Fd\bar{3}m$: $D - DT \triangleq {}^{227}\langle (III)_{5/2}^{-\pi/4}; (220) \rangle$ (000 at $\bar{4}3m$). The relative contributions of the two structure factors have been optimized to barely prevent the formation of singularities. If $S(220)$ is too large, then bubbles will form at $\frac{1}{4}\frac{1}{4}\frac{1}{4}$. The relation of the two $S(hkl)$ to each other is therefore not arbitrary. Ill. 23.a also depicts the extrema graphs of the generating function, which has the same characteristic as the D^* graph, although it has different values (see Table 12). When calculating this PNS centrically, it is clear that this surface is merely a mild modulation of the D^* surface (Ill. 2.i, p. 56).

In 1991 Savin et al. succeeded in calculating the electron localization function (ELF) of solid materials.^[137] The function developed by Becke and Edgecombe^[138] corresponds to the probability of one electron to encounter another electron at a given location having the same spin. In principle ELF is observable like the electron density $\rho(xyz)$, to which it adds an additional quality. Ill. 23.b shows a cross section along $\{101\}$ of an ELF calculation for the diamond unit cell.^[139] The coloration follows the pattern of geographical maps with white indicating a high localization value and blue a low value. The D^* surface has been superimposed onto this image with the equivalent orientation. The ELF along the PNS has a medium value (green). If depicting this medium value as a surface, it is topologically identical to the corresponding POPS and PNS. Hence, there exist topologically identical three-dimensional periodic surfaces both of constant electron density as well as of a constant ELF value. These surfaces, however, have little to do with the contours of the carbon atoms. They are determined by the symmetry of the generating translational group.

6.2.2. α -Manganese

α -Manganese is the most complex of all element structures.^[140] It is based on four crystallographically independent atomic positions in the space group $\bar{I}43m$, with three different coordination numbers (2×16 , 1×13 , 1×12).^[141] Neutron diffraction experiments have revealed that these four positions are occupied by Mn atoms with different magnetic moments.^[142] This allows the assumption that each different Mn atom has different spatial needs. The structure of α -P₄ can be regarded as a higher order of this type, as in this case each Mn position is occupied by the center of a P₄ tetrahedron.^[143] Here as well the four different sets of P₄ tetrahedra occupy very different amounts of space, which shows up in their different thermal motions. In a sense this complex structure type is therefore a prototype for a spatial arrangement of units with different sizes.

The organization of this structure can be described in various ways:

- a) Without Ill.: Hellner and Koch have described α -Mn as a network and highlighted parallels to structurally related compounds.^[144]
- b) Ill. 23.c: Mn₁₃ clusters, centered around one Mn atom each on 000 (coordination no: 12) plus 12 Mn in the shape of a truncated tetrahedron. These Friauf polyhedra are separated from one another by the PNS $P^* \triangleq {}^{221}\langle 100 \rangle^{229}$. The remaining Mn atoms wrap these clusters, most of them close to the surface. This rendering is symmetrical-ly inappropriate, however, since identical clusters are separated from one another and because the tetrahedral symmetry of this space group is not included.
- c) Ill. 23.d: here α -Mn is organized by the PNS $II_{xxx}W^* - I_{xxx} \triangleq {}^{217}\langle (211)^{-\pi/4} \rangle$ (a PNS without degrees of freedom), exhibiting the proper symmetry $\bar{I}43m$ of this structure. The four different positions of Mn atoms are rendered in different colors. This PNS separates different positions, which are either located on the surface or within the partial spaces.

6.3. Compounds

6.3.1. Compounds of the Cr₃Si type

The phases of the Cr₃Si type (also frequently and erroneously called A15 phases) crystallize in the space group $Pm\bar{3}n$. A structural relationship between the PNS $P_2 - IW_z \triangleq {}^{223}\langle (110)_2^{\pi}; (200)_4^{\pi}; (210) \rangle$ and the construction principle of the “A15” superconductors

and the sodium platinum oxides ($\text{Na}_x\text{Pt}_3\text{O}_4$) deserves attention. In Nb_3Sn and Nb_3Ge (Cr_3Si type, the latter one with a particularly high critical temperature) Nb occupies the position $0\frac{1}{2}\frac{1}{2}$ (Wyckoff position 6b, $PC J^*$), i.e., they are lined up along the constant line graph $x\ 0\frac{1}{2}$ ($12g, W_z$) of the PNS $P_2 - IW_z$ (Ill. 3.g, p. 58).^[145] The existence of constant, linear extrema with this PNS of $\text{Pm}\bar{3}n$ symmetry along the Nb positions of the superconductors Nb_3Sn and Nb_3Ge gives rise to the speculation whether this is a peculiarity of this particular space group. Apparently its symmetry forces, under certain circumstances, the formation of constant values or properties along certain straight channels throughout the entire crystal.

Mackay surmised that new insights about the mechanisms of superconduction could be gained by structuring oxidic compounds of lower symmetry with the help of minimal surfaces.^[146]

The platinum bronzes^[147] of the general composition $\text{M}_x\text{Pt}_3\text{O}_4$ have been investigated first by Waser and McClanahan^[148] and later have been diversified and characterized by Scheer, v. Arkel, and Heyding,^[149] by Cahen et al.^[150,151] as well as by Bergner and Kohlhaas,^[152] among others. Of particular interest is the metallic conductivity of single crystals of many of these compounds. The parent structure is a network of platinum (Wyckoff position 6c, $\frac{1}{4}0\frac{1}{2}$), which is planar-quadratically coordinated by oxygen ($8e, \frac{1}{4}\frac{1}{4}\frac{1}{4}$). The platinum forms Pt–Pt bonds (277 pm) in all three directions of space, resulting in metallic conductivity.^[150] In Ill. 8.h (p. 90) the extrema graph of one partial space of the PNS $P_2 - IW_z \triangleq {}^{223}\langle(110)_2^\pi; (200)_4^\pi; (210)\rangle$ has been included. It is topologically equivalent to the network formed by oxygen and platinum consisting of 8-membered rings of alternately three (O) and fourfold (Pt) connected atoms. Following Well's nomenclature,^[108] this is a $(8\frac{3}{4})$ network. The only difference between the PNS graph and the chemical structure is that in case of the PNS the position 6d ($\frac{1}{2}0\frac{1}{4}$) is used to generate the network whereas the compound uses the equivalent position 6c. These positions are interchangeable, though, by simply changing the setup (rotation by 90°). If leaving the PNS, however, the surface separates the oxygen from the platinum, which are then all located on the constant extrema of the three-rod packing (graph $W(x, 0, \frac{1}{2})_{x=0}^{x=1}$, Ill. 3.g, p. 58). The metallically conducting Pt–Pt bonds then run exactly along these constant extrema of the PNS's function. This reveals a similar feature as postulated for the “A15” superconductors.

On the importance of rod packings in solid state chemistry see [153].¹³

¹³ See also and more recently: S. Lidin, M. Jacob, S. Andersson, “A mathematical analysis of rod pack-

6.3.2. Barium Cuprate, BaCuO₂

Müller-Buschbaum has been focussing for quite a while on the investigation of ternary oxo-cuprates,^[154-158] and by so doing built an important foundation for the discovery of oxidic high-temperature superconductors, which attracted enormous attention some time later. Besides the influence of the kind of alkali-earth metal the main focus has been on the effect of the stoichiometric ratio of oxygen and copper on the coordination sphere of copper. Several ways of connecting the usually planar-quadratically coordinated Cu²⁺ atoms have been observed: squares of CuO_{4/2}²⁻ linked two-dimensionally to planes, one-dimensionally to plane or waved ribbons and double-ribbons, as well as isolated clusters. In addition oxo-halogeno cuprates(II) exhibit a distorted octahedral coordination explicable with the normal ion radii.^[157,158] Particular emphasis has been given to newly discovered isolated clusters of several CuO_{4/2}²⁻ units combined to polyhedra, as in Ba₉Cu₇O₁₅Cl₁₂ as a minority component,^[158] but then also as a pattern dominating the structure of BaCuO₂ (space group Im $\bar{3}$ m).^[159]

This highly complex and highly symmetrical structure is depicted in Ill. 23.f together with the PNS $IJ^* - P_2 \triangleq {}^{229}\langle(110);(200)\rangle$, which has been calculated beyond the borders of the unit cell along one edge. Oxygen is represented by blue, copper by red, and barium by yellow spheres. The quadratic CuO₅ pyramids oriented to one another with their bases, visible in the narrow ‘bottle necks’ of the PNS, are statistically occupied to only 50%, which is why they can be positioned so closely together. The two identical labyrinth systems generated by the PNS perfectly enwrap the hexaicosahedra formed by the 21 CuO_{4/2}²⁻ units. They separate them from the hexagonal prisms of 6 CuO_{4/2}²⁻ units which are centered around the position $\frac{1}{4}\frac{11}{44}$ orthogonally to the threefold axes. Except for one position all Ba atoms are located on the PNS itself. Another detail can be gleaned from Ill. 24.a: the function generating the PNS $IJ^* - P_2$ has a minor extremum at the position $\frac{1}{2}00$ (point configuration J*), as a result of which the surface is a little bulged in the middle of the tunnel. The quadratic pyramids mentioned above are located at exactly this spot. Hence, if one intended to wrap this polyhedron network with a skin, it would assume the shape of the PNS shown here down to the tiniest detail. The PNS therefore ensheathes the covalently bound poly-anion framework and separates it from the barium cations, which are located close to the PNS and thus close to the poly-anion. This example highlights the stunning congruency of fundamental, symmetrical patterns of the

ings”, *J. Solid State Chem.* **114** (1995) pp. 36-41.

space group $\text{Im}\bar{3}\text{m}$ with the entire structure of BaCuO_2 .

The double tunnel system of this PNS contains only some 60% of the space of the third, partial space separating them (Table 13, p. 86). Hence, each tunnel labyrinth has only ca. 30% of the volume of the separating partial space. If assuming that the PNS is completely enwrapping the cuprate network, then this network occupies only some 37% of the entire volume of this structure ($\frac{59}{100+59}$), while the rest is occupied by the hexagonal cuprate prisms and most of all by the very voluminous barium cations.

6.3.3. $\text{Bi}_{22}\text{Sr}_{36}\text{Al}_{48}\text{O}_{141}$

While exploring ternary and quaternary metal oxides in the context of searching further superconducting oxides, Popp came across a most complex structure, in which chemically different regions are formed by the generation of an onion-like spherical shell assembly embedded in an hyperbolic network.^[160] The pervasive hyperbolic aluminate network consists of condensed AlO_4 tetrahedra. This network creates caverns of ca. 19 Å diameter, in which several closed spheres of Sr, Bi, and O of various sizes encapsulate one another. The empty center ($\varnothing \approx 5$ Å) is enclosed by a pure Bi(III) oxide shell whose single electron pairs point toward the center. Next follows a covalently bonded oxo-bismuthate(III) shell with single electron pairs pointing outward. The inner part of this multi-layered sphere assembly therefore consists exclusively of Bi and O atoms ($\varnothing \approx 8\text{--}9$ Å) with a strong radial polarity gradient. The subsequent spherical shell around this consisting of Sr^{2+} ions is at once the outermost sphere acting like an interface between the elliptically curved bismuthate(III)-bismuth oxide core and the hyperbolically curved aluminate wrapping. A small amount of additional Sr^{2+} cations is octahedrally coordinated by 6 O atoms of a star-shaped arrangement of 12 AlO_4 tetrahedra, which form at once an intersection of the hyperbolic network. Since the distribution of Sr, BiO and AlO clusters in this space group $\text{F}\bar{4}3\text{m}$ resembles an fcc packing, this structure is sufficiently well adapted by the PNS $\text{FF}_{\text{zx}} - \text{FP}_2 \triangleq {}^{225}\langle(III)_2;(220)^\pi\rangle$ ($\text{Fm}\bar{3}\text{m}$, Ill. 24.b).

Ill. 24.c shows one octant of the unit cell. The yellow AlO_3 framework follows the PNS in the silver-colored partial space. The Sr^{2+} cations (orange) are located close to the PNS, whereas the bismuthate(III)-bismuth(III) oxide shell (blue) is located in the cavern of the green partial space, which has 12 exits in accordance with the cuboctahe-

dral environment of an fcc packing. Hence, this PNS organizes the covalently bound ${}^2_{\infty}[\text{AlO}_n]^{n-}$ network and the bismuthate(III)- bismuth(III) oxide shells in a different partial space, separated by the Sr^{2+} shells, which are connected to the other two structures by electrovalent interactions.

6.3.4. Molybdato-Phosphates

Haushalter has focused on the chemistry of molybdato-phosphates.^[161-166] Two of these compounds will be considered here.

The molybdato-phosphate of stoichiometry $[\text{Et}_4\text{N}]_6[\text{Na}_{14}\text{Mo}_{24}\text{P}_{17}\text{O}_{97}(\text{OH})_{31}] \cdot x \text{H}_2\text{O}$ crystallizing in the space group $\text{Pn}\bar{3}$, is characterized by three different building units: a network-like distribution of Et_4N^+ (N=blue, C=white), a molybdato-phosphate sandwich cluster (MoO_6 octahedra green, PO_4 octahedra red) with a Na^+ ion (yellow) as central atom, as well as ‘free’ phosphoric acid in large cavities, see Ill. 24.d.^[167]

The space group $\text{Pn}\bar{3}$ has only one characteristic point configuration. Except for the general position 24h, all point configurations are characteristic for the supergroups $\text{Im}\bar{3}\text{m}$, $\text{Fm}\bar{3}\text{m}$, $\text{Pn}\bar{3}\text{m}$, and $\text{Im}\bar{3}$.^[105] As explained in chapter 3.2.3., only few characteristic structure factors $S(hkl)$ exist in such a case, which in addition are relatively distant from the origin. In such cases it is usually more conducive to use a PNS of a supergroup whose point configurations are occupied by the respective structure. In the present case this is the point configuration of the positions 2a and 4b (characteristic for $\text{Im}\bar{3}\text{m}$) as well as 8e ($\text{Pn}\bar{3}\text{m}$). Hence nodal surfaces of these space groups have been used to describe the structure.

In Ill. 24.e the above compound has been combined with the PNS $\text{I}_{\text{xxx}} - \text{J}^* \triangleq {}^{229}\langle(110);(200)^\pi\rangle$ (analogous to PMS I – WP) with the origin at $\frac{1}{4}\frac{1}{4}\frac{1}{4}$ from $\bar{3}\text{m}$. At the bottom on the left-hand side a piece has been omitted to free a view into the silver-colored partial space. Also included is the line graph $\text{I}(\text{x},\text{x},\text{x})_{\text{x}=0}^{\text{x}=1}$ of the partial space containing line segments of constant values. The nodal surface separates the Et_4N^+ cations from the molybdato-phosphate anions. The anion clusters, consisting of two rings of six edge-wise connected ($\text{MoO}_2\text{O}_{4/2}$) octahedra¹⁴ and coordinating one Na^+ ion in their center, are centered like wheels on an axle by the constant line graph $\text{I}(\text{x},\text{x},\text{x})_{\text{x}=0}^{\text{x}=1}$. The free phos-

¹⁴ Since the octahedra hexagons are capped by phosphate tetrahedra (red), three of whose four oxygen atoms belong to the octahedra, the simplified coordination $\text{MoO}_2\text{O}_{4/2}$ is not quite correct. It should be $\text{MoO}_2\text{O}_{3/2}\text{O}_{1/3}$.

phoric acid molecule omitted here is located at the intersections of the I_{xxx} -graphs. From Ill. 24.f can be gleaned that the nitrogen atoms (blue) of the Et_4N groups are located exactly on the line segment graph $J^*(x, 0, \frac{1}{2})_{x=0}^{x=1/2}$.

Illustration 25.a shows the same compound together with the PNS $F-I \triangleq {}^{224}\langle(110);(111)^{-\pi/2}\rangle$, which has been calculated up to 1.2 cell units in direction of the y axis. In this case the two molybdate octahedra rings of the sandwich are located on surface patches at opposite sides of the blue partial space, at the C_2 axes of the double-tetrahedron tunnel system generated by this PNS. Whereas the ammonium and coordinated sodium cations are located in the blue partial space, all phosphate tetrahedra capping the sandwiches as well as all phosphoric acid tetrahedra are located in the violet partial space centered around the point position with $\bar{4}3m$ symmetry (Wyckoff position 2b in $\text{Pn}\bar{3}m$).

We therefore can confirm Haushalter's conjecture that this compound can be elegantly organized by three-dimensional periodic surfaces,^[167] despite the difficulties arising from the space group $\text{Pn}\bar{3}$.

In 1989 Haushalter, Strohmaier, and Lai were successful in their pursuit of the ambitious goal to generate cavernous networks similar to the zeolites with the exclusive help of oxometallates of transition metals.^[168] The structure of $(\text{Me}_4\text{N})_{1.3}(\text{H}_3\text{O})_{0.7}[\text{Mo}_4\text{O}_8(\text{PO}_4)_2] \cdot 2\text{H}_2\text{O}$ ($\bar{4}3m$), depicted in Ill. 25.b together with the PNS $I_{xxx}-J^* \triangleq {}^{229}\langle(110);(200)^\pi\rangle$, is characterized by a three-dimensional network of phosphate tetrahedra (violet) and distorted Mo_4O_4 hetero-cubanes (yellow). The distortion is caused by two Mo-Mo bonds (261.7 pm, red). The PNS $I_{xxx}-J^*$ separates the hollow space from the molybdate phosphate network, which is topologically similar to NbO. This compound can reversibly store water up to 25% of its own volume. There are so far no data about the location of this water, but it most likely stays close to the PNS caused by hydrogen bonds to the oxide framework.

In Ill. 25.c the PNS $IJ^*-P_2 \triangleq {}^{229}\langle(110);(200)\rangle$ separates the hetero-cubanes (in the blue double tunnel system) from the phosphate tetrahedra.

6.3.5. Lithium Nitrido-Silicate, Li_2SiN_2

In the early 1990s Curda et al.^[169] prepared Li_2SiN_2 , which has a filled ZnI_2 structure.^[170] In principle this is a structure of the Cu_2O type (OCu_2) ,^[171] i.e., two independ-

ent interpenetrating tetrahedral networks ${}^3\infty[\text{AB}_{4/2}]$. In the present case, however, the tetravalent A atoms have been replaced by adamantane units (A_4B_6), which are connected to one another via additional B atoms: ${}^3\infty[(\text{A}_4\text{B}_6)\text{B}_{4/2}]$. This is also the structure of the nitride-silicate anion ${}^3\infty[(\text{Si}_4\text{N}_6)\text{N}_{4/2}]^{8-}$. The reduced symmetry from $\text{Fd}\bar{3}\text{m}$ or $\text{Pn}\bar{3}\text{m}$, respectively, down to Pbca is caused by steric distortions of the adamantane groups necessary to link them together, which does not effect the structural principle, though. The Li^+ cations are located in the free space connecting both networks. Similar structures have also been discovered for crystalline organic acids linked via hydrogen bonds, some of which even come with three- and fivefold interpenetrating diamond networks.^[171-173]

The structure of Lithium nitrido silicate is also related to several ternary chalcogenides of the third main group.^[174-178] In these cases, however, the adamantane units form layered structures topologically resembling the orange HgI_2 structure.^[179]

The topological relation of Li_2SiN_2 to diamond permits the use of PNS with $\text{Fd}\bar{3}\text{m}$ and $\text{Pn}\bar{3}\text{m}$ symmetry after adjusting cell orientation and transforming the cell's metrics. Since Li_2SiN_2 has the symmetry $\text{I}4_1/\text{acd}$, the following holds for the transformation:

$$a' = \frac{1}{2}(a + b); \quad b' = \frac{1}{2}(a - b); \quad c' = c \quad (40)$$

When performing the respective hkl transformations for the $S(hkl)$ permutations for the PNS D^* and $\text{F} - \text{I}$ and adding a phase shift for the moved origin, where needed, the appropriate PNS in tetragonal setup are obtained.

Ill. 25.d-f show Li_2SiN_2 as such, together with the PNS $\text{D}^* \triangleq {}^{227}\langle 111 \rangle^{224}$ and with the PNS $\text{F} - \text{I} \triangleq {}^{224}\langle (110); (111) \rangle$, respectively. In tetragonal symmetry these surfaces are generated by the structure factors $\text{D}_{\text{tetr.}}^* \triangleq {}^{141}\langle 101 \rangle$ and $\text{F} - \text{I}_{\text{tetr.}} \triangleq {}^{141}\langle (202); (112)^\pi; (200)^\pi \rangle$. Whereas the $\text{D}_{\text{tetr.}}^*$ surface separates the two adamantane networks from each other while organizing the Li^+ cations close to the surface, the $\text{F} - \text{I}_{\text{tetr.}}$ surface parallel to the first PNS almost perfectly separates the two anion networks from the Li^+ cations. If considering that each partial space of this PNS enwrapping the anion network has only 22% of the total volume of the structure, it cannot surprise that a few nitrogen atoms protrude into the partial space with the cations (see Table 13, p. 86). This PNS nevertheless separates the areas dominated by covalent interactions (anion network) fairly well from those dominated by ionic interactions (cation partial space).

6.3.6. $\text{Na}_2\text{Ca}_3\text{Al}_2\text{F}_{14}$

In 1988 Courbion and Ferey proposed a new way of looking at several fluorides, initiated by the newly discovered structure of $\text{Na}_2\text{Ca}_3\text{Al}_2\text{F}_{14}$ crystallizing in the space group $\text{I}2_13$.^[180] They depicted the structure both by using AlF_6 octahedra (Ill. 26.a) and by using $[\text{FCa}_{3/2}\text{Na}]$ tetrahedra, i.e., with the anion as central atom, indicating that this perspective could be expanded to other structures.^[181] They apparently overlooked that Bergerhoff had defined such “metallo complexes” more than 30 years earlier and had suggested them for the description of structures.^[182]

Since this structure is topologically related to that of garnet, crystallizing in a subgroup of second order of $\text{Ia}\bar{3}\text{d}$, an analysis has been conducted using PNS of the symmetry $\text{Ia}\bar{3}\text{d}$. And in fact, the threefold vertex-sharing fluoride coordination polyhedra (yellow) form a hyperbolic layer structure following the PNS Y^* (Ill. 26.a), whereby the F^- central anion lies in immediate vicinity of the surface. Since the $(\text{FCa}_{3/2})$ -polyhedra are rather large, they do not quite fit into the mirroring, green partial space of the PNS $\text{I}_2 - \text{Y}^{**}\text{V}^*$ (Ill. 26.b), which, after all, comprises 55.5% of the unit cell's volume (Table 13, p. 86). At one side a Na^+ cation (orange) at the top of the trigonal pyramid protrudes deeply into the red partial space, while the three Ca^+ cations (yellow) at the other side reach similarly deeply into the red labyrinth of the Y^{**}V^* graph. The orientation of the base of these trigonal pyramids follows the orientation of the surface. Hence, the organization of the structural parts follows not so much the hyperbolic interaction of $(\text{FM}_4)^{3+}/(\text{AlF}_6)^{3-}$ with a separation of the metallo cations as firmly bound units rather than the hyperbolic curvature of the $(\text{FM}_4)^{3+}$ network as such.

6.3.7. $\text{Ta}_6\text{Cl}_{15}$

Cu_2O forms a structure of two interpenetrating networks. They are tetrahedral networks of the β -cristobalite type. Interpenetration can be realized only if the majority component consists of the smaller atoms. Hence one cannot find them for SiO_2 but only in case of OCu_2 , iceVII, or the adamantane compounds $(\text{M}_4\text{X}_6)\text{X}_2$ with the large, complex minority component (M_4X_6) . In analogy to this, it can be deduced for an interpenetrating octrahedral network $\text{MX}_{6/2}$ that for this also a large minority component is necessary. A structure with two ReO_3 -like networks is known for the cluster-forming compound $\text{Nb}_6\text{F}_{15} = {}^3_\infty[\text{Nb}_6\text{F}_{12}]_{6/2}^{\text{a-a}} \triangleq \text{GX}_3$ in which the large minority component

$G = [\text{Nb}_6\text{F}_{12}^{\text{i}}]$.^[183] v. Schnering and Nesper have shown how the PNS $^{221}\langle 100 \rangle^{229}$ is organizing this structure (SG $\text{Im}\bar{3}\text{m}$, No. 229).^[35] Both networks are separated by van-der-Waals interactions, where the linear connections of the clusters in cI packing always go to the second next six neighbors instead of to the closest eight neighbors.

This is different for the analogous cluster compounds $\text{Ta}_6\text{Cl}_{15}$ and $\text{Br}_6\text{Cl}_{15}$.^[184] Here as well the clusters are cI packed and accordingly linked following the pattern $^3[\text{Ta}_6\text{X}_{12}^{\text{i}}]\text{X}_{6/2}^{\text{a-a}}$, yet here only one network is formed with *non-linear* connections of the clusters via $\text{X}^{\text{a-a}}$ bridges. By so going, this bridging connects 6 of the 8 *closest* neighbors. This variety is realized in a huge cubic cell of 16 clusters with $\text{Ia}\bar{3}\text{d}$ symmetry.

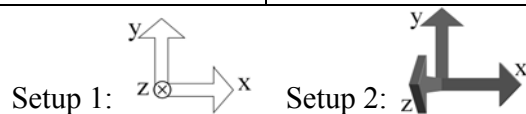
Ill. 26.c shows the PNS $\text{Y}^{**} \triangleq ^{214}\langle (110)^{\pi/2} \rangle^{230}$ completely sheeting the $\text{Ta}_6\text{Cl}_{15}$ network. The $\text{Cl}^{\text{a-a}}$ bridges follow the surface while the clusters not directly linked together are located on parallel surface patches opposing one another, here connected by the four-rod packing. Hence this is a non-Euclidian layer structure. The PNS $\text{I}_2 - \text{Y}^{**}\text{V}^* \triangleq ^{230}\langle (211); (220) \rangle$ parallel to Y^{**} furls its two independent, intertwined partial spaces containing the van-der-Waals region (red partial spaces, Ill. 26.d) around the covalently bound network area (green).

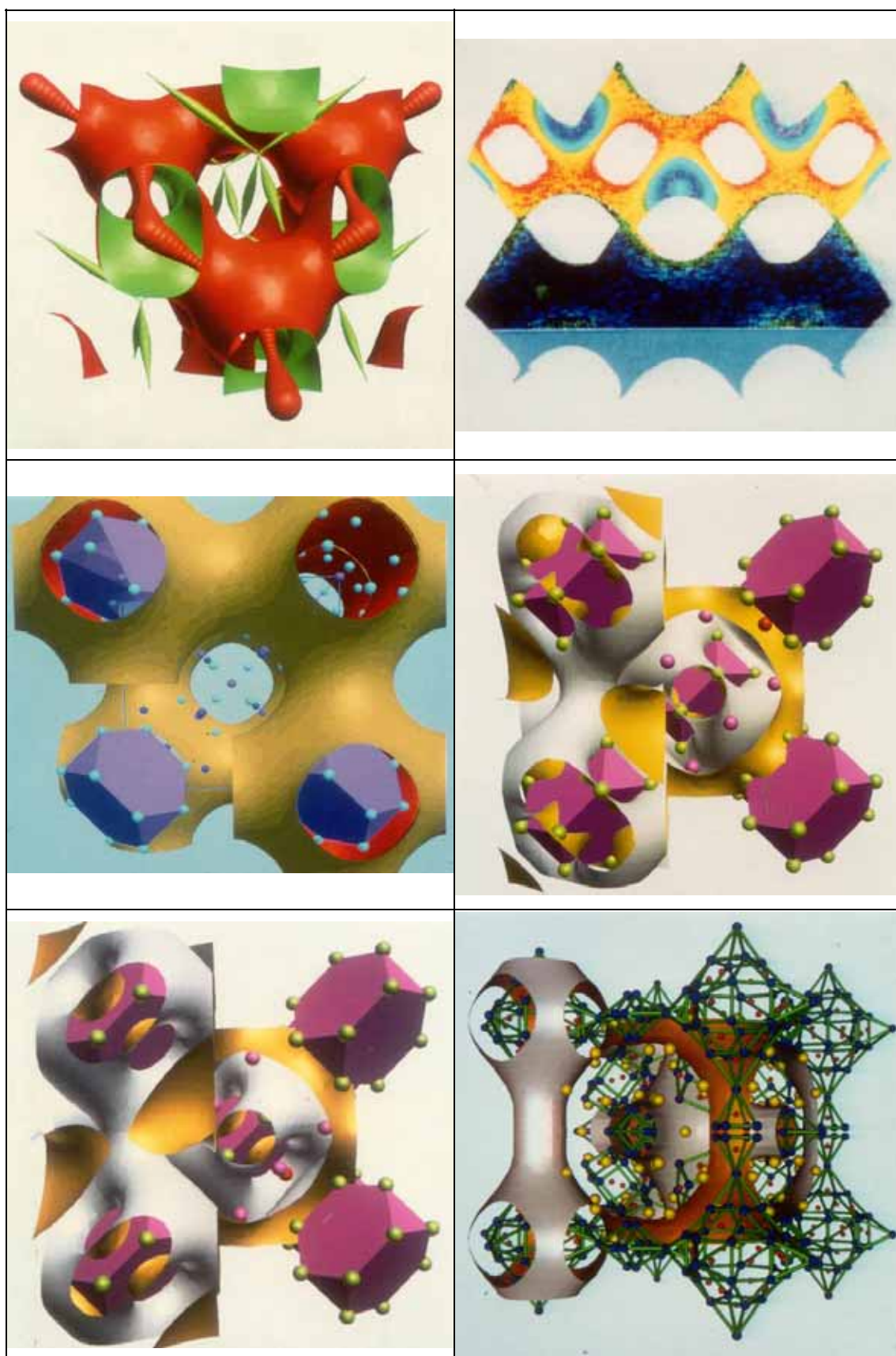
Here as well a non-Euclidian layer structure of this type can not be formed by compounds of the type MeX_3 (e.g. BiI_3 ^[185]), if the minority component is too small, since the shortest distance between X atoms of adjacent MX_6 octahedra can reach only 60% of the intra-octahedral X—X distance. On the other hand, $\text{Ta}_6\text{Cl}_{15}$ cannot form a Euclidian layer structure of edge-sharing octahedra like BiI_3 , because then the $\text{Cl}^{\text{a-a}}$ bridge atoms would come too close to the Cl^{i} atoms.

6.3.8. Zeolites

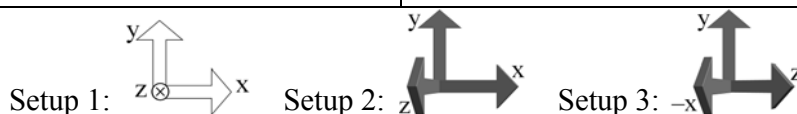
Both regarding synthesis and application zeolites are a particularly interesting research area of inorganic chemistry.^[186] From a structural point of view these compounds fascinate with their amazing variability and complexity.^[187,188] Especially Andersson and Fälvth have dedicated much effort to describe zeolite structures by means of combining various elementary building units.^[29,189-191] Koch and Hellner described zeolites as networks and strived to show patterns and relationships.^[192] Here I will try to elucidate the sometimes simple, but sometimes also very complicated structures of a series of mostly cubic zeolites by organizing them with the help of PNS.

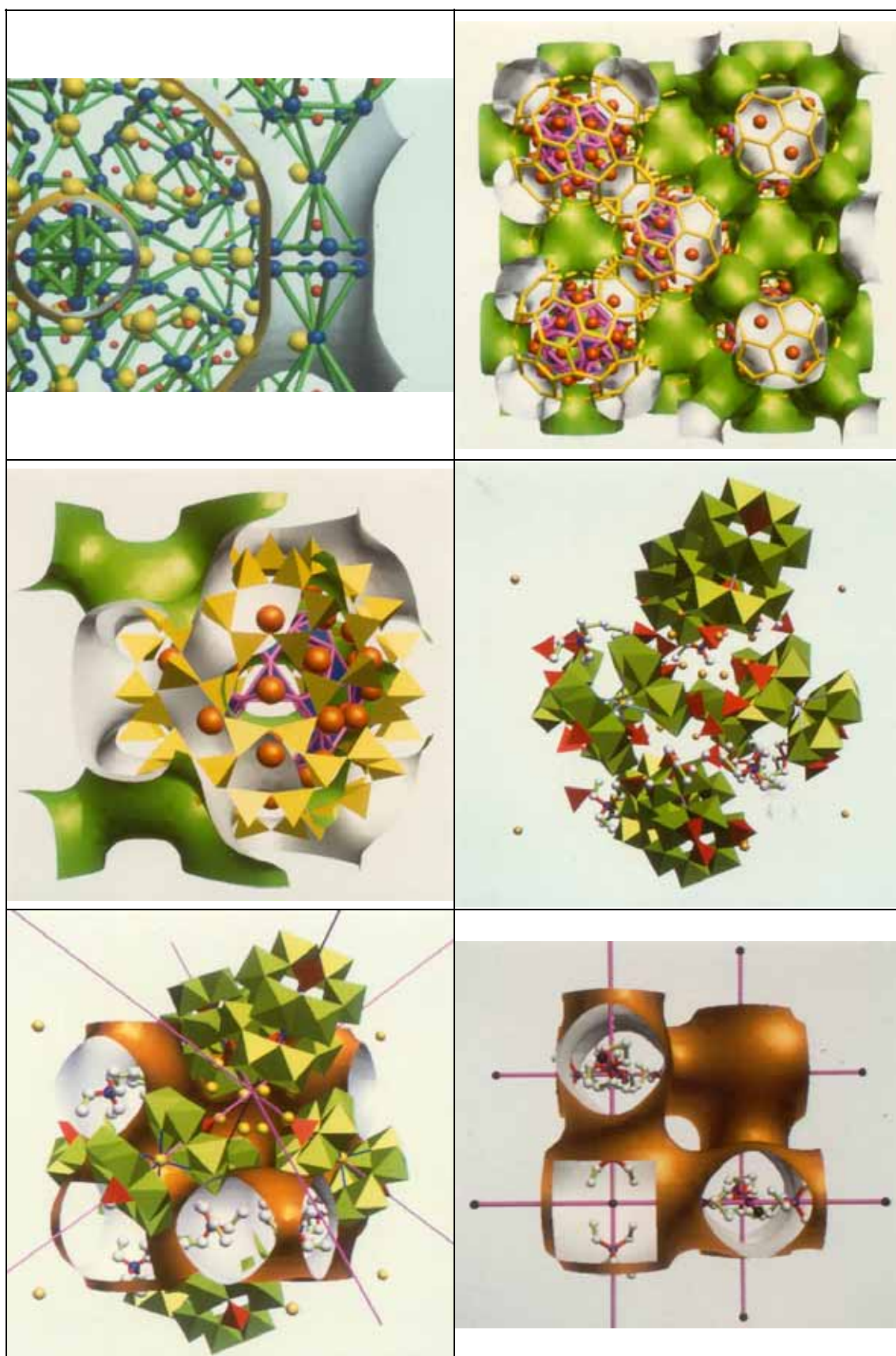
<p>Ill. 23.a</p> <p>D – DT</p> $^{227}\langle(111)^{-\pi/4};(220)\rangle$ <p>000 at 43m; with extrema graph; thickness of graph corresponds to relative function value; Setup 2</p>	<p>Ill. 23.b</p> <p>Electron Localization Function (ELF) of diamond cut along (101); with PNS D* $^{227}\langle(111)^{224}$ in same setup</p>
<p>Ill. 23.c</p> <p>α-Mangan</p> <p>Coordination polyhedral around site 000 (coord. no. = 12)</p> <p>PNS P* (with cutout)</p> $^{221}\langle(100)^{229}\rangle; x,y,z, \text{ from } -0,5 \text{ to } 1,5$ <p>Mn atoms at different positions are colored accordingly; Setup 1</p>	<p>Ill. 23.d</p> <p>α-Mangan</p> <p>with PNS $\Pi_{xxx}W^* - I_{xxx}$</p> $^{217}\langle(211)^{-\pi/4}\rangle$ <p>coloration like Ill. 23.c; Setup 1</p>
<p>Ill. 23.e</p> <p>α-Mangan</p> <p>with PNS $\Pi_{xxx}W^* - I_{xxx}$</p> $^{217}\langle(211)^{-\pi/4}\rangle;$ <p>PNS, 90° rotated against structure; coloration like Ill. 23.c; Setup 1</p>	<p>Ill. 23.f</p> <p>BaCuO₂ acc. to^[159]</p> <p>with PNS $IJ^* - P_2$</p> $^{229}\langle(110);(200)\rangle;$ <p>blue: O; red: Cu; yellow: Ba; Setup 2</p>



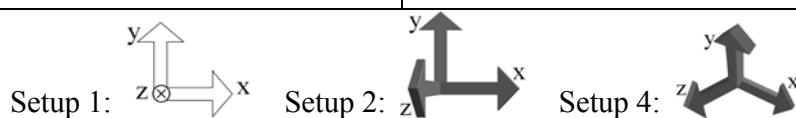


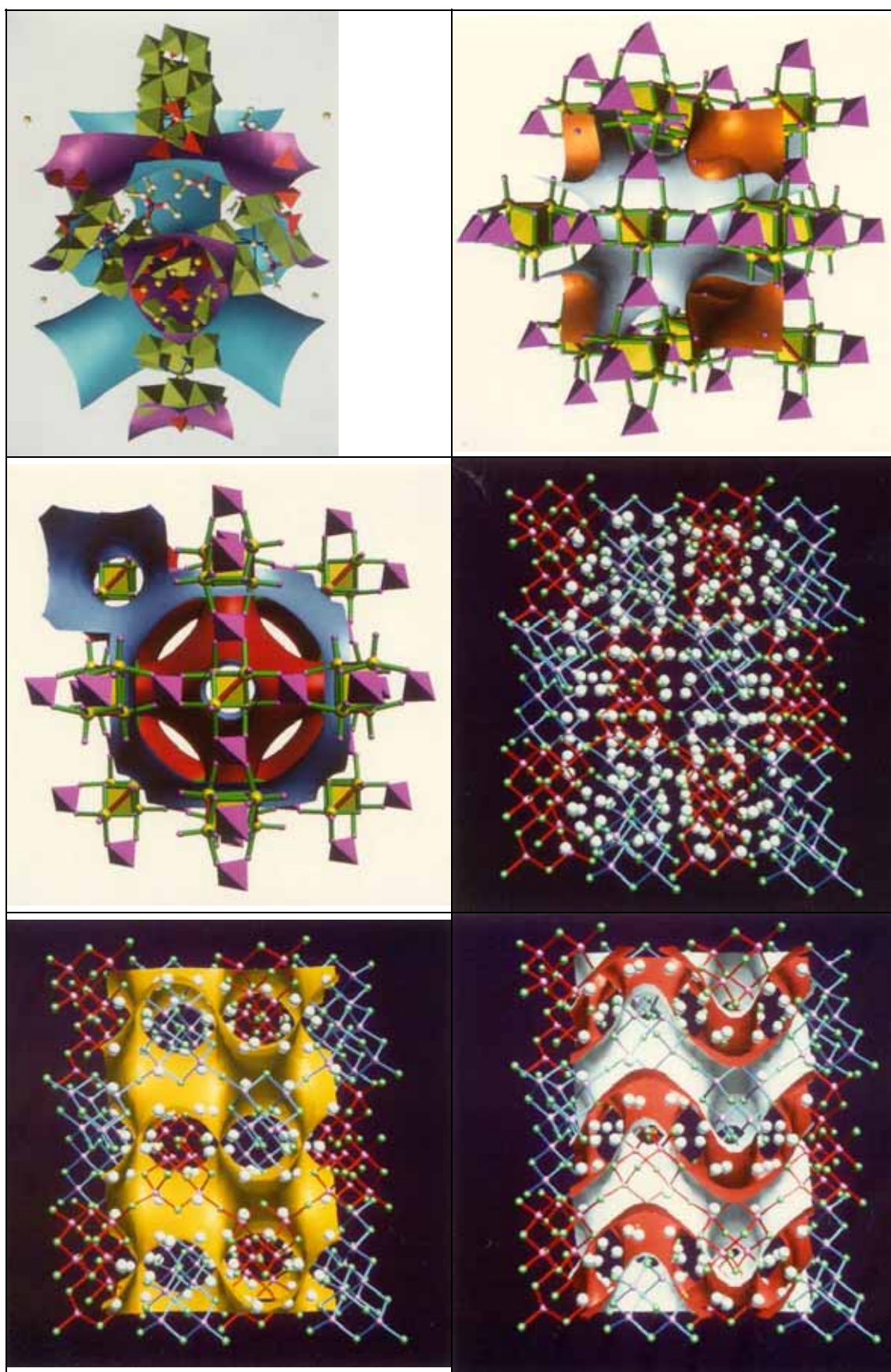
<p>Ill. 24.a</p> <p>BaCuO₂</p> <p>Section of Ill. 23.f around the edge of the unit cell, see text; arrow points to statistically occupied CuO₅ pyramids; roughly Setup 1</p>	<p>Ill. 24.b</p> <p>8 unit cells of PNS FF_{zx} – FP₂ ²²⁵$\langle(111)_2;(220)^\pi\rangle$, cut-out at left; yellow: aluminate framework Bi₂₂Sr₃₆Al₄₈O₁₄₁; orange: Sr²⁺; blue-violet: bismuthate framework; Setup 1</p>
<p>Ill. 24.c</p> <p>Hollow aluminate sphere of Bi₂₂Sr₃₆Al₄₈O₁₄₁ with FF_{zx} – FP₂ ²²⁵$\langle(111)_2;(220)^\pi\rangle$, z from 0 to 0.8; coloration as in Ill. 24.b; Setup 3</p>	<p>Ill. 24.d</p> <p>Tetra-ethyl ammonium molybdate phosphate [Et₄N]₆[Na₁₄Mo₂₄P₁₇O₉₇(OH)₃₁] · x H₂O, acc. to Haushalter et al.^[167]; green: Mo-O octahedra; red: phosphate tetrahedra; yellow: Na⁺; blue: N; white: CH_{2/3}; Setup 2</p>
<p>Ill. 24.e</p> <p>Compound as in Ill. 24.d with PNS I_{xxx} – J* ²²⁹$\langle(110);(200)^\pi\rangle$ (Original at $\frac{1}{4}\frac{1}{4}\frac{1}{4}$ from $\bar{3}m$) and graph I(x,x,x)_{x=0}^{x=1}; coloration as in Ill. 24.d; Setup 2</p>	<p>Ill. 24.f</p> <p>Tetra-ethyl ammonium groups from Ill. 24.d, PNS from Ill. 24.e and graph J*(x,0,$\frac{1}{2}$)_{x=0}^{x=1/2}; coloration as in Ill. 24.d; Setup 1</p>



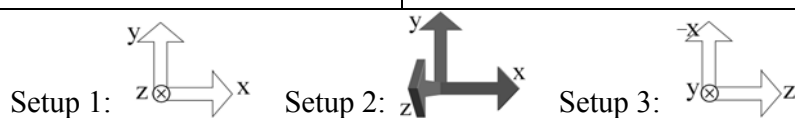


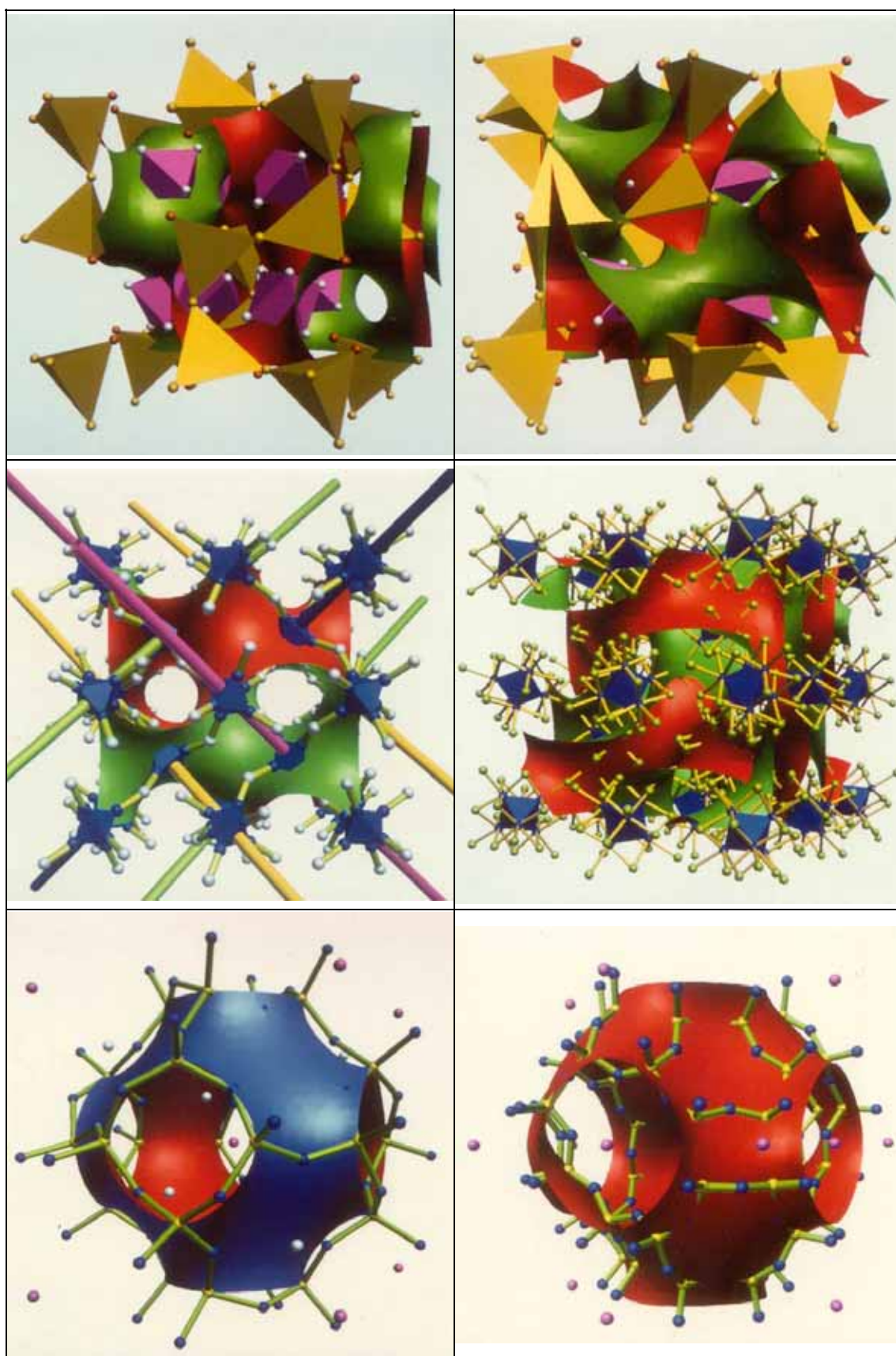
<p>Ill. 25.a</p> <p>Compound as in Ill. 24.d with PNS F – I $^{224}\langle(110);(111)^{-\pi/2}\rangle$, x from 0 to 1.2; (000 at $\frac{1}{4}\frac{1}{4}\frac{1}{4}$ from $\bar{3}m$); coloration as in Ill. 24.d; Setup 4</p>	<p>Ill. 25.b</p> <p>3D network with Mo-Mo bonds (red): $(Me_4N)_{1.3}(H_3O)_{0.7}[Mo_4O_8(PO_4)_2]$ ac. to^[168] with PNS $I_{xxx} - J^*$ $^{229}\langle(110);(200)^\pi\rangle$; yellow: Mo_4O_4-Heterokuban; violet: phosphate tetrahedra; red: Mo-Mo bonds; Setup 2</p>
<p>Ill. 25.c</p> <p>Compound as in Ill. 25.b with PNS $IJ^* - P_2$ $^{229}\langle(110);(200)\rangle$; Setup 1</p>	<p>Ill. 25.d</p> <p>Li_2SiN_2 with adamantane networks in different colors; pink: Si; green: N; white: Li^+; Setup 1</p>
<p>Ill. 25.e</p> <p>Li_2SiN_2 with PNS D_{tet}^* $^{227}\langle 111 \rangle^{224}$ or $^{141}\langle 101 \rangle$ after transformation (see text); Setup 1</p>	<p>Ill. 25.f</p> <p>Li_2SiN_2 with PNS $F - I_{tetr.}$ $^{224}\langle(110);(111)\rangle$ or $^{141}\langle(202);(112);(200)^\pi\rangle$ after transformation (see text); Setup 1</p>



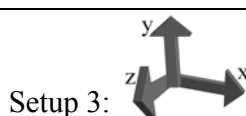
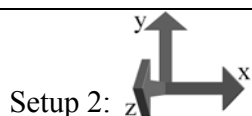


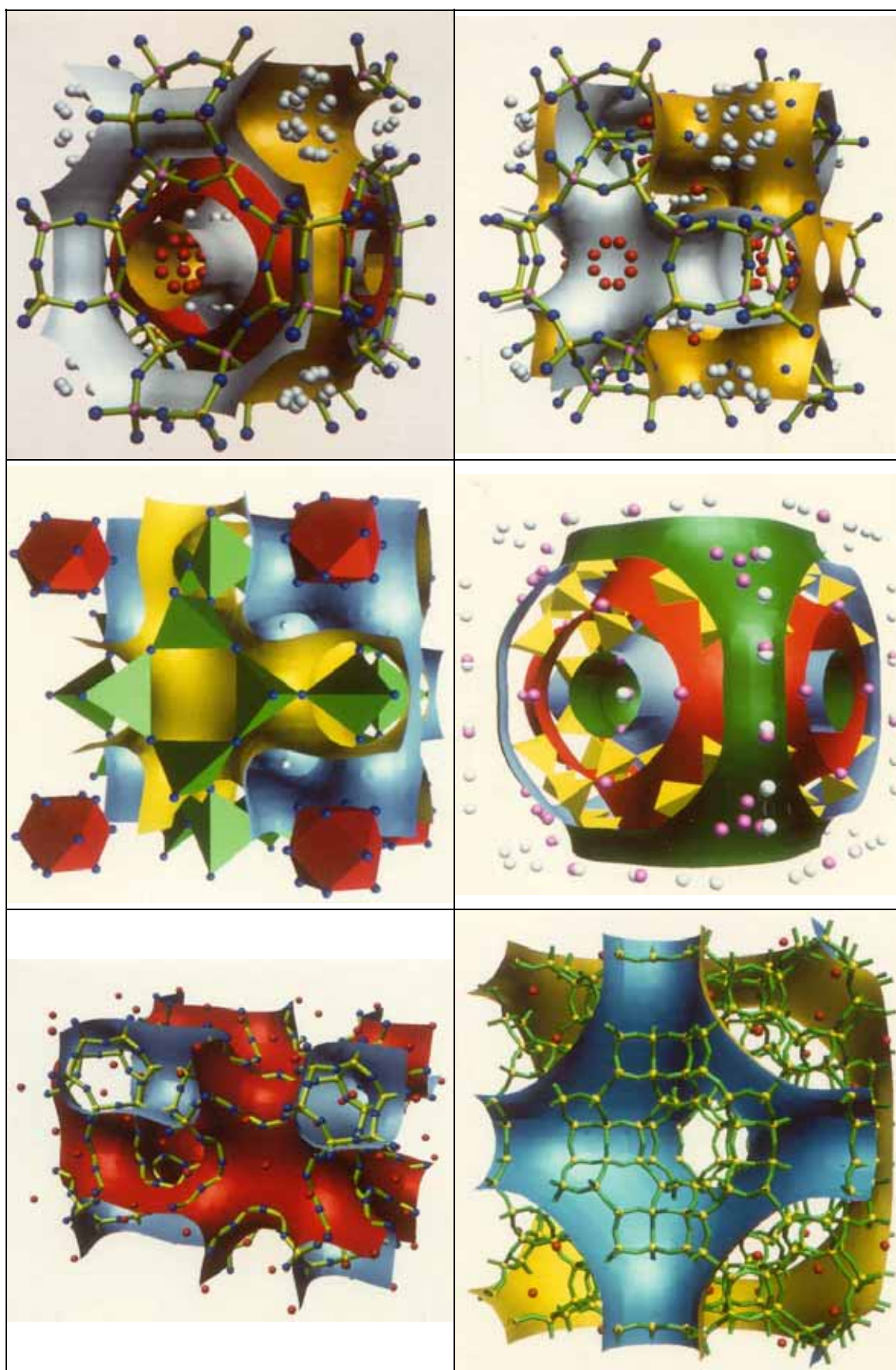
<p>Ill. 26.a</p> <p>$\text{Na}_2\text{Ca}_3\text{Al}_2\text{F}_{14}$ with PNS Y^{**} $^{214}\langle(110)^{\pi/2}\rangle^{230}$, z from 0 to 1.3; white: F; violet: AlF_6-Oktaeder; yellow: FCa_3Na-Polyeder /Ca^{2+}; orange: Na; Setup 3</p>	<p>Ill. 26.b</p> <p>$\text{Na}_2\text{Ca}_3\text{Al}_2\text{F}_{14}$ with PNS $I_2 - Y^{**}V^*$ $^{230}\langle(211);(220)\rangle$, x,z from 0 to 1.3; Setup 1</p>
<p>Ill. 26.c</p> <p>$\text{Ta}_6\text{Cl}_{15}$ with PNS Y^{**} $^{214}\langle(110)^{\pi/2}\rangle^{230}$; blue: Ta_6-Oktaeder; white: $\text{Cl}^{\text{a-a}}$ atoms; four-rod packing; Setup 1</p>	<p>Ill. 26.d</p> <p>$\text{Ta}_6\text{Cl}_{15}$ with PNS $I_2 - Y^{**}V^*$ $^{230}\langle(211);(220)\rangle$; blue: Ta_6-Oktaeder; bright green: Cl; Setup 2</p>
<p>Ill. 26.e</p> <p>Sodalite, acc. to $^{[194]}$ with PNS P^* $^{221}\langle 100 \rangle^{229}$; yellow: Si und Al; blue: O; white: Na; violet: Cl; Setup 2</p>	<p>Ill. 26.f</p> <p>ρ-Zeolite, acc. to $^{[196]}$ with PNS $(\text{PP}_{\text{xxx}})^*$ $^{215}\langle(100);(111)^{\pi/2}_{4.35}\rangle^{217}$; yellow: Si/Al; blue: O; violet: Cations; Setup 2</p>



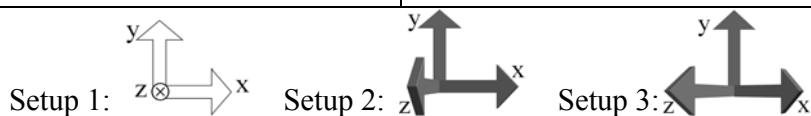


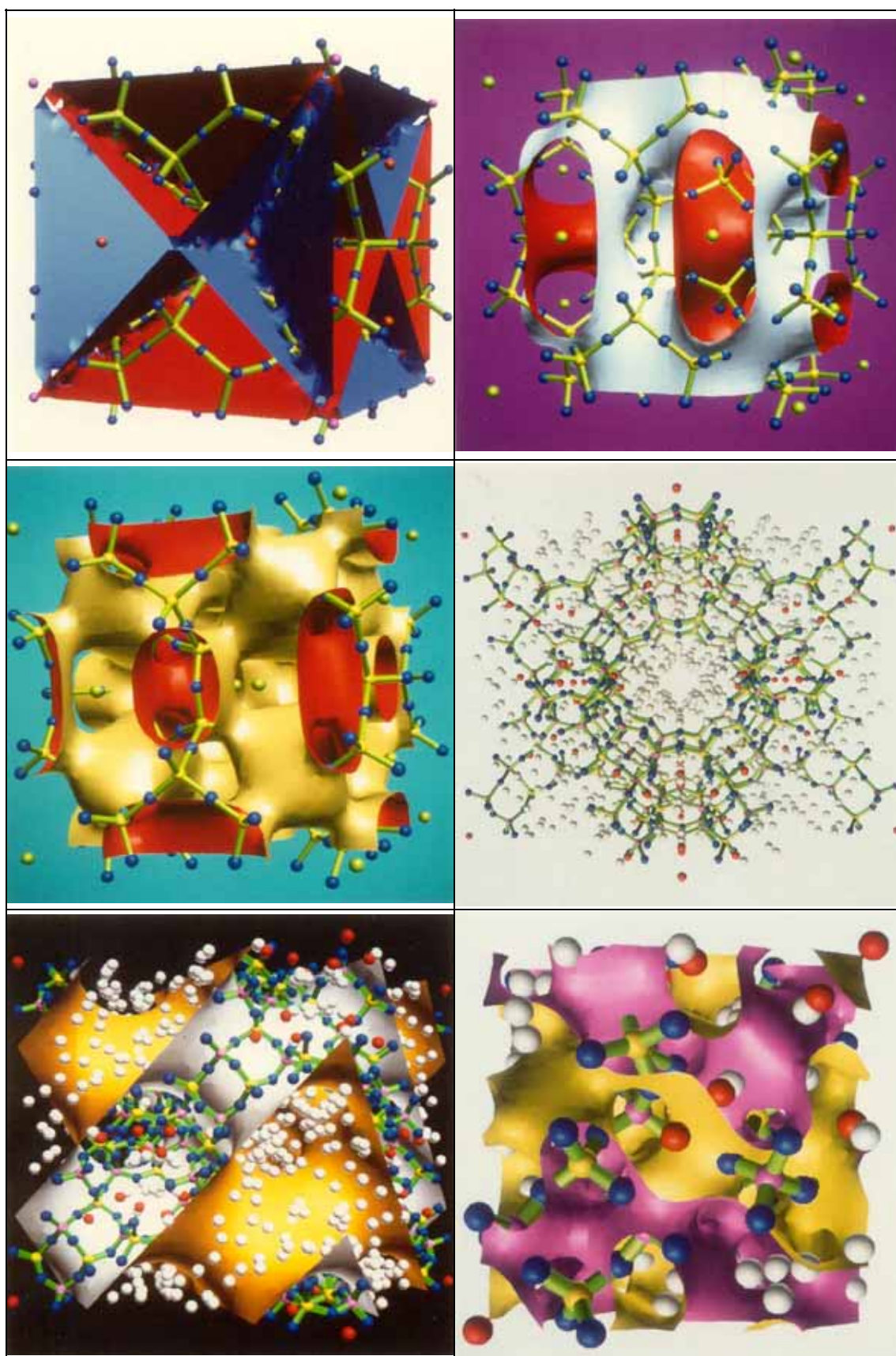
<p>Ill. 27.a</p> <p>Linde A or Harmatom-Zeolith, acc. to^[198] with P^* ($^{221}\langle 100 \rangle^{229}$; red) and PNS $IJ^* - P_2$ $^{229}\langle (110); (200) \rangle$, y from -0.2 to 1, z from 0 to 1.2; yellow: Si/Al; blue: O; red: Cations; white: H₂O; Setup 2</p>	<p>Ill. 27.b</p> <p>Compound and coloration as in Ill. 27.a with PNS $I_{xxx} - J^*$ $^{229}\langle (110); (200)^\pi \rangle$, y, z from 0 to 1.25; Setup 2</p>
<p>Ill. 27.c</p> <p>Aluminate sodalite, acc. to^[202] with PNS $I_{xxx} - J^*$ $^{229}\langle (110); (200)^\pi \rangle$, y, z from 0 to 1.25; green: aluminate tetrahedra; red: chromate cuboctahedra; Setup 2</p>	<p>Ill. 27.d</p> <p>ZK-5 Zeolite, acc. to^[203]; with P^* ($^{221}\langle 100 \rangle^{229}$, rot) and PNS $IJ^* - P_2$ $^{229}\langle (110); (200) \rangle$; yellow: SiO_{4/2}-Tetraeder; white / pink: inclusions (heer BaCl); Setup 2</p>
<p>Ill. 27.e</p> <p>ZK-5-Zeolith; with PNS $I_{xxx} - J^*$ $^{229}\langle (110); (200)^\pi \rangle$, x from -0.5 to 1; yellow: Si/Al; blue: O; red: Cations; Setup 3</p>	<p>Ill. 27.f</p> <p>Half a unit cell of Paulingite with half the PNS $IJ^* - P_2$ $^{229}\langle (110); (200) \rangle$; yellow: Si/Al; O atoms omitted; red: Cations (Ca²⁺, Na⁺, Mg²⁺ ...); note the zeolite's tunnels followed by the PNS; Setup 2</p>



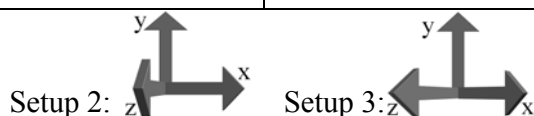


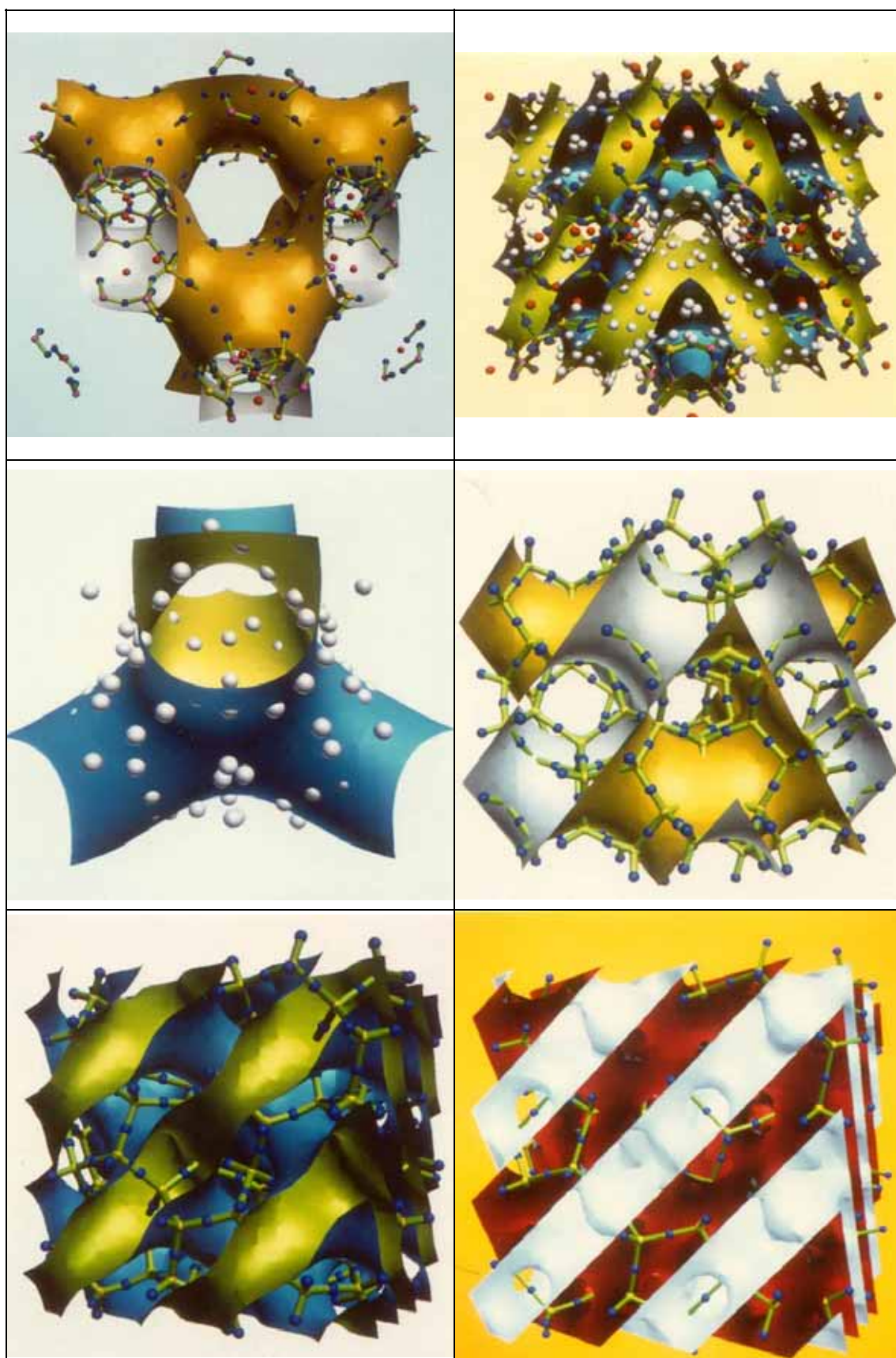
<p>Ill. 28.a</p> <p>Melanophlogite with PNS W^* $^{223}\langle 210 \rangle^{229}$; yellow: Si; blue: O; red/violet: gas inclusions; Setup 2</p>	<p>Ill. 28.b</p> <p>Melanophlogite with PNS $P_2 - IW_z$ $^{223}\langle (110)_2; (200)_4; (210)^n \rangle$; yellow: Si; blue: O; green: gas inclusions; Setup 2</p>
<p>Ill. 28.c</p> <p>Melanophlogite with PNS $IWI_{zx} - J^*P_2$ $^{223}\langle (210); (211)_2; (220)_4 \rangle$; coloration as in Ill. 28.b; Setup 2</p>	<p>Ill. 28.d</p> <p>Faujasite; yellow: Si; violet: Al; blue: O; red: Na; white: H_2O; Setup 3</p>
<p>Ill. 28.e</p> <p>Faujasite with PNS D^* $^{227}\langle III \rangle^{224}$; coloration as in Ill. 28.d; Setup 2</p>	<p>Ill. 28.f</p> <p>1st octand of Faujasite with 1st octand of PNS $^{203}\langle 531 \rangle$; x,y,z from 0 to 0.5 coloration as in Ill. 28.d; Setup 1</p>



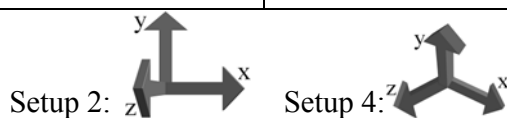


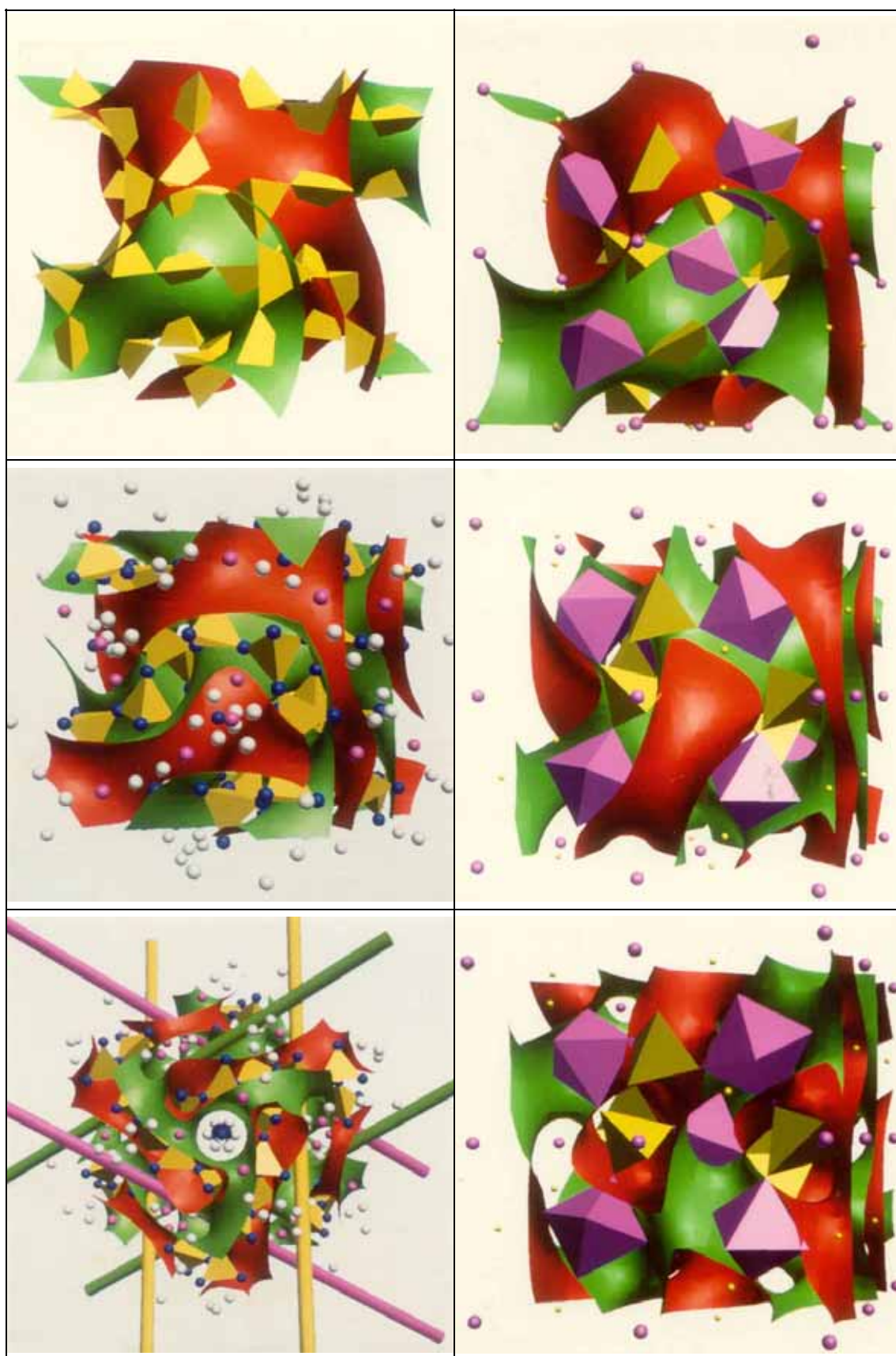
<p>Ill. 29.a</p> <p>Faujasite without water with PNS D – DT $^{227}\langle(111)_{5/2}^{-\pi/4};(220)\rangle$; coloration as in Ill. 28.d; Setup 2</p>	<p>Ill. 29.b</p> <p>Faujasite with 8 unit cells of PNS F – I $^{224}\langle(110);(111)\rangle$; coloration as in Ill. 28.d; Setup 3</p>
<p>Ill. 29.c</p> <p>Water of Faujasite (white) with tetrahedral of PNS F – I $^{224}\langle(110);(111)\rangle$; Setup 3</p>	<p>Ill. 29.d</p> <p>Clathrate ZSM-39 with PNS D* $^{227}\langle 111 \rangle^{224}$; yellow: Si; blue: O; Setup 2</p>
<p>Ill. 29.e</p> <p>Clathrate ZSM-39 with PNS F – I $^{224}\langle(110);(111)\rangle$, 000 at $\frac{1}{4}\frac{1}{4}\frac{1}{4}$ from $\bar{3}m$; 8 unit cells; coloration as in Ill. 29.d; Setup 2</p>	<p>Ill. 29.f</p> <p>Clathrate ZSM-39 with PNS IF_{xx} – I_{xxx}W* $^{224}\langle(111);(211)\rangle$, 000 at $\frac{1}{4}\frac{1}{4}\frac{1}{4}$ from $\bar{3}m$ 8 unit cells; coloration as in Ill. 29.d; Setup 2</p>





<p>Ill. 30.a</p> <p>SiO_{4/2} tetrahedra of analcime with PNS Y** $^{214}\langle(110)^{\pi/2}\rangle^{230}$ Setup 2</p>	<p>Ill. 30.b</p> <p>Coordination polyhedral of Garnet with PNS Y** $^{214}\langle(110)^{\pi/2}\rangle^{230}$; violet: AlO_{6/2} octahedra; yellow: SiO_{4/2} tetrahedra; Setup 2</p>
<p>Ill. 30.c</p> <p>Analcime with PNS I₂ – Y**J* $^{230}\langle(211);(220)\rangle$; yellow: SiO_{4/2} tetrahedra; blue: O; violet: Na⁺; white: H₂O; Setup 2</p>	<p>Ill. 30.d</p> <p>Garnet with PNS I₂ – Y**V* $^{230}\langle(211);(220)\rangle$, z from 0 to 0.8; coloration as in Ill. 30.b; Setup 2</p>
<p>Ill. 30.e</p> <p>Analcime with PNS I_{xxx} – S* $^{230}\langle(211);(220)^{\pi}\rangle$; with four-rod packing (I_{xxx} graph); coloration as in Ill. 30.c; Setup 4</p>	<p>Ill. 30.f</p> <p>Garnet with PNS I_{xxx} – S* $^{230}\langle(211);(220)^{\pi}\rangle$, z from 0 to 0.8; coloration as in Ill. 30.b; Setup 2</p>





6.3.8.1. Zeolites of the Sodalite Type

A major part of known zeolites form networks topologically similar or at least closely related to that of sodalite. They all have in common the symmetry $\text{Im}\bar{3}\text{m}$ or a slightly acentric distortion toward $\text{I}\bar{4}3\text{m}$. Already Pauling^[193] correctly assigned sodalite ($\text{Na}_4\text{Si}_6\text{Al}_6\text{O}_{24}\text{Cl}_2$) to its proper space group $\text{P}\bar{4}3\text{n}$, which in contrast to $\text{I}\bar{4}3\text{m}$ (direct supergroup with index 2) permits an ordered distribution of Si and Al atoms.^[194,195] If regarding the tetrahedrally coordinated central atoms as identical and if ignoring minor distortions, then this structure can be described by PNS of the space group $\text{Im}\bar{3}\text{m}$ (indirect supergroup of index 4). Ill. 26.e shows sodalite of the true unit cell with the PNS $\text{P}^* \triangleq {}^{221}\langle 100 \rangle$ ²²⁹. The description of this structure as a covalent membrane along the nodal surface can be improved by using the tetrahedral PNS $(\text{PP}_{\text{xxx}})^* \triangleq {}^{215}\langle (100); (111)^{\pi/2} \rangle$ ²¹⁷ generated from $\text{P}\bar{4}3\text{m}$, in Ill. 26.f merged with the ρ -zeolite.^[196,197] The ρ -zeolite differs from sodalite by having twice as many tetrahedrally coordinated atoms in the Si_8O_8 rings orthogonal to $\{100\}$, as a result of which additional Si_4O_4 rings are formed orthogonally to $\{110\}$. The PNS $(\text{PP}_{\text{xxx}})^*$ is variable due to the adjustable ratio of the structure factor values used. Here we used the ratio 1:4.35 ($|S|(100):|S|(111)$), as in that case the Si atoms are located exactly on the surface. The ratio of the structure factors therefore allows quantitative conclusions about the degree of tetrahedral deformation of such structures.

If considering the tetrahedrally coordinated atoms as equivalent, then ρ -zeolite is topologically identical with several other zeolites like for instance with Linde A (space group $\text{Pm}\bar{3}\text{m}$ or $\text{Fm}\bar{3}\text{c}$).^[198] The zeolites harmatome and phillipsite, which are topologically identical with ρ -zeolite as well, have different symmetries due to certain distortions ($\text{Im}\bar{3}\text{m}$, $\text{P}2_1/\text{m}$).^[199-201] Since primarily the topology of a compound is important for its organization with PNS, cubic PNS can easily be transformed to lower symmetries in case of topological isomorphism (see footnote 9, p. 92).

The inclusions described by Parise et al.^[197] are located together with most cations in the labyrinth of the double tunnel system formed by the $\text{IJ}^* - \text{P}_2$ (Ill. 27.a). This is true for sodalite as well as for ρ -zeolite and their topological relatives. Hence the PNS separates the covalent part of the compound from that one which is dominated by van-der-Waals and electrovalent interactions. The PNS $\text{I}_{\text{xxx}} - \text{J}^*$ separates the inclusions from both the silicate network and the cations (Ill. 27.b).

Depmeier et al. have shown that the relative amount of aluminium has a decisive in-

fluence on the distortion of zeolites.^[202] The zeolite depicted in Ill. 27.c is a pure aluminate sodalite ($\text{AlO}_{4/2}^{2-}$ tetrahedra rendered green). The strange quasi-cuboctahedral surroundings of Cr(VI) (red) result from an orientation disorder of the CrO_4^{2-} tetrahedra. This sodalite is free of distortions ($\text{Im}\bar{3}\text{m}$). The PNS $\text{I}_{\text{xxx}} - \text{J}^* \triangleq {}^{229}\langle(110);(200)^\pi\rangle$ added in Ill. 27.c wraps the aluminate network and separates it from the CrO_4^{2-} anions.

The zeolite ZK-5 possesses a double tetrahedral network, quite in contrast to sodalite.^[203] This is separated by the P^* surface $\triangleq {}^{221}\langle 100 \rangle^{229}$ (red), Ill. 27.d. The separation of the inclusions from the silicate networks succeeds with the PNS $\text{IJ}^* - \text{P}_2 \triangleq {}^{229}\langle(110);(200)\rangle$. The positions in the second double tunnel system (Ba=pink, Cl=white, in other cases Cs and K on similar positions^[204]) are only statistically occupied. The PNS $\text{I}_{\text{xxx}} - \text{J}^* \triangleq {}^{229}\langle(110);(200)^\pi\rangle$ neatly embeds the silicate network (Ill. 27.e, inclusions omitted). As in the case of harmatome, Line A, and ρ -zeolite, the topology of the silicate framework can be described by the PNS $\text{I}_{\text{xxx}} - \text{J}^*$ and $\text{IJ}^* - \text{P}_2$, because the only relevant difference between these zeolites is the different amount of Si_4O_4 rings, which is a topologically neutral element for fourfold connected systems.

6.3.8.2. Paulingite

Gordon, Samson, and Kamb have thoroughly characterized Paulingite crystallographically, which is a zeolite with one of the largest unit cells ($\text{Im}\bar{3}\text{m}$, $a = 35.1 \text{ \AA}$, more than 2000 atoms).^[205] Ill. 27.f shows one half of the unit cell (yellow: Si, red: cations, O atoms omitted), together with equally half a unit cell of the PNS $\text{IJ}^* - \text{P}_2$. The silicate network forms an independent tunnel system within this complex structure (blue partial space). The cations are in the other, yellow partial space.

6.3.8.3. Melanophlogite

According to Gies, Liebau, and Gerke^[206-208] the mineral melanophlogite, a gas-containing clathrasile, crystallizes in the space group of the three rod packing ($\text{Pm}\bar{3}\text{n}$) with the structure of the gas hydrates $\text{Xe}_8(\text{H}_2\text{O})_{46}$. Characteristic for this clathrate-I structure are linked pentagon dodecahedra and tetradecahedra (14 faces) formed by Si atoms and interconnected via O bridges. Ill. 28.a-c show melanophlogite with three different PNS of the generating space group $\text{Pm}\bar{3}\text{n}$ (No. 223). The PNS W^* has the eigen symmetry $\text{Im}\bar{3}\text{m}$. It consists of intersecting planes with 24 partial spaces, all converging at singularities at 000 and $\frac{1}{2}\frac{1}{2}\frac{1}{2}$. This results in an organization of clathrasile

with respect to the dodecahedra. The covalent silicate network lies in 12 segments of the one partial space (red), the atoms of the inclusions in the other (blue). Since this PNS has many intersections, PNS free of intersections have been sought for a long time. In order to organize the entire clathrate network in one partial space it would be necessary to generate topological units of cuboctahedral or icosahedral symmetry around the point configuration I, which has not been successful so far (Ill. 28.b und c).

6.3.8.4. Faujasite and Dodecasile-3C

Faujasite, in certain variations also called Linde type X and Y, was discovered in the mid-19th century and used to be considered as having $Fd\bar{3}m$ symmetry.^[209-212] However, if the Al and Si atoms are located on separate positions, then the space group $Fd\bar{3}$ results (Ill. 28.d).^[213]

There are only a few characteristic $S(hkl)$ in $Fd\bar{3}$, the closest to the origin being $S(531)$. But since we are not interested in distinguishing Si and Al from each other, the PNS $D^* \triangleq {}^{227}\langle 111 \rangle^{224}$ from the direct supergroup of $Fd\bar{3}$ ($Fd\bar{3}m$) is depicted in Ill. 28.e together with the cubic faujasite. The PNS separates the covalent silicate network from the inclusions (H_2O). Ill. 28.f shows an octand of the unit cell of both the PNS ${}^{203}\langle 531 \rangle$ and faujasite. Even though this PNS separates Al and Si atoms from one another, it obscures the organization of the covalent network and the inclusions. Ill. 29.a shows the nodal surface $D - DT \triangleq {}^{227}\langle (111)_{5/2}^{-\pi/4}; (220) \rangle$ with faujasite but without the water structure in its cavities. This PNS has $Fd\bar{3}m$ not only as its generating but also as its eigen symmetry (see p. 56). It enwraps the silicate framework like a tight skin. Ill. 29.b shows eight unit cells of the PNS $F - I \triangleq {}^{224}\langle (110); (111) \rangle$, generated in the direct supergroup of $Fd\bar{3}m$, $Pn\bar{3}m$ (Index 2), the eigen symmetry of the D surface. While the silicate network lies around one of the tunnel systems, the water is close to the surface of the other tunnel system. When considering the relatively large standard deviation of the H_2O positions, the accuracy of the localization of water close to the nodal surface is astounding. It should also be noted that the diameter of the $F - I$ labyrinth tunnel is ca. 3Å ($1/8 a$), which roughly corresponds to the O-O distance in water ($\approx 2.75\text{Å}$). Ill. 29.c shows a segment of the PNS $F - I$ with the O atoms of water viewed from $\{131\}$. As far as we know, it has so far not been reported that the water in faujasite forms a network analogous to the silicate framework. The inclusion of water in the hollow space probably involves the formation of hydrogen bonds while at the same time keeping a certain distance to the silicate network.^[213] This is therefore a heterogeneous double network as it

has been shown to exist in homogeneous form for instance for certain lipid and polymer phases.^[17,27] The data given in Table 13 (p. 86) permit further conclusions about this structure using the PNS concept. We can, for example, give the area of the PNS F – I ‘covered’ with H₂O, which can be interpreted as an ‘inner’ water surface area of faujasite. It is 1.65 times the surface area of $A = 1.65 a^2 \approx 1000 \text{ \AA}^2$ ($a = 25 \text{ \AA}$). With roughly 170 water molecules per unit cell, this yields an average area of some 6 \AA^2 per H₂O. If taking the shortest O-O distance in water (2.75 \AA) as twice the radius of the circle area available for each H₂O, then this too yields 6 \AA^2 per H₂O. If considering the effective free area in water given by the mol volume, then we obtain a value of some 10 \AA^2 per H₂O. The occupation density in faujasite therefore lies at the upper limit.

Schlemker et al. discovered a novel clathrasile in 1981 crystallizing in $Fd\bar{3}m$, the supergroup of faujasite: ZSM-39.^[214] This clathrate, which has also been systematically investigated by Gies,^[215] is shown in Ill. 29.d-f with various PNS. In this case the silicate framework lies around the D* surface. A complete separation of the covalent framework from the free tunnel labyrinth or an embedding of all Si atoms on the surface fails, however. As in the case of melanophlogite, here, too, the dodecahedral arrangement of the building units of the silicate network requires the discovery of a periodic PNS consisting of topological units with dodecahedral or icosahedral symmetry.

6.3.8.5. Analcime and Garnet

The structure of analcime, which has been determined by Taylor^[216] and which has been confirmed and refined by means of neutron diffraction,^[217] has the symmetry $Ia\bar{3}d$ (with a variety in $I4_1/acd$). It consists of 48 vertex-sharing $O_{4/2}$ tetrahedra per unit cell which are statistically occupied by Al and Si. This zeolite also contains 16 water molecules and Na⁺ ions per unit cell: $16 \text{ Na}[\text{AlSi}_2\text{O}_6](\text{H}_2\text{O})$.

If the number and size of the hetero rings M_nO_n of this structure is to be maintained, it is impossible to connect all regular tetrahedra in such a way via vertices that an arrangement ensues corresponding to a close polyhedra packing. Nature’s solution for this problem is given by the example of analcime. Ill. 30.a shows the $\text{MO}_{4/2}$ tetrahedra together with the PNS $Y^{**} \triangleq {}^{214}\langle(110)^{\pi/2}\rangle^{230}$. The tetrahedrally coordinated central atoms are located exactly on the surface, thus forming a hyperbolic, evenly curved network. The illustration containing the PNS $I_2 - Y^{**}V^* \triangleq {}^{230}\langle(211);(220)\rangle$ shows how the tetrahedra smoothly wind along the green partial space separating the two mirror-symmetrical red tunnel systems from each other (Ill. 30.c). Embedding this structure

into the PNS $I_{xxx} - S^* \triangleq {}^{230}\langle(211);(220)^\pi\rangle$ leads to an impressive separation of the silicate framework from the water (Ill. 30.e). In particular the perspective along the space diagonal $\{111\}$ with added I_{xxx} graph (four-rod packing) reveals the highly ordered organization of the water along this graph.

The organizing effect of the PNS $Y^{**} \triangleq {}^{214}\langle(110)^{\pi/2}\rangle^{230}$ (corresponding to the PMS ‘Gyroide’) on garnet can be gleaned from Ill. 30.b. The structure of garnet, which exists in many variations, has been determined long ago by Menger.^[218] It has the general composition $M_3^{II}Al_2Si_3O_4$ ^[219,220] and fascinates by its seemingly complicated structure of alternately tipped $AlO_{6/2}$ octahedra (violet) and $SiO_{4/2}$ tetrahedra (yellow). Rendering the compound together with the ‘Gyroide’-like PNS reveals that this, too, is a non-Euclidian layer structure like analcime. In this case the curvature is caused by the vertex-sharing of octahedra and tetrahedra in a stoichiometric ratio of T:O = 3:2. The PNS $I_2 - Y^{**}V^* \triangleq {}^{230}\langle(211);(220)\rangle$ reveals the cyclicly tilted octahedra (Ill. 30.d). They follow the orientation of the surface, positioning the oxygen atoms close to the surface. Embedding this structure into the PNS $I_{xxx} - S^* \triangleq {}^{230}\langle(211);(220)^\pi\rangle$ elucidates the difference to analcime (Ill. 30.f). While all tetrahedra of analcime are in one partial space together with the graph $Y^{**}(x,y,z)_{x=5/16, y=1/16, z=3/8}^{x=3/8, y=0, z=1/4}$, all octahedra of garnet are located on the I_{xxx} graph, hence are centered by the rods of the four-rod packing around the $\bar{3}$ axes.

6.3.9. Hyperbolic Surface Area Demand of Several Zeolites

As a quantity for the porosity of zeolites, which is decisive for their ion exchange capacity, the framework density is given as the number of tetrahedrally coordinated atoms per volume. Brunner and Meier^[221] as well as Stixrude and Bukowinski^[222] have shown that the framework density is directly determined by the size of the smallest rings in the network, whereby the density decreases with reduced ring size. This is easily understandable if considering the result of our chapter 5. In a network with fourfold connected atoms, rings with four furcation points are neutral elements which can form only parabolic objects (planes, cylinders, cones \triangleq Euclidian layer silicates). With increasing number of M_4O_4 rings in a silicate the size of cavities and pores grows by inflating the Euclidian parts of the framework. The increase of the average ring size, however, forces the channels and cavities to shrink due to the increasing hyperbolic curva-

ture of the network. The values extrapolated by Brunner and Meier for frameworks densities of zeolites containing three membered tetrahedra rings (M_3O_3) do not have to be correct, however, since hetero hexagons lead to the formation of elliptic objects (island silicates), so their exclusive use would prevent the formation of networks.

Embedding the tetrahedrally coordinated atoms of non-Euclidian silicates – zeolites – in nodal surfaces enables us to calculate the surface area which is at the disposal of each tetrahedron on the respective curved surface, which in turn permits a comparison with Euclidian layer silicates.

The right-most column of Table 20 (p. 150) lists the surface area available for each tetrahedrally coordinated atom on the respective PNS. Two PNS have been used to describe faujasite. The PNS F – I lies too far inside of the structure, its surface area is therefore too small. The D – DT, on the other hand, enwraps the outer oxygen atoms, hence gives too high a value. Since the surface values for the PNS F – I listed in Table 13 (p. 86) are given for the unit cell in $Pn\bar{3}m$, eight such unit cells have to be used for $Fd\bar{3}m$. But due to the changed normalization (the unit cell's surface area in $Pn\bar{3}m$ has only a quarter of the value of that in $Fd\bar{3}m$) and because only one of the two labyrinth systems of this surface is used, we end up with the same value as given in Table 13.

As another comparative value the formal surface area available for the $SiO_{4/2}$ tetrahedra in quartz can be taken. At a mol volume of 22.6 cm^3 this results in an available area of 11.2 Å^2 per tetrahedron.

In each of the Euclidian layer silicates listed in Table 20 threefold connected tetrahedrally coordinated atoms form hetero-twelve rings (Si_6O_6 as the topologically neutral element of triple connections). If embedding sodalite into the P^* surface, all rings located on the surface have 12 members as well. In addition to that, all other silicates listed possess a minimum number of hetero-eight rings on the surface, which reduce the surface area available for each tetrahedron in comparison to sodalite. Only as a result of this reduced occupancy can these zeolites reach an areal density similar to that of Euclidian layer silicates. In sodalite each tetrahedron has an area available on the hyperbolic surface which is one third larger than that available in Euclidian layer silicates. If calculating the areal density of sodalite not with PNS but by means of regular polyhedra, a similar area available per tetrahedron results as for Euclidian layer silicates. At a distance of $d(Si-Si) = d(O-O) = 2.62\text{ Å}$ one Si_6O_6 ring has an area of 17.8 Å^2 . A unit cell with eight heterotwelve rings therefore yields 142.4 Å^2 . Hence, one tetrahedron has on average 11.87 Å^2 , which resembles the available area of Euclidian layer silicates. The

Tabelle 20: Available Area per Tetrahedrally Coordinated Atom T in Hyperbolic and Euclidian Layer Silicates							
a/b = Cell Axis, $n(T)$ = Number of T on Observed Area $a^2 / a \cdot b \cdot \sin \gamma$, F_R from Table 13, p. 86							
Zeolite	a [Å]	$n(T)$	Reference	PNS	F_R (PNS)	$a^2 \cdot F_R$ [Å ²]	$\frac{a^2 \cdot F_R}{n(T)}$ [Å ²]
Sodalite	8.9 – 9.0	12	[194,195]	P*	2.4	192	16
ρ-Zeolite	14.7–15.0	48	[197]	(PP _{xxx})*	2.5 ¹	550	11.5
Linde A	12.3	48	[198]	I _{xxx} –J*	3.6	544	11.3
Harmatome ²	14.4	48	[199,200]	P*	2.4	499	10.4
ZK5	18.7–18.8	96	[203,204]	I _{xxx} –J*	3.6	1260	13.1
Faujasite	25.0	192	[213]	F–I/D–DT	3.3 ³ /3.8	2062/2375	10.7/12.4
ZSM-39	19.4	128	[214]	D*	3.8	1425	11.13
Analcime	13.7	48	[217]	Y**	3.1	586	12.2
Garnet	11.8–12.6	24T + 16O	[219,220]	Y**	3.1	437–490	10.9–12.3
Mineral	a, b [Å]	$n(T)$	Reference	–	–	$a \cdot b \cdot \sin \gamma$ ⁴	$\frac{a \cdot b \cdot \sin \gamma}{n(T)}$ [Å ²]
Serpentine	$a_{\min} = 5.16$	4 each	[223]	–	–	Min.: 46.1	Min.: 11.53
Kaolinite	$a_{\max} = 5.3$		[224]				
Talcite	$b_{\min} = 8.9$		[225]				
Mica	$b_{\max} = 9.46$		[226]			Max.: 50.0	Max.: 12.5

¹ $S(111):S(100) = 1:4.35$; ² Setup as with ρ-Zeolite and Linde A; ³ $a^2(224) = \frac{1}{4} a^2(227)$, 8 unit cells, half a double surface, see text; ⁴ monoclinic ($\gamma = 90^\circ$) or triclinic (γ between 89 and 85°).

increased surface area values per tetrahedron listed in Table 20 therefore result from the curvature of the describing surface.¹⁵

6.4. Summarizing Overview

In this chapter on the organization of chemical structures with PNS we have mainly used such PNS which either had been known before or were discovered during the early phase of this investigation. A broad variety of chemical compounds selected primarily but not exclusively for their complexity, has been embedded into them. This has been done in search for an answer to the question whether or not these nodal surfaces can lead us to a novel or improved understanding of structural relationships particularly of complex structures and if such insights are independent of the kind of material explored.

Restricting this investigation to the application of only a selected few of the PNS introduced in this work has proved not to have been an impediment, as the nodal surfaces used here can be called fundamental in many cases. This means that most of the other PNS are either generated by $S(hkl)$ distant from the reciprocal origin or that they are mere modulations of existing PNS (e.g. with reduced symmetry).

¹⁵ See also the similar, more mathematical-analytical observations by S. Hyde et al. (footnote 1 on p. 7) pp. 58–66.

It has turned out that, with the PNS used here, a broad variety of different structures can be organized with at times astounding accuracy. In some cases (“A15” superconductors and platinum bronzes) connections to physical properties (conductivity) can be implied. Frequently a separation of structural areas occurs, which are dominated by different kinds of interactions (covalent-electrovalent or covalent-van-der-Waals).

For the large group of zeolites the PNS concept has managed to reveal at times fascinating organizational relationships, like for instance the separation of templates/inclusions and silicate frameworks by the PNS as well as the highly symmetrical arrangement of water in cavities (faujasite, analcime). In particular the non-Euclidian layer structures of $\text{Ta}_6\text{Cl}_{15}$, garnet, and analcime highlight the fact that a Euclidian perspective as it has been standard until now may perhaps have prevented a deeper understanding of structural relationships. Since the method of the – mostly hyperbolic – nodal surfaces is predestined to be used in order to explore structural relationships of non-Euclidian geometry, it cannot surprise that most of the examples studied here can be regarded as hyperbolic and elliptic structures, permitting novel, unconventional interpretations. We have therefore been able to show that the organization of crystalline structures as non-Euclidian regions of different interactions is more common than assumed so far. On closer inspection it therefore turns out that the mathematically unlikely case of a Euclidian structure, which up to date has dominated structural descriptions in solid state chemistry, is indeed only one perspective among many, which occasionally may even prove disadvantageous.¹⁶ A broad field of new insights may open up for structural chemistry.¹⁷

¹⁶ As a sidenote it may be remarked that the hyperbolic and the elliptic concepts can be kind of merged by defining “curved polyhedra”, see: S. Andersson, “Curved Polyhedra”, *Z. Anorg. Allg. Chem.* **631** (2005) pp. 499-501; see also M. O’Keefe, “Three-periodic nets and tilings: regular and related infinite polyhedral”, *Acta. Cryst. A* **64** (2008) pp. 425-429.

¹⁷ As representative, but by no means complete, examples of the application of PNS (exclusively by von Schnering’s group) for the elucidation of chemical structures in more recent years see, e.g.:

- Y. Grin, U. Wedig, F. Wagner, H. G. von Schnering, A. Savin, “The analysis of ‘empty space’ in the PdGa_5 structure”, *J. Alloys Comp.* **255** (1997) pp. 203-208.
- Y. Grin, U. Wedig, H.G. von Schnering, “Hyperbolic Lone Pair Structure in RhBi_4 ”, *Angew. Chem. Int. Ed. Engl.* **34** (1995) pp. 1204-1206; German: *Angew. Chem.* **107** (1995) 1317-1318.
- A. Zürn (see footnote 5 on p. 42).
- M. Somer, U. Herterich, J. Čurda, W. Carrilo-Cabrera, A. Zürn, K. Peters, H.G. von Schnering, “Darstellung, Kristallstruktur und Schwingungsspektren neuer ternärer Verbindungen mit dem Anion $(\text{N-B-N})^{3-}$ ”, *Z. Anorg. Allg. Chem.* **626** (2000) pp. 625-633.
- H.G. von Schnering, J.-H. Chang, M. Freiberg, K. Peters, E.-M. Peters, A. Ormeci, L. Schröder, G. Thiele, G. Röhr, “Structure and Bonding of the Mixed-Valent Platinum Trihalides PtCl_3 and PtBr_3 ”, *Z. Anorg. Allg. Chem.* **630** (2004) pp. 109-116.
- H.G. von Schnering, A. Zürn, J.-H. Chang, M. Baitinger, Y. Grin, “The Intrinsic Shape of the cubic cP124 Clathrate Structure”, *Z. Anorg. Allg. Chem.* **633** (2007) pp. 1147-1153.
- J.-H. Chang, A. Zürn, H.G. von Schnering, “Hyperbolic Cation Diffusion Path in $\alpha\text{-RbAg}_4\text{I}_5$ Type Su-

-
- perionic Conductors”, *Z. Anorg. Allg. Chem.* **634** (2008) pp. 2156-2160.
- A. Zörn, H.G. von Schnering, “Topological Analysis of Mesoporous Solids and Their Ordered Pore Structure by Periodic Nodal Surfaces, PNS”, *Z. Anorg. Allg. Chem.* **634** (2008) pp. 2761-2764.

7. Potential Areas of Application of the PNS Method

This chapter will briefly touch upon areas to which the PNS method could be expanded. These areas either suggested themselves during research for this thesis or they have been suggested by others, while there has not been enough time to investigate them any further.^[227]

7.1. Bonding Theory of the Solid State

Bertaut has observed that linear relations exist between Madelung factors of various cubic systems.^[228] Madelung factors can be calculated via Fourier sums following Bertaut's equation for lattice energies (eq. (5), p. 17).^[57] This is analogous to the calculation of PNS. Bertaut personally suggested investigating whether there are linear relations between single structure factors used to generate relevant PNS.

Nesper has pointed out that structural contributions to the lattice energy of the pseudo-potential theory are also introduced by way of Fourier sums.^[229] He also indicated that the Fermi surfaces of metals frequently look similar to minimal surfaces.¹⁸ Hence, an investigation of correlations between the Fermi surfaces of pseudo-potential theory and nodal surfaces may be promising.

7.2. Phase Transitions

In his PhD thesis Oehme presented a fair amount of examples emphasizing the usefulness of potential and nodal surfaces for the description of phase transitions.^[39] By way of continuously transforming the P^* surface in hexagonal setup (along $\{111\}$) toward the Q^* surface, v. Schnering and Nesper have demonstrated that this method is very well suited to elucidate structural relationships.^[61] During preparatory work for the present thesis many similar transformations have been calculated. It is worthwhile to explore for second order phase transitions whether the spatial parameters of structural units can be described by appropriate, continuously transformed nodal surfaces.

¹⁸ A relationship first observed by Mackay in 1988, see [58].

Another option is the investigation of the behavior of Fermi surfaces during phase transitions.

7.3. Physics of Interfaces

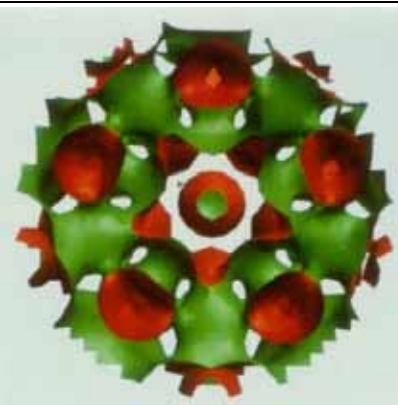
The multifaceted focus on minimization problems in tenside and polymer mixtures referred to at the beginning of this work (see pp. 13 ff.) is restricted almost exclusively to minimal surfaces, which is explicable with direct physical relationships. But as mentioned earlier, the concept of minimal surfaces has mathematical limitations. Both due to its similarity and due to its broader flexibility, the PNS method is a much more convenient model for the description of such problems. Diamond double networks, for instance, can be described much better with the PNS F – I as introduced here than with the PMS D*, but the former surface is unobtainable with the minimal surface method. It turned out, moreover, that more recently discovered two-dimensional water-tenside networks of tetragonal symmetry can only be described using the PNS approach.^[230] This discovery has also highlighted the fact that in dynamical systems interface networks do not always assume the shape of minimal surfaces. Finally and as already mentioned, phase transitions of lipid-water mixtures can be handled much easier by models using PNS.

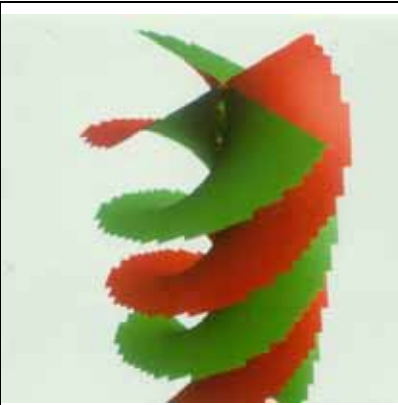
7.4. Description of Non-Crystalline Systems

Already in 1990 Nesper, Oehme, and v. Schnering^[231] demonstrated the possibility to describe non-periodic, quasi-crystalline structures by using $S(hkl)$ with irrational numbers.¹⁹ It is for instance quite simple to generate a quasi-crystalline nodal surface of

¹⁹ The problems posed by non-crystalline yet well-ordered structures, be they quasi-crystalline, semi-amorphous, or incommensurable, are a challenge for chemists and physicists not to be underestimated. See in this regard for instance:

- S. Andersson, S. Lidin, M. Jacob, O. Terasaki, "Über den quasi-kristallinen Zustand", *Angew. Chem.* **103** (1991) pp. 771-775.
- B.W. Ninham, S. Lidin, "Some Remarks on Quasi-Crystal Structures", *Acta Cryst. A* **48** (1992) pp. 640-649.
- S. Hyde et al. (footnote 1 on p. 7) pp. 66-72, 80-83.
- A.L. Mackay, "Generalised crystallography", *J. Molecular Structure* **336** (1995) pp. 293-303; anew: *Structural Chemistry* **13** (2002) pp. 215-220.
- A. Zürn, H. G. von Schnering, (see footnote 15 on p. 152).
- Bertrand Toudic et al., "Hidden Degrees of Freedom in Aperiodic Materials", *Science* **319** (4.1.2008) pp. 69-71.

Table 21: Permutations of $S(hkl)$ for a Truncated Dodecahedron		
$\alpha = 0^\circ, S = 1, \tau = 1/2 (\sqrt{5} + 1)$		
$\tau^{-1} \tau 0$		
$0 \tau^{-1} \tau$	$1 \ 1 \ 1$	
$\tau 0 \tau^{-1}$	$\bar{1} \ 1 \ 1$	
$\tau^{-1} \tau^{-1} 0$	$1 \ \bar{1} \ 1$	
$0 \tau^{-1} \tau^{-1}$	$1 \ 1 \ \bar{1}$	
$\tau^{-1} 0 \tau^{-1}$		
III. 31: PNS from $S(hkl)$ of Tab. 21, Truncated Dodecahedron, along Fivefold Axis $\{1\tau 0\}$.		

		
III. 32: Helical PNS from $S(hkl)$ of Tab. 22 along $\{011\}$		

five- or ten-fold symmetry. The $S(hkl)$ permutation laws for the icosahedral point group can be gleaned from the International Tables, resulting in the permutations as given in Table 21.^[232] Characteristic for quasi-crystalline systems is the irrational number of the golden section τ :

$$\tau = 2 \cdot \cos(36^\circ) = \frac{1}{2}(\sqrt{5} + 1) \approx 1.61803 \quad (41)$$

The PNS resulting from this structure factor is shown in Ill. 31. Its relevance for the organization of quasi-crystalline compounds has yet to be determined, though.

Equally by means of irrational numbers it is possible to generate helices which are equivalent to helical minimal surfaces.^[74] If distributing $S(hkl)$ cyclicly in the h - k plane of reciprocal space with $l = 1$, then one obtains various helices depending on the kind of continuously varied phase angle in the circular h - k plane of the $S(hkl)$. Table 22 lists the hk permutations for a fourfold helix as depicted in Ill. 32. This is the result of investigations initiated by the discovery of multiple helices in oligomer-water mixtures.^[233] A continuously varied phase angle, by the way, also exists for the structure factors of those crystalline space groups having screw axes.

Table 22: hk Permutations for the Generation of a Quadruple Helix; $S = 1, l = 1$								
h	k	α	h	k	α	h	k	α
$\cos(0^\circ)$	$\sin(0^\circ)$	0°	$\cos(252^\circ)$	$\sin(252^\circ)$	252°	$\cos(504^\circ)$	$\sin(504^\circ)$	504°
$\cos(36^\circ)$	$\sin(36^\circ)$	36°	$\cos(288^\circ)$	$\sin(288^\circ)$	288°	$\cos(540^\circ)$	$\sin(540^\circ)$	540°
$\cos(72^\circ)$	$\sin(72^\circ)$	72°	$\cos(324^\circ)$	$\sin(324^\circ)$	324°	$\cos(578^\circ)$	$\sin(578^\circ)$	578°
$\cos(108^\circ)$	$\sin(108^\circ)$	108°	$\cos(360^\circ)$	$\sin(360^\circ)$	360°	$\cos(612^\circ)$	$\sin(612^\circ)$	612°
$\cos(144^\circ)$	$\sin(144^\circ)$	144°	$\cos(396^\circ)$	$\sin(396^\circ)$	396°	$\cos(648^\circ)$	$\sin(648^\circ)$	648°
$\cos(180^\circ)$	$\sin(180^\circ)$	180°	$\cos(432^\circ)$	$\sin(432^\circ)$	432°	$\cos(684^\circ)$	$\sin(684^\circ)$	684°
$\cos(216^\circ)$	$\sin(216^\circ)$	216°	$\cos(468^\circ)$	$\sin(468^\circ)$	468°			

7.5. Electron Localization Function ELF

Already while discussing diamond (p. 118) we indicated that the usual ball-and-stick models used to depict chemical structures are too much reduced in information to be reliable. It is therefore conducive to use more realistic descriptions, which are linked to chemical and generally also physical properties like, for example, electron density and localization. Since the early 1990^[234] the ELF values of structures are being calculated throughout three-dimensional space, leading to the depiction of certain ELF values as closed surfaces.²⁰ Caused by the symmetry laws of crystalline structures, there are inevitable correlations between nodal surfaces and surfaces of constant ELF values, since both are subjected to the same laws.

²⁰ See A. Savin, R. Nesper, S. Wengert, T. S. Fässler, “ELF: The Electron Localization Function”, *Angew. Chem. Int. Ed. Engl.* **36** (1997), pp. 1808-1832, with further references; German: *Angew. Chem.* **109** (1997) pp. 1892-1918.

8. Summary

8.1. Since the early 1970s relationships between the properties of periodic minimal surfaces (PMS) and a variety of phenomena from different disciplines of the natural sciences are being investigated. In the mid-1980s these investigations were expanded to encompass periodic potential surfaces (POPS) and since the late 1980s also nodal surfaces (PNS). The concept of periodic nodal surfaces is, quite in contrast to both other methods, free of any physical implications and offers a broad variability while constraint by strict symmetry laws.

8.2. One main focus of this thesis is the complete analysis of *characteristic structure factors* $S(hkl)$ for the systematic generation of periodic nodal surfaces. This analysis departs from the implicitly known, yet never comprehensively summarized symmetry selection laws of the reciprocal lattice vectors including their phase permutations. In analogy to the characteristic point configurations in real space, the *characteristic structure factors* $S(hkl)$ of a certain symmetry are deducted for the reciprocal space. Tables are produced for the cubic, hexagonal, and trigonal crystal systems, which list the correlation between symmetry and structure factor type. Also considered are phase shifts caused by shifted origins. An interesting detail is the fact that structure factor types with $\sum h_i = 2n$ exist in two cF space groups which have exclusive cF character and are therefore unable to generate cI symmetry in the same (centric) symmetry class: $Fd\bar{3}m$ and $Fd\bar{3}$.

8.3. Based on these results, numerous periodic nodal surfaces are introduced and analyzed, which have been calculated rather easily with Fourier sums. The analysis of mathematical properties regarding topology and symmetry yields a series of results which have been known from the other methods. Decisive new insights are gained, however, while analyzing the distribution of extrema of the generating Fourier series. They frequently exhibit constant or only slightly varying values along certain lines. Hence, besides the *nodes* it is particularly these *line* and *line segment graphs* which permit a characterization of PNS. Furthermore the surface areas and volumes of partial spaces separated by the surfaces can be determined easily, which is important for special questions of structural chemistry.

8.4. The exploration of hyperbolic, graphite-like networks reveals topological and

symmetrical patterns regarding the existence and variability of hypothetical new graphite modifications. This topological excursion into non-Euclidian geometry leads to generally valid relationships between frameworks of chemical compounds and mostly hyperbolic periodic nodal surfaces PNS.

8.5. The organization of chemical structures by periodic nodal surfaces is investigated, with many examples. It is demonstrated that already a relatively small amount of surface types permits the analysis and – sometimes very detailed – characterization of a broad range of different compounds. In some cases the concept of non-Euclidian layer structures leads to an improved understanding of complicated structures and to the discovery of overlooked details, for instance the layered organization of Labyrinth water in faujasite.

8.6. Several topics are finally listed as suggestions for further research, where the concept of periodic nodal surfaces (PNS) could be applied just as successfully.

9. Acknowledgements

- ✿ I am foremost grateful that my late teacher Prof. Dr. Dr. h.c. Hans Georg von Schnering gave me the opportunity to prepare this dissertation in his research group and under his direct supervision, whereby he gave me many liberties to be creative, because or although he entrusted me with his favorite topic;
- ✿ I owe thanks to Prof. Dr. Reinhard Nesper for his many suggestions and for his support during many a shoptalk;
- ✿ next I'd like to highlight Prof. Dr. Sten Andersson and Dr. Sven Lidin who occasionally accompanied me with help and advice in this lonely desert of unexplored scientific territory;
- ✿ I am obliged to Dr. Liane Schröder and particularly to Dipl.-Math. Astrid Jähde, the latter of whom has remained a close and dear friend to this day, for their many discussions and multifarious aid to solve numerous details in and about this work;
- ✿ I am particularly appreciative for Dr. Thomas Popp's vital help during the first weeks of my investigations, as a newcomer to a field without any swimming aid always fears to drown; Thomas took that fear away;
- ✿ a warm thank you goes to all coworkers of the research group of Prof. von Schnering for cordially accepting me in their midst, especially to Dr. Ulrich Wedig for his computational support and to my room colleagues Dr. Frank Wagner and Dr. Dagobert Thiery for their friendly reception;
- ✿ last but not least I am gratefully indebted to the Max Planck Society for the Advancement of Science for their generous scholarship.

10. Annex

10.1. References

References added to this thesis after its initial version had been completed back in early 1993 have been included in footnotes throughout the text, as the text itself did not require any additions or amendments.

- [1] M.H. Schwarz, *Gesammelte mathematische Abhandlungen*, Springer Verlag, Berlin 1890.
- [2] E.R. Neovius, *Bestimmung zweier spezieller periodischer Minimalflächen*, Frenckel & Sohn, Helsinki 1883.
- [3] O. Bonnet, “Note sur la théorie générale des surfaces”, *Compt. Rend.*, **37** (1853) 529-532.
- [4] K. Weierstrass, *Mathematische Werke*, Abh. 3, Johnson Reprint Corp., New York 1967, 39-52.
- [5] A.H. Schoen, *Infinite periodic minimal surfaces without self-intersection*, NASA Technical Note D-5541, Washington 1970.
- [6] H.-U. Nissen, “Crystal orientation and plate structure in echinoid skeletal units”, *Science* **166** (1969) 1150-1152.
- [7] G. Donnay, D.L. Pawson, “X-ray diffraction studies of echinoderm plates”, *Science* **166** (1969) 1147-1150.
- [8] L.E. Scriven, “Equilibrium bicontinuous structure”, *Nature* **263** (1976) 123-125.
- [9] K. Larsson, “The structure of mesomorphic phases and micelles in aqueous glyceride systems”, *J. Phys. Chem.* **56** (1967) 173-198.
- [10] V. Luzzati, P.A. Spegt, “Polymorphism of lipids”, *Nature* **215** (1967) 701-704.
- [11] V. Luzzati, A. Tardieu, T. Gulik-Krzywicki, E. Rivas, F. Reiss-Husson, “Structure of the cubic phases of lipid-water systems”, *Nature* **220** (1968) 485-488.
- [12] A. Tardieu, V. Luzzati, “Polymorphism of lipids – a novel cubic phase – a cage-like network of rods with enclosed spherical micelles”, *Biochim. Biophys. Acta* **219** (1970) 11-17.
- [13] G. Lindblom, K. Larsson, L. Johansson, K. Fontell, S. Forsén, “The cubic phase of monoglyceride-water systems. Arguments for a structure based upon lamellar bilayer units”, *J. Am. Chem. Soc.* **101** (1979) 5465-5470.
- [14] M. Kléman, “Dislocations vis et surfaces minima dans les smectiques A”, *Philos. Mag.* **34** (1976) 79-87.
- [15] K. Larsson, K. Fontell, N. Krog, “Structural relationships between lamellar, cubic and hexagonal phases in monoglyceride-water systems. Possibility of cubic structures in biological systems”, *Chem. Phys. Lip.* **27** (1980) 321-328.
- [16] K. Fontell, “Liquid crystallinity in lipid-water systems”, *Mol. Cryst. Liq. Cryst.* **63** (1981) 59-82.

- [17] W. Longley, T.J. McIntosh, "A bicontinuous tetrahedral structure in a liquid-crystalline lipid", *Nature* **303** (1983) 612-614.
- [18] K. Larsson, "Two cubic phases in monoolein-water system", *Nature* **304** (1983) 664.
- [19] S.T. Hyde, S. Andersson, B. Ericsson, K. Larsson, "A cubic structure consisting of a lipid bilayer forming an infinite periodic minimum surface of the gyroid type in the glycerol-monooleat-water system", *Z. Kristallogr.* **168** (1984) 213-219.
- [20] A. Marmur, "Minimal surface area as an equilibrium condition", *J. Coll. Interface Sci.* **97** (1984) 587-590.
- [21] Gulik, V. Luzzati, M. de Rosa, A. Gambacorta, "Structure and polymorphism of bipolar isopranyl ether lipids from archaebacteria", *J. Molec. Biol.* **182** (1985) 131-149.
- [22] S.T. Hyde, S. Andersson, "Differential geometry of a model membrane consisting of a lipid bilayer with a regular array of protein units", *Z. Kristallogr.* **174** (1986) 237-245.
- [23] P. Kekicheff, B. Cabane, "Between cylinders and bilayers: structures of intermediate mesophases of the SDS/water system", *J. Physique* **48** (1987) 1571-1583.
- [24] E.L. Thomas, D.B. Alward, D.J. Kinning, D.C. Martin, "Ordered bicontinuous boublediamond structure of star block copolymers: A new equilibrium microdomain morphology", *Macromolecules* **19** (1986) 2197-2202.
- [25] H. Hasegawa, H. Tanaka, K. Yamasaki, T. Hashimoto, "Bicontinuous microdomain morphology of block copolymers. 1. Tetrapod-network structure of polystyrene-polyisoprene diblock polymers", *Macromolecules* **20** (1987) 1651-1662.
- [26] D.S. Herman, D.J. Kinning, E.L. Thomas, "A compositional study of the morphology of 18-armed poly (styrene-isoprene) star block copolymers", *Macromolecules* **20** (1987) 2940-2942.
- [27] E.L. Thomas, D.M. Anderson, C.S. Henkee, D. Hoffman, "Periodic area-minimizing surfaces in block copolymers", *Nature* **334** (1988) 598-601.
- [28] E.L. Thomas, J.R. Reffner, J. Bellare, "A menagerie of interface structures in copolymer systems", *J. Physique, Colloq.* **C7** (1990) 363-374.
- [29] S. Andersson, "Eine Beschreibung komplexer anorganischer Kristallstrukturen", *Angew. Chem.* **95** (1983) 67-80; *Angew. Chem. Int. Ed. Engl.* **22** (1983) 69.
- [30] S. Andersson, S.T. Hyde, H.G. von Schnering, "The intrinsic curvature of solids", *Z. Kristallogr.* **168** (1984) 1-17.
- [31] R. Nesper, H.G. von Schnering, "Periodische Äqui-Potentialflächen (PEPS)", *Z. Kristallogr.* **170** (1985) 138-140.
- [32] M. Oehme, Beiträge zur Berechnung und kristallchemischen Anwendung periodischer 3D-Potentialflächen, Master Thesis, Stuttgart 1985.
- [33] R. Nesper, H.G. von Schnering, "Periodische Potentialflächen in Kristallstrukturen", *Angew. Chem.* **98** (1986) 111-113; *Angew. Chem. Int. Ed. Engl.* **25** (1986) 110.
- [34] H.G. von Schnering, "Äquipotentialflächen in Kristallen", *Z. Kristallogr.* **174** (1986) 182-185.
- [35] H.G. von Schnering, R. Nesper, "Die natürliche Anpassung von chemischen Strukturen an gekrümmte Flächen", *Angew. Chem.* **99** (1987) 1097; *Angew. Chem. Int. Ed. Engl.* **26** (1987) 1058.

- [36] P.P. Ewald, "Die Berechnung optischer und elektrostatischer Gitterpotentiale", *Ann. Phys.* **64** (1921) 253-287.
- [37] I.S. Barnes, S.T. Hyde, B.W. Ninham, "The Caesium Chloride zero potential surface is not the Schwarz P*-surface", *J. Physique, Colloq.* **C7** (1990) 19-24.
- [38] A. Fogden, private communication to H.G. von Schnering, Lund 1992; see also A. Fogden, S.T. Hyde, "Parametrization of triply periodic minimal surfaces. I. Mathematical basis of the construction algorithm for the regular class", *Acta Cryst.* **A48** (1992) 442-451; A. Fogden, S.T. Hyde, "... II. Regular class solutions", *ibid.*, 575-591.
- [39] M. Oehme, Nullpotentialflächen und ihre Anwendung in der Kristallchemie, PhD Thesis, Stuttgart 1989.
- [40] S.T. Hyde, *Infinite periodic minimal surfaces and crystal structures*, PhD Thesis, Monash University, Canberra, Australien 1986.
- [41] S. Andersson, S.T. Hyde, J.-O. Bovin, "On the periodic minimal surfaces and the conductivity mechanism of α -AgI", *Z. Kristallogr.* **173** (1985) 97-99.
- [42] Z. Blum, S. Lidin, "The carcerand, an organic structure on a minimal surface", *Acta chem. scand.* **B42** (1988) 332-335.
- [43] Z. Blum, "The 'Caesium effect' revisited", *Acta chem. scand.* **43** (1989) 248-250.
- [44] K. Larsson, "Structure of the starch granule – a curved crystal", *Acta chem. scand.* **45** (1991) 840-843.
- [45] W. Fischer, E. Koch, "On 3-periodic minimal surfaces", *Z. Kristallogr.* **179** (1987) 31-52.
- [46] E. Koch, W. Fischer, "On 3-periodic minimal surfaces with non-cubic symmetry", *Z. Kristallogr.* **183** (1988) 129-152.
- [47] E. Koch, W. Fischer, Serie: "New surface patches for minimal balance surfaces": "I. Branched catenoids", *Acta Cryst.* **A45** (1989) 166-169; "II. Multiple catenoids", *ibid.*, 169-174; "III. Infinite stripes", *ibid.*, 485-490; "IV. Catenoids with spout-like attachments", *ibid.*, 558-563.
- [48] W. Fischer, E. Koch, "Genera of minimal balance surfaces", *Acta Cryst.* **A45** (1989) 726-732.
- [49] S.T. Hyde, S. Andersson, "A systematic net description of saddle polyhedra and periodic minimal surfaces", *Z. Kristallogr.* **168** (1984) 221-254.
- [50] S.T. Hyde, S. Andersson, "Differential geometry of crystal structure descriptions, relationships and phase transformation", *Z. Kristallogr.* **170** (1985) 225-239.
- [51] S.T. Hyde, S. Andersson, "The martensite transition and differential geometry", *Z. Kristallogr.* **174** (1986) 225-236.
- [52] S.T. Hyde, "A topological characterisation of chemical structures", *Z. Kristallogr.* **179** (1987) 53-65.
- [53] S.T. Hyde, "The topology and geometry of infinite periodic surfaces", *Z. Kristallogr.* **187** (1989) 165-185.
- [54] S. Lidin, S.T. Hyde, "A construction algorithm for minimal surfaces", *J. Physique* **48** (1987) 1585-1590.
- [55] S. Lidin, "Symmetry restrictions on minimal surfaces related by the Bonnet-transformation", *Z. Kristallogr.* **188** (1989) 121-129.

- [56] R. Nesper, M. Oehme, H.G. von Schnering, "Periodic potential surfaces", *Wissenschaftlicher Tätigkeitsbericht MPI FKF – Stuttgart – Grenoble für den Zeitraum 1. Jan. 1987 bis 31. Dez. 1987*, Stuttgart 1988, as well as private communication by H.G. von Schnering.
- [57] F. Bertaut, "L'énergie électrostatique de réseaux ioniques", *J. Physique* **13** (1952) 499-505.
- [58] A.L. Mackay, "Äquipotentialflächen für periodische Ladungsverteilungen", *Angew. Chem.* **100** (1988) 867-868; *Angew. Chem. Int. Ed. engl.* **25** (1986) 110.
- [59] Kittel, *Introduction to solid state physics*, 6th ed., Wiley, New York 1976, 231.
- [60] H.G. von Schnering, "Die Krümmung chemischer Strukturen", *Nova acta Leop. NF* **65**, **277** (1991) 89-103; English as: "The curvature of chemical structures", *J. Physique, Colloq.* **C7** (1990) 383-396.
- [61] H.G. von Schnering, R. Nesper, "Nodal surfaces of fourier series: fundamental invariants of structured matter", *Z. Physik B – Cond. Matter* **83** (1991) 407-412.
- [62] H.G. Schnering, M. Oehme, G. Rudolf, "Three-dimensional periodic surfaces which envelope the threefold and fourfold cubic rod packings", *Acta chem. scand.* **45** (1991) 873-876.
- [63] E. Dubois-Violette, B. Pansu (eds.), International Workshop on Geometry and Interfaces, *J. Physique, Colloq.* **C7** (1990).
- [64] H. Karcher, "The triply periodic minimal surfaces of Alan Schoen and their constant mean curvature companions", *Manus. math.* **64** (1989) 291-337.
- [65] J.C.C. Nitsche, "Ein Einschließungssatz für Minimalflächen", *Math. Ann.* **165** (1966) 71-75.
- [66] J.C.C. Nitsche, *Vorlesungen über Minimalflächen*, Springer, Berlin 1975; Engl.: *Lectures on minimal surfaces*, Cambridge University Press, Cambridge 1989.
- [67] J.C.C. Nitsche, "The existence of surface patches for periodic minimal surfaces", *J. Physique, Colloq.* **C7** (1990) 265-271.
- [68] J.C.C. Nitsche, "Periodic surfaces which are extremal for energy functionals containing curvature functions", *IMA Preprint Series* 785, Minneapolis, March 1991.
- [69] J.C.C. Nitsche, "Boundary value problems for variational integrals involving surface curvature", *IMA Preprint Series* 856, Minneapolis, August 1991.
- [70] C.F. Gauss, "Theoria figurae fluidorum in statu aequilibrri", in: Gauss, C.F., *Werke*, Vol. 5, 2nd ed., Königliche Gesellschaft der Wissenschaften, Göttingen 1877, 29-77.
- [71] C.F. Gauss, *Allgemeine Flächentheorie*, 5th ed., Akademische Verlagsgesellschaft, Leipzig 1921.
- [72] A. Fogden, "Weierstrass representation of periodic minimal surfaces", *J. Physique, Colloq.* **C7** (1990) 149-156.
- [73] F. Gachstatter, "H. Hopf's quadratic differential and a Weierstrass formula for general surfaces and surfaces of constant mean curvature", *J. Physique, Colloq.* **C7** (1990) 163-168.
- [74] Hoffman, "The computer-aided discovery of new embedded minimal surfaces", *Math. Intell.* **9** (1987) 8-21.

- [75] W. Fischer, E. Koch, *Minimalflächen in der Kristallographie*, typescript to a lecture series on IPMS, Marburg 1991, unpublished.
- [76] A. Gulik, V. Luzzati, M. de Rose, "Structure and polymorphism of bipolar isopranyl ether lipids from archaebacteria", *J. Molec. Biol.* **182** (1985) 131-149.
- [77] S.D. Kohlwein, "Biological membranes", *J. Chem. Ed.* **69** (1992) 3-9.
- [78] R. Lipowsky, "Critical behavior of vesicles and membranes", *J. Physique, Colloq.* **C7** (1990) 243-248.
- [79] K. Larsson, "Periodic minimal surface structures of cubic phases formed by lipides and surfactants", *J. Coll. Interface Sci.* **113** (1986) 299-300.
- [80] J. Charvolin, J.F. Sadoc, "Periodic systems of frustrated fluid films and 'bicontinuous' cubic structures in liquid crystals", *J. Physique* **48** (1987) 1559-1569.
- [81] I.S. Barnes, S.T. Hyde, B.W. Ninham, P.-J. Derian, M. Drifford, T.N. Zemb, "Small-angle x-ray scattering from ternary microemulsions determines microstructure", *J. Phys. Chem.* **92** (1988) 2286-2293.
- [82] J. Egberts, H. Sloot, A. Mazure, "Minimal surface tension, squeeze-out and transition temperatures of binary mixtures of dipalmitoylphosphatidylcholine and unsaturated phospholipids", *Biochem. Biophys. Acta* **1002** (1989) 109-113.
- [83] S.T. Hyde, "Microstructure of bicontinuous surfactant aggregates", *J. Phys. Chem.* **93** (1989) 1458-1464.
- [84] R. Strey, "Grenzflächen", *Nachr. Chem. Tech. Lab.* **40** (1992) 213-216.
- [85] F. Morgan, "Minimal surfaces, crystals, shortest networks, and undergraduate research", *Math. Intell.* **14** (1992) 37-44.
- [86] S. Andersson, S.T. Hyde, K. Larsson, S. Lidin, "Minimal surfaces and structures: From inorganic and metal crystals to cell membranes and biopolymers", *Chem. Rev.* **88** (1988) 221-242.
- [87] J. Hoppe, H. Nicolai, "Relativistic minimal surfaces", *Phys. Lett. B* **196** (1987) 451-455.
- [88] V. Tapai, "The geometrical meaning of the harmonic gauge for minimal surfaces", *Nuovo Cim.* **103B** (1989) 441-445.
- [89] H.G. von Schnering, *Beiträge zur Chemie binärer und ternärer Halogeno- und Oxoverbindungen der Metalle*, Habilitation Thesis, University of Münster, 1963, 54-64; Program MADKUG for the calculation of Madelung constants and lattice potentials, H.G. v. Schnering, Münster 1962.
- [90] H.G. von Schnering, "Zusammenhänge zwischen Coulomb-Potentialen und Protonenlagen bei kristallinen Hydroxoverbindungen", *Angew. Chem.* **78** (1966) 113; *Angew. Chem. Int. Ed. Engl.* **5** (1966) 133.
- [91] S.T. Hyde, "Minimal surfaces and fast ion conductors", *Philos. Mag.* **57** (1988) 691-702.
- [92] W.J. Moore, D.O. Hummel, *Physikalische Chemie*, 3rd ed., Walter de Gruyter, Berlin 1983, 1118.
- [93] Lax (ed.), *Taschenbuch für Chemiker und Physiker*, Vol. 1, Springer-Verlag, Berlin 1967.
- [94] R.C. Weast, *Handbook of Chemistry and Physics*, 66th ed., CRC Press, Boca Raton, Florida 1986, F62.
- [95] R.C. Weast, *ibid.*, evaporation enthalpies B230, melting enthalpies B223.

- [96] W.I. Smirnow, *Lehrgang der höheren Mathematik*, Teil 2, VEB Deutscher Verlag der Wissenschaften, Berlin 1967, 363.
- [97] J.S. Kasper, K. Lonsdale (eds.), *International Tables for X-Ray Crystallography*, Vol. I, The Kynoch Press, Birmingham 1967, 353-355.
- [98] S. Haussühl, *Kristallstrukturbestimmung*, Verlag Chemie, Weinheim 1979, 83ff.
- [99] J.S. Kasper, K. Lonsdale (eds.), *International Tables for X-Ray Crystallography*, Vol. 1, The Kynoch Press, Birmingham 1967, 373-425; particularly also *ibid.*, Vol. 2, 147; see also the listed phase laws for the direct method of phase determination, J.A.- Ibers, W.C. Hamilton (eds.), *ibid.*, Vol. 4, 337ff.
- [100] H. Wondratschek, "Extraordinary orbits of the space groups. Theoretical considerations", *Z. Kristallogr.* **143** (1976) 460-470.
- [101] P. Engel, T. Masumoto, G. Steinmann, H. Wondratschek, *The non-characteristic Orbits of the Space Groups*, Suppl. 1 to *Z. Kristallogr.*, Oldenbourg, Munich 1984.
- [102] P. Engel, "Zur Theorie der kristallographischen Orbits", *Z. Kristallogr.* **163** (1983) 243-249.
- [103] A. Bienenstock, P.P. Ewald, "Symmetry of Fourier Space", *Acta Cryst.* **15** (1962) 1253-1261.
- [104] H. Wondratschek, private communication to H.G. von Schnering of 11 March 1993.
- [105] T. Hahn (ed.), *International Tables for Crystallography*, Vol. A, 2nd revised ed., Kluwer Academic Publishers, Dordrecht 1989, 825-854.
- [106] – Program 'rapture' for the display and manipulation of 3D objects, U. Wedig, Max Planck Institute for Solid State Research, Stuttgart 1990;
– Program 'fourier' for the manipulation of input files (transformations), with tools for numerical analysis of funktion values (determination of extrema etc.), for continuous surface transformations, -translations and for the calculation of surface subsections, U. Wedig, G. Rudolf, R. Nesper, Max Planck Institute for Solid State Research, Stuttgart 1989ff.
- [107] Hellner, E. Koch, A. Reinhardt, A., "The homogeneous frameworks of the cubic crystal structures", *Verwandtschaftskriterien von Kristallstrukturtypen*, part XI, Physik Daten No. 16-2, Fachinformationszentrum Energie · Physik · Mathematik GmbH, Karlsruhe 1981.
- [108] A.F. Wells, *Three-dimensional nets and polyhedra*, Wiley & Sons, London 1977.
- [109] W. Fischer, E. Koch, "Crystallographic aspects of minimal surfaces", *J. Physique, Colloq.* **C7** (1990) 131-147.
- [110] H.S.M. Coxeter, *Regular Polytopes*, 3rd ed., Dover, New York 1973, 6.
- [111] A.L. Loeb, *Space Structures*, Addison Wesley Publ. Comp., Reading, MA 1976, 92.
- [112] S.J. Chung, T. Hahn, W.E. Klee, "Nomenclature and generation of three-periodic nets: the vector method", *Acta Cryst.* **A40** (1984) 42-50.
- [113] W.E. Klee, "The topology of crystal structures: Invariants", *Z. Kristallogr.* **179** (1987) 67-76.
- [114] A. Beukemann, W.E. Klee, "Minimal nets", *Z. Kristallogr.* **201** (1992) 37-51.
- [115] J.R. Weeks, *The shape of space*, Marcel Dekker Inc., New York 1985.

- [116] B.M. Sen, "On double surfaces", *Proc. Lond. Math. Soc.* **20** (1922) 417-434, quoted acc. to [53].
- [117] Koch, W. Fischer, "Three-periodic minimal balance surfaces: a correction", *Acta Cryst.* **A49** (1993) 209-210.
- [118] M. do Carmo, *Differential geometry of curves and surfaces*, Prentice-Hall Inc., Eaglewood Cliffs, N.J. 1976.
- [119] D.E.H. Jones, *New Scient.* **32** (1966) 245.
- [120] C. Zammattio, A. Marinoni, A.M. Brizio, *Leonardo der Forscher*, Belser, Stuttgart 1981, 99.
- [121] H.W. Kroto, J.R. Heath, S.C. O'Brien, R.F. Curl, R.E. Smalley, " C_{60} : Buckminsterfullerene", *Nature* **318** (1985) 162-163.
- [122] W. Krätschmer, L.D. Lamb, K. Fostiropoulos, D.R. Huffman, "Solid C_{60} : a new form of carbon", *Nature*, **347** (1990) 354-358.
- [123] R.F. Curl, R.E. Smalley, "Fullerenes", *Sci. Amer.* **10** (1991) 32-41.
- [124] H.W. Kroto, " C_{60} : Buckminsterfulleren, die Himmelsspäre, die zur Erde fiel", *Angew. Chem.* **104** (1992) 113-133; *Angew. Chem. Int. Ed. Engl.* **31** (1992) 111.
- [125] S. Iijima, "Helical microtubules of graphitic carbon", *Nature* **357** (1991) 56-58.
- [126] D.E.H. Jones, "Ghostly graphite", *Nature* **351** (1991) 526.
- [127] Schuh (ed.), *Enzyklopädie Naturwissenschaft und Technik*, Verlag Moderne Industrie, Munich 1980, 1635-1637.
- [128] J.H. Lindsay, "An elementary treatment of the imbedding of a graph in a surface", *Am. Math. Mon.*, **66** (1959) 117-118.
- [129] M.R. Garey, D.S. Johnson, *Computers and intractability, a guide to the theory of np-completeness*, W.H. Freeman & Cie., San Fransisco 1979.
- [130] J. Terno, *Numerische Verfahren der diskreten Optimierung*, Teubner Texte zur Mathematik, Vol. 36, Teubner Verlagsgesellschaft, Leipzig 1981, 52 ff.
- [131] A.W.M. Dress, R. Franz, "Zu einer Frage von Herrn S. Bilinski Pflasterungen von Brezelflächen betreffend", *Jugoslavenska Akademija Znanosti i Umjetnosti*, Zagreb 1987.
- [132] T. Lenosky, X. Gonze, M. Teter, V. Elser, "Energetics of negatively curved graphitic carbon", *Nature* **355** (1992) 333-335.
- [133] G.B. Adams, O.F. Sankey, J.B. Page, M. O'Keeffe, D.A. Drabold, "Energetics of large fullerenes: balls, tubes, and capsules", *Science* **256** (1992) 1792-1795.
- [134] S.J. Townsend, T.J. Lenosky, D.A. Muller, C.S. Nichols, V. Elser, "Negatively curved graphitic sheet model of amorphous carbon", *Phys. Rev. Lett.* **69** (1992) 921-924.
- [135] M. O'Keeffe, G.B. Adams, O.F. Sankey, "Predicted new low energy forms of Carbon", *Phys. Rev. Lett.* **68** (1992) 2325-2328.
- [136] A.L. Mackay, H. Terrones, "Hypothetical graphite structures with negative Gaussian curvature", *Phil. Trans. R. Soc. Lond.* **A 343** (1993) 113-127.
- [137] A. Savin, A.D. Becke, J. Flad, R. Nesper, H. Preuss, H.G. von Schnering, "Ein neuer Blick auf die Elektronenlokalisierung", *Angew. Chem.* **103** (1991) 421-424; *Angew. Chem. Int. Ed. Engl.* **30** (1991) 409.
- [138] A.D. Becke, K.E. Edgecombe, "A simple measure of electron localization in atomic and

- molecular systems”, *J. Chem. Phys.* **92**(9) (1990) 5397-5403.
- [139] A. Savin, O. Jepsen, J. Flad, O.K. Anderson, H. Preuß, H.G. von Schnering, “Die Elektronenlokalisierung in den Festkörperstrukturen der Elemente: die Diamantstruktur”, *Angew. Chem.* **104** (1992) 186-188; *Angew. Chem. Int. Ed. Engl.* **31** (1992) 187.
- [140] C.P. Gazzara, R.M. Middleton, R.J. Weiss, “A refinement of the parameters of α -Manganese”, *Acta Cryst.* **22** (1967) 859-862.
- [141] F.C. Frank, J.S. Kasper, *Acta Cryst.* **11** (1958) 184, quoted acc. to: C.W. Kimball, W.C. Phillips, M.V. Nevitt, R.S. Preston, “Magnetic hyperfine interactions and electric quadrupolar coupling in alloys of iron with the alpha-Manganese structure”, *Phys. Rev.* **146** (1966) 375-378.
- [142] J.A. Oberteuffer, J.A. Marcus, L.H. Schwartz, G.P. Felcher, “Magnetic structure of a single crystal of alpha manganese”, *Phys. Lett.* **28A** (1968) 267-268; J.S. Kasper, B.W. Roberts, *Phys. Rev.* **101** (1955) 537.
- [143] H.G. von Schnering, unpublished works, private communication; see also D.E.C. Corbridge, E.J. Lowe, “Structure of white phosphorus: Single crystal X-ray examination”, *Nature* **170** (1952) 629.
- [144] E. Hellner, E. Koch, “Cluster of framework considerations for the structures of Ti_7Sb_2 , α -Mn, Cu_5Zn_8 and their variations”, *Acta Cryst.* **A37** (1981) 1-6.
- [145] S.E. Rasmussen, “Preparation of single phases and single crystals of niobium-germanium compounds”, *Acta chem. scand.* **A31** (1977) 79-82; S.E. Rasmussen, R.G. Hazell, “Structure and order parameter of a A15-type niobium germanium single crystal”, *Acta Cryst.* **B35** (1979) 1677-1679.
- [146] A.L. Mackay, “New geometries for superconduction and other purposes”, *Spec. Sci. Tech.* **11** (1988) 4-8.
- [147] S.M. Jørgensen, *J. Prakt. Chem.* **16** (1877) 344, quoted acc. to [150].
- [148] J. Waser, E.D. McClanahan, “The structure of NaPt_3O_4 ”, *Exper.* **6** (1950) 379-380; same authors, “The crystal structure of NaPt_3O_4 ”, *J. Chem. Phys.* **19** (1951) 413-416.
- [149] J.J. Scheer, A.E. van Arkel, R.D. Heyding, “Oxide complexes formed in the systems platinum metals : alkali carbonates : oxygen”, *Can. J. Chem.* **33** (1955) 683.
- [150] D. Cahen, J.A. Ibers, R.D. Shannon, “Structure and properties of $\text{Ni}_{0.25}\text{Pt}_3\text{O}_4$. A new platinum bronze”, *Inorg. Chem.* **11** (1972) 2311-2315.
- [151] D. Cahen, J.A. Ibers, R.D. Shannon, “Platinum bronzes. IV. Preparation, crystal chemistry, and physical properties”, *Inorg. Chem.* **13** (1974) 1377-1388.
- [152] D. Bergner, R. Kohlhaas, “Neue Verbindungen vom $\text{Na}_x\text{Pt}_3\text{O}_4$ -Strukturtyp”, *Z. anorg. allg. Chem.* **401** (1973) 15-20.
- [153] M. O’Keeffe, S. Andersson, “Rod packings and crystal chemistry”, *Acta Cryst.* **A33** (1977) 914-923.
- [154] C.L. Teske, H. Müller-Buschbaum, “Über Erdalkalimetall-Oxocuprate. I Zur Kenntnis von CaCuO_3 ”, *Z. anorg. allg. Chem.* **370** (1969) 134-143.
- [155] C.L. Teske, H. Müller-Buschbaum, “Über Erdalkalimetall-Oxocuprate. II Zur Kenntnis von Sr_2CuO_3 ”, *Z. anorg. allg. Chem.* **371** (1969) 325-332.
- [156] C.L. Teske, H. Müller-Buschbaum, “Über Erdalkalimetall-Oxocuprate. V Zur Kenntnis von CaCuO_3 und Sr_2CuO_3 ”, *Z. anorg. allg. Chem.* **379** (1970) 234-241.

- [157] R. Kipka, H. Müller-Buschbaum, "Über Oxocuprate, XI Zur Kenntnis von $\text{Ba}_3\text{Cu}_2\text{O}_4\text{Cl}_2$ ", *Z. anorg. allg. Chem.* **422** (1976) 231-236.
- [158] R. Kipka, H. Müller-Buschbaum, "Über Oxocuprate, XVI $\text{Ba}_9\text{Cu}_7\text{O}_{15}\text{Cl}_{12}$ mit Cu^{2+} in neuer Koordination", *Z. Naturforsch.* **31b** (1976) 1067-1069.
- [159] R. Kipka, H. Müller-Buschbaum, "Über Oxocuprate, XX: Ein Erdalkalioxocuprat(II) mit geschlossenen Baugruppen: BaCuO_2 ", *Z. Naturforsch.* **32b** (1977) 121-123.
- [160] T. Popp, *Konkurrierende Phasen bei der Synthese von supraleitenden Materialien im System Bi-Sr-Ca-Cu-O*, PhD Thesis, Max Planck Institute for Solid State Research, Stuttgart 1990, pp. 98 ff.
- [161] K.-H. Lii, R.C. Haushalter, "Layer and tunnel structures in new molybdenophosphates: $\text{Cs}_2\text{Mo}_4\text{P}_6\text{O}_{26}$ and $\text{M}_4\text{Mo}_8\text{P}_{12}\text{O}_{52}$ ($\text{M} = \text{Cs}, \text{Rb}, \text{K}, \text{Tl}$)", *J. Solid State Chem.* **69** (1987) 320-328.
- [162] K.-H. Lii, D.C. Johnston, D.P. Goshorn, R.C. Haushalter, "Crystal structure and magnetic properties of a new molybdenophosphate: $\text{AgMo}_5\text{P}_8\text{O}_{33}$ ", *J. Solid State Chem.* **71** (1987) 131-138.
- [163] K.-H. Lii, R.C. Haushalter, " CsMoP_2O_7 : a molybdenopyrophosphate containing isolated Mo^{3+} cations", *Acta Cryst.* **C43** (1987) 2036-2038.
- [164] K.-H. Lii, R.C. Haushalter, C.M. O'Connor, " $\text{Cs}_3\text{Mo}_5\text{P}_6\text{O}_{25}$, ein neues Molybdatophosphat mit einem cubanartigen Mo_4O_4 -Cluster mit sechs Mo-Mo-Bindungen", *Angew. Chem.* **99** (1987) 576-577; *Angew. Chem. Int. Ed. Engl.* **26** (1987) 549.
- [165] R.C. Haushalter, F.W. Lai, "Synthesis and structure of $\text{Cs}_4\text{Mo}_{10}\text{P}_{18}\text{O}_{66}$ ", *J. Solid State Chem.* **76** (1988) 218-223.
- [166] R.C. Haushalter, F.W. Lai, "Synthesis of a new one-dimensional sodium molybdenum phosphate polymer: structure of $[(\text{H}_3\text{O})_2\text{NaMo}_6\text{P}_4\text{O}_{24}(\text{OH})_7]^{2-}$ ", *Inorg. Chem.* **28** (1989) 2904-2905.
- [167] R.C. Haushalter, F.W. Lai, " $[\text{Et}_4\text{N}]_6[\text{Na}_{14}\text{Mo}_{24}\text{P}_{17}\text{O}_{97}(\text{OH})_{31}] \cdot x\text{H}_2\text{O}$, ein mit zwölf Na^+ -Ionen und einem H_3PO_4 -Molekül gefüllter Hohlraumcluster", *Angew. Chem.* **101** (1989) 802-805; *Angew. Chem. Int. Ed. Engl.* **28** (1989) 743.
- [168] R.C. Haushalter, K.G. Strohmaier, F.W. Lai, "Structure of a three-dimensional, microporous molybdenum phosphate with large cavities", *Science* **246** (1989) 1289-1291, as well as private communication from 30.4.1991.
- [169] H. Hillebrecht, J. Curda, L. Schröder, H. G. von Schnering, " Li_2SiN_2 – eine aufgefüllte ZnI_2 -Struktur mit $[\text{Si}_4\text{N}_6]\text{N}_{4/2}$ -Netzen", *Z. Kristallogr. Suppl.* **6** (1993), 80. B. Eisenmann has found a similar, undistorted structure with Na_2SnAs_2 , private communication to H. Hillebrecht.
- [170] P.H. Fourcroy, D. Carré, J. Rivet, "Structure cristalline de l'Iodure de Zinc ZnI_2 ", *Acta Cryst.* **B 34** (1978) 3160-3162.
- [171] A.F. Wells (ed.), *Structural Inorganic Chemistry*, 5th ed., Oxford University Press, New York 1984; NaTiI : 1300; $\text{Cu}_2\text{O}/\text{SiO}_2$ and many other examples for diamond multiple networks: 127ff.
- [172] O. Ermer, "Fivefold-diamond structure of adamantane-1,3,5,7-tetracarboxylic acid", *J. Am. Chem. Soc.* **110** (1988) 3747-3754.
- [173] O. Ermer, A. Eling, "Verzerrte Dreifach-Diamantstruktur von 3,3-

- Bis(carboxymethyl)glutarsäure ('Methantetraessigsäure')", *Angew. Chem.* **100** (1988) 856-860; *Angew. Chem. Int. Ed. Engl.* **27** (1988) 829.
- [174] B. Krebs, "Thio- und Selenverbindungen von Hauptgruppenelementen – neue anorganische Oligomere und Polymere", *Angew. Chem.* **95** (1983) 113-134; *Angew. Chem. Int. Ed. Engl.* **22** (1983) 113.
- [175] D. Müller, H. Hahn, "Untersuchungen über ternäre Chalkogenide XXIV: Zur Struktur des TlGaSe_2 ", *Z. anorg. allg. Chem.* **138** (1978) 258-272; see also: D. Thiery, *Beiträge zur Strukturbestimmung bei tiefen Temperaturen am Beispiel der ferroelektrischen Phase TlGaSe_2* , PhD Thesis, Stuttgart 1992, 158 S.
- [176] B. Eisenmann, A. Hofmann, "Crystal structure of sodium phyllo-diselenidoaluminate, NaAlSe_2 ", *Z. Kristallogr.* **197** (1991) 171-172.
- [177] B. Eisenmann, A. Hofmann, "Crystal structure of potassium phyllo-dithioindate(III), KInS_2 ", *Z. Kristallogr.* **195** (1991) 318-319.
- [178] P. Lemoine, D. Carré, M. Guittard, "Structure du sulfure de gallium et de potassium, KGaS_2 ", *Acta Cryst.* **C40** (1984) 910-912.
- [179] F. Lévy, *Structural chemistry of layer-type phases*, D. Reidel Publishing Company, Dordrecht 1976, 136ff.
- [180] Courbion, G. Ferey, " $\text{Na}_2\text{Ca}_3\text{Al}_2\text{F}_{14}$: A new example of a structure with 'independent F' – a new method of comparison between fluorides and oxides of different formula", *J. Solid State Chem.* **76** (1988) 426-431.
- [181] R. Domesle, R. Hoppe, "The crystal structure of Ca_2AlF_7 ", *Z. Kristallogr.* **153** (1980) 317-328.
- [182] G. Bergerhoff, "Über Metallokomplexe", Habilitationsschrift, University of Bonn 1962; see also G.B. Kauffman, M. Karbassi, G. Bergerhoff, "Metallo complexes: an experiment for the undergraduate laboratory", *J. Chem. Ed.* **61** (1984) 729-737.
- [183] Schäfer, H.G. von Schnering, K.-J. Niehues, H.G. Nieder-Vahrenholz, "Niobfluoride", *J. Less-common Metals* **9** (1965) 95-104.
- [184] D. Bauer, H.G. von Schnering, "Die Struktur der Tantalhalogenide $\text{Ta}_6\text{Cl}_{15}$ und $\text{Ta}_6\text{Br}_{15}$ ", *Z. anorg. allg. Chem.* **361** (1968) 259-276.
- [185] B.G. Hyde, S. Andersson, *Inorganic crystal Structures*, John Wiley & Sons, New York 1989, 116f.
- [186] On their application see, e.g.: J. Weitkamp, "New directions in zeolite catalysis", *Stud. Surf. Sci. Catal.* **65** (1991) 21-46.
- [187] W.M. Meier, D.H. Olson, *Atlas of zeolite structure types*, 2nd ed., Butterworth & Co., Stoneham, MA, 1987.
- [188] M.E. Davis, R.F. Lobo, "Zeolite and molecular sieve synthesis", *Chem. Mater.* **4** (1992) 756-768.
- [189] S. Hansen, L. Fäth, S. Andersson, "Structural relationships in tetrahedral frameworks: Reflections on Cristobalite", *J. Solid State Chem.* **39** (1981) 137-141.
- [190] L. Fäth, S. Andersson, "Crystalstructure of the synthetic zeolite N $\text{NaAlSiO}_4 \cdot 1.35 \text{H}_2\text{O}$ ", *Z. Kristallogr.* **160** (1982) 313-316.
- [191] S. Hansen, S. Andersson, L. Fäth, "A description of the feldspar framework", *Z. Kristallogr.* **160** (1982) 9-17.

- [192] E. Koch, E. Hellner, "The framework of sodalite-like structures and of tetrahedrite-like structures", *Z. Kristallogr.* **154** (1981) 95-114.
- [193] L. Pauling, "The structure of soldalite and helvite", *Z. Kristallogr.* **74** (1930) 213-225.
- [194] Löns, H. Schulz, "Strukturverfeinerung von Sodalith, $\text{Na}_8\text{Si}_6\text{Al}_6\text{O}_{24}\text{Cl}_2$ ", *Acta Cryst.* **23** (1967) 434-436.
- [195] C. Baerlocher, W.M. Meier, "Synthese und Kristallstruktur von Tetramethylammonium-Sodalith", *Helv. Chim. Acta* **52** (1969) 1853-1860.
- [196] L.B. McCusker, C. Baerlocher, R. Nawaz, "Rietveld refinement of the crystal structure of the new zeolite mineral gobbinsite", *Z. Kristallogr.* **171** (1985) 281-289.
- [197] J.B. Parise, T.E. Gier, D.R. Corbin, D.E. Cox, "Structural changes occurring upon dehydration of zeolite rho. A study using neutron powder diffraction and distance-least-squares structural modeling", *J. Phys. Chem.* **88** (1984) 1635-1640.
- [198] V. Gramlich, W.M. Meier, "The crystal structure of hydrated NaA: A detailed refinement of a pseudosymmetric zeolite structure", *Z. Kristallogr.* **133** (1971) 134-149.
- [199] R.M. Barrer, F.W. Bultitude, I.S. Kerr, "Some properties of, and a structural scheme for, the harmatome zeolites", *J. Chem. Soc.* (1959) 1521-1528.
- [200] H. Steinfink, "The crystal structure of the zeolite, phillipsite", *Acta Cryst.* **15** (1962) 644-651.
- [201] R. Rinaldi, J.J. Pluth, J.V., Smith, "Zeolites of the phillipsite family, refinement of the crystal structures of phillipsite and harmatome", *Acta Cryst.* **B30** (1974) 2426-2433.
- [202] W. Depmeier, H. Schmid, N. Setter, M.L. Werk, "Structure of cubic aluminate sodalite, $\text{Sr}_8[\text{Al}_{12}\text{O}_{24}](\text{CrO}_4)_2$ ", *Acta Cryst.* **C43** (1987) 2251-2255.
- [203] R.M. Barrer, D.J. Robinson, "The structures of the salt-bearing aluminosilicates, species P and Q", *Z. Kristallogr.* **135** (1972) 374-390.
- [204] J.B. Parise, R.D. Shannon, E. Prince, D.E. Cox, "The crystal structures of the synthetic zeolites (Cs,K)-ZK5 and (CS,D)- ZK5 determined from neutron powder diffraction data", *Z. Kristallogr.* **165** (1983) 175-190.
- [205] E.K. Gordon, S. Samson, W.B. Kamb, "Crystal structure of the zeolite Paulingite", *Science* **154** (1966) 1004-1007.
- [206] H. Gies, F. Liebau, "Melanophlogite: Composition, thermal behavior and structure refinement", *Acta Cryst.* **A37** (1981) C-187-188.
- [207] H. Gies, F. Liebau, H. Gerke, "'Dodecasile' – eine neue Reihe polytyper Einschlußverbindungen von SiO_2 ", *Angew. Chem.* **94** (1982) 214-215; *Angew. Chem. Int. Ed. Engl.* **21** (1982) 206.
- [208] H. Gies, "Studies on clathrasils III", *Z. Kristallogr.* **164** (1983) 247-257; see also F. Liebau, "Zeolites and clathrasils – two distinct classes of framework silicates", *Zeolites* **3(3)** (1983) 191-193; H. Gies in: J.L. Atwood, J.E.D. Davies, D.D. MacNicol (eds.), *Inclusion Compounds*, Oxford University Press, Oxford 1991, 1-36.
- [209] G. Bergerhoff, W.H. Baur, W. Nowacki, "Über die Kristallstruktur des Faujasites", *N. Jb. Miner.* (1958) 193-200.
- [210] Damour, *Ann. Mines* **1** (1842) 395, quoted acc. to [209].
- [211] F. Delprato, L. Delmotte, J.L. Guth, L. Huve, "Synthesis of new silica-rich cubic and

- hexagonal faujasites using crown-ether-based supramolecules as templates”, *Zeolites* **10** (1990) 546-552.
- [212] Broussard, D.P. Shoemaker, “The structures of synthetic molecular sieves”, *J. Amer. Chem. Soc.* **82** (1960) 1041-1051.
- [213] D.H. Olson, “A reinvestigation of the crystal structure of the zeolite hydrated NaX”, *J. Phys. Chem.* **74** (1970) 2758-2764.
- [214] J.L. Schlenker, F.G. Dwyer, E.E. Jenkins, W.J. Rohrbaugh, G.T. Kokotailo, W.M. Meier, “Crystal structure of a synthetic high silica zeolite – ZSM-39”, *Nature* **294** (1981) 340-342.
- [215] H. Gies, “Studies on clathrasils VI”, *Z. Kristallogr.* **167** (1984) 73-82.
- [216] W.H. Taylor, “The structure of analcite ($\text{NaAlSi}_2\text{O}_6 \cdot \text{H}_2\text{O}$)”, *Z. Kristallogr.* **74** (1930) 1-19.
- [217] G. Ferraris, D.W. Jones, J. Yerkess, “A neutron-diffraction study of the crystal structure of analcime, $\text{NaAlSi}_2\text{O}_6 \cdot \text{H}_2\text{O}$ ”, *Z. Kristallogr.* **135** (1972) 240-252.
- [218] G. Menzer, “Die Kristallstruktur der Granate”, *Z. Kristallogr.* **69** (1928) 300-396.
- [219] S.C. Abrahams, S. Geller, “Refinement of the structure of a grossularite garnet”, *Acta Cryst.* **11** (1958) 437-441.
- [220] C. Addad, P. Ducros, “Études de la substitution du groupement SiO_4 par $(\text{OH})_4$ dans les Composés $\text{Al}_2\text{Ca}_3(\text{OH})_{12}$ et $\text{Al}_2\text{Ca}_3(\text{SiO}_4)_2 16(\text{OH})_{3,36}$ de type Grenat”, *Acta Cryst.* **23** (1967) 220-230.
- [221] G.O. Brunner, W.M. Meier, “Framework density distribution of zeolite-type tetrahedral nets”, *Nature*, **337** (1989) 146-147.
- [222] Stixrude, M.S.T. Bukowinski, “Rings, topology, and the density of tectosilicates”, *Am. Mineral.*, **75** (1990) 1159-1169.
- [223] A.F. Holleman, N. Wiberg, *Lehrbuch der Anorganischen Chemie*, Walter de Gruyter, Berlin 1985, 771.
- [224] L. Smrcok, D. Gyepesova, M. Chmielova, “New X-ray Rietveld refinement of Kaolinite from Keokuk, Iowa”, *Cryst. Res. Technol.* **25** (1990) 105-110.
- [225] B. Perdikatsis, H. Burzlaff, “Strukturverfeinerung am Talk $\text{Mg}_3[(\text{OH})_2\text{Si}_4\text{O}_{10}]$ ”, *Z. Kristallogr.* **156** (1981) 177-186.
- [226] H. Tateyama, S. Shimoda, T. Sudo, “The crystal structure of synthetic Mg^{IV} mica”, *Z. Kristallogr.* **139** (1974) 196-206.
- [227] See also the examples in: A.L. Mackay, “Lonsdale Invariants - Periodic Nodal Surfaces”, *Per. Mineral.* **59** (1990) 149-155; A.L. Mackay, “Crystallographic surfaces”, *Proc. R. Soc. Lond. A* **442** (1993) 47-59.
- [228] F. Bertaut, “Sur les relations linéaires entre constantes de Madelung”, *C. Rend. Acad. Sci.* **239** (1954) 234-235.
- [229] R. Nesper, “Chemische Bindungen - intermetallische Verbindungen”, *Angew. Chem.* **103** (1991) 805-834; *Angew. Chem. Int. Ed. Engl.* **30** (1991) 789.
- [230] P. Kekicheff, G.J.T. Tiddy, “Structure of the intermediate phase and its transformation to lamellar phase in the lithium perfluorooctanoate/water system”, *J. Phys. Chem.* **93** (1989) 2520-2526.

- [231] R. Nesper, M. Oehme, H.G. von Schnering, unpublished works, Max Planck Institute for Solid State Research, Stuttgart.
- [232] T. Hahn (ed.), *International Tables for Crystallography*, op. cit. (note 105), 783-786.
- [233] J. Köning, C. Boettcher, H. Winkler, E. Zeitler, Y. Talmon, J.-H. Fuhrhop, "Magic angle (54.7°) gradient and minimal surfaces in quadruple micellar helices", *J. Am. Chem. Soc.* **115** (1993) 693-700.
- [234] A. Savin, unpublished work at the conclusion of research for this thesis, University of Stuttgart; but see footnote 20 on p. 156.

10.2. List of Abbreviations and Symbols

$^+R/-R$	volume with positive/negative function values	gSG	number of the generating space group
\bigcirc	partly characteristic $S(hkl)$	H	average curvature
\bullet	characteristic $S(hkl)$	h,k,l	reciprocal lattice coefficients
∇	non-characteristic $S(hkl)$	hP	hexagonal primitive
A	surface area	I_{hkl}	Intensity of an x-ray reflex hkl
α	phase angle	\mathcal{K}	number of edges/lines of a network (N_l)
a,b,c	crystallographic cell axes	$k_{1/2}$	main curvature
χ	Euler-Poincaré characteristic ($2 - t$)	k_α	curvature, $f(\alpha)$
cF	cubic face-centered	n	number of corners of a polygon
cI	cubic body-centered	N_i	i-dimensional element of a network
C_n	n -fold rotational axis	P	lattice potential
cP	cubic primitive	p	connectivity of a polygon's corner
d^*	reciprocal lattice plane distance	Θ	diffraction angle
$\Delta H_{V/F}$	evaporation and melting enthalpies, respectively	PC	name of point configuration
\mathcal{E}	number of furcation points of a network (N_0)	q	electric charge
eSG	space group number of the eigen symmetry	ρ	electron density
Φ	Fourier transform of charge distribution	R, r	distance in polar coordinates
F	crystallographic structure factor	SG	space group
\mathcal{F}	number of polygons of a network (N_2)	Σ	sum of reciprocal coefficients h,k,l
\mathcal{F}_n	number of n -fold polygons	S	geometric structur factor
F_R	volume-reduced surface area	t	number of tunnels of a network
F_R^0	volume-reduced surface area of a primitive unit cell	τ	golden section = $2 \cdot \cos(36^\circ)$
G	Gaussian curvature	trP	trigonal primitive
γ	crystallographic cell angle $\angle a,b$	trR	trigonal rhombohedral
g	even-numbered reciprocal coefficient $h/k/l$	U	lattice energy
g	genus of a body	u	odd reciprocal coefficient $h/k/l$
		V	cell volume
		x,y,z	real lattice coefficients in fractions of cell axes
		\mathcal{J}	centricity index of a unit cell
		Z	number of cycles of a graph

10.3. List of Illustrations and Charts

	page
III. 1:	Minimal surface in tetrahedral frame, taken from ^[32] 14
III. 2-7:	Illustrations of cubic PNS from Table 8 56-66
III. 8.a-c:	Double surfaces $F - I$, $IJ^* - P_2$, and $I_2 - Y^{**}V^*$ with their mirror surfaces 90
III. 8.d-g:	'Frames' of the PNS P^* , $(PJ)^*$ (No. 221), and $(PP_{xxx})^*$, $(PJ)^*$ (No. 215) 90
III. 8.h-k:	Labyrinth graphs of the PNS $P_2 - IW_z$, $I_{xxx} - J^*$ und $Y_{xxx}^{**} - V^*$ 90
III. 9.a-d:	Bodies of genus $g = 1$ bzw. 2, taken from ^[115] 92
III. 10:	Möbius ribbon, a non-orientable surface, taken from ^[40] 93
III. 11:	Connectivity pattern of the Buckminster fullere network 102
III. 12:	Pattern of tunnel separation of a periodical unit, taken from ^[40] 103
III. 13-15:	Trigonal-planar network units made of hexagons and heptagons (6,7) with genus $g = 1\frac{1}{2}$ 108-109
III. 16:	Tetrahedral network unit (6,7) with genus $g = 2$ 112
III. 17:	Hexagonal network unit (6,7) with genus $g = 2\frac{1}{2}$ 112
III. 18:	Octahedral network unit (6,7) with genus $g = 3$ 112
III. 19:	Pentagonal-bipyramidal network unit (6,7) with genus $g = 3\frac{1}{2}$ 112
III. 20:	Cubic network unit (6,7) with genus $g = 4$, and tetragonal-planar network unit (6,7) with genus $g = 2$ 112
III. 21:	Non-translative, cubic network unit (6,7) with genus $g = 4$ 112
III. 22:	Cuboctahedral network unit (6,7) with genus $g = 6$ 113
III. 23-30:	Structures of various compounds with PNS 128-142
III. 31:	PNS from $S(hkl)$ in shape of a truncated dodecahedron 155
III. 32:	Helical PNS 155
Charts 1+2:	Reciprocal lattice distances as function of c/a ration of a trP and tI unit cell, respectively 100

10.4. List of Tables

	page
Tab. 1: Relation between melting enthalpy ΔH_M and evaporation enthalpy ΔH_E of some elements and compounds.....	18
Tab. 2: α -Permutations in $Im\bar{3}m$ with and without phase shift.....	29
Tab. 3: α -Permutations in $Fd\bar{3}m$	29
Tab. 4: Permutations of $S(531)$ in $F\bar{4}3m$	31
Tab. 5.1: Characteristic structure factors, cI space groups.....	33
Tab. 5.2: Characteristic structure factors, cF space groups	34
Tab. 5.3: Characteristic structure factors, cP space groups	35
Tab. 6.1: Characteristic $S(hkl)$, cI space groups.....	36
Tab. 6.2: Characteristic $S(hkl)$, cF space groups.....	36
Tab. 6.3: Characteristic $S(hkl)$, cP space groups.....	37
Tab. 7: Possible combinations of two $S(hkl)$ close to the origin in space group $I\bar{4}3d$	40
Tab. 8: Some 3D periodic, cubic nodal surfaces.....	44
Tab. 9.1.1: Characteristic structure factors, hP space groups, Patterson symmetry 6/mmm.....	70
Tab. 9.1.2: Characteristic structure factors, hP space groups, Patterson symmetry 6/m	71
Tab. 9.2: Characteristic structure factors, trP space groups.....	72
Tab. 9.3: Characteristic structure factors, trR space groups.....	73
Tab. 10.1: Characteristic $S(hkl)$, hP space groups	74
Tab. 10.2: Characteristic $S(hkl)$, trP space groups.....	75
Tab. 10.3.1: Characteristic $S(hkl)$, trR space groups in trR setup	75
Tab. 10.3.2: Characteristic $S(hkl)$, trR space groups in trP setup	75
Tab. 11: Some 3D periodic hexagonal and trigonal nodal surfaces.....	77
Tab. 12: Some graph-generating nodal surfaces	84
Tab. 13: Volume distribution and surface areas of some nodal surfaces	86
Tab. 14: Genus g of some nodal surfaces	97
Tab. 15: Curvature of various combinations of two m - and one n -polygon	102
Tab. 16: Number of n -polygons \mathfrak{T}_n in topologically repetitive unit as a function of number of tunnel faces t with $p = 3$	106
Tab. 17: Tessellation of space with pentagons and octagons by topological units with $g = 2$	106
Tab. 18: Symmetry of topological units of 3D networks with $p = 3$	110
Tab. 19: Comparison of PMS and PNS with hypothetical graphite networks	114
Tab. 20: Available area per tetrahedrally coordinated atom T in hyperbolic and euclidian layer silicates.....	150
Tab. 21: Permutations of $S(hkl)$ for a truncated dodecahedron.....	155
Tab. 22: hk Permutations for the generation of a quadruple helix	155



The periodic nodal surface $\Pi_{xxx}W^* - I_{xxx}$ ("orchid")
 $^{217}\langle(211)^{-\pi/4}\rangle$; x, y, z from $-1/4$ to $1/4$, see p. 60f.

